AFTR -58-74
AD0047410. Copy #1
CATALOGED BY SEPRR
TI- *

AF TECHNICAL REPORT 5874

DO NOT DESTROY
RETURN TO
TECHNICAL INFORMATION LIBRARY
ASAPRL

DO NOT DESTROY
RETURN TO
TECHNICAL INFORMATION LIBRARY
SEPRR

20090520 144

INFRARED DEFROSTING AND DEICING

WRIGHT-PATTERSON
TECHNICAL LIBRARY
WPAFB, O.

RETURN TO SEPIR BY:
28 NOV 1966

HARRY DORNBRAND

REPUBLIC AVIATION CORPORATION

JANUARY 1952

WRIGHT AIR DEVELOPMENT CENTER

NOTICE

When Government drawings, specifications, or other data are used for any purpose other than in connection with a definitely related Government procurement operation, the United States Government thereby incurs no responsibility nor any obligation whatsoever; and the fact that the Government may have formulated, furnished, or in any way supplied the said drawings, specifications, or other data, is not to be regarded by implication or otherwise as in any manner licensing the holder or any other person or corporation, or conveying any rights or permission to manufacture, use, or sell any patented invention that may in any way be related thereto.

AF TECHNICAL REPORT 5874

AD-047410

INFRARED DEFROSTING AND DEICING

Harry Dornbrand

Republic Aviation Corporation

January 1952

Equipment Laboratory
Contract No. AF33(038)-12917
RDO No. 664-802

Wright Air Development Center
Air Research and Development Command
United States Air Force
Wright-Patterson Air Force Base, Ohio

Carpenter Litho & Prtg. Co., Springfield, O.
100 - 23 November 1954

FOREWORD

This report was prepared by Republic Aviation Corporation on Contract AF33(038)-12917. RDO No. 664-802, Prevention and Removal, Ice and Frost, Aircraft Surfaces, is applicable to this report. It was administered under the direction of the Equipment Laboratory, with D. M. Patterson acting as project engineer. J. S. Martin, Chief Research Engineer, was responsible for the administration of this program at Republic Aviation Corporation. This is the final report on the project; it contains all of the useful data presented in the previous progress reports.

The author wishes to express his appreciation to W. R. Bush for his helpful suggestions and guidance throughout the program and to H. Towle for his valuable suggestions and assistance in the preparation of the material on reflector design. Other members of the Republic Aviation Corporation staff who, at some time during this program, contributed by conducting experimental tests, gathering data and etc., are: Edward Lee, Sidney Gravitz, Herbert A. Grumm, Robert Kamerow, Ronald W. McCaffrey, Joseph L. Poggie and Robert B. Revenko.

ABSTRACT

Data are presented herein, useful in the design of infra-red defrosting and deicing systems. The data can be subdivided into two main parts. One part deals with the pertinent physical properties of receiver, reflector, filter and source materials. The physical properties include spectral reflection, transmission, absorption and etc. The data have been gathered for the wavelength band immediately beyond the visible, 0.75 to 10.0 microns. The other section is devoted to methods of predicting the distribution and magnitude of the radiant energy impinging on a receiver from a source-reflector combination. Results of an experimental test on the magnitude and distribution of radiant energy issuing from a cylindrical source within a parabolic reflector and impinging on a plexiglas receiver, are shown to compare favorably with predicted results based upon the data herein contained.

PUBLICATION REVIEW

This report has been reviewed and is approved.

FOR THE COMMANDER:

RICHARD STOLLE
Colonel, USAF
Chief, Equipment Laboratory

CONTENTS

		Page
LIST OF ILLUSTRATIONS		vi
INTRODUCTION		xi
SECTION I	- Properties of Plexiglas and Lucite, Glass, and Vinyl	1
SECTION II	- Properties of Water, Frost, Ice and Fog	8
SECTION III	- Properties of Radiator and Reflector Materials	13
SECTION IV	- Theoretical Reflector Design Considerations.	17
SECTION V	- Experimental Reflector Tests	29
SECTION VI	- Magnitude of Radiation Interception	32
BIBLIOGRAPHY		39
APPENDIX I	Reflected Energy Distribution from Paraboloid	43
APPENDIX II	Total Radiation Intensity Distribution on a Line Above a Parabolic Reflector Containing a Point Source (Two Dimensional)	46
APPENDIX III	Distribution of the Reflected Energy Intensity at One of the Foci of a Two Dimensional Elliptical Reflector for a Point Source Located at the Other Focus	48
APPENDIX IV	Total Radiation Intensity Distribution Impinging Upon a Receiving Surface Above an Infinitely Long Parabolic Reflector Containing a Finite Diameter Source	55
APPENDIX V	Correction for Chart Method of Radiation Distribution to Account for Finite Length Source	62

CONTENTS
(CONT'D)

		Page
APPENDIX VI	Correction for Chart Method of Radiation Distribution to Account for Finite Length Source and Receiver Reflection.....	65
APPENDIX VII	Correction for Chart Method of Radiation Distribution to Account for Reflection (Two Dimensional).....	75
APPENDIX VIII	Correction for Blockage.....	77
APPENDIX IX	Sample Calculation for Experimental Reflector Tests.....	85
APPENDIX X	Reflection From a Water Droplet.....	89a

LIST OF ILLUSTRATIONS

Figure		Page
1	Light Paths Thru a Transparent Panel	90
2	Dispersion - Lucite and Plexiglas	91
3	Dispersion - Silica Glass	92
4	Theoretical Average Reflection VS Angle of Incidence	93
5	Index of Refraction VS Temperature	94
6	Schematic - Portable Spectrometer	95
7	Portable Spectrometer Set-Up	96
8	Reflection VS Angle of Incidence - Lucite (0.068)	97
9	Reflection VS Angle of Incidence - Glass (0.116 ANN. L.O.F.)	98
10	Spectral Reflection (Two Surfaces) of Glass, Plexiglas and Vinyl	99
11	Normal Transmission - Lucite 202	100
12	Normal Transmission - Lucite 201	101
13	Normal Transmission - Plexiglas II	102
14	Normal Transmission - Plexiglas IA	103
15	Normal Transmission - Plate Glass	104
16	Transmission Comparison of Annealed and Tempered Glass	105
17	Transmission Comparison of Regular Glass From Two Manufacturers	106
18	Transmission Comparison of White Glass from Two Manufacturers	107
19	Normal Transmission - Vinyl	108
20	Normal Transmission - Laminated Glass	109
21	Comparison of Experimental and Predicted Data for Laminated Glass - A	110

Figure		Page
22	Comparison of Experimental and Predicted Data for Laminated Glass - B	111
23	Comparison of Experimental and Predicted Data for Laminated Glass - C	112
24	Transmission VS Temperature	113
25	Transmission - Lucite and Plexiglas	114
26	Transmission - Glass	115
27	Transmission - Vinyl Plastic (Du Pont)	116
28	Transmission - Vinyl Plastic (Monsanto)	117
29	Transmission - Vinyl Plastic (L.O.F. Co.)	118
30	Transmission - Laminated Glass	119
31	Absorption Coefficients of Transparent Materials	120
32	Absorption Coefficients of Transparent Materials from Two References	121
33	Total Absorption of Glass and Methyl Methacrylate for Normal Black Body Radiation VS Thickness	122
34	Spectral Reflection of Water and Ice	123
35	Transmission - Water in Quartz Containers	124
36	Transmission - Water in Plexiglas Containers	125
37	Total Transmission of Water and Ice for Normal Black Body Radiation	126
38	Absorption Coefficient - Water	127
39	Transmission of Glaze Ice Collected Atop of Mt. Washington	128
40	Transmission - Corning Glass Filters	129
41	Transmission - Plexiglas Container (1/16" Wall) with 1/8" Water and Corning Glass Filter 7-57	130

Figure		Page
42	Transmission - Polaroid Infra-red Band Filter (Type C-3).....	131
43	Transmission of Clear Ice - A.....	132
44	Transmission of Clear Ice - B.....	133
45	Comparison of Clear Ice and Water Transmission....	134
46	Transmission Rime Ice (.09" Thickness).....	135
47	Reflection of Snow.....	136
48	Laboratory Frost Accretion Setup.....	137
49	Spectral Distribution of Black Body Radiation.....	138
50	Black Body Spectral Transmission Thru Corning Glass Filter 7-56 (Low Temperature).....	139
51	Black Body Spectral Transmission Thru Corning Glass Filter 7-56 (High Temperature).....	140
52	Black Body Spectral Transmission Thru Corning Glass Filter 7-57 (Low Temperature).....	141
53	Black Body Spectral Transmission Thru Corning Glass Filter 7-57 (High Temperature).....	142
54	Total Black Body Transmission Thru Corning Glass Filters - 7-56, 7-57.....	143
55	Transmission - Highly Transparent Glass.....	144
56	Total Transmission - Highly Transparent Glass.....	145
57	Emissivity Test Schematic.....	146
58	Emissivity - Oxidized Cast Iron.....	147
59	Emissivity - Oxidized Cold Roll Steel.....	148
60	Emissivity - Porcelain Tile.....	149
61	Spectral Emissivity of Several Radiator Materials.	150
62	Emissivity - Nernst Radiator.....	151

Figure		Page
63	Emissivity - Alclad	152
64	Emissivity - Monel	153
65	Emissivity - Inconel	154
66	Emissivity - Inconel X	155
67	Emissivity - Titanium	156
68	Emissivity - Stainless Steel	157
69	Emissivity - Chrome Plated Steel	158
70	Spectral Reflectivity of Several Materials	159
71	Reflection of Various Metals	160
72	Distribution of Reflected Energy from Paraboloid Containing a Point Source at Focus	161
73	Distribution of Reflected Energy from a Point Source Enclosed Within a Parabolic Reflector (Two Dimensional)	162
74	Distribution - Parabolic Reflectors	163
75	Typical Total Energy Distribution on a Receiver from a Point Source within a Parabolic Reflector (Two Dimensional)	164
76	The Distribution of Energy at the Focus of an Elliptical Reflector with a Point Source at the Other Focus (Two Dimensional) - A	165
77	The Distribution of Energy at the Focus of an Elliptical Reflector with a Point Source at the Other Focus (Two Dimensional) - B	166
78	The Distribution of Energy at the Focus of an Elliptical Reflector with a Point Source at the other Focus (Two Dimensional) - C	167
79	Design Chart for Determining Energy Distribution from Parabolic Reflector with Finite Diameter Source - Source Diameter = 1/8"	168

Figure		Page
80	Design Chart for Determining Energy Distribution from Parabolic Reflector with Finite Diameter Source - Source Diameter = 1/4".....	169
81	Design Chart for Determining Energy Distribution from Parabolic Reflector with Finite Diameter Source - Source Diameter = 3/8".....	170
82	Design Chart for Determining Energy Distribution from Parabolic Reflector with Finite Diameter Source - Source Diameter = 1/2".....	171
83	Design Chart for Determining Energy Distribution from Parabolic Reflector with Finite Diameter Source - Source Diameter = 3/4".....	172
84	Design Chart for Determining Energy Distribution from Parabolic Reflector with Finite Diameter Source - Source Diameter = 1".....	173
85	Typical Energy Distribution on Plate Above a Parabolic Reflector Containing A Finite Diameter Source of Finite Length.....	174
86	Correction for Finite Length Source.....	175
87	Reflection VS Angle of Incidence - Comparison of Two Methods.....	176
88	Correction for Finite Length and for Reflection.....	177
89	Radiant Energy Passing Thru Surface of Glass or Plexiglas VS Angle of Incidence.....	178
90	Comparison of the $(\cos^{-1} ay)^8$ to the First Two Terms of Its Infinite Series.....	179
91	Blockage of an Infinitely Long Cylindrical Source within a Parabolic Reflector.....	180
92	Plexiglas Receiver Instrumented with Surface Thermocouples.....	181
93	Experimental Reflector Test Setup.....	182
94	Comparison of Experimental and Predicted Reflector Results.....	183
95	Ratio of Convection to Radiation Transfer from Cylindrical Source.....	184

INTRODUCTION

Recent studies have indicated the superiority of infra-red over other systems for defrosting, anti-icing and de-icing of certain aircraft cockpit transparent enclosures. A simple infra-red system for heating panels, may consist of a radiating source and a reflector to efficiently direct the radiant energy upon the panel.

The scarcity of infra-red optical data has hindered the design of infra-red heating systems. The purpose of the subject research project is to gather and compile this data, in a form readily usable by the designer. Basic data are presented on the total and spectral absorption, reflection and transmission of aircraft transparent materials and water, frost and ice. Also presented are data on the total and spectral emissivity of materials suitable for use as a radiating source and the total and spectral absorption and reflection of materials suitable for use as a reflector. In addition, a general analytical method has been developed for determining the magnitude and distribution of radiant energy impinging or absorbed by a receiver from any source-reflector combination.

SECTION I

PROPERTIES OF PLEXIGLAS AND LUCITE, GLASS, LAMINATED GLASS AND VINYL

Plexiglas and Lucite, glass, laminated glass and vinyl are the transparent materials generally used in aircraft enclosures. The physical laws that govern the reflection, transmission and absorption of these materials are presented in this section. Pertinent data, gathered from many sources, are also presented and discussed.

Theoretical Relationships

Of the total incident energy, E, impinging on a transparent material, a portion, E_R, is reflected another portion, E_A, is absorbed and the remainder, E_T, is transmitted.

$$E = E_R + E_A + E_T \tag{1}$$

1. Reflection

The specular reflection from a polished surface can be expressed in terms of the polarized rays vibrating parallel and perpendicular to the incident surface, by Fresnel's equations.

$$r_{\parallel} = \tan^2(i-i') / \tan^2(i+i') \tag{2}$$

$$r_{\perp} = \sin^2(i-i') / \sin^2(i+i') \tag{3}$$

If the incident energy is composed of equal amounts of both polarized components, the average reflection can be expressed as:

$$r = \frac{1}{2}\left[\frac{\tan^2(i-i')}{\tan^2(i+i')} + \frac{\sin^2(i-i')}{\sin^2(i+i')}\right] \tag{4}$$

i = angle of incidence
i' = angle of refraction
r = fraction of incident energy reflected

For the special case of unpolarized, normal incident radiation, the reflection from the surface of a material immersed in air, is:

$$r = (n-1)^2 / (n+1)^2 \tag{5}$$

n = refractive index with respect to air = $\frac{\sin i}{\sin i'}$

2. Transmission

Each differential layer of a semi-transparent material will absorb a constant percent of the radiation entering the layer. In differential form, the decrease in intensity in passing thru the differential layer may be expressed as:

$$\frac{dE_E}{dl} = -KE_E \tag{6}$$

dE_E/dl = transmitted light gradient
E_E = intensity of light entering layer
K = absorption coefficient

Integrating the above expression, the radiation transmitted thru a layer of material, is:

$$E_{T_1} = E_E e^{-KL} \tag{7}$$

E_{T_1} = transmitted radiation energy thru a thickness of semi-transparent material (no reflection)
e = base of natural logarithm
L = thickness of material

3. Absorption

The absorption of radiant energy is calculated indirectly by use of equation (1) after the reflected and transmitted energy has been determined. If reflection occurred only at the front surface, the previously presented relationships for reflection and transmission could be simply applied and the absorbed energy determined for a pane of transparent material with known values of n and K. However, due to multiple-reflection, illustrated in Fig. 1, the relationships are more complicated. Also, at angles of incidence other than normal to the surface, the increased radiation path length thru the material must be considered. The length of the radiation path, L', thru the material at various incident angles may be determined from:

$$L' = \frac{L}{\sqrt{1-\left(\frac{\sin\psi}{n}\right)^2}} \tag{8}$$

Now, the expression for transmission, modified to account for the increased radiation path length, is:

$$E_{T_1} = gE_E = e^{-K\left(\frac{L}{\sqrt{1-\left(\frac{\sin\psi}{n}\right)^2}}\right)} E_E \tag{9}$$

The term, g, is defined by equation (9). It is discussed more fully in Ref. 33. As can be seen from Fig. 1, the total transmitted energy is given by the following infinite series:

$$E_T = Eg(1-r)^2\left[1 + (rg)^2 + (rg)^4 + (rg)^6 + \text{----}\right] \tag{10}$$

The sum of this infinite series can be expressed as:

$$E_T = E\,\frac{(1-r)^2 g}{1-(rg)^2} \qquad (11)$$

Since $g<1$, and for the materials under consideration the magnitude of r is approximately 0.04, the term $(rg)^2$ may be neglected, yielding:

$$E_T \simeq E(1-r)^2 g \qquad (12)$$

Note that the above expression can be developed directly from equation (10) by neglecting the transmitted rays other than the first. A similar expression can be derived for the total multiple reflection (See Fig. 1).

$$E_R = E\left[r + \frac{rg^2(1-r)^2}{1-(rg)^2}\right] \qquad (13)$$

If all but the first reflection is neglected, then:

$$E_R \simeq Er \qquad (14)$$

Substituting the exact expressions for reflection and transmission into equation (1), the absorbed energy is:

$$E_A = E\left[1-r-\frac{(1-r)^2 g}{1-rg}\right] \qquad (15)$$

And by the approximate relationships:

$$E_A \simeq E\left[1-r-g(1-r)^2\right] \qquad (16)$$

Experimental and Theoretical Data

1. Reflection

The refractive indicies of Lucite and Plexiglas as a function of wavelength are presented in Fig. 2. The refractive index of glass is shown in Fig. 3. The greater portion of the available data are for the visible range. The refractive index changes rapidly in the ultraviolet and only slightly in the infra-red range. This suggests that a constant value of n may be selected for the infra-red range under investigation for the purpose of engineering calculations. The average value selected for all the transparent materials investigated is $n = 1.48$. The variation in reflection as a function of angle of incidence, based on equation (4), is shown in Fig. 4. Also shown is a comparison of reflection values over a range of refractive indicies from 1.44 to 1.52. This range of indicies is greater than the expected variation of all the materials in the entire test wavelength band. The greatest variation, at any angle of incidence, between the reflection at an extreme value of n compared to the mean value of n is but 1 % of the incident energy.

The effect of temperature on index of refraction and hence on reflection is small as shown in Fig. 5. Within the range of -65 to +160°F the variation may be neglected for the purpose of engineering calculations. As an example, the difference in the first reflection from the glass of Fig. 5 at -65°F compared to +160°F, calculated from equation 5, is but 0.06% of the incident radiation.

An experimental check of Fresnel's relationship between angle of incidence and reflection was made on the portable spectrometer schematically illustrated in Fig. 6 and photographed with auxillary equipment in Fig. 7. The optics are essentially the same as the Perkin-Elmer 12B spectrometer. The ability to change the position of the detector, an Eppley Thermopile, permits measurements of transmission at various angles of incidence other than zero degrees; measurements which can not be made with a standard spectrometer. For at angles of incidence other than zero degrees, the ray transmitted thru a transparent material is translated parallel to the incident ray. In order to measure the true energy of the transmitted ray, the detector must be translated a like amount. This is illustrated in Fig. 6. Briefly, the method employed in these tests consisted of transmission measurements at various angles of incidence from which the percent reflection was calculated. It was assumed that the index of refraction was equal to 1.48, and the normal reflection was calculated from equation (5). The absorption coefficient for the material under consideration was next determined by a transmission measurement at normal incidence and substitution of the results into equations (9) and (12). Once the absorption coefficient was known, the reflection at the various angles of incidence could be calculated from the test results and equations (9) and (12). Since this method involves the computation of the absorption coefficient, a possible source of error, only filters limiting the radiant energy to band widths of high transparency, for the particular test specimen, were used. Figs. 8 and 9 show the test results compared to the theoretical curves obtained by Fresnel's relationship as given by equations (2) and (3). The test data follows the general shape of the average theoretical curve but are a few percent low. This slight deviation may be due to inaccuracy in angle measurement, error in determination of the absorption coefficient, or possibly slight polarization of incident radiation. The agreement is sufficient to confirm the use of the theoretical relationship for calculating the reflection at any angle of incidence.

Normal spectral reflection measurements of plexiglas, glass and vinyl specimens were made for Republic Aviation Corporation at the New York Naval Shipyard with a reflectometer described in Ref. 7.

The results are presented in Fig. 10. The reflection measured is the total reflection and hence is affected by thickness and absorption coefficient. At wavelengths of high absorption, the reflection decreases because the only contribution is from the initial ray at the front surface. Although not shown in this data, reflection peaks, sometimes occurring near absorption bands, have negligible effect on the reflection when averaged over a sizable wavelength band width.

2. Transmission

Experimental spectral transmission tests were made, by use of a Beckman Spectrometer in the wavelength range between 0.75 and 1.1 microns and a Perkin Elmer Model 12 Spectrometer was used in the wavelength region between 1.1 and 10.0 microns. These tests were conducted at the Westinghouse Plant in Bloomfield, New Jersey. Several thicknesses of each of the following materials were tested.

a. Lucite 202
b. Lucite 201
c. Plexiglas IA
d. Plexiglas II
e. Glass (annealed and tempered, regular and water white, manufactured by Libbey-Owens-Ford and Pittsburgh Plate Glass Companies)
f. Vinyl bonding material
g. Laminated glass

The results are presented in Figs. 11-20. A comparison of the data for the methyl methacrylate samples reveals that the transmission properties are essentially the same for both the high and low temperature materials and for the products of both manufacturers (Figs. 11-14). This material has very noticeable absorption bands between 0.75 and 2.2 microns; beyond 2.2 microns it can be considered opaque. The transmission properties may be affected to a slight extent by aging.

Figs. 15-18 show the spectral transmission properties of plate glass. The transmission decreases sharply at 2.7 microns and is negligible after 4.6 microns. A comparison of the transmission of annealed and tempered glass, both manufactured by Pittsburgh Plate Glass Company, is shown in Fig. 16. Heat treating glass does not appreciably change its transmission properties. Fig. 17 is a comparison of the transmission of regular glass from two manufacturers. The Pittsburgh Plate Glass Company regular glass has a somewhat lower transmission than that of the Libbey-Owens-Ford Company probably due to the greater iron content which also gives

the glass a greener tint. White glass samples from the two manufacturers are compared in Fig. 18. There is a smaller variation between the samples of white glass from the two manufacturers than in regular glass. In general, white glass has a considerably higher transmission than regular glass. Note that glass samples from the same manufacturer but prepared from different batches, may differ slightly.

The transmission of the vinyl bonding material, used by Pittsburgh Plate Glass in the manufacture of laminated glass, is presented in Fig. 19. There are many sharply defined absorption bands and a large region between 2.7 and 3.8 microns in which there is no transmission. For the thicker specimens, transmission may be considered negligible past 2.7 microns.

The transmission of laminated glass is shown in Fig. 20. As can be observed, the transmission is dependent upon the color of the glass. The laminated glass was built to Air Force Specification No. AN-DD-G-551, Amendment 1, except for the 1 1/2 inch thick specimen which was built to Air Force Specification No. 34012. The latter specification is more rigid as to light transmission in the visible range. It requires a minimum transmission in the visible range of 80% compared to the 70% called for by Specification No. AN-DD-G-551, Amendment 1. To meet the higher transmission requirements, it is usually necessary for the manufacturer to use water white glass instead of regular glass.

The transmission of the laminated glass may be predicted from the data gathered on its components, glass and vinyl. The internal reflection loss between two materials with approximately equal indicies of reflection is small. As an example, the loss at a surface formed by two materials of n equal to 1.5 and 1.4 is 0.1%. Hence in calculating the transmission thru laminated glass, internal reflection losses can normally be neglected. In this case, equation (12) becomes:

$$\frac{E_T}{E} = e^{-\left[K_g(L_1+L_3+L_5+\cdots)+K_v(L_2+L_4+L_6+\cdots)\right]}(1-r)^2 \qquad (17)$$

wherein g and the odd number subscripts refer to the glass and v and the even number subscripts refer to the vinyl. Using a constant value of r equal to 0.0375 and the absorption coefficients as determined in a following section from the glass and vinyl transmission tests, the transmission of the laminated glass was calculated. A comparison of calculated and test results is presented in Figs. 21-25. The computed transmission agrees fairly well with the experimental results. The 1 1/2 inch bullet resistant glass, shows higher transmission than can be calculated, in the wavelength

region near the visible. It is believed that this is due to the use of a "whiter" glass than was singly tested.

The variation of the transmission of glass, methyl methacrylate and vinyl with temperature, in the range between -65°F and 160°F, was checked by use of the portable filter spectrometer, previously described. The spectrometer was alternately set up in an oven and refrigerated room to obtain the entire temperature range. As Fig. 24 shows, there is no appreciable variation in transmission of any of the test materials in this temperature range.

As a matter of interest, transmission data for the same materials from other sources are presented in Figs. 25-30.

3. Absorption

The absorption coefficient, K, may be calculated from transmission data in several ways by use of equation (12). For normal incidence, this equation reduces to:

$$\frac{E_T}{E} = e^{-KL}(1-r)^2 \qquad (18)$$

Given the transmission of two thicknesses of the same material, a ratio based on equation (18) may be made which will eliminate the reflection term as follows:

$$\frac{E_{T_1}}{E_1} \Big/ \frac{E_{T_2}}{E_2} = \frac{e^{-KL_1}}{e^{-KL_2}} \qquad (19)$$

wherein the subscripts 1 and 2 designate the two different thicknesses. Solution of the above equation for K yields:

$$K = \frac{\log\left[\frac{E_{T_1}}{E_1} \Big/ \frac{E_{T_2}}{E_2}\right]}{L_2 - L_1} \qquad (20)$$

Another method, useful when data from more than two or more thicknesses are available, is a graphical one. Equation (18) expressed in logarithm form is:

$$\log\left(\frac{E_T}{E}\right) = \log(1-r)^2 - KL \qquad (21)$$

Hence, if the transmission is plotted versus length on log-log paper, the slope of the straight line will represent -K. Also, the intercept at L = 0, will represent $(1-r)^2$. A third possible method is to estimate r from the index of refraction and solve for K directly from equation (18). Methods 1 and 2 are extremely sensitive to the inherent experimental error involved in the high transmission range. A check revealed that, even with the slight variation in reflection to be expected, method 3 yielded results as or more consistent than methods 1 and 2. Using a value of r equal to 0.0375, the absorption coefficient for the various materials was determined and plotted in Fig. 31 as a function of wavelength.

Data collected from other sources are presented in Fig. 32.

4. Total Transmission and Absorption

Up to now, only spectral transmission, i.e., the per cent of incident light, composed of a very narrow wavelength band that passes through a transparent material, has been considered. Data of this type have been presented for a large range of wavelengths. A radiant source at a particular temperature will radiate varying amounts of energy at each wavelength. This is discussed more fully in a later section. The total transmission, i.e. the per cent of the total radiation emitted from the source that will be transmitted thru the material is evidently a function of the radiating characteristics of the source as well as the transmission characteristics of the receiver. Knowing both characteristics, the radiant energy transmitted at each wavelength may be computed. This result, energy transmitted per unit wavelength may be plotted versus wavelength. Integration of this curve will yield the per cent of the total radiation transmitted. Assuming a constant 4 % total reflection for glass and plexiglas the amount of energy absorbed may then be calculated. This last assumption is very closely true when there is very little transmission as in the greater portion of the infra-red region.

The total absorption of various thicknesses of methyl methacrylate and glass for black body radiation at several temperatures have been calculated and the results are shown in Fig. 33. The absorption of energy in the wavelength region below 0.75 microns was considered negligible. Black body radiation is discussed more fully in a later section on radiation sources. The greater absorption of methyl methacrylate as compared to glass is noticeable from the figure. All methyl methacrylate thicknesses considered, absorbed more than 90 % of the incident energy for source temperatures below 2000°R.

SECTION II
PROPERTIES OF WATER, FROST, ICE AND FOG

The general theoretical relationships on reflection, transmission and absorption, discussed in the previous section, are applicable to substances mentioned herein.

Water

1. Reflection

The reflectivity of water as a function of wavelength is presented in Fig. 34. The reflectivity varies only slightly. A constant value of r equal to 2% appears to be a good approximation for use in engineering calculations. This corresponds to an index of refraction, $n = 1.33$.

2. Transmission

Experimental data on the spectral transmission of water are presented in Figs. 35 and 36. The data were gathered by use of both a Beckman and Perkin Elmer Spectrometer. The practical transmission limit for water is 1.8 microns. The total transmission of water as a function of black body source temperature is presented in Fig. 37. The data, taken from Ref. 7b indicate that 90% of the incident radiant energy from a black body source at 1000°F will be absorbed by a layer of water 0.02 inches thick. Calculations, based upon the spectral transmission data, yields 98% absorption of the incident energy for a .04 inch thick water layer.

3. Absorption

The absorption coefficient calculated from the experimental transmission data is presented in Fig. 38. Similar data from another source are included in Fig. 31.

Ice

Ice that appears transparent to visible light is known as clear or glaze ice. It is formed when water freezes slowly permitting the entrapped air to escape. Ice that is not transparent in the visible range and has the appearance of snow is known as rime ice. Ice formations are often found within these extreme limits, and unfortunately an exact classification is difficult.

1. Reflection

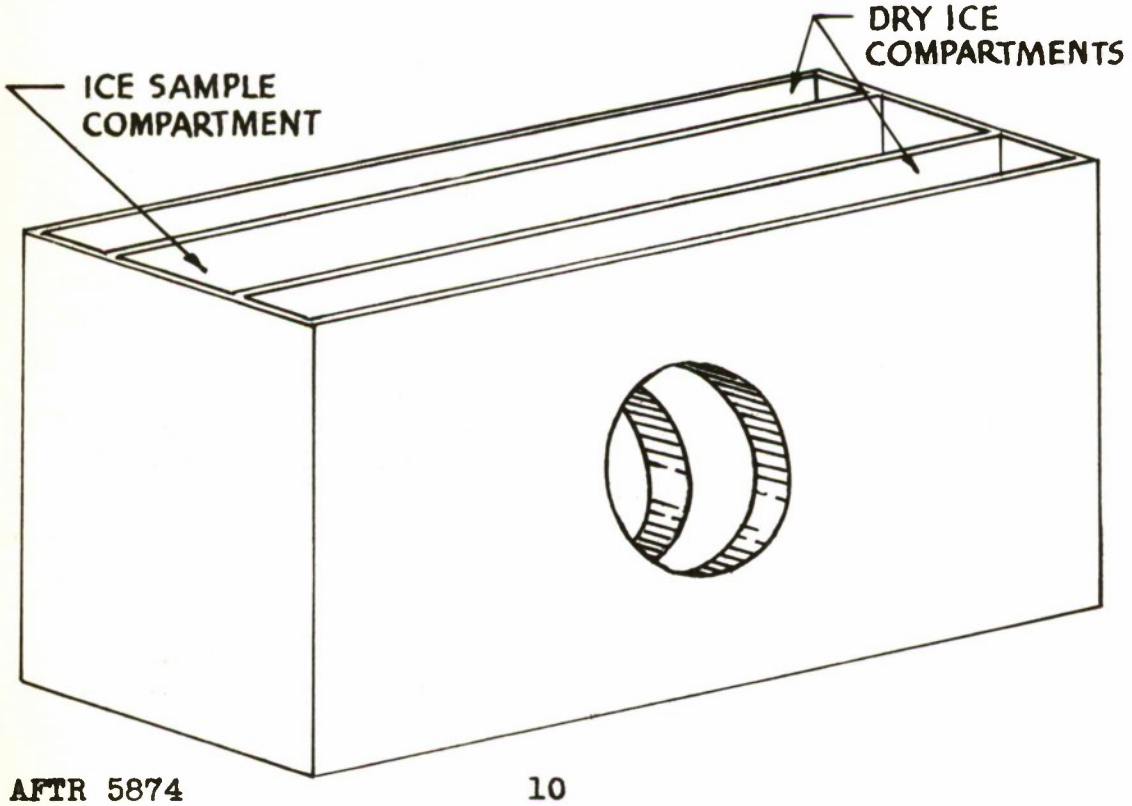
The normal reflectivity of clear ice is presented in Fig. 34 and is very similar to that of water. The reflectivity of rime type ice is somewhere between that of clear ice and snow, depending upon the structure. The reflectivity of snow is discussed in a following section under the heading of "Frost".

2. Transmission

Tests were made on natural and artificial ice formations. The former tests were made atop of Mt. Washington, New Hampshire at the facilities of the Aeronautical Ice Research Laboratory between

January 23 and February 12, 1951. During this period, the majority of the ice formations were of the rime type. Transmission tests with the portable filter spectrometer (Fig. 7) indicated that rime ice, as thin as 1/16", does not transmit any appreciable amount of infra-red radiation. Transmission data on glaze type ice are shown in Fig. 39. The filters used in connection with the portable spectrometer in these tests are shown in Figs. 40-42. There is considerable scatter in the data. The samples were collected on several days and the degree of ice clearness differed noticeably. The specimens also were not of uniform thickness. Similar tests made on rime type ice formed in the laboratory, yielded the similar results shown in Figs. 43 and 44. Here again the ice samples varied somewhat in the degree of clearness. The results indicate that ice is transparent only in the infra-red region near the visible. This is confirmed by the spectral transmission tests made in the laboratory.

The spectral normal transmission of various thicknesses of ice were determined on a Perkin Elmer Spectrometer. The ice was placed in a container illustrated in the sketch below, to prevent the ice from melting too rapidly. Difficulties encountered included, local melting due to absorption of some of the incident radiation and frost coatings. Frost has a low transmission and hence greatly affected the experimental results. The amount of dry ice in the compartments was adjusted to permit a slow rate of melting in order to prevent the accumulation of frost. The transmission of clear ice is compared to that of water in Fig. 45. The ice and water curves are very similar.



It is suggested that water transmission data be used to determine the transmission of clear ice because of the greater scatter in the ice data. Fig. 46 shows the transmission of a sample of rime ice. The transmission is small. Other samples of rime ice, depending upon the structure, will have somewhat differing transmission characteristics. The total transmission of clear ice for black body radiation (Ref. 7b) is presented in Fig. 37.

3. Absorption

Since the reflection and transmission of clear ice and water are so similar, the absorption will be very much the same. Indeed the absorption coefficient of ice and water are considered identical in the data of Ref. 18, presented in Fig. 32.

Frost

Frost and snow are formed by inverse sublimation, water vapor changing directly from the vapor into the solid state. Hence, the more available data on snow should be applicable to frost.

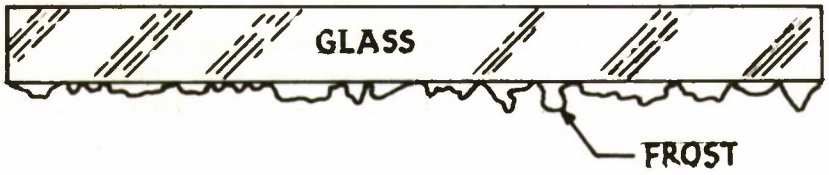
1. Reflection

The diffuse reflectivity of snow, as taken from Ref. 7b and attributed to E.O. Hulbert, is presented in Fig. 47. The values are relative, that for the wavelength region 0.4-0.8 microns, being arbitrarily taken as 100%. Ref. 11, lists this same data but uses a value of 40% reflectivity in the range between 0.4-0.8 microns. This value appears to be too low. The Handbook of Chemistry and Physics lists the diffuse reflectivity of snow for "incandescent" light as 93%. This absolute value appears more reasonable than 40% for 0.4-0.8 micron wavelength region.

2. Transmission

An attempt was made to gather frost under controlled surface and air dewpoint temperatures. A schematic sketch of the apparatus, used to form the frost and check the transmission thru it, is shown in Fig. 48. A glass square, upon which the frost formed, was placed in a hole in the oven door such that the inside surface was in contact with the controlled dewpoint air within the oven. Inside surface temperature of the glass square was controlled by means of a dry ice container in contact with the outer surface of the glass. When frost accumulated on the oven side of the glass, the glass square with the frost sample was removed from the oven door and placed on the sample holder of the portable spectrometer. The room temperature was maintained at

30°F in an attempt to prevent the frost from melting. A comparison of the transmission of the glass square, with and without the frost accumulation was used to measure the effect of frost. Frost was obtained under various contract specified combinations of of surface and dewpoint temperatures. However, a thin uniform frost accretion could not be obtained on the glass surface. The frost built up in the manner shown in the sketch below, a non-uniform coat with many minute voids.



In testing the frost sample on the portable spectrometer, the finite width beam impinged on sections of frost of varying thickness, including zero thickness. Also, in the short time interval required for measurement, the frost thickness decreased because of the absorption of heat. Because of the two foregoing reasons, the data are inconsistent as illustrated in the following table. The erratic data indicate that the transmission that does occur is mainly in the region near 1.0 micron in accord with the water transmission data.

RATIO OF TRANSMISSION OF FROST SAMPLES ON GLASS TO THAT OF GLASS ALONE

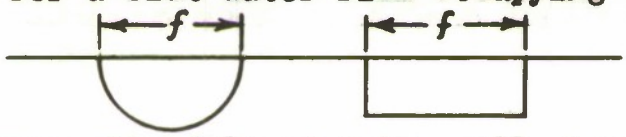
FROST THICKNESS	TRANSMISSION FOR RADIATION EMITTED FROM GLOBAR AT 2400°F AND PASSING THRU THE LISTED FILTERS		
	LUCITE + CORNING GLASS 7-69 (APPROX. TRANSMISSION BAND .7-1.1 MICRONS)	CORNING GLASS 7-57 (APPROX. TRANSMISSION BAND .75-2.7 MICRONS)	CORNING GLASS 7-85 (APPROX. TRANSMISSION BAND .8-1.1 MICRONS)
.01 inches	50 %	20 %	30 %
.05 inches	80 %	10 %	50 %

It was noticed during the spectral transmission of clear ice, that the formation of a thin layer of frost of approximately 1/64 inch thickness on the ice surface eliminated all transmission. For this reason it is believed that frost will absorb all of the incident energy between 1.0 and 10.0 microns that is not reflected from the front surface.

Fog

Experimental attempts to obtain Fog on a glass surface, with the same apparatus used for Frost, were not successful. The water droplets condensed on the surface non-uniformly. During the transfer of the specimen from the oven door to the sample holder of the portable spectrometer, and during the short time interval that the radiation from the globar impinged upon the sample, the fog formation deteriorated still further. Because of this condition and the consequent poor experimental data, an attempt was made to theoretically predict the absorption of radiation by fog based upon the available water film data.

The reflection or normal incident radiation from the surface of a hemi-spherical droplet was determined by a form of graphical integration (Appendix X). For an index or refraction, h, equal to 1.33, 6 % of the incident radiation will be reflected, compared to 2 % for a flat water film occupying the same projected area.



Since a very thin film of water will absorb all the radiation past 1.8 microns that is not reflected, the water droplet will absorb 94 % of the incident radiation compared to the 98 % of the flat water film.

If the droplet is closely surrounded by other droplets, a portion of the reflection will impinge on the neighboring droplets. More important than this reflection phenomena may be the droplet spacing. If the droplets cover but 70 % of the surface, then 30 % of the normal radiation will not impinge on the droplets at all. The amount absorbed may be calculated for a known droplet spacing.

SECTION III
PROPERTIES OF RADIATOR AND REFLECTOR MATERIALS

Radiators

1. General

The theoretical "black body" radiates the greatest amount of energy possible at any temperature. The dependence of the total

emissive power of a black body on its temperature is given by the Stefan-Boltzman law:

$$W = \sigma T^4 \tag{22}$$

W = total emissive power, BTU/hr, ft^2
σ = constant, 0.173×10^{-8} BTU/hr, $ft^2/{}^oR^4$
T = absolute temperature, ^oR

A theoretical grey body, defined as a body that will emit a constant proportion of the energy radiated by a black body at any wavelength, will radiate by definition:

$$W = \varepsilon \sigma T^4 \tag{23}$$

ε = emissivity

Grey bodies do not exist in practice; the emissivity of a body varies with wavelength. However, this concept is still used by defining ε for any body such that equation (23) will yield the actual value of the total emissive power. This value of ε will change with temperature because the proportion of radiant energy at any wavelength to the total radiant energy emitted is a function of temperature.

The spectral distribution of black body radiation can be evaluated from Plank's law:

$$\omega_\lambda = \frac{C_1}{\lambda^5} \frac{1}{\left[e^{\frac{C_2}{\lambda T}} - 1\right]} \tag{24}$$

$C_1 = 1.172 \times 10^8$ BTU/hr ft^2, $micron^4$
$C_2 = 25800$ microns/^oR
λ = microns
T = absolute temperature, ^oR
ω_λ = black body monochromatic emissive power, BTU/hr, ft^2/micron

The wavelength at which the intensity is a maximum is an inverse function of the absolute temperature. The relationship, known as Wien's Displacement Law, is:

$$\lambda_{max} = \frac{5193}{T} \tag{24a}$$

The spectral distribution of black body radiation between 0-15 microns for a temperature range of 1000-4000^{o}R, as determined from equation (23), is presented in Fig. 49.

A simplified formula for the natural convection coefficient from a long cylinder (Reference 27) is:

$$h_c = .27\left(\frac{\Delta t}{D}\right)^{.25} \qquad (24b)$$

h_c = coefficient of natural convection, BTU/hr, ft^2, °F

Δt = temperature difference between air and surface, °F

D = cylinder diameter, ft

A similar coefficient may be computed for radiation from a black body.

$$h_r = .173\frac{\left[\left(\frac{T}{100}\right)^4 - \left(\frac{T_s}{100}\right)^4\right]}{T - T_s} \qquad (24c)$$

h_r = coefficient of radiation, BTU/hr, ft^2 °F

T = surface temperature, °R

T_s = temperature of surroundings, °R

The ratio of convection to radiation emmision is then:

$$\frac{\text{convection}}{\text{radiation}} = \frac{h_c}{h_r}$$

A plot of this ratio is shown in Fig. 95 assuming the air and surroundings to be at 70°F. The comparative heat transfer by convection becomes small at high temperatures but is considerable at low temperatures. An open reflector surrounding a radiator will hinder heat transfer by natural convection, the amount of interference depending on the geometrical configuration. Neglecting this effect, approximately 70 % at 1000°F and 90 % at 2000°F of the total energy imput to a cylindrical radiator is available for radiation heat transfer. When a filter is used in combination with the source and reflector, so that the radiator is completely enclosed, the convection loss from the source will be negligible.

2. Ideal Radiator

Ref. 12 makes mention of experimental work on other than thermal type radiators. However, thermal type radiators are the only practical ones available to date. Ref. 14 reports on experimental work of thermal radiators emitting line or band type spectra in the infra-red. However, the emitted radiation is too small when compared to the power input. Hence, the usual thermal radiator, depending on elevated temperature and high emissivity, is the only one available at present.

The desirable spectral characteristics of an ideal infra-red thermal radiator are a very high emissivity in the wavelength region above 0.75 microns and a very low emissivity, below. For use in an airplane cockpit, elimination of visible radiation is desirable. The ideal radiator characteristic is approximated to an extent by certain materials. Materials that have a high emissivity in both the visible and near-infra-red may be operated at relatively low temperatures or at high temperatures in conjunction with the proper filter to more closely approximate the ideal. The former restriction can be best understood by glancing at the black body spectral distribution graph, Fig. 49. Below approximately 1000°F, the intensity of energy in the visible range is not sufficiently great for the eye to perceive. In addition, at low source temperatures, the absorption of radiant energy that passes thru the receiver surface is practically complete for the materials herein considered. As examples, the percent normal incident radiation from a black body source at a 1000°F which is absorbed by 1/4" thick specimens of glass and methyl methacrylate are 86 and 95 % respectively. A thin film of water, 0.04 inches thick will absorb approximately 98 %; clear ice absorption will be much the same. Fog will be somewhat lower due to incomplete coverage of the surface and slightly increased reflection. Rime ice or frost having the appearance of snow will absorb only 50 % because of the higher reflection. Unfortunately, operating below 1000°F limits the total emissive power available. The second alternative, use of a suitable filter, permits higher emissive power but at the expense of efficiency.

The Corning Glass filters 7-56, and 7-57, shown in Fig. 40, are the type that do not transmit much visible radiation but transmit infrared. However, these filters, being basically glass, decrease sharply in transmission at 2.7 microns and cut-off completely around 4.5 microns. Figs. 50-53 show the spectral distribution of black body radiation thru these filters. The ratio of the total energy transmitted thru the filters compared to the energy radiated from the black body source is presented in Fig. 54. The highest efficiency, at about 4000°R, is but 67 %. At lower temperatures the efficiency is considerably lower. On the same figure the ratio

of $(1460/T)^4$ is plotted. The intersection of this curve with the filter curves is the temperature at which the energy transmitted thru a filter source is equal to energy radiated from a non-filter source at 1000°F. This evidence indicates that the temperature range between 1000 and 1500°F should not be used since the transmitted filtered energy is less than that obtainable with a non-filtered source at 1000°F. Reradiation of a portion of the energy absorbed by the filter has not been considered.

For de-icing purposes it may be desired to use radiation which will not be absorbed by the transparent window and so be available for absorption by the ice directly. At the high temperature of 4000°R, 52 % of the normal incident energy from a black body will pass through a 1/4 inch thick piece of glass; only 37 % will pass through methyl methacrylate 1/4 inch thick. If it is necessary to remove visible radiation, by enclosing the source within a filter such as Corning Glass 7-57, 43 % and 25 % respectively, will reach the ice surface. These typical values were calculated from the data contained in this report. Of course, a portion of energy absorbed by the transparent panel will reach the ice surface by conduction.

It may be necessary to enclose the radiating source, even at operating temperatures below 1000°F, to prevent pilot burns or fire caused by inflammable objects accidently coming in contact with the radiator. A highly transmitting glass, such as reported in Ref. 8 may be desirable for such use. Fig. 55 shows the spectral transmission of two of the glasses reported on in this reference. The per cent total transmission of these glasses for black body radiation at various temperatures is presented in Fig. 56. At temperatures below approximately 1460°R, even these highly transmitting glasses, decrease the available radiant energy by 50 % . One possible advantage of enclosing the source will be the decreased convection losses.

3. Emissivity

The total normal emissivity of several materials were experimentally determined by a comparison method. The specimens were heated by inserting them in an opening in an oven wall. The radiation emitted in a normal direction was measured with a directional Eppley Thermopile Detector sensitive to approximately 9 microns. A schematic of the set-up is shown in Fig. 57. The emissivity at any temperature was obtained by comparing the emitted energy to that of a black body at that temperature. The black body values were obtained by measuring the radiant energy from a sample of asbestos and correcting for the variation from a black body. The asbestos emissivity was considered to vary linearly with temperature having a value of 0.93 at 100°F and 0.945 at 700°F. The results are presented in Figs. 58-60. The accuracy is estimated to be ±5 %. The total emissivity of Oxidized Cast Iron, Oxidized Cold Roll Steel and Porcelain Tile is high.

The spectral reflectivity of these and other materials were measured at the New York Naval Shipyard on the apparatus described in Ref. 7. The spectral emissivity determined from these measurements are presented in Fig. 61. The Porcelain Tile data unaccountably differs from that of the total emissivity test. The Globar (silicon carbide) is another material of high emissivity.

The emissivity of a Nernst Glower, a source sometimes used in infra-red work, is presented in Fig. 62. Glass, another possible source, appears to be a material of high emissivity. Black Carrara, a glass manufactured by Pittsburgh Plate Glass Company and which transmits infra-red radiation only, was heated to 1100° F to check whether it emits visible radiation; it does.

Ref. 31 reports that gold-black films have been prepared that have a specular reflectance (at 45 degree incidence) of less than 0.01 per cent in the region between 2 to 15 microns.

Reflectors

The total emissivity, (1- reflectivity), for various good reflector materials are shown in Figs. 63-69. The data were gathered experimentally by the same method as that for the good radiator materials. The spectral reflectivity for several of these materials as determined at the New York Naval Shipyard, is shown in Fig. 70. Additional spectral reflectivity data from the literature are contained in Fig. 71

SECTION IV
THEORETICAL REFLECTOR DESIGN CONSIDERATIONS

An ideal reflector is one which will reflect all of the energy impinging on it onto the receiving surface such that a uniform receiver absorption rate is obtained. This ideal reflector is easier to approach for certain receiver configurations than others. Of necessity, the source-reflector combination cannot be centrally located in an airplane cockpit. Usually the only space available is close to the bottom or top of the receiver. This makes the uniform distribution of the radiant energy much more difficult.

The parabola and the ellipse were the curved reflector surfaces mainly studied. The former reflects light in a parallel beam from a point source located at the focus; the latter collects the light and concentrates the energy onto a second focus. The parabolic shaped reflector with some variations appears to be the most promising.

Methods are presented in this section for determining the distribution of radiant energy upon a receiving surface from a:

A. Point source within a
   1. Paraboloid reflector
   2. Parabolic reflector (2 dimensional)
   3. Elliptic reflector (2 dimensional)
B. Finite size source within
   1. Infinitely long reflectors
   2. Reflectors of finite length

In addition, corrections for reflection from the receiver and blockage of reflected radiation by the source are also included. The reflector material is considered to have 100 % reflectivity, but correction for other values may be made. The semi-graphical method presented for finite diameter size sources may be used for curved reflector surfaces other than parabolic.

Point Source Reflectors

The cases considered in the following are for point sources within a reflector. This is approximated in practice when the ratio of the source size to the reflector is very small.

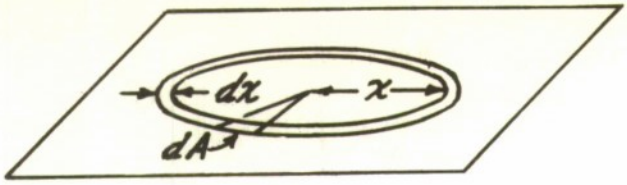
1. Paraboloid

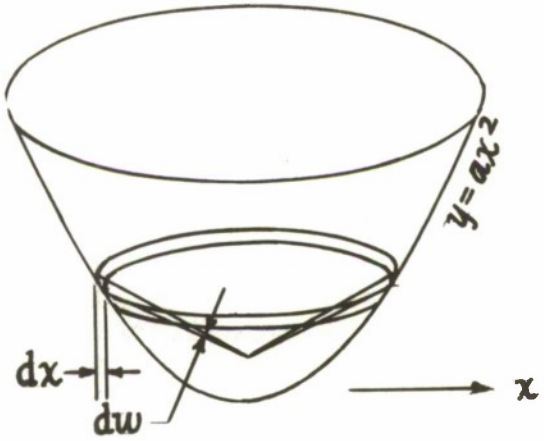
Consider a paraboloid reflector with a spherical point source at the focus. The solid angle, $d\omega$, subtended by the element, $2\pi X\,dX$, on the surface, is:

$$d\omega = \frac{16a^2(2\pi X\,dX)}{(1+4a^2X^2)^2} \qquad (25)$$

Symbols are identified in accompanying sketch. The solid angle subtended is directly proportional to the radiant energy received by the element of area. Since a paraboloid will reflect the radiant energy emitted at the focus parallel to the Y axis, the intensity of the reflected energy intercepted at a point on a horizontal plane above the paraboloid can be determined as function of the radial distance, X. In the following expression, $d\delta/dA$ represents the intensity of reflected energy at a point on a horizontal surface above a paraboloid.

$$\frac{d\omega}{2\pi X\,dX} = \frac{d\delta}{dA} = \frac{16a^2}{(1+4a^2X^2)^2} \qquad (26)$$



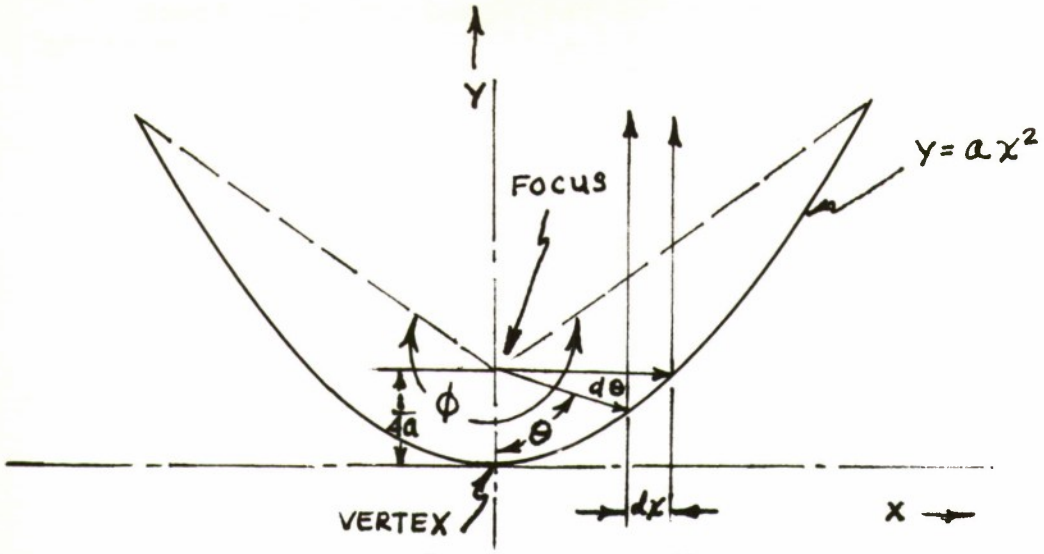


The derivation of this expression is presented in Appendix I. The intensity distribution, as given by equation 26, is presented in graphical form as a function of X, in Fig. 72. The variation is large, since $d\Phi/dA$ varies inversely as the fourth power of X. The total energy emitted from the point sphere is 4π steradians.

2. Parabola

Consider a two dimensional parabolic reflector with a point source at the focus. Any point on the parabola can be located by the following relationship between θ and X:

$$\theta = \cot^{-1}\left(\frac{1-4a^2x^2}{4ax}\right) \qquad (27)$$



The rays in the angle, $d\theta$, given off by the source at the focus are intercepted by a segment of the parabola surface and are all reflected parallel to the Y axis. This segment is subtended by a distance, dX, along the X axis, within which all the reflected rays remain. Since $d\theta$ is directly proportional to the radiant energy emitted, $d\theta/dX$ is a measure of the reflected intensity in the differential length, dX. Differentiating the previous equation:

$$\frac{d\theta}{dX} = \frac{4a}{(1+4a^2X^2)} \qquad (28)$$

Note the similarity between this expression and that for the paraboloid. The reflected energy intensity variation for several parabolas, as determined from equation (28), is shown in Fig. 73. The variation in intensity increases sharply with increase of the parabola constant, a. The total energy emitted from a point source in one plane is 2π radians. If the efficiency is defined as the ratio of the controlled energy (that intercepted by the reflector) to the total energy radiated from a point, then:

$$\text{Efficiency} = \frac{100\int_{\theta_1}^{\theta_2} d\theta}{2\pi} = 100\frac{\phi}{2\pi} \qquad (29)$$

Fig. 74 shows that the uniformity of the reflected energy decreases whereas the efficiency increases, for a given width parabolic reflector, as the parabola constant, a , becomes larger.

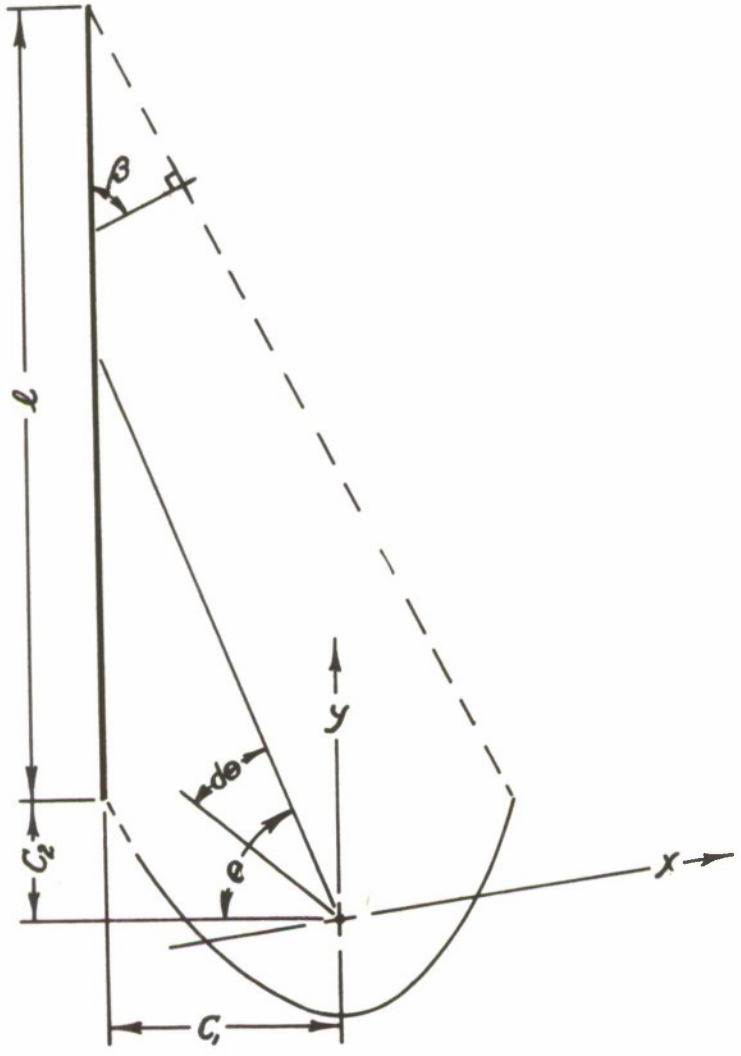
To determine the total energy intensity distribution incident on a line above a two dimensional parabolic reflector, as shown in the following sketch, equation (30) was derived (Appendix II).

The total energy includes both the reflected and the direct radiation components. The first term of the equation represents the reflected energy, the second is the direct radiation,

$$\frac{d\theta_T}{dy} = \frac{4a\cos\beta}{1+4a^2\left[\left(y-\frac{l}{2}-C_2\right)\cos\beta\right]^2} + \frac{C_1^2}{C_1^2+y^2} \qquad (30)$$

$\frac{d\theta_I}{dy}$ = total incident radiant energy intensity at a point, y, on the receiver, radians/inch

and the remainder of the symbols can be identified on the sketch.



A typical total energy distribution on a 12 inch line above a point source-parabolic reflector is shown in Fig. 75 as determined

from equation (30).

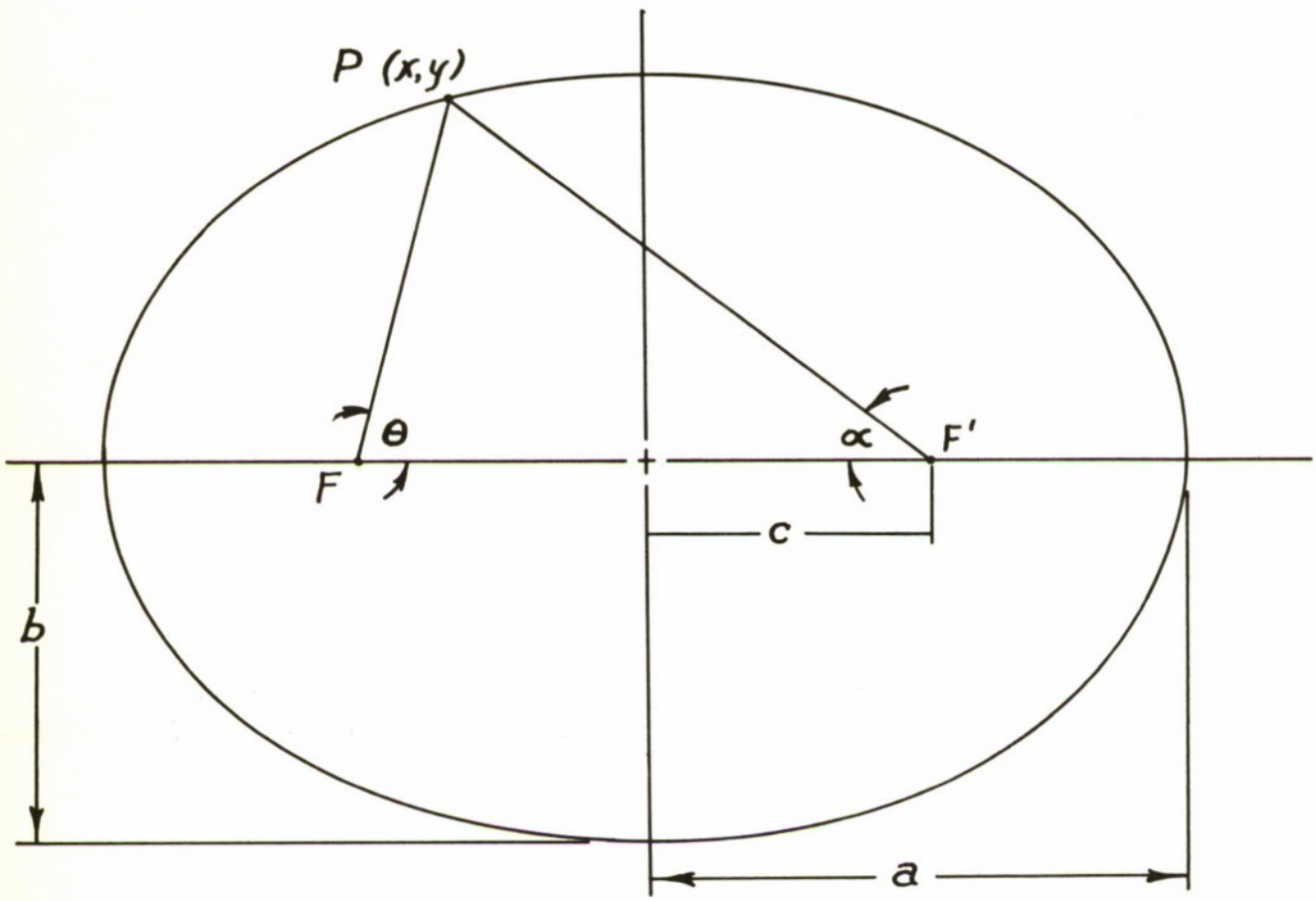
5. Ellipse

The distribution of the reflected energy intensity at the second focus of a two dimensional elliptic reflector, for a point source located at the other focus, is given by:

$$\frac{d\theta}{d\alpha} = - \frac{(-2ac\cos\alpha + a^2 + c^2)}{b^2 + \frac{4a^2c^2}{b^2}\sin^2\alpha} \qquad (31)$$

$\frac{d\theta}{d\alpha}$ = radiant energy intensity at angle α, radians/radian and the other symbols can be identified in accompanying sketch.

The derivation of this relationship is presented in Appendix III. Equation (31) has been used to determine the intensity distribution as a function of the angle α; the results are presented in Figs. 76-78. It can be seen that the greatest concentration of energy is in the region of $\alpha = 0$. This means that a small portion of an elliptical reflector may be used to control a good portion of the energy of the reflector. Unfortunately, it also indicates that a good portion of the energy from a finite size source will be reflected back onto the source.



Finite Diameter Infinite Length Source-Reflector Combinations

The cases considered in the following are for a finite diameter source but of infinite length, enclosed within an infinitely long reflector.

1. Parabola

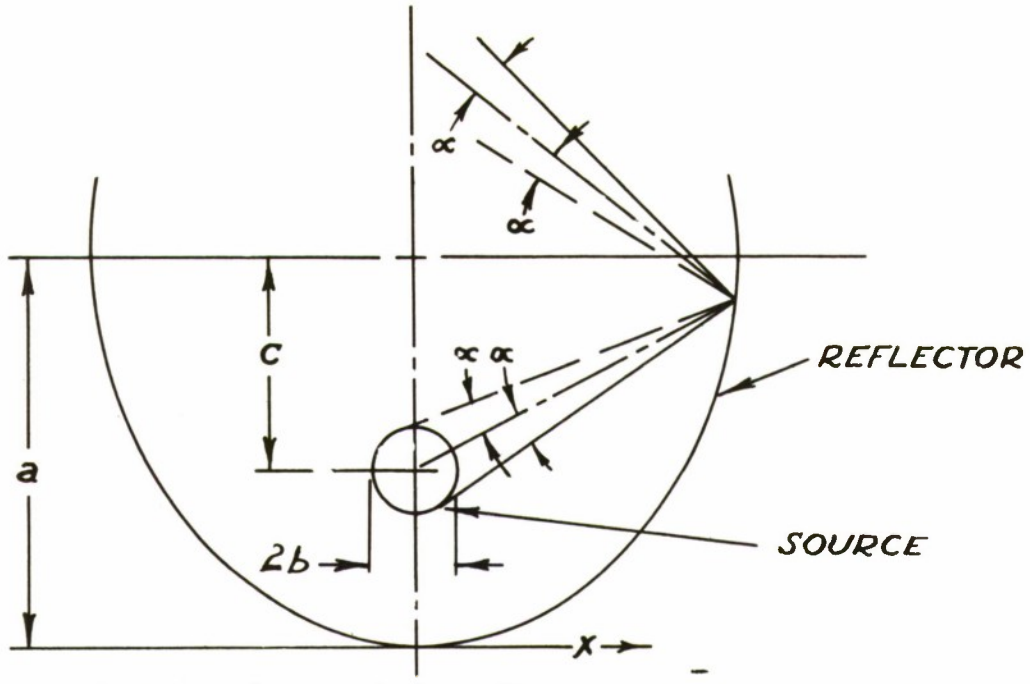
A semi-graphical method has been developed to determine the actual distribution of incident energy upon a receiver above a parabolic reflector containing a finite size source of infinite length. The method depends upon graphically determining, from any point on the receiver, the total projected angle thru which the source can be 'seen' directly or by reflection. Figs. 79-84 are design charts which greatly simplify the mechanics of this process. These charts can be used to determine the energy distribution on a plane or curved surface above any combination of reflector and source diameter. Their construction and use are explained in detail in Appendix IV. Special cases of multiple reflection from reflector and from receiver are also considered.

Using this semi-graphical method, the energy distribution impinging upon a 12 inch long receiving surface, from a 1/2 inch diameter source enclosed with an infinitely long parabolic reflector, has been determined and is presented in Fig. 85. The configuration selected for this illustrative case is typical of an anti-fogging installation in an airplane cockpit. The size of the reflector is necessarily small and it has to be located close to the base of the receiver. As can be seen, a ten to one variation in intensity exists between the top and the bottom of the plate for this case.

2. Ellipse and Other Curved Surfaces

The same method used for the parabolic reflector can be used in determining the distribution of energy upon a receiver above an elliptical reflector containing a finite size source of infinite length. The design charts can be constructed similarly to the method shown in Appendis IV. However, the equation for the askew lines in this case, is:

$$\alpha = \sin^{-1} \frac{b}{\left(a - \frac{cx}{a}\right)} \qquad (32)$$



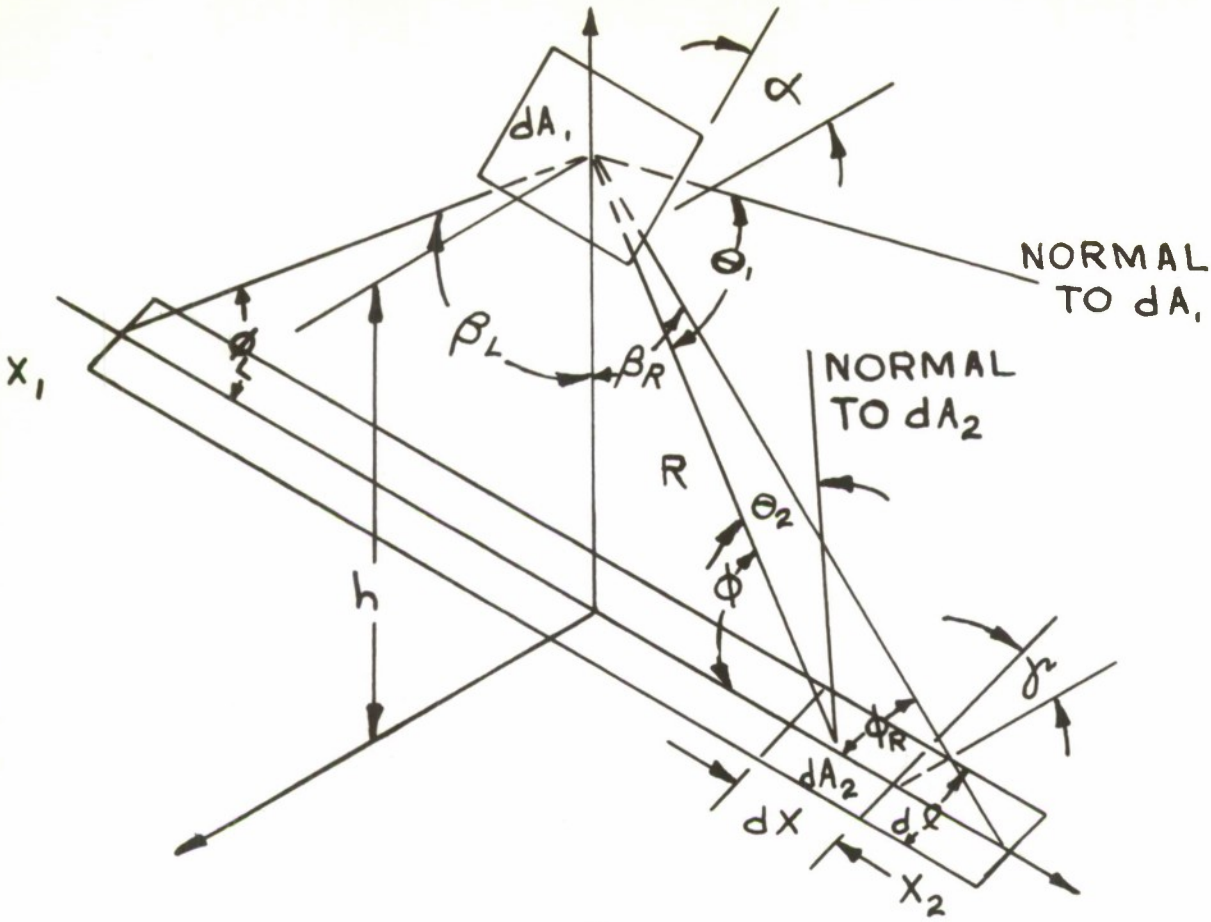
This method may be used for all curved surfaces. The askew lines of the design chart may be calculated from the equation of the curve or may be graphically determined by setting the angle of incidence equal to the angle of reflection at any point on the reflector (Appendix IV). The charts may be prepared by the latter method for sources other than cylindrically shaped ones.

Finite Diameter Finite Length Source-Reflector Combinations

A correction factor has been developed for use, with the method explained in the previous paragraphs and Appendix IV, in determining the radiant intensity distribution from a finite length source. To compute the energy distribution incident upon a receiver from a finite length and diameter source, determine the distribution by the semi-graphical method for the infinitely long source and multiply by the correction factor, as given in equation (33). The factor will vary for different points on the receiving surface. The development of this factor, its use and limitations, are presented in Appendix V.

$$F = \frac{1}{\pi}\left[\left(\frac{1}{2}\sin 2\beta_R + \beta_R\right) + \left(\frac{1}{2}\sin 2\beta_L + \beta_L\right)\right] \qquad (33)$$

The angles are defined in the sketch below. It is assumed that the source-reflector combination is relatively narrow.



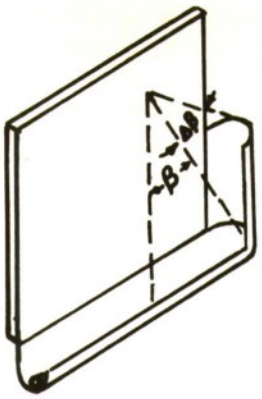
To facilitate tabulation of the factor, F, it has been broken down into two components, F_R and F_L. The latter accounts for the correction due to the finite length of the source to the left of the point on the receiver and the former accounts for the right hand side.

$$F = F_R + F_L \qquad (34)$$

The factors F_R and F_L may be individually determined from Fig. 86 and then added to determine F instead of solving equation (33). Note that in this figure, $F_{L\,or\,R}$ is plotted vs $(90-\beta_{L\,or\,R})$ or $\phi_{L\,or\,R}$.

End Reflectors

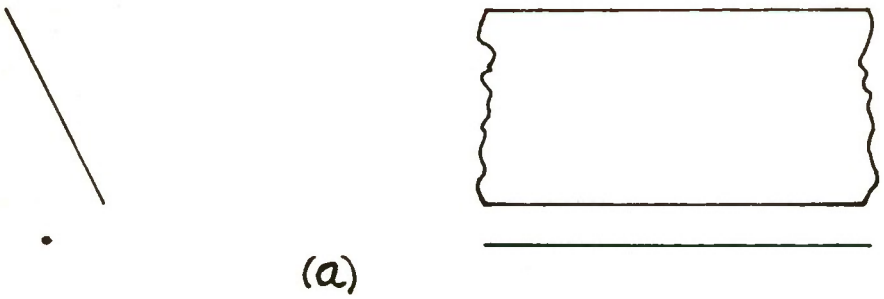
In some applications it may be possible to use end reflectors to increase and more evenly distribute the energy impinging on the receiver.

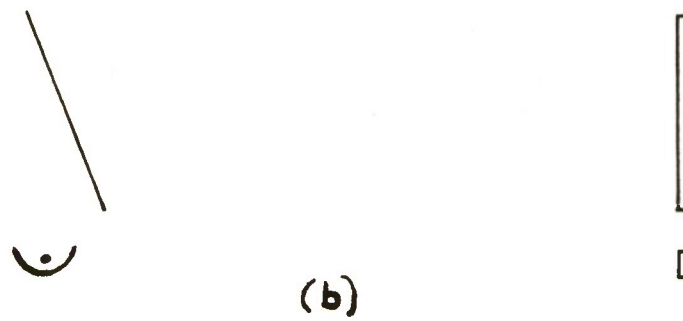


If the angle thru which a point on the surface can see the source is increased from β to $\beta+\Delta\beta$, the correction factor for finite length, F_R, will be increased as given by Fig. 86.

Receiver Reflection Correction

All of the energy impinging on a receiver such as glass or plexiglas will not penetrate the material because of reflection from the surface. The effect of reflection is difficult to analyze exactly. Two configuration simplifications were made in order to estimate the effect of the reflection phenomena. The two configuration simplifications are shown below; each one was analyzed separately.





In case (a), the reflector-source combination is considered to be a line of finite length in the source axis direction. In case (b), the reflector-source combination is considered to have finite width, but together with the receiver have but differential length in the direction of the source axis.

It was assumed that reflection from glas and plexiglas does not vary greatly with wavelength in the region between 0.75 and 10.0 microns. Furthermore, the complex Fresnel equation for reflection as a function of angle of incidence was closely approximated for these materials ($n = 1.48$) by the somewhat simpler equation:

$$r = .04 + .96\left(\frac{\theta}{\pi/2}\right)^8 \qquad (35)$$

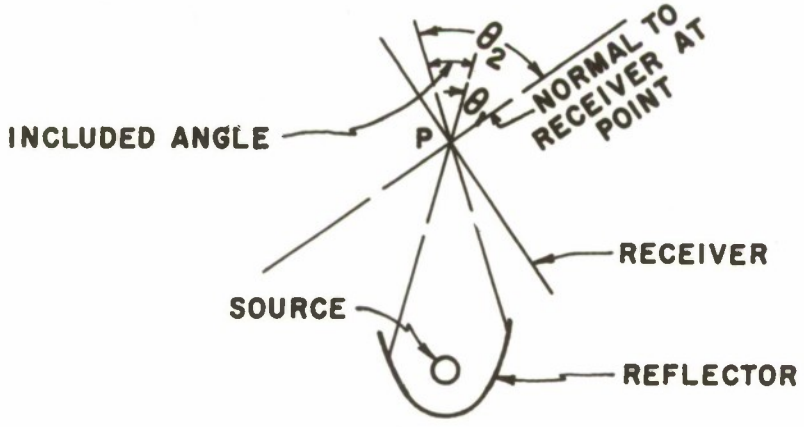
r = fraction reflected
θ = angle of incidence

A comparison of the above equation and that of Fresnel, for angles of incidence from 0 to 90° is shown in Fig. 87.

The analysis for case (a) is presented in Appendix VI, and that for case (b) in Appendix VII. The results are presented in graphical form in Figs. 88 and 89 respectively.

For case (a) the following procedure is to be used in conjunction with Fig. 88. Read the F' values corresponding to $\phi_{L \text{ or } R}$ from Fig. 88 and add the two. The result is the proportion of energy intensity impinging on the surface, as determined by the semi-graphical method of Appendix IV, which passes thru the surface of the receiver at that point. The correction for finite length is included in Fig. 88.

To use Fig. 89, determine the included angle of irradiation at any point on the receiver by use of the charts explained in Appendix IV. Read the values corresponding to the angles θ_1, and θ_2 and subtract the smaller from the larger. The value thus



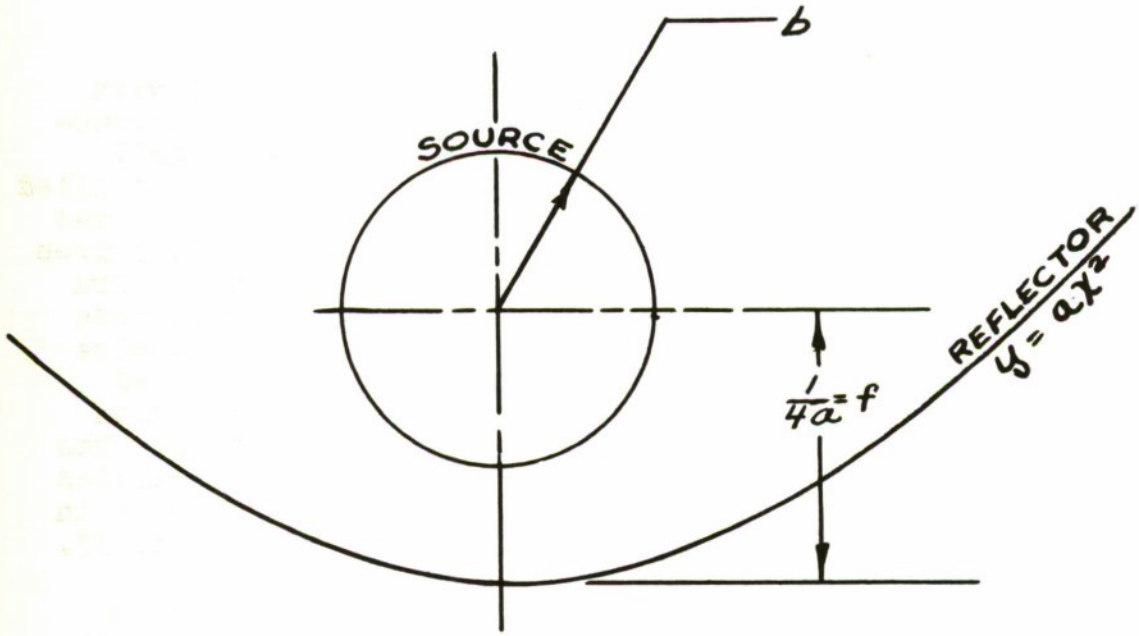
determined is the intensity of energy that passes thru the surface at that point, when an infinitely long radiator-reflector combination is assumed to radiate only in the plane of the point on the receiver. The energy intensity is expressed in terms of W, which is defined by equation (23). The correction factor for finite length (Appendix IV) is then applied.

In most applications, simplification (a) will yield results closer to the actual. This method may be made more exact by dividing the reflector width into two or more strips and determining separate correction factors for each.

Blockage

Blockage is herein defined as the fraction of the total radiation from a radiator within a reflector which is reflected back onto the radiator. The reflector is considered made out of material of 100% reflectivity. An expression for blockage for a source within a parabolic reflector is derived in Appendix VIII. Blockage is a complex function of the ratio of source diameter to focus length of the parabolic reflector. The exact expression is:

$$\text{Blockage} = \frac{1}{\pi}\left[\pi - \frac{f}{b}\sqrt{\sqrt{\left(\frac{b}{f}\right)^2+\frac{1}{4}}+\frac{1}{2}} - \tan^{-1}\frac{f}{b}\sqrt{\sqrt{\left(\frac{b}{f}\right)^2+\frac{1}{4}}+\frac{1}{2}} - \cot^{-1}\frac{b}{f} + \tan\left(\cot^{-1}\frac{b}{f}\right)\right] \quad (36)$$



Using this equation, the blockage has been determined for the complete range of b/f, 0.0 to 1.0. The results are presented in Fig. 91. After plotting the results, it was noticed that the curve can be represented by a straight line with but slight error. Hence, the blockage may be expressed by the following simple relationship:

$$\text{Blockage} = 0.307 \left(\frac{b}{f}\right) \qquad (37)$$

For a perfect reflector and black body radiator, the blocked out energy is returned in entirety to the radiator. There is no energy loss due to blockage. As an example, consider two identical radiators surrounded by different reflectors. Let the blockage of one combination be 5 % and that of the other 20 %; i.e., 5 and 20 % respectively of the energies emitted by the source are returned to the source. Only 95 and 80 % respectively of the total source radiation will be available to receivers above the reflectors. It is for this reason that high blockage is undesirable. If the sources are maintained at the same temperature, less power input will be required by the source with the higher blockage, since it emits less net radiation.

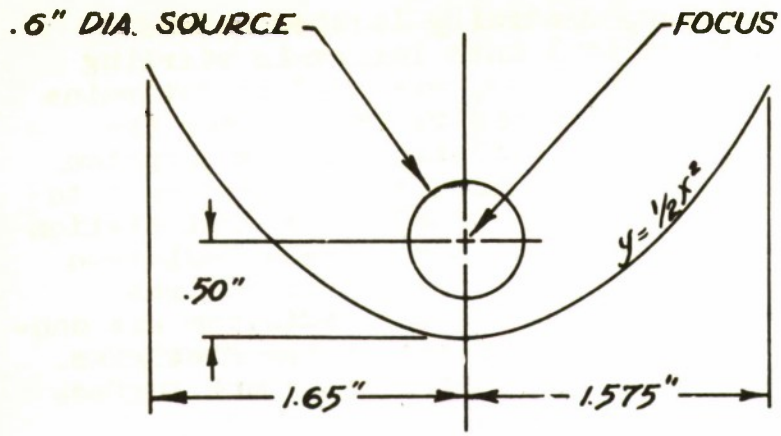
SECTION V
EXPERIMENTAL REFLECTOR TESTS

A set of tests were made to check some of the theoretical reflector relationships of the previous section.

Apparatus

A 12 inch Plexiglas square, 1/4" thick, was spotted with surface thermocouples as shown in Fig. 92. The surface thermocouples were applied in the following manner. Two very small holes, large enough to permit #30 gage wire through, were drilled from the back to front surface, 3/8" apart. A thin scratch was then made on the front surface between the two holes. Bare iron thermocouple wire was pushed thru one hole and constantan thru the other. A fine, butt-type, solder connection was then made between the two holes on the front side and the connected wire was fitted into the scratch on the Plexiglas surface, pulled taut and cemented in place with solvent. The wire insulation and tape shown in Fig. 92 are all behind the back surface. The thermocouples were attached to a Brown Recorder. The Plexiglas square was mounted in a frame and could be oriented properly in regard to the source-reflector combination as shown in Fig. 93.

G.E. Calrod, 0.6 inch diameter cylindrical heaters were the sources used. A thermocouple was welded to the source surface. The power input to the source was controlled by a variac and measured by means of a voltmeter and ammeter. The parabolic reflectors were made of Alclad. The reflector cross-section varied somewhat along the length because costly dies were not used in their manufacture. The nominal cross-section is shown below.

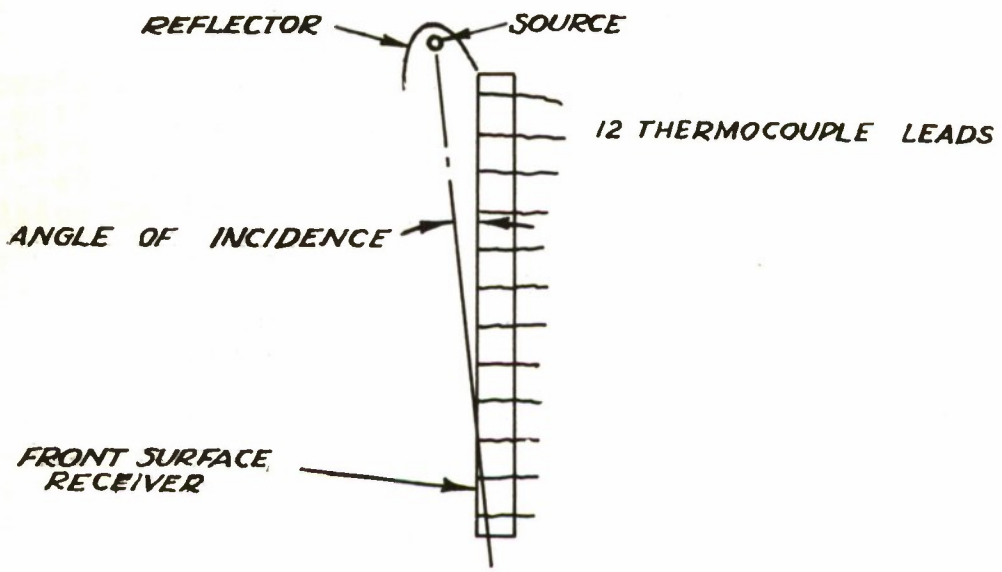


Procedure

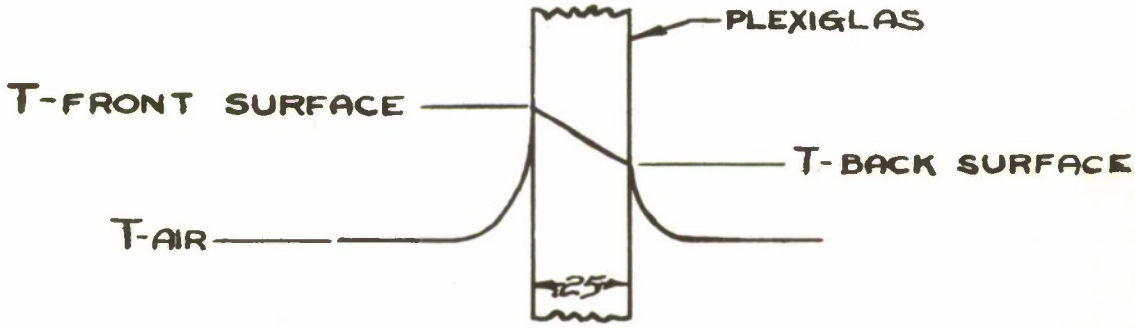
Tests were made at relatively low source temperatures, 605-735°F, to prevent excessive temperatures on the Plexiglas receiver. At this source temperature, all of the impinging energy, which is not reflected from the receiver front surface is absorbed in a relatively thin layer near the Plexiglas front surface (Fig. 33).

The majority of the tests were made with one source-reflector combination and several with two. In all but one of the former tests the source-reflector combination was located above instead of below the receiver in an attempt to eliminate the effect of convection heat transfer. In the latter tests, a combination was located symmetrically at both the top and bottom.

The reflector was located such that the edge of the smaller side was in contact with the receiver edge.



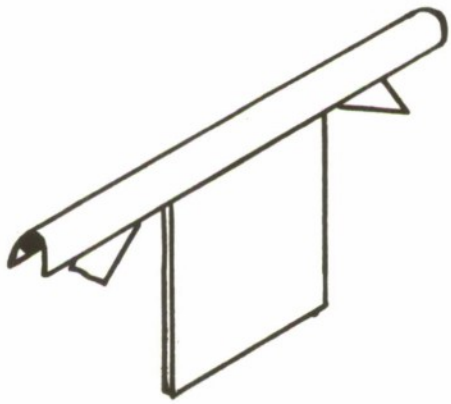
A row of 12 thermocouples, centrally located on the front surface of the receiver, at 1 inch intervals starting 1/2 inch from the base of the receiver, was used to determine the vertical variation in radiation distribution. For the purpose of determining the maximum variation, the absorption at each station was considered to be directly proportional to the temperature difference between the surface at that station and the surrounding air. The value of the average radiation absorption intensity along this row of thermocouples was determined in the following manner. All the radiation was considered to be absorbed at the front surface of the Plexiglas. The heat energy flows along two paths; from the front surface



by natural convection and radiation to the surroundings and from the front surface thru the plexiglas by conduction and then to the surroundings by natural convection and radiation. Any heat transfer thru the plexiglas other than normal to the surfaces was neglected. This set of calculations is illustrated in Appendix IX for a typical run. Also shown in this appendix, are the mechanics for utilizing the theoretical relationships of the previous section to predict the radiant energy absorption distribution.

Results

A table of the test results and predicted values are shown in Fig. 94. In the first three runs, the angle of inclination of the source-reflector combination to the receiver was varied. In the fourth run, the effective length of the source was decreased by locating end reflectors as shown. This opened possible



sources of error but the end reflectors were used because Calrod heaters of this type are not obtainable in 12 inch lengths. In run 5 the source temperature was elevated to the maximum value without exceeding 200°F local Plexiglas surface temperature. The reflector-source combination was located at the bottom of the receiver in run 6 for purposes of estimating the additional effect of convection heat transfer from the source. The data were used in predicting the results for the two combination case of run 7.

A comparison of predicted and experimental results for maximum temperature variation and average radiation absorption rate shows good agreement, considering the test apparatus and possible sources of error.

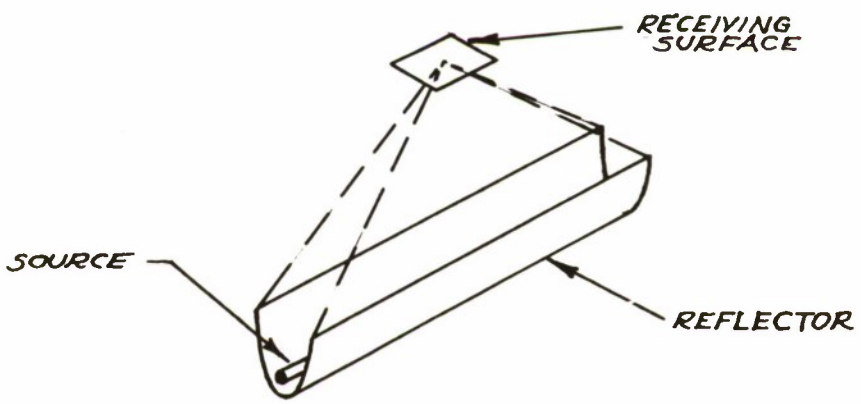
SECTION VI
MAGNITUDE OF RADIATION INTERCEPTION

Estimates of radiation interception by an infra-red receiver are presented herein. A comparison is also made, between the method of this report and that in the literature, to compute incident radiation intensity.

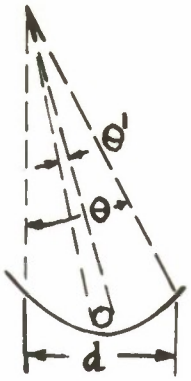
Comparison of Method Herein to Compute Incident Radiation Intensity with that in Literature

As a check of the semi-graphical method to compute incident radiation intensity, presented herein, two special cases treated in Ref. 26, were analyzed. The results by both methods, are identical. The method of Ref. 26 is limited to the cases wherein the receiving and radiating surfaces are parallel or perpendicular. The method presented herein may be used for these two limits and for all angles in between.

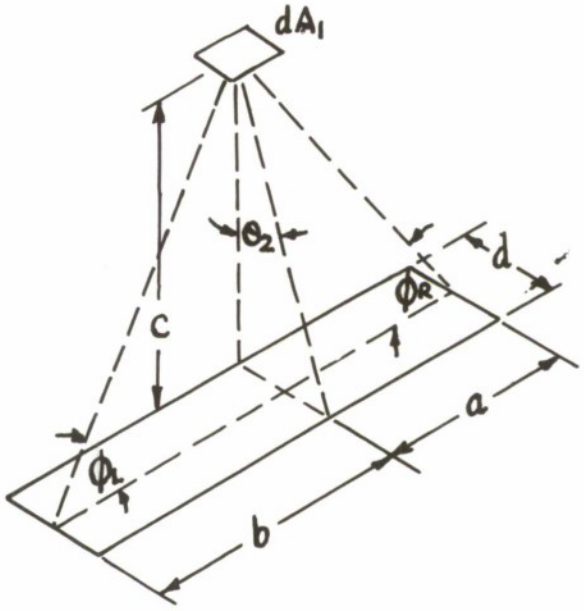
Consider the configuration shown in the following sketch.



The effect of the reflector is to permit the receiver to "see" the source through a larger angle, θ.



It effectively makes the source width equal to the distance, d. Hence, sketch (a) may be replaced by the following sketch.



Let $a = 3''$, $b = 9''$, $c = 6''$, $d = 3''$

From equations 2 and 3, Appendix IV, for an infinitely long radiator, the radiation intensity on dA_1, is:

$$\frac{Q}{dA_1} = \frac{W}{2} \sin\theta \Big]_0^{\theta_2}$$

$$= \frac{W}{2} \frac{3}{\sqrt{(6)^2+(3)^2}} = .223W$$

To correct for finite source length, find φ_E and φ_L.

$$\varphi_E = \tan^{-1} \frac{\sqrt{(1.5)^2+(6)^2}}{3} = \tan^{-1} 2.06 = 64.1^\circ$$

$$\varphi_L = \tan^{-1} \frac{\sqrt{(1.5)^2+(6)^2}}{6} = \tan^{-1} 1.03 = 45.8^\circ$$

From Fig. 86, for the above values of φ:

$F_E = .270$
$F_L = .403$

Corrected for finite length the intensity on dA_1 is:

$$\frac{Q}{dA_1} = (F_E + F_L).223W$$
$$= .15\,W \quad BTU/hr, ft^2$$

If dA_1 is perpendicular to the radiator instead of parallel, then:

$$\theta_1 = \operatorname{sen}^{-1} \frac{6}{\sqrt{(3)^2+(6)^2}} \qquad \text{and } \theta_2 = \frac{\pi}{2}$$

$$\frac{Q}{dA_1} = \frac{W}{2}\left[1.0 - .895\right] = .052W$$

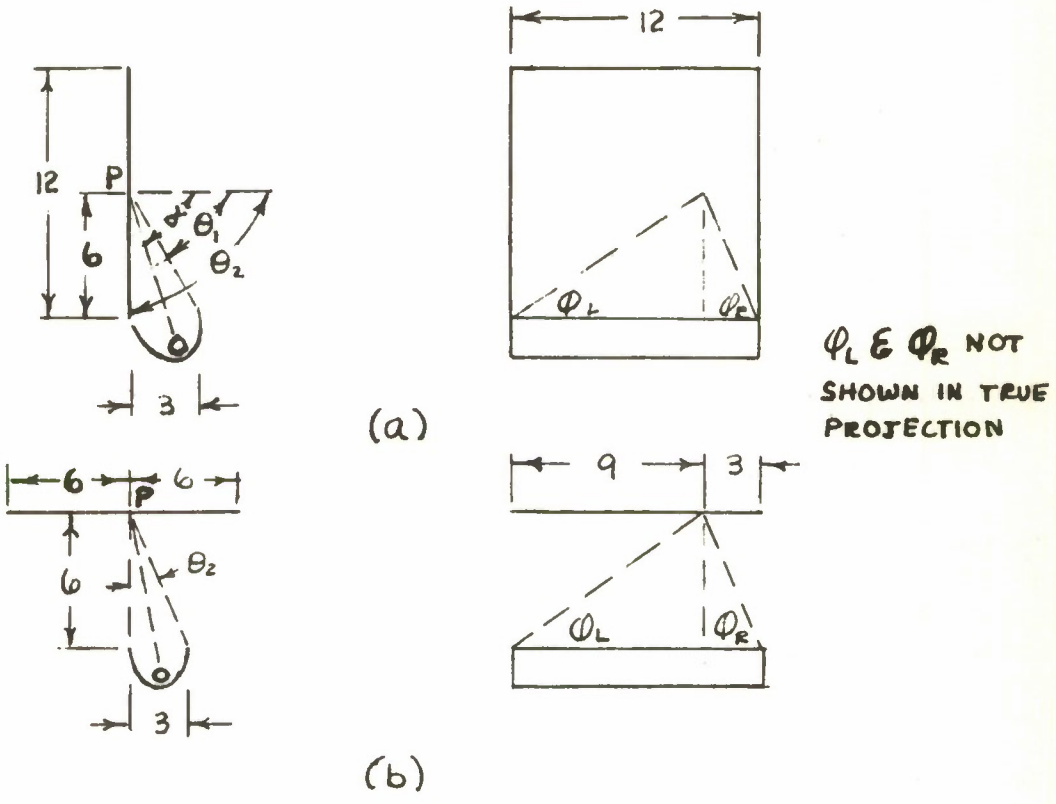
F_E and F_L are the same as in the previous case, and so corrected for finite length:

$$\frac{Q}{dA_1} = .673 \times .052W = .035 \; BTU/hr, ft^2$$

The value obtained from the charts of Ref. 26 for both cases are the same as calculated above.

Estimate of Absorption Rate Magnitudes

Consider the two extreme configurations shown below. Each receiver has a mean point, P, 6 inches from an edge of the reflector and 3 inches from one end. Consider the reflectors designed such that the point, P, can 'see' the source through an angle that includes the entire reflector width, an optimum condition. The conditions are the same as that of the two examples in the previous paragraph. It is desired to include the effect of reflection and hence, the correction factors, F', from Fig. 88 shall be used instead of F.



For case (a), $\alpha = \text{cotan}^{-1} \frac{1.5}{6} = 76°$, and for case (b), $\alpha = \tan^{-1} \frac{1.5}{6} = 14°$. As in the previous example, $\Phi_R = 64.1°$ and $\Phi_L = 45.8°$. The values of F' obtained from Fig. 88 for these conditions are listed below.

case (a)	$F_R' = .19$	$F_L' = .305$
case (b)	$F_R' = .255$	$F_L' = .385$

Corrected for finite length and reflection, the intensity of radiation passing thru the surface at point P, is:

case (a) $\frac{Q'}{dA_1} = (F_e' + F_L') \frac{Q}{dA_1} = .495 \times .223 W = .11 W$

case (b) $\frac{Q'}{dA_1} = (F_e' + F_L') \frac{Q}{dA_1} = .64 \times .223 W = .143 W$

Consider possible values of W. Assume an effective source emissivity of 0.9, a feasible value. The effective emissivity includes the slight absorption effect of the reflector.

$$W = .173 \times .9 \left(\frac{T}{100}\right)^4$$

T	W
1460°R	7529 BTU/hr, ft^2
4000°R	424,192 BTU/hr, ft^2

The maximum intensity for a source temperature of 1000°F is therefore:

$$\frac{Q'}{dA_1} = .143 \times 7529 = 1080 \text{ BTU/hr ft}^2$$

The more practical configuration would yield:

$$\frac{Q'}{dA_1} = .11 \times 7529 = 830 \text{ BTU/hr, ft}^2$$

By use of end reflectors these values might be increased 10-20 %. Plexiglas, 1/4 inch thick, will absorb 99% of the 1000 °F radiation passing thru the surface. Hence these intensities also represent the intensity of the absorbed energy for a plexiglas receiver. Therefore, for a configuration not better than that of the illustration, a 1000 BTU/hr, ft^2 maximum absorption rate can be obtained at the mean point with a source at 1000°F by radiation transfer only. (Loss due to convection may be estimated from Fig. 95.) Using two source-reflector combinations, one located near the bottom of the receiver and the other near the top, approximately twice the radiation intensity can be obtained. This type of configuration also permits more uniformity of energy distribution.

Consider the source to be at 4000°R and to be enclosed within Corning Glass 7-55 filter. The total transmission at 4000°R (Fig. 54) is 66%. The maximum intensity of radiant energy entering the receiver, is:

$$\frac{Q'}{dA_1} = .143 \times .66 \times 424,192 = 40,100 \text{ BTU/hr, ft}^2$$

It was mentioned in a previous section that 37 % of the radiant energy from a black body source enclosed within Filter 7-57 will pass thru Plexiglas. Hence 63 % less approximately 4 % for

reflection, or 59%, will be absorbed. Therefore, the absorbed energy, is:

$$\text{Absorbed energy} = 40{,}100 \times .59 = 25{,}600 \text{ BTU/hr, ft}^2$$

This amount is many times greater than will be required for defrosting or de-icing purposes. Heat transfer by radiation and convection to the receiver from the filter has not been considered.

Theoretical attempts were made with the configuration (a) to obtain a uniform distribution of radiant energy along the vertical centerline of the receiver. Various parabolas and angles of inclination were tried. Uniformity of distribution could be increased but at the expense of lowering the average intensity. For an intensity variation of 9/1, an average intensity radiation entering the receiver of .04w(BTU/hr, ft^2) was obtained. Before being corrected for finite length and reflection, the variation and average intensities were 4/1 and .055w respectively. In this latter correction, the angle α (Fig. 88) was considered a constant and equal to the inclination of the receiver from the parabola centerline. Experimental results indicate that due to conduction the actual surface temperature variation will be 2/3 this value. The sizable advantage of using two source-reflector combinations, one located at the bottom and the other at the top of the receiver is shown by the following theoretical results. Corrected for finite length and reflection, the maximum variation for this case is 1.7/1 and the average intensity is .08w.

A 12" radius semi-circular canopy with a reflector-source combination located symmetrically at each end was studied. Without correcting for finite length, the intensity variation, in the design calculations, could be reduced considerably below 2/1. In this particular case each reflector source combination had an orientation such that one combination could contribute either direct or reflected radiation to the entire canopy. This presents the problem of radiation interception by the pilot.

In general, it has been more difficult to uniformly irradiate a flat plate receiver than a gently curved receiver.



Parabolic Reflector Variations

Various modifications of the parabolic type reflector were tried theoretically in an attempt to obtain more uniform distributions and higher average intensities. The source was moved above, below and to the side of the parabola focus. Sources other than cylindrically shaped were tried. All these attempts were unsuccessful. Blackening portions of the reflector and decreasing the emissivity of portions of the source helped decrease the intensity variation but at the expense of the average intensity. Combinations of parabolic and elliptical reflectors were tried as well as combinations of different parabolas. The latter combination showed some promise. Two narrow reflectors were substituted instead of one wide one with poor results. A rotating source-reflector combination which could be directed at the portion of the receiver furthest away for longer time intervals than nearby portions would help but would greatly complicate mechanical design.

BIBLIOGRAPHY

1. Anon. Summary of Research on Materials for Infra-red Transmitting Windows, Period 1 Dec. 1946 to 14 May 1948. Institutum Divi Thomae Foundation, Cincinnati, Ohio. May 1948.

2. Barnes, R. B. and Bonner, L. G. The Christiansen Filter Effect in the Infra-red. Phys. Rev. Volume 49, No. 10. 1936. pp. 732-740.

3. Blau, H. H. Glass to Transmit Infra-red Radiations. Ohio State University Research Foundation, Project 314, Report 10, Columbus, Ohio. October 31, 1949.

4. Boelter, L.M.K., Bromberg, R. and Gier, J. T. An Investigation of Aircraft Heaters, XV-The Emissivity of Several Materials. NACA ARR No. 4A21. University of California. Jan. 1944.

5. Clark, Walter. Photography by Infra-red. Second Edition. John Wiley & Sons Publishing Co., New York. 1947. pp. 131-174, 410-440.

6. Denning, L.S. Spectral Reflectance and Transmittance Measurements on Infra-red Materials for U. S. Air Force Contractor NE 020730. Report transmitted with letter dated Dec. 3, 1951 from Commander New York Naval Shipyard to Chief of the Bureau of Ships (816) (8). Project Order Number 67964/50.

7. Derksen, W. and Monahan, T. I. Report on a Reflectometer for Measuring Diffuse Reflectance in the Infra-red Region. N. Y. Naval Shipyard, Material Lab. Lab. Project 5046, Part 9. October 1950.

7b. Dorsey, Ernst N. Properties of Ordinary Water-Substance. Reinhold Publishing Corp., N. Y., 1940.

8. Dunkle, R. V., Gier, J. T., Test, A. J., Possner, L. and Bevans, J. T. The Spectral and Total Transmissivity Characteristics of Plexiglas in the Wavelength Range Between 0.4 and 15 Microns. University of California Dept. of Engineering. Report No. 8. California, March 23, 1949.

9. Fischer, Heinz. The Influence of the Spectral Transmission of Optics and the Atmosphere on the Sensitivity of Infra-red Detectors. United States Air Force Technical Report No. F-TR-2104-ND. United States Air Force, Air Materiel Command. October 1946.

10. Fleischer, R. The Energy of Infra-red Radiation Between 8 and 14μ of a Radiator of Low Temperature at Different Heights and Lateral Positions from the Radiator. Deutsche Forschungsanstalt Fur Segeflung, E. V. Darmstadt. April 1941. ZWB/FB/1435. (German)

11. Fowle, F. E. Smithsonian Physical Tables. Smithsonian Institution, Washington, D.C. 1934. pp. 313-325, 347-396.

12. Fry, W. J., Van Velzer, H. L. and Dunn, F. Infra-red Sources. University of Illinois, Electrical Engineering Research Laboratory, Report No. IR4, Urbana, Illinois. December 24, 1949.

13. Gier, J. T., Possner, L., Test, A. J., and Others. The Absolute Spectral Reflectivity of Certain Pigments and Metals in the Wavelength Range Between 2 and 15 Microns. University of California, Dept. of Engineering, Report No. 7, California. February 1949.

14. Ginsburg, N. Final Engineering Report on Infra-red Sources for Use as Radiators in the Spectrum Band from 1 Micron to 25 Microns (July 1, 1946 - June 30, 1948). Syracuse University, Physics Report No. 102-7, N. Y. October 1948.

15. Hahner, C. H. The Preparation and Measurements of Glasses for Transmitting Infra-red Energy. U. S. Dept. of Commerce, National Bureau of Standards. Reference No. 9.2. Oct. 27, 1948.

16. Hamilton, D. C., Sibbitt, W. L. and Hawkins, G. A. Radiant Interchange Configuration Factors. A.S.M.E. Advance Copy of Paper No. 50-A-104 to be Presented at Annual Meeting Nov. 26-Dec. 1, New York, New York.

17. Hamilton, J. Arthur. Near Infra-red Filters. Corps of Engineers, Fort Belvoir, Report No. 968, Va. February 1946.

18. Hasinger, S. H. and Larsen, L. V. Infra-red Heating for Anti-Icing, De-Icing, and Defrosting of Aircraft Transparent Areas. United States Air Force Technical Report No. 6113. United States Air Force, Air Materiel Command. March 1950.

19. Hesthal, C. E. and Schaffer, W. H. Interference Type Filters for Use in the Infra-red - April 1 to June 1, 1949. Ohio State University, Research Foundation Report No. IER-16. June 1949.

20. Hottel, H.C. Radiant Heat Transmission. Mech. Eng. Vol. 52, No. 7. July 1930, Section One. pp. 699-704.

21. Hottel, H. C. Radiant Heat Transmission Between Surfaces Separated by Non-Absorbing Media. Trans. of the A.S.M.E. Fuels and Steam Power. Vol 53, No. 14. pp. 265-273.

22. Jones, R. C. A New Classification System for Radiation Detectors. Jour. Opt. Soc. Am. Volume 39, No. 5. May 1949. pp. 327-43.

23. Jones, R. C. Factors of Merit for Radiation Detectors. Jour. Opt. Soc. Am. Volume 39, No. 5. May 1949. pp. 344-56.

24. Jones, R. C. The Ultimate Sensitivity of Radiation Detectors. Jour. Opt. Soc. Am. Volume 37. 1949. p. 879.

25. Land, E. H. Final Report on Improved Infra-red Transmitting Filters (Covering Period from Aug. 21, 1943 to Oct. 31, 1945). Polaroid Corporation, Cambridge, Mass. Oct. 1945.

26. Mackey, C. O., Wright Jr., L.T., Clark, R.E. and Gray, N.R. Radiant Heating and Cooling, Part I. Cornell University Experiment Station. Bulletin No. 32. Ithaca, N. Y. Aug. 1943.

27. McAdams, W. H. Heat Transmission. Second Edition. McGraw-Hill Book Co., New York. 1942.

28. Miller, R. A. and Black, L.V. Transmission of Radiant Energy Through Glass. Heating, Piping & Air Conditioning. Volume 4, No. 10. February 1932. pp. 143-148.

29. Morey, George W. Properties of Glass. Reinhold Publishing Corporation, New York. 1947. pp. 365-440.

30. Mouzon, J. C. and Dyer, C. A. Low Temperature Radiation Pyrometry in Industry. Jour. Opt. Soc. Am. Volume 39, No. 3. March 1949. pp. 203-10.

31. Naiman, Mark L. and Carlson, George R. Cannonball I. Illinois Institute of Technology, Armour Research Foundation, Project No. 90-656D. Report No. 20, Chicago. June 1950.

32. National Research Council. International Critical Tables. Volume 5. McGraw-Hill, New York. 1929. pp. 237-270.

33. Parmelee, George W. The Transmission of Solar Radiation Through Flat Glass Under Summer Conditions. Heating, Piping & Air Conditioning. Volume 17, No. 10. October-November 1945. pp. 562-576.

34. Pfund, A. H. Infra-red Filters of Controllable Transmission. Phys. Rev. Volume 36, No. 1. July 1930. pp. 71-76.

35. Pfund, A. H. Rayleigh's Law of Scattering in the Infra-red. Jour. Opt. Soc. Am. Volume 24, No. 6. June 1934. pp. 143-46.

36. Pfund, A. H. and Silverman, S. The Absorption of Infra-red Radiation by Small Particles. Phys. Rev. Volume 39, No. 1. Jan. 1, 1932. pp. 64-71.

37. Pfund, A. H. The Dispersion and Transmission of Methyl Methacrylate Polymer. Jour. Opt. Soc. Am. Volume 29, No. 7. July 1939. pp. 291-293.

38. Plummer, J. H. Transmissions of Powder Films to the Infra-red Spectrum. Jour. Opt. Soc. Am. Volume 26, No. 12. Dec. 1936. pp. 434-438.

39. Schorr, W. E. An Experimental Investigation of Defrosting of Transparent Panels by Means of Infra-red Radiation. Report No. ERF-10. Republic Aviation Corporation, Farmingdale, N. Y.

40. Seemann, H. H. An Analytical Investigation of Radiant Defrosting of Transparent Panels. Unpublished Research Department Report, Republic Aviation Corporation, Farmingdale, N. Y.

41. Strong, J. Procedures in Experimental Physics. Prentice-Hall, Inc., New York. 1938. pp. 305-395.

42. Sutherland, G. B. B. M. Recent Developments in the Technique of Infra-Red Spectroscopy with Some Applications to Scientific and Industrial Problems. Instr. Prac. March 1949. p. 190.

43. Williams, V. Z. Infra-Red Instrumentation and Techniques. The Review of Scientific Instruments. Volume 19, No. 3. March 1948. pp. 135-178.

44. Williamson, D. E. Infra-Red Interference Filter Used in Calibration. Jour. Opt. Soc. Am. Volume 39, No. 7. July 1949. pp. 613-614.

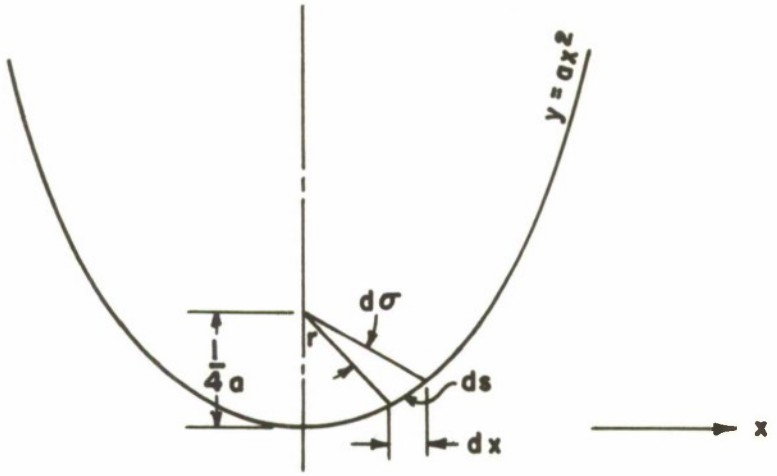
45. Wolf. Transmittance of Infra-red Rays Through Round Glass Windows. Zeiss, Carl, Jena. (German)

46. Wood, Robert W. Physical Optics. Third Edition. The Macmillan Co., New York. 1942.

APPENDIX I

REFLECTED ENERGY DISTRIBUTION FROM PARABOLOID

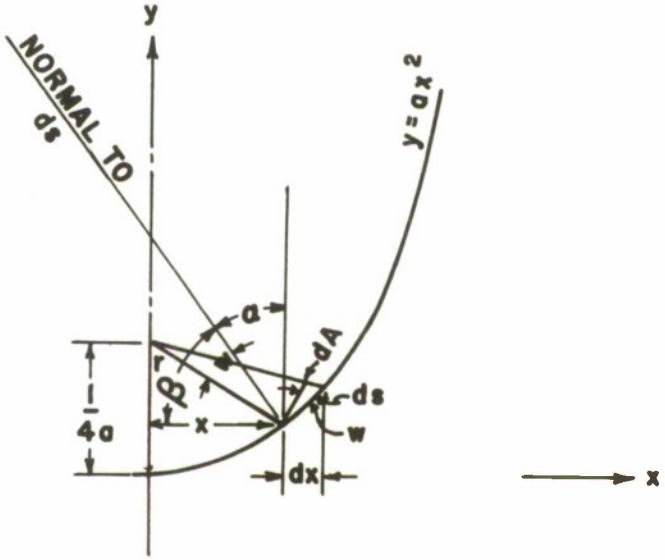
Consider the paraboloid cross section shown below.



The amount of energy reflected in the annular element, **dx**, is proportional to the solid angle, **dw**, intercepted by the annular arc **ds**. The projection of the solid angle, **dw**, is represented by $d\sigma$.

$$dw = \frac{dA}{r^2} \qquad (1)$$

dA is the projection of **ds** onto a sphere.



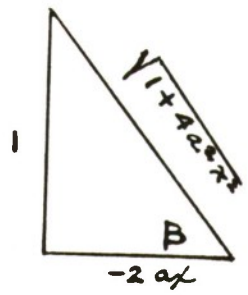
$$dA = 2\pi x\, ds \cos\gamma \qquad (2)$$

$\alpha = \gamma$ (PROPERTY OF PARABOLOID)

$\beta + \alpha = \frac{\pi}{2}$ $\qquad$ $\beta + \gamma = \frac{\pi}{2}$

$\cos\gamma = \sin\beta$

$\beta = -\frac{1}{dy/dx} = \tan^{-1}\left(-\frac{1}{2}ax\right)$



$$\cos\gamma = \frac{1}{\sqrt{1+4a^2x^2}} \qquad (3)$$

$$ds = dx\sqrt{1+\left(\frac{dy}{dx}\right)^2} = dx\sqrt{1+4a^2x^2} \qquad (4)$$

$$r^2 = x^2 + \left(\frac{1}{4a} - y\right)^2 = x^2 + \left(\frac{1}{4a} - ax^2\right)^2 = \left(\frac{1}{4a}\right)^2\left(1+4a^2x^2\right)^2 \qquad (5)$$

SUBSTITUTING INTO (1)

$$dw = \frac{2\pi x\, dx\sqrt{1+4a^2x^2}}{\left(\frac{1}{4a}\right)^2\left(1+4a^2x^2\right)^2\sqrt{1+4a^2x^2}}$$

$$= \frac{32\pi a^2 x\, dx}{\left(1+4a^2x^2\right)^2} \qquad (6)$$

Equation (6) represents the solid angle intercepted by an annular element, $d\delta$, of the paraboloid. To determine the intensity of reflected energy, $d\delta/dA$ at a point on a horizontal surface above the paraboloid, divide by $2\pi x dx$:

$$\frac{d\delta}{dA} = \frac{16a^2}{(1+4a^2x^2)^2} \qquad (7)$$

APPENDIX II

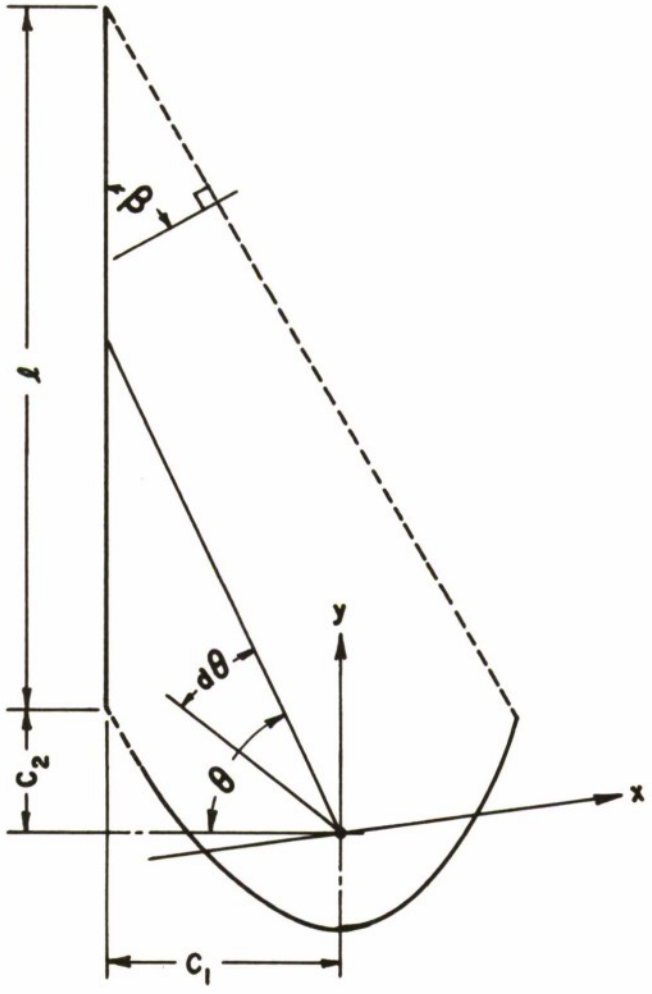
TOTAL RADIATION INTENSITY DISTRIBUTION ON LINE ABOVE A PARABOLIC REFLECTOR CONTAINING A POINT SOURCE

A point on a line above a reflector may receive both reflected and direct energy. The distribution of reflected energy from a parabolic reflector containing a point source was derived previously, and is:

$$\frac{d\theta_R}{dx} = \frac{4a}{1+4a^2x^2} \tag{1}$$

Since the energy is impinging on the receiving surface at an angle other than normal, the intensity on the receiving surface is:

$$\frac{d\theta_R}{dy} \quad \frac{4a\cos\beta}{1+4a^2x^2} \tag{2}$$



The angle, θ, made by a line from the focus of the parabola and intersecting the receiver plane, is

$$\theta = \tan^{-1}\left(\frac{y}{c_1}\right) \tag{3}$$

Hence, $\frac{d\theta_D}{dy}$, which represents the direct radiation intensity component, is:

$$\frac{d\theta_D}{dy} = \frac{c_1^2}{c_1^2 + y^2} \tag{4}$$

The total radiation intensity impinging on the receiver at any point is then:

$$\frac{d\theta_T}{dy} = \frac{4a\cos\beta}{1+4a^2x^2} + \frac{c_1^2}{c_1^2+y^2} \tag{5}$$

Now, x, may be expressed as:

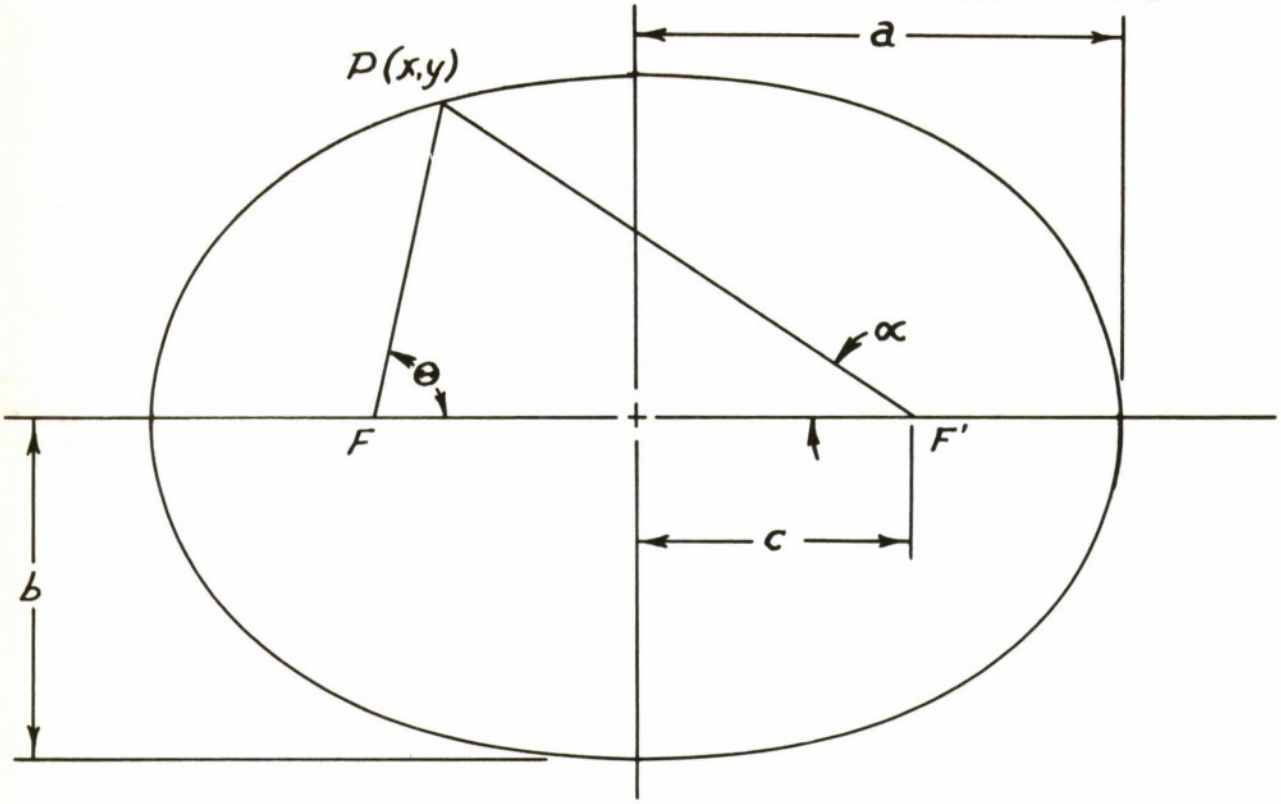
$$x = \mp\left[y - \left(\frac{\ell}{2} + c_2\right)\right]\cos\beta \tag{6}$$

and hence may be eliminated from Eq. (5), yielding the final form:

$$\frac{d\theta_T}{d\ell} = \frac{d\theta_T}{dy} = \frac{4a\cos\beta}{1+4a^2\left[\left(y-\frac{\ell}{2}-c_2\right)\cos\beta\right]^2} + \frac{c_1^2}{c_1^2+y^2} \tag{7}$$

APPENDIX III

DISTRIBUTION OF THE REFLECTED ENERGY INTENSITY AT ONE OF THE FOCI OF A TWO DIMENSIONAL ELLIPTICAL REFLECTOR FOR A POINT SOURCE LOCATED AT THE OTHER FOCUS



F= POINT SOURCE

$$\frac{x^2}{a^2} + \frac{y^2}{b^2} = 1 \qquad (1)$$

$$a^2 = b^2 + c^2 \qquad (2)$$

$$\tan\theta = \frac{y}{c-x} \qquad (3)$$

$$\tan\alpha = \frac{y}{c+x} \qquad (4)$$

$$\tan\theta = \frac{(c+x)\tan\alpha}{c-x} \qquad (5)$$

$$\frac{x^2}{a^2} + \frac{y^2}{b^2} = 1$$

$$x^2b^2 + y^2a^2 = a^2b^2$$

$$x^2b^2 + (c+x)^2 \tan^2\alpha (a)^2 = a^2b^2$$

$$x^2b^2 + a^2c^2\tan^2\alpha + 2a^2cx\tan^2\alpha + a^2x^2\tan^2\alpha - a^2b^2 = 0$$

$$x^2(b^2 + a^2\tan^2\alpha) + x(2a^2c\tan^2\alpha) + a^2(c^2\tan^2\alpha - b^2) = 0$$

$$x = \frac{-2a^2c\tan^2\alpha \pm \sqrt{4a^4c^2\tan^4\alpha - 4a^2(c^2\tan^2\alpha - b^2)(b^2 + a^2\tan^2\alpha)}}{2(b^2 + a^2\tan^2\alpha)}$$

$$x = \frac{-a^2c\tan^2\alpha \pm a\sqrt{a^2b^2\tan^2\alpha - c^2b^2\tan^2\alpha + b^4}}{b^2 + a^2\tan^2\alpha}$$

$$x = \frac{-a^2c\tan^2\alpha \pm ab\sqrt{(a^2 - c^2)\tan^2\alpha + b^2}}{b^2 + a^2\tan^2\alpha}$$

$$x = \frac{-a^2c\tan^2\alpha \pm ab^2\sqrt{\tan^2\alpha + 1}}{b^2 + a^2\tan^2\alpha}$$

$$x = \frac{-a^2c\tan^2\alpha \pm ab^2\sec\alpha}{b^2 + a^2\tan^2\alpha}$$

$$\tan\theta = \frac{(c+\gamma)\tan\alpha}{c-\gamma}$$

$$= \frac{\left[c + \frac{(-a^2c\tan^2\alpha \pm ab^2\sec\alpha)}{b^2+a^2\tan^2\alpha}\right]\tan\alpha}{c - \frac{(-a^2c\tan^2\alpha \pm ab^2\sec\alpha)}{b^2+a^2\tan^2\alpha}}$$

$$\therefore \tan\theta = \frac{(b^2c \pm ab^2\sec\alpha)\tan\alpha}{b^2c + 2a^2c\tan^2\alpha \mp ab^2\sec\alpha}$$

DIFFERENTIATING WITH RESPECT TO α

$$\sec^2\theta\frac{d\theta}{d\alpha} = \frac{(b^2c + 2a^2c\tan^2\alpha \mp ab^2\sec\alpha)\left[b^2c\sec^2\alpha \pm ab^2(\sec\alpha\tan^2\alpha + \sec^3\alpha)\right]}{(b^2c + 2a^2c\tan^2\alpha \mp ab^2\sec\alpha)^2}$$

$$- \frac{(b^2c \pm ab^2\sec\alpha)\tan\alpha(4a^2c\tan\alpha\sec^2\alpha \mp ab^2\sec\alpha\tan\alpha)}{(b^2c + 2a^2c\tan^2\alpha \mp ab^2\sec\alpha)^2}$$

BUT $\sec^2\theta = 1+\tan^2\theta = 1 + \frac{(b^2c \pm ab^2\sec\alpha)^2\tan^2\alpha}{(b^2c + 2a^2c\tan^2\alpha \mp ab^2\sec\alpha)^2}$

$$= \frac{(b^2c + 2a^2c\tan^2\alpha \mp ab^2\sec\alpha)^2 + (b^2c \pm ab^2\sec\alpha)^2\tan^2\alpha}{(b^2c + 2a^2c\tan^2\alpha \mp ab^2\sec\alpha)^2}$$

(6) $$\frac{d\theta}{d\alpha} = \frac{(b^2c \pm 2a^2c\tan^2\alpha \mp ab^2\sec\alpha)\left[b^2c\sec^2\alpha \pm ab^2(\sec\alpha\tan^2\alpha + \sec^3\alpha)\right]}{(b^2c + 2a^2c\tan^2\alpha \mp ab^2\sec\alpha)^2 + (b^2c \pm ab^2\sec\alpha)^2\tan^2\alpha}$$

$$- \frac{(b^2c \pm ab^2\sec\alpha)\tan\alpha(4a^2c\tan\alpha\sec^2\alpha \mp ab^2\sec\alpha\tan\alpha)}{(b^2c + 2a^2c\tan^2\alpha \mp ab^2\sec\alpha)^2 + (b^2c \pm ab^2\sec\alpha)^2\tan^2\alpha}$$

Using the top signs of the plus or minus, minus or plus signs, gives the values of $d\Theta/d\alpha$ for angles of α from 0° to 90°. The lower signs give the values of $d\Theta/d\alpha$ for angles of α from 90° to 180° even though angles of α from 0 to 90° are used. This is because of the sign condition where tangent and secant are both positive in the 1st quadrant and negative in the second quadrant. If we respect these signs, then the top signs of the equation will hold throughout.

For example: If we respect the top signs and α varies from 0° to 90°, then the signs are:

$$\frac{d\Theta}{d\alpha} = \frac{[(+)+(+)-(+)][(+)+(+)+(+)]-[(+)+(+)][+][(+)-(+)]}{[(+)+(+)-(+)]^2+[(+)+(+)]^2[(+)]^2} \quad (7a)$$

If we respect the top signs and α varies from 90° to 180°, then the signs are:

$$\frac{d\Theta}{d\alpha} = \frac{[(+)+(+)-(-)][(+)+(-)+(-)]-[(+)+(-)][-][(-)-(+)]}{[(+)+(+)-(-)]^2+[(+)+(-)]^2[(+)]^2} \quad (7b)$$

If we respect the lower signs and α varies from 0° to 90°, then the signs are:

$$\frac{d\Theta}{d\alpha} = \frac{[(+)+(+)+(+)][(+)-(+)-(+)]-[(+)-(+)][+][(+)+(+)]}{[(+)+(+)+(+)]^2+[(+)-(+)]^2[(+)]^2} \quad (7c)$$

Equations (7b) and (7c) give the same numerical answer and sign.

It was noticed, after plotting the distribution determined from expression (6) on polar coordinate paper, that the distributions formed ellipses of minor axis $2b = 2$ (see Fig. 78). This permitted finding a simpler expression for the distribution as shown in the following.

For the case where $\alpha = 0$, then $\tan\alpha = 0$, $\sec\alpha = 1$

$$\frac{d\Theta}{d\alpha} = \frac{(b^2c \mp ab^2)(b^2c \pm ab^2)}{(b^2c \mp ab^2)^2} = \frac{c-a}{c+a} \text{ or } \frac{c+a}{c-a}$$

Assuming these two values to be the extremities of another ellipse of major axis a_1 and minor axis b_1 and allowing $b_1 = 1$, we can find a_1, b_1, and c_1 in terms of a, b, and c in the following way:

$$a_1 = \frac{1}{2}\left(\frac{c-a}{c+a} + \frac{c+a}{c-a}\right) = \frac{c^2+a^2}{c^2-a^2} = -\left(\frac{a^2+c^2}{b^2}\right) \text{ since } b^2 = a^2-c^2$$

and

$$c_1 = \sqrt{a_1^2 - b_1^2} = \sqrt{\left(\frac{-a^2+c^2}{b^2}\right)-1} = \sqrt{\frac{a^4+2a^2c^2+c^4-b^4}{b^4}}$$

but

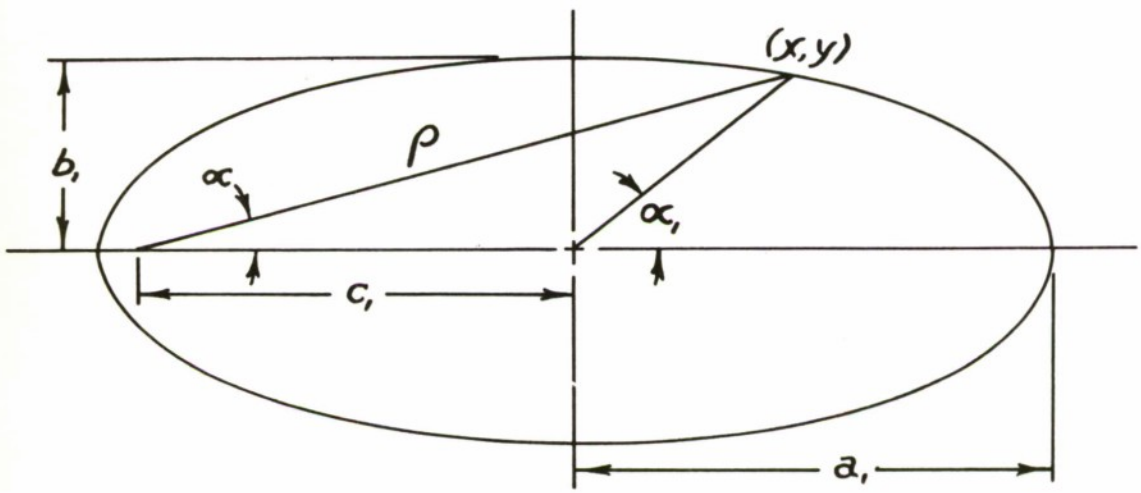
$$b^4 = (a^2-c^2)^2 = a^4-2a^2c^2+c^4$$

so that

$$c_1 = \sqrt{\frac{4a^2c^2}{b^4}} = \pm \frac{2ac}{b^2}$$

These values of a_1, b_1, and c_1 are used in the ellipse in the following.

Suppose ρ the radius vector from one of the foci represented the value $\frac{d\theta}{d\alpha}$



$$\frac{x_1^2}{a_1^2} + \frac{y_1^2}{b_1^2} = 1 \tag{8}$$

$$y_1 = \rho_1 \sin\alpha_1 = \rho \sin\alpha \tag{9}$$

so that $y_1^2 = \rho_1^2 \sin^2\alpha_1 = \rho^2 \sin^2\alpha$

$$x_1 = \rho\cos\alpha - c_1 \tag{10}$$

so that $x_1^2 = \rho^2\cos^2\alpha + c_1^2 - 2\rho c_1 \cos\alpha$

$$b_1^2 x_1^2 + a_1^2 y_1^2 - a_1^2 b_1^2 = 0$$

$$b_1^2(\rho^2\cos^2\alpha + c_1^2 - 2\rho c_1\cos\alpha) + a_1^2\rho^2\sin^2\alpha - a_1^2 b_1^2 = 0$$

$$\rho^2(b_1^2\cos^2\alpha + a_1^2\sin^2\alpha) - \rho(2b_1^2 c_1\cos\alpha) - b_1^4 = 0$$

$$\rho = \frac{2b_1^2 c_1\cos\alpha \pm \sqrt{4b_1^4 c_1^2\cos^2\alpha + 4b_1^4(b_1^2\cos^2\alpha + a_1^2\sin^2\alpha)}}{2(b_1^2\cos^2\alpha + a_1^2\sin^2\alpha)}$$

$$\rho = \frac{2b_1^2 c_1\cos\alpha \pm \sqrt{4b_1^4 c_1^2\cos^2\alpha + 4b_1^4(b_1^2 + c_1^2\sin^2\alpha)}}{2(b_1^2\cos^2\alpha + a_1^2\sin^2\alpha)}$$

$$\rho = \frac{b_1^2 c_1\cos\alpha \pm b_1^2\sqrt{b_1^2 + c_1^2}}{b_1^2 + c_1^2\sin^2\alpha}$$

$$\therefore \rho = \frac{b_1^2 c_1\cos\alpha \pm a_1 b_1^2}{b_1^2 + c_1^2\sin^2\alpha}$$

$$\rho = \frac{b_1^2 C_1 \cos\alpha \pm a_1 b_1^2}{b_1^2 + C_1^2 \sin^2\alpha}$$

If we substitute the values of a, b, and c, for a', b' and c' as found previously, we arrive at a new expression for ρ.

$$b_1^2 = b_1 = 1$$

$$a_1 = -\left(\frac{a^2+c^2}{b^2}\right)$$

$$C_1 = \pm \frac{2ac}{b^2}$$

so

$$\rho = \frac{\pm \frac{2ac}{b^2}\cos\alpha \mp \frac{a^2+c^2}{b^2}}{1 + \frac{4a^2c^2}{b^4}\sin^2\alpha} = \frac{\pm 2ac\cos\alpha \mp (a^2+c^2)}{b^2 + \frac{4a^2c^2}{b^2}\sin^2\alpha}$$

Using the top signs and remembering that c is a negative number:

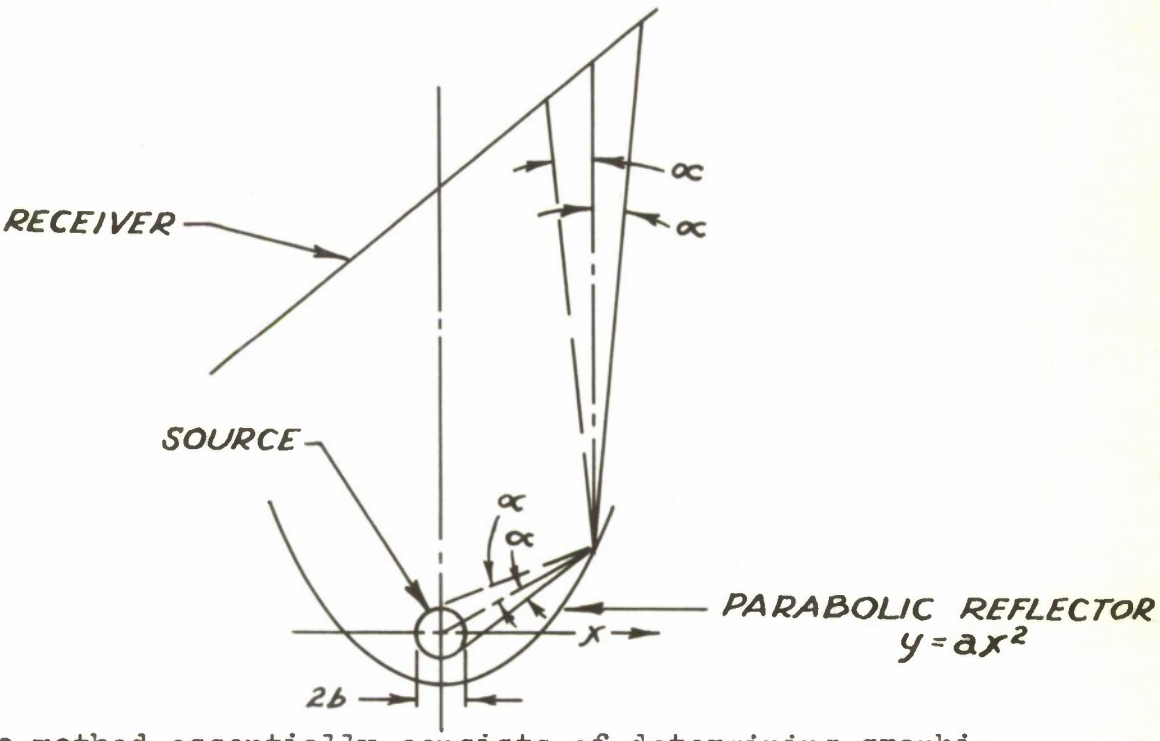
$$\rho = \frac{+2ac\cos\alpha - (a^2+c^2)}{b^2 + \frac{4a^2c^2}{b^2}\sin^2\alpha} \qquad 0° < \alpha < 180°$$

The reflected energy distribution for an ellipse is graphically shown in Figs. 76 and 77.

APPENDIX IV

TOTAL RADIATION INTENSITY DISTRIBUTION IMPINGING UPON A RECEIVING SURFACE ABOVE AN INFINITELY LONG PARABOLIC REFLECTOR CONTAINING A FINITE DIAMETER SOURCE

A semi-graphical method may be used to determine the radiation intensity distribution impinging on a receiving surface above an infinitely long parabolic reflector containing a finite diameter source. It is assumed the receiving surface contains elements parallel to the source such that a profile or end view of the receiving surface may be represented as a line.



The method essentially consists of determining graphically, in the profile view, the total angle over which a number of points on the receiver can see the source directly or by reflection. To reduce the amount of work involved in this process, six design charts, Figs. 79 - 84, have been constructed. The askew lines on the charts represent rays from either top or bottom extremities of the source reflected by any point on the surface of the reflector. The dashed lines represent rays from the top of the source, the solid lines are rays from the bottom of the source. The angle, α, made by these lines can be computed from:

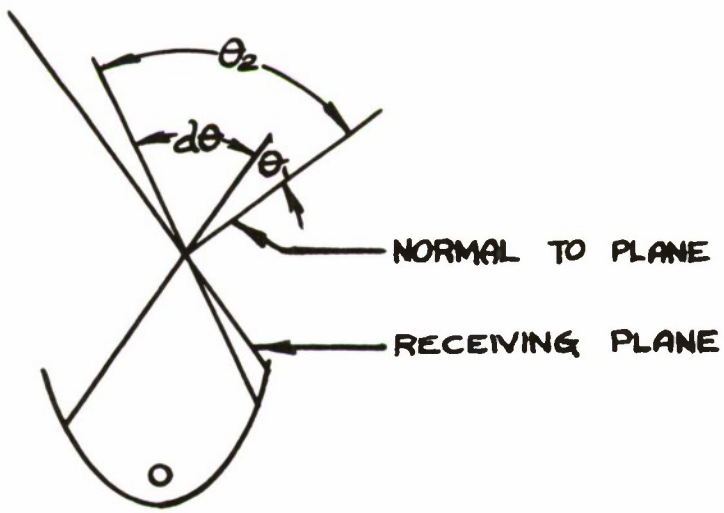
$$\alpha = \sin^{-1} \frac{b}{\left(\frac{1}{4a} + ax^2\right)} \qquad (1)$$

The design charts permit a simple determination of the two dimensional total angle through which the source can be 'seen' directly or by reflection.

To use the chart, place a line representing the receiver above the parabola at the desired location and orientation. (In the photographic reproduction of these charts, the scale has been reduced. To compensate, draw line representing receiver to the same scale. The scale can be determined by taking the ratio of the measured source diameter to the original source diameter printed on the chart.) Divide the receiver into any number of equal segments depending on the accuracy desired. Any point on the plate will receive both direct and reflected radiant energy.

To find the included angle, within which reflected radiation is incident on a point of the receiver, use the askew lines on the chart. If the point falls at the intersection of two of these lines, the angle between these lines is the angle within which the point receives reflected energy. If the point does not fall at an intersection, which will be the usual case, interpolate between the two sets of enclosing lines and thus determine the included angle.

To find the included angle in which direct radiation is incident on a point of the receiver, draw two lines tangent to each side of the radiating source and passing through the point on the receiver. Often this angle will fall within the angle determined for reflected radiation. This indicates that the source blocks out this amount of reflected energy and that the receiver obtains this radiation directly from the source. Hence this angle should be included but once.



The radiation intensity impinging on the receiver element from an infinitely long radiator, Q/dA_1, is simply:

$$\frac{Q}{dA_1} = \frac{\pi I}{2} \sin\theta \Big]_{\theta_1}^{\theta_2} \tag{2}$$

$$I = \frac{w}{\pi} = \frac{\varepsilon \sigma T^4}{\pi} \tag{3}$$

I = intensity of normal incident radiation, BTU/hr, ft.^{2}

w = total emissive power, BTU/hr, ft.^{2}

ε = emissivity of radiator

σ = constant, 0.173 x 10^{-8} BTU/hr, ft^2/$^\circ$R4

T = temperature of source, $^\circ$R

θ_1 and θ_2 = limits of included angle measured from normal to receiver surface

Therefore, after obtaining θ_1 and θ_2 graphically, multiply the difference of their sines by the constant, $\frac{\pi I}{2}$, to obtain the incident radiation intensity at the point on the receiver. If this procedure is followed for several points along the receiver, the distribution of the total incident energy can be determined. To substantiate Eq. (2), the following proof is offered.

Assume an area, dA_1, on the receiver parallel to an infinitely long radiator of which dA_2 is an element.

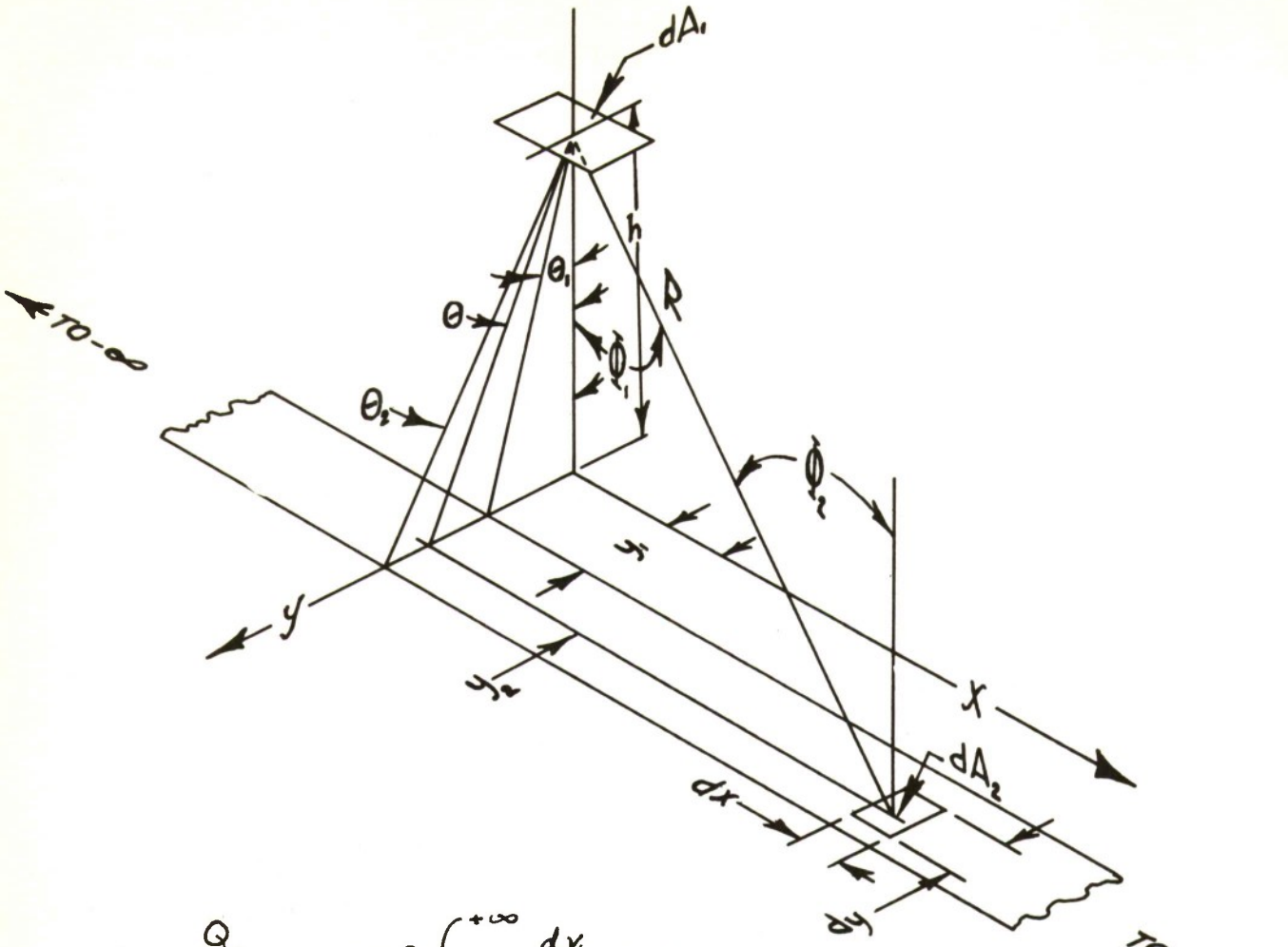
Starting with the general radiation equation:

$$\frac{dQ}{dA_1} = \frac{I\, dA_2 \cos\phi_1 \cos\phi_2}{R^2}$$

$$\cos\phi_1 = \cos\phi_2 = \frac{h}{\sqrt{x^2+y^2+h^2}}$$

$$R^2 = x^2+y^2+h^2$$

$$dA_2 = dx \cdot dy$$



$$\frac{Q}{\frac{dA_1}{dy}} = Ih^2 \int_{-\infty}^{+\infty} \frac{dx}{(x^2+y^2+h^2)^2}$$

$$= Ih^2 \left[\frac{x}{2(y^2+h^2)(x^2+y^2+h^2)} + \frac{1}{2(y^2+h^2)^{3/2}} \tan^{-1} \frac{x}{a} \right]_{-\infty}^{+\infty}$$

$$= \frac{Ih^2\pi}{2(y^2+h^2)^{3/2}}$$

$$\frac{Q}{dA_1} = \frac{Ih^2\pi}{2} \int_{y_1}^{y_2} \frac{dy}{(y^2+h^2)^{3/2}}$$

$$= \frac{Ih^2\pi}{2} \left[\frac{y}{h^2(y^2+h^2)^{1/2}} \right]_{y_1}^{y_2}$$

$$= \frac{\pi I}{2} \sin\theta \Big]_{\theta_1}^{\theta_2}$$

The above is identical to Eq. (2).

The design charts have been prepared for identical parabolas but with different source diameters. However, these charts can be used for other parabolic reflectors by the method explained in the following.

For any combination of reflector and source, obtain the value of the source radius multiplied by the characteristic constant of the parabola, a, ($y = ax^2$). Select a design chart which has the same value of radius multiplied by the characteristic constant. This design chart will now represent the particular combination of reflector and source, but to a different scale. All dimensions are to a scale determined by the ratio of desired source radius to chart source radius. Hence, when positioning the receiver above the chart, draw it to the proper length considering the new scale. An example, to further clarify this process is presented in the following.

Given:

Source Radius = 1/8

Parabolic Reflector Equation, $y = 2x^2$

$b \times a = 1/8 \times 2 = 1/4$

Therefore select chart with same b x a value.

$y_o = 1/2\ x^2$

$b_o = 1/2$

$b_o \times a_o = 1/4$

The scale of this chart is:

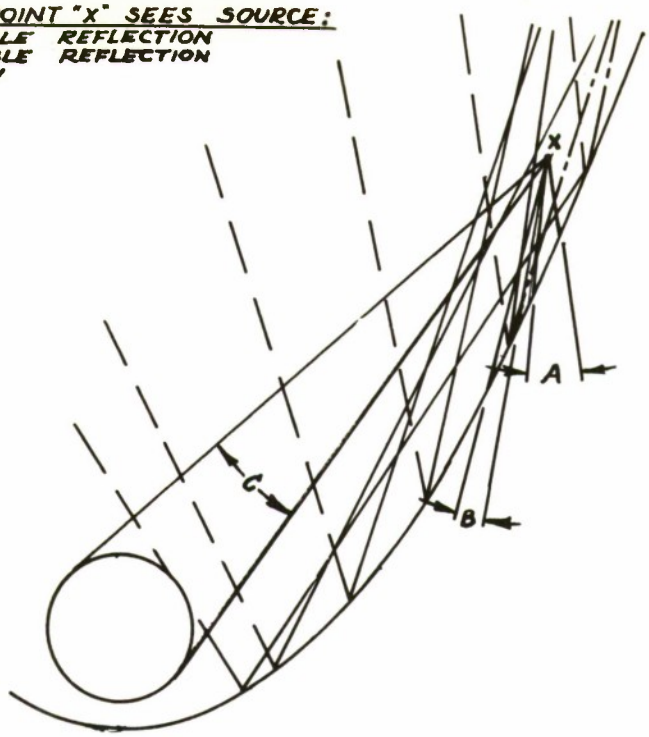
$$\frac{b}{b_o} = \frac{1/8}{1/2} = 1/4$$

Hence 1" on chart represents 1/4" and a receiver 6" true length would be drawn on the chart 24" long. The angles formed are true and hence the calculated intensity need not be multiplied by the scale factor.

Double Reflection from Reflector

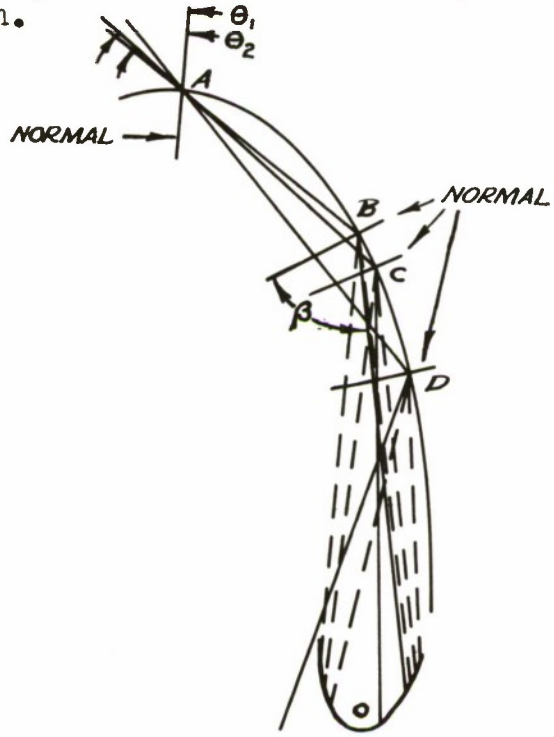
When the source is large compared to the enclosing parabola focus, radiation may impinge on the receiver by double reflection from the reflector. Double reflection lines, have been included on the 3/4" and 1" source diameter charts. This phenomena of double reflection from the reflector will be negligible in the great majority of cases; it is included herein for the sake of completeness. The use of the charts containing double reflection lines is illustrated by the following sketch.

ANGLE THRU WHICH POINT "X" SEES SOURCE:
ANGLE A ~ BY SINGLE REFLECTION
ANGLE B ~ BY DOUBLE REFLECTION
ANGLE C ~ DIRECTLY



Multiple Reflection from Receiver

On a curved receiver, radiation from the source-reflector combination may be reflected from one point onto another point of the receiver. A semi-graphical method of determining the radiant energy contribution at any point by reflection from other points along the receiver surface, is illustrated by the following sketch.



From any point, A, draw straight 'lines of sight' to other points on the receiver. The angle of incidence is equal to the angle of reflection and hence the 'lines of sight' may be continued beyond these points, B, C, D, etc., toward the reflector-source combination. If the reflected 'line of sight' falls within the angle through which B, C, D, etc. receive radiation from the source-reflector combination, then reflected radiation from these points impinge on point A. In this manner it is possible to determine the limits of the angle at A through which once reflected radiation will reach point A. The intensity of the rays within this angle are not uniform. The intensity will be a function of the angle of incidence, β, made by the ray from the source-reflector combination and the normal at the point on the receiver surface on which it first impinges. For Lucite (Plexiglas) and glass, Figures 8 and 9, the variation is slight up to incident angles of 45°. Hence, the incident energy at point A, by first reflection from other points on the receiver, may be evaluated from:

$$\frac{Q_R}{dA_1} = \frac{.04 I \Pi}{2} \sin\theta \Big]_{\theta_1}^{\theta_2}$$

For β angles larger than 45°, the portion of the angle greater than 45° should be divided into a number of small divisions and the energy contributed by each division evaluated by:

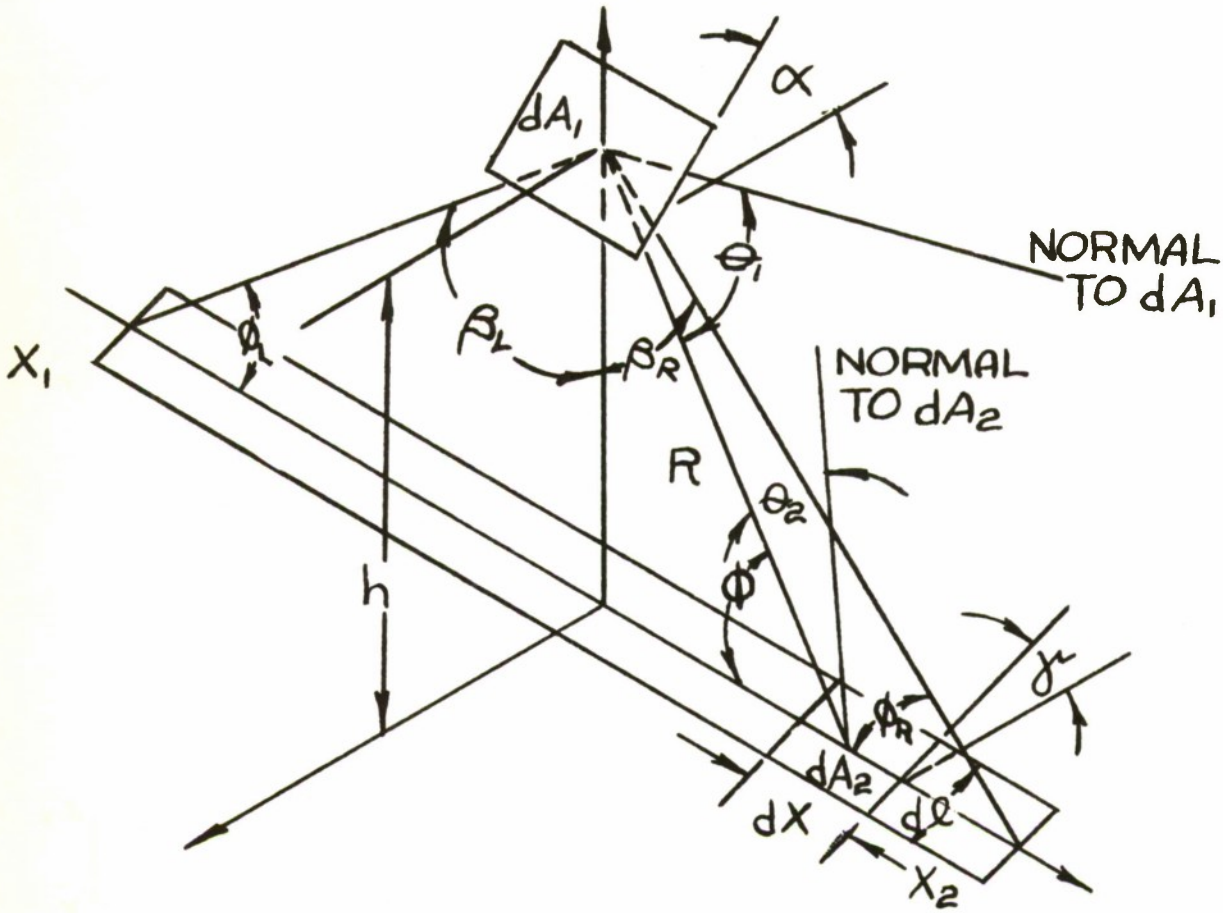
$$\frac{Q_R}{dA_1} = \frac{r I \Pi}{2} \sin\theta \Big]_{\theta_1}^{\theta_2}$$

r = fraction reflected by the mean ray of the angle division and is a function of β (Figures 8 and 9).

Multiple reflection effects can be evaluated by a similar method.

APPENDIX V

CORRECTION FOR CHART METHOD OF RADIATION DISTRIBUTION TO ACCOUNT FOR FINITE LENGTH SOURCE



Consider an element on the source, dA_2, inclined at angle of $\gamma°$ from the horizontal radiating to dA_1 on the receiver which is inclined at an angle $\alpha°$ from the horizontal (see sketch above). The energy impinging upon dA_1 is

$$\frac{Q}{dA_1} = \int_{X_1}^{X_2} \frac{I \cos\theta_1 \, dA_2 \cos\theta_2}{R^2}$$

$\frac{Q}{dA_1}$ = impinging radiant energy, BTU/hr, ft^2

I = intensity of normal incident radiation, BTU/hr, ft^2

and the other symbols are defined by the sketch.

NOW:

$$\cos\theta_1 = \frac{h\cos\alpha}{\sqrt{x^2+h^2}}$$

$$\cos\theta_2 = \frac{h\cos\gamma}{\sqrt{x^2+h^2}}$$

$$R = \sqrt{x^2+h^2}$$

AND LET

$$dA_2 = dl \cdot dy$$

THEN

$$\frac{Q}{dA_1} = \int_{x_1}^{x_2} \frac{I\,h^2\cos\alpha\cos\gamma\,dl\,dy}{(x^2+h^2)^2}$$

$$= I h^2 dl \cos\alpha \cos\gamma \int_{x_1}^{x_2} \frac{dx}{(x^2+h^2)^2}$$

$$\frac{Q}{dA_1} = I h^2 dl \cos\alpha \cos\gamma \left[\frac{x}{2h^2(x^2+h^2)} + \frac{1}{2h^3}\tan^{-1}\frac{x}{h}\right]_{x_1}^{x_2}$$

The ratio of energy impinging upon dA_1 for a source of finite length to that from an infinite length source is:

$$F = \frac{\left(\frac{Q}{dA_1}\right)_{\text{FINITE LENGTH SOURCE}}}{\left(\frac{Q}{dA_1}\right)_{\text{INFINITE LENGTH SOURCE}}} = \frac{\cos\alpha I h^2 dl \cos\psi \left[\frac{x}{2h^2(x^2+h^2)} + \frac{1}{2h^3}\tan^{-1}\frac{x}{h}\right]_{x_1}^{x_2}}{\cos\alpha I h^2 dl \cos\psi \left[\frac{x}{2h^2(x^2+h^2)} + \frac{1}{2h^3}\tan^{-1}\frac{x}{h}\right]_{-\infty}^{+\infty}}$$

$$F = \frac{\left[\frac{x_2}{2h^2(x_2^2+h^2)} + \frac{1}{2h^3}\tan^{-1}\left(\frac{x_2}{h}\right)\right] - \left[\frac{x_1}{2h^2(x_1^2+h^2)} + \frac{1}{2h^3}\tan^{-1}\left(\frac{x_1}{h}\right)\right]}{\pi/2h^3}$$

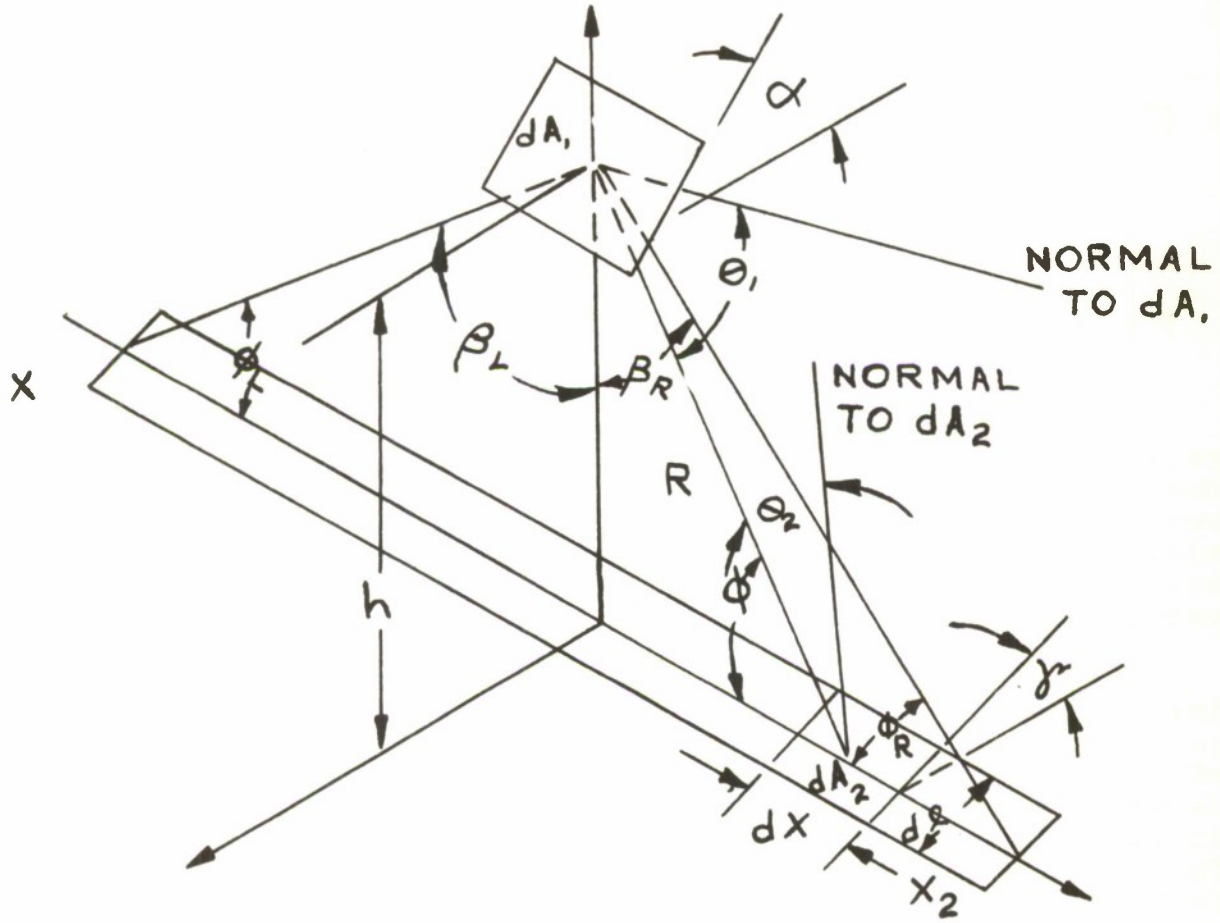
$$F = \frac{1}{\pi}\left[\left(\frac{1}{2}\sin 2\beta_R + \beta_R\right) + \left(\frac{1}{2}\sin 2\beta_L + \beta_L\right)\right]$$

As in Appendix IV it is assumed that the receiver and radiator contain parallel elements. Also herein, it is assumed that the source-reflector combination is narrow and can be represented by a differential width strip. Where the source width is large, this method may be applied by dividing the source into narrow strips and determining separate factors for each.

Since the chart method of Appendix IV for determining intensity distribution is for an infinite length source-reflector combination, the factor F, when multiplied by the chart results will correct for finite source length. The factor, F, has to be determined for each point on the receiver. To simplify the calculations involved, the factor has been plotted in Fig. 86 as a function of $\varphi_{LOR}(90-\beta_{LOR})$. To use the chart determine the factors for φ to the right and left of the point on the receiver and add the two values. The factor will be, one, for an infinitely long source on both sides of the receiver and less than one for all other cases.

APPENDIX VI

CORRECTION FOR CHART METHOD OF RADIATION DISTRIBUTION TO ACCOUNT FOR FINITE LENGTH SOURCE AND RECEIVER REFLECTION



This correction was derived in order to determine by use of the chart method the amount of radiant energy passing thru the surface at any point on the receiver. The energy passing thru the surface is less than that impinging, by the amount reflected from the surface. Correction for finite source length, as derived in Appendix V, is included in this factor F'. It was assumed that the reflector-source combination could be represented by a narrow strip.

The energy impinging on dA_1 and which is not reflected at the surface, is

$$\frac{Q'}{dA_1} = \int_{x_1}^{x_2} \frac{I \cos\theta_1 \, dA_2 \cos\theta_2 \, (1-r)}{R^2} \qquad (1)$$

wherein

$\frac{Q'}{dA_1}$ = impinging radiant energy passing through surface, BTU/hr, ft²

I = intensity of normal incident radiation, BTU/hr, ft²

r = fraction of incident energy that is reflected

and the other symbols are identified on the diagram.

Reflection as a function of angle of incidence is expressed by the somewhat complex Fresnel relationship, It was found that the following equation, expressing this relationship, could be more readily used, and that it differed by a negligible amount from Fresnel's equation for glass and plexiglas (see Fig. 87 for comparison of the two equations).

$$r = .04 + .96\left(\frac{\theta_1}{\pi/2}\right)^8 \qquad (2)$$

SUBSTITUTING EQ (2) in EQ (1)

$$\frac{Q'}{dA_1} = \int_{x_1}^{x_2} \frac{.96 I \cos\theta_1 dA_2 \cos\theta_2}{\ell^2} - \int_{x_1}^{x_2} \frac{.96 I \cos\theta_1 dA_2 \cos\theta_2 \left(\frac{\theta_1}{\pi/2}\right)^8}{\ell^2} \qquad (3)$$

AND AS IN APPENDIX V

$$dA_2 = dx \cdot dl$$

$$\cos\theta_1 = \frac{h\cos\alpha}{\sqrt{x^2+h^2}} \qquad \theta_1 = \cos^{-1}\frac{h\cos\alpha}{\sqrt{x^2+h^2}}$$

$$\cos\theta_2 = \frac{h\cos\gamma}{\sqrt{x^2+h^2}} \qquad \ell = \sqrt{x^2+h^2}$$

$$\frac{Q'}{dA_1} = .96 I h^2 \cos\alpha \cos\gamma\, dl \int_{x_1}^{x_2} \frac{dx}{(x^2+h^2)^2} - \frac{\left(\cos^{-1}\frac{h\cos\alpha}{\sqrt{x^2+h^2}}\right)^8 dx}{(x^2+h^2)(\pi/2)^8} \qquad (4)$$

As mentioned in the previous appendix, use of the chart is a graphical means of determining the energy impinging on the receiver element from an infinite length receiver. This energy intensity was denoted by the symbol, $\frac{Q}{dA_1}$, and was shown to equal

$$\frac{Q}{dA_1} = Ih^2 \cos\alpha \cos\gamma \, dl \int_{-\infty}^{\infty} \frac{dx}{(x^2+h^2)^2}$$

$$= Ih^2 \cos\alpha \cos\gamma \, dl \, \frac{\pi}{2h^3} \tag{5}$$

The correction factor F' is defined as:

$$\frac{\left(\frac{Q'}{dA_1}\right)_{\text{FINITE LENGTH SOURCE}}}{\left(\frac{Q}{dA_1}\right)_{\text{INFINITE LENGTH SOURCE}}} = F' \tag{6}$$

$$F' = \frac{.96 Ih^2 \cos\alpha \cos\gamma \, dl \int_{x_1}^{x_2} \frac{dx}{(x^2+h^2)^2} - \frac{\left(\cos^{-1}\frac{h\cos\alpha}{\sqrt{x^2+h^2}}\right)^8}{(x^2+h^2)^2\left(\frac{\pi}{2}\right)^8} dx}{Ih^2 \cos\alpha \cos\gamma \, dl \, \frac{\pi}{2h^3}}$$

$$= .96 \frac{2}{\pi} h^3 \int_{x_1}^{x_2} \frac{dx}{(x^2+h^2)^2} - \frac{\left(\cos^{-1}\frac{h\cos\alpha}{\sqrt{x^2+h^2}}\right)^8}{(x^2+h^2)^2\left(\frac{\pi}{2}\right)^8} dx \tag{7}$$

To simplify the following mathematics and the later tabulations, the factor F' was divided into its two components, one covering the correction for the source to the left and the other to the right

$$F' = F_L' + F_R' \tag{8}$$

In explaining the derivation, F_R' will be used, but similar procedure could be used for F_L'.

$$F_2' = .96\left(\frac{2}{\pi}\right) h^3 \int_0^{x_2} \frac{dx}{(x^2+h^2)^2} - \frac{\left(\cos^{-1}\frac{h\cos\alpha}{\sqrt{x^2+h^2}}\right)^8}{(x^2+h^2)^2\left(\frac{\pi}{2}\right)^8}\,dx$$

let $x = h\tan\beta$

$dx = h\sec^2\beta\, d\beta$

then

$$\int_0^{x_2} \frac{dx}{(x^2+h^2)^2} = \int_0^{\tan^{-1}\frac{x_2}{h}} \frac{h\sec^2\beta\, d\beta}{[h^2(\tan^2\beta+1)]^2}$$

$$= \frac{1}{h^3}\int_0^{\tan^{-1}\frac{x_2}{h}} \cos^2\beta\, d\beta$$

$$= \frac{1}{h^3}\left[\frac{\beta}{2} + \frac{1}{4}\sin 2\beta\right]_0^{\tan^{-1}\frac{x_2}{h}}$$

$\beta = \frac{\pi}{2} - \phi$

$$= \frac{1}{h^3}\left[\frac{\frac{\pi}{2}-\phi}{2} + \frac{1}{4}\sin(\pi - 2\phi)\right]_{\pi/2}^{\tan^{-1}\frac{h}{x_2}}$$

$$= \frac{1}{h^3}\left[\frac{\pi}{4} - \frac{\phi}{2} + \frac{1}{4}\sin 2\phi\right]_{\pi/2}^{\tan^{-1}\frac{h}{x_2}}$$

$$F_2' = .96\,\frac{2}{\pi}\left\{\left[\frac{\pi}{4} - \frac{\phi}{2} + \frac{1}{4}\sin 2\phi\right]_{\pi/2}^{\tan^{-1}\frac{h}{x_2}} - \frac{h^3}{\left(\frac{\pi}{2}\right)^8}\int_0^{x_2} \frac{\left(\cos^{-1}\frac{h\cos\alpha}{\sqrt{x^2+h^2}}\right)^8}{(x^2+h^2)^2}\,dx\right\}$$

let $y = (x^2+h^2)^{-1/2}$

$$dy = -\tfrac{1}{2}(x^2+h^2)^{-3/2}(2x)\,dx$$
$$= -x(x^2+h^2)^{-3/2}\,dx$$
$$= -xy^3\,dx$$

$$x = \sqrt{\left(\tfrac{1}{y}\right)^2 - h^2}$$

$$dx = -\frac{dy}{y^3\sqrt{\left(\frac{1}{y}\right)^2 - h^2}}$$

then

$$\frac{-h^3}{\left(\frac{\pi}{2}\right)^8}\int_0^{x_2}\frac{\left(\cos^{-1}\frac{h\cos\alpha}{\sqrt{x^2+h^2}}\right)^8}{(x^2+h^2)^2}\,dx = +\frac{h^3}{\left(\frac{\pi}{2}\right)^8}\int_{\frac{1}{h}}^{(x_2^2+h^2)^{-\frac{1}{2}}}\frac{(\cos^{-1}yh\cos\alpha)^8}{\frac{1}{y^3}\sqrt{\left(\frac{1}{y}\right)^2-h^2}}\,dy$$

let $h\cos\alpha = a$

$$= \frac{h^3}{\left(\frac{\pi}{2}\right)^8}\int_{\frac{1}{h}}^{(x_2^2+h^2)^{-1/2}}\frac{y(\cos^{-1}ay)^8}{\sqrt{\left(\frac{1}{y}\right)^2-h^2}}\,dy$$

In order to integrate, the $\cos^{-1}ay$ term was expanded into its infinite series form. The first term of the expansion, $\left(\frac{\pi}{2}-ay\right)^8$, is compared to $(\cos^{-1}ay)^8$ in Fig. 90 for $\cos^{-1}ay$ ranging from 0 to $\pi/2$. The two curves agreed well and hence only the first term of the expansion was used.

$$-\frac{h^3}{\left(\frac{\pi}{2}\right)^8}\int_0^{x_2}\frac{\left(\cos^{-1}\frac{h\cos\alpha}{\sqrt{x^2+h^2}}\right)^8}{(x^2+h^2)^2}\,dx = \frac{h^3}{\left(\frac{\pi}{2}\right)^8}\int_{\frac{1}{h}}^{(x_2^2+h^2)^{-\frac{1}{2}}}\frac{y\left(\frac{\pi}{2}-ay\right)^8}{\sqrt{\left(\frac{1}{y}\right)^2-h^2}}\,dy$$

$$= \frac{h^3}{(\pi/2)^8} \int_{\frac{1}{h}}^{(x_2^2+h^2)^{-1/2}} \frac{y^2\,dy}{\sqrt{1-y^2h^2}} \left[\left(\frac{\pi}{2}\right)^8 - 8\left(\frac{\pi}{2}\right)^7 ay + \frac{8\cdot7}{2}\left(\frac{\pi}{2}\right)^6 a^2y^2 - \frac{8\cdot7\cdot6}{2\cdot3}\left(\frac{\pi}{2}\right)^5 a^3y^3 \right.$$

$$+ \frac{8\cdot7\cdot6\cdot5}{2\cdot3\cdot4}\left(\frac{\pi}{2}\right)^4 a^4y^4 - \frac{8\cdot7\cdot6\cdot5\cdot4}{2\cdot3\cdot4\cdot5}\left(\frac{\pi}{2}\right)^3 a^5y^5 + \frac{8\cdot7\cdot6\cdot5\cdot4\cdot3}{2\cdot3\cdot4\cdot5\cdot6}\left(\frac{\pi}{2}\right)^2 a^6y^6$$

$$\left. - \frac{8\cdot7\cdot6\cdot5\cdot4\cdot3\cdot2}{2\cdot3\cdot4\cdot5\cdot6\cdot7}\left(\frac{\pi}{2}\right) a^7y^7 + a^8y^8 \right]$$

let $y = \frac{1}{h}\sin\varphi$

$dy = \frac{1}{h}\cos\varphi\,d\varphi$ $\qquad \sqrt{1-y^2h^2} = \sqrt{1-\sin^2\varphi} = \cos\varphi$

$$= h^3 \int_{\pi/2}^{\varphi_c} \frac{\cos\varphi\,d\varphi}{h\cos\varphi} \left[\frac{1}{h^2}\sin^2\varphi - 8\left(\frac{2}{\pi}\right)\frac{a}{h^3}\sin^3\varphi + 28\left(\frac{2}{\pi}\right)^2\frac{a^2}{h^4}\sin^4\varphi \right.$$

$$- 56\left(\frac{2}{\pi}\right)^3\frac{a^3}{h^6}\sin^5\varphi + 70\left(\frac{2}{\pi}\right)^4\frac{a^4}{h^6}\sin^6\varphi - 56\left(\frac{2}{\pi}\right)^5\frac{a^5}{h^7}\sin^7\varphi$$

$$\left. + 28\left(\frac{2}{\pi}\right)^6\frac{a^6}{h^8}\sin^8\varphi - 8\left(\frac{2}{\pi}\right)^7\frac{a^7}{h^9}\sin^9\varphi + \left(\frac{2}{\pi}\right)^8\frac{a^8}{h^{10}}\sin^{10}\varphi \right] \qquad (9)$$

$$\int \sin^2\varphi\,d\varphi = \frac{\varphi}{2} - \frac{1}{4}\sin 2\varphi$$

$$\int \sin^3\varphi\,d\varphi = -\frac{1}{3}\sin^2\varphi\cos\varphi + \frac{2}{3}(-\cos\varphi)$$

$$= -\frac{1}{3}\cos\varphi\,(\sin^2\varphi + 2)$$

$$\int \sin^4\varphi\,d\varphi = -\frac{1}{4}\sin^3\varphi\cos\varphi + \frac{3}{4}\int \sin^2\varphi\,d\varphi$$

$$= -\frac{1}{4}\sin^3\varphi\cos\varphi + \frac{3}{8}\left(\varphi - \frac{1}{2}\sin 2\varphi\right)$$

$$\int \sin^5\varphi\, d\varphi = -\tfrac{1}{5}\sin^4\varphi\cos\varphi + \tfrac{4}{5}\int \sin^3\varphi\, d\varphi$$
$$= -\tfrac{1}{5}\sin^4\varphi\cos\varphi - \tfrac{4}{15}\cos\varphi\,(\sin^2\varphi + 2)$$

$$\int \sin^6\varphi\, d\varphi = -\tfrac{1}{6}\sin^5\varphi\cos\varphi + \tfrac{5}{6}\int \sin^4\varphi\, d\varphi$$
$$= -\tfrac{1}{6}\sin^5\varphi\cos\varphi - \tfrac{5}{24}\sin^3\varphi\cos\varphi + \tfrac{15}{48}\left(\varphi - \tfrac{1}{2}\sin 2\varphi\right)$$

$$\int \sin^7\varphi\, d\varphi = -\tfrac{1}{7}\sin^6\varphi\cos\varphi + \tfrac{6}{7}\int \sin^5\varphi\, d\varphi$$
$$= -\tfrac{1}{7}\sin^6\varphi\cos\varphi - \tfrac{6}{35}\left[\sin^4\varphi\cos\varphi + \tfrac{4}{3}\cos\varphi(\sin^2\varphi + 2)\right]$$

$$\int \sin^8\varphi\, d\varphi = -\tfrac{1}{8}\sin^7\varphi\cos\varphi + \tfrac{7}{8}\int \sin^6\varphi\, d\varphi$$
$$= -\tfrac{1}{8}\sin^7\varphi\cos\varphi + \tfrac{7}{48}\left[-\sin^5\varphi\cos\varphi + \tfrac{5}{4}\left\{-\sin^3\varphi\cos\varphi + \tfrac{3}{2}\left(\varphi - \tfrac{1}{2}\sin 2\varphi\right)\right\}\right]$$

$$\int \sin^9\varphi\, d\varphi = -\tfrac{1}{9}\sin^8\varphi\cos\varphi + \tfrac{8}{9}\int \sin^7\varphi\, d\varphi$$
$$= -\tfrac{1}{9}\sin^8\varphi\cos\varphi - \tfrac{8}{63}\left[\sin^6\varphi\cos\varphi + \tfrac{6}{5}\left\{\sin^4\varphi\cos\varphi + \tfrac{4}{3}\cos\varphi(\sin^2\varphi + 2)\right\}\right]$$

$$\int \sin^{10}\varphi\, d\varphi = -\tfrac{1}{10}\sin^9\varphi\cos\varphi + \tfrac{9}{10}\int \sin^8\varphi\, d\varphi$$
$$= -\tfrac{1}{10}\sin^9\varphi\cos\varphi + \tfrac{9}{10}\left\{-\tfrac{1}{8}\sin^7\varphi\cos\varphi + \tfrac{7}{48}\left(-\sin^5\varphi\cos\varphi + \tfrac{5}{4}\left[-\sin^3\varphi\cos\varphi + \tfrac{3}{2}\left(\varphi - \tfrac{1}{2}\sin 2\varphi\right)\right]\right)\right\}$$

also $\frac{a}{h} = \cos\alpha$

substituting in Eq (9)

$$-\frac{h^3}{\left(\frac{\pi}{2}\right)^8}\int_0^{\chi_2}\frac{\left(\cos^{-1}\frac{h\cos\alpha}{\sqrt{\chi^2+h^2}}\right)^8}{(\chi^2+h^2)^2}\,d\chi = \left[\frac{\phi}{2}-\frac{1}{4}\sin 2\phi+\frac{8}{3}\left(\frac{2}{\pi}\right)\cos\alpha\cos\phi(\sin^2\phi+2)\right.$$

$$+7\left(\frac{2}{\pi}\right)^2\cos^2\alpha\left[-\sin^3\phi\cos\phi+\frac{3}{2}\left(\phi-\frac{1}{2}\sin 2\phi\right)\right]+\frac{56}{5}\left(\frac{2}{\pi}\right)^3\cos^3\alpha\left[\sin^4\phi\cos\phi\right.$$

$$\left.+\frac{4}{3}\cos\phi(\sin^2\phi+2)\right]+\frac{35}{3}\left(\frac{2}{\pi}\right)^4\cos^4\alpha\left[-\sin^5\phi\cos\phi-\frac{5}{4}\sin^3\phi\cos\phi\right.$$

$$\left.+\frac{15}{8}\left(\phi-\frac{1}{2}\sin 2\phi\right)\right]+8\left(\frac{2}{\pi}\right)^5\cos^5\alpha\left[\sin^6\phi\cos\phi+\frac{6}{5}\left\{\sin^4\phi\cos\phi\right.\right.$$

$$\left.\left.+\frac{4}{3}\cos\phi(\sin^2\phi+2)\right\}\right]+\frac{7}{2}\left(\frac{2}{\pi}\right)^6\cos^6\alpha\left[\sin^7\phi\cos\phi+\frac{7}{6}\left\{-\sin^5\phi\cos\phi\right.\right.$$

$$\left.\left.+\frac{5}{4}\left(-\sin^3\phi\cos\phi+\frac{3}{2}\left[\phi-\frac{1}{2}\sin 2\phi\right]\right)\right\}\right]+\frac{8}{9}\left(\frac{2}{\pi}\right)^7\cos^7\alpha\left[\sin^8\phi\cos\phi\right.$$

$$\left.+\frac{8}{7}\left\{\sin^6\phi\cos\phi+\frac{6}{5}\left[\sin^4\phi\cos\phi+\frac{4}{3}\cos\phi(\sin^2\phi+2)\right]\right\}\right]$$

$$+\frac{1}{10}\left(\frac{2}{\pi}\right)^8\cos^8\alpha\left[-\sin^9\phi\cos\phi+\frac{9}{8}\left\{-\sin^7\phi\cos\phi+\frac{7}{6}\left(-\sin^5\phi\cos\phi\right.\right.\right.$$

$$\left.\left.\left.+\frac{5}{4}\left[-\sin^3\phi\cos\phi+\frac{3}{2}\left(\phi-\frac{1}{2}\sin 2\phi\right)\right]\right)\right\}\right]\Bigg]_{\pi/2}^{\phi_2} \qquad (10)$$

$$F_e' = .96\frac{\pi}{2}\left\{\left[\frac{\pi}{4} - \frac{\phi}{2} + \frac{1}{4}\sin 2\phi + \frac{\phi}{2} - \frac{1}{4}\sin 2\phi + \frac{8}{3}\left(\frac{2}{\pi}\right)\cos\alpha\cos\phi\left(\sin^2\phi + 2\right)\right.\right.$$

$$+ 7\left(\frac{2}{\pi}\right)^2\cos^2\alpha\left[-\sin^3\phi\cos\phi + \frac{3}{2}\left(\phi - \frac{1}{2}\sin 2\phi\right)\right] + \frac{56}{5}\left(\frac{2}{\pi}\right)^3\cos^3\alpha\left[\sin^4\phi\cos\phi\right.$$

$$\left. + \frac{4}{3}\cos\phi\left(\sin^2\phi + 2\right)\right] + \frac{35}{3}\left(\frac{2}{\pi}\right)^4\cos^4\alpha\left[-\sin^5\phi\cos\phi - \frac{5}{4}\sin^3\phi\cos\phi\right.$$

$$\left. + \frac{15}{8}\left(\phi - \frac{1}{2}\sin 2\phi\right)\right] + 8\left(\frac{2}{\pi}\right)^5\cos^5\alpha\left[\sin^6\phi\cos\phi + \frac{6}{5}\left\{\sin^4\phi\cos\phi\right.\right.$$

$$\left.\left. + \frac{4}{3}\cos\phi\left(\sin^2\phi + 2\right)\right\}\right] + \frac{7}{2}\left(\frac{2}{\pi}\right)^6\cos^6\alpha\left[-\sin^7\phi\cos\phi - \frac{7}{6}\sin^5\phi\cos\phi\right.$$

$$\left. + \frac{35}{24}\left\{-\sin^3\phi\cos\phi + \frac{3}{2}\left[\phi - \frac{1}{2}\sin 2\phi\right]\right\}\right] + \frac{8}{9}\left(\frac{2}{\pi}\right)^7\cos^7\alpha\left[\sin^8\phi\cos\phi\right.$$

$$\left. + \frac{8}{7}\sin^6\phi\cos\phi + \frac{48}{35}\left\{\sin^4\phi\cos\phi + \frac{4}{3}\cos\phi\left(\sin^2\phi + 2\right)\right\}\right]$$

$$+ \frac{1}{10}\left(\frac{2}{\pi}\right)^8\cos^8\alpha\left[-\sin^9\phi\cos\phi - \frac{9}{8}\sin^7\phi\cos\phi + \frac{63}{48}\left\{-\sin^5\phi\cos\phi\right.\right.$$

$$\left.\left. + \frac{5}{4}\left[-\sin^3\phi\cos\phi + \frac{3}{2}\left(\phi - \frac{1}{2}\sin 2\phi\right)\right]\right\}\right]\Bigg]_{\pi/2}^{\phi_e}\Bigg\}$$

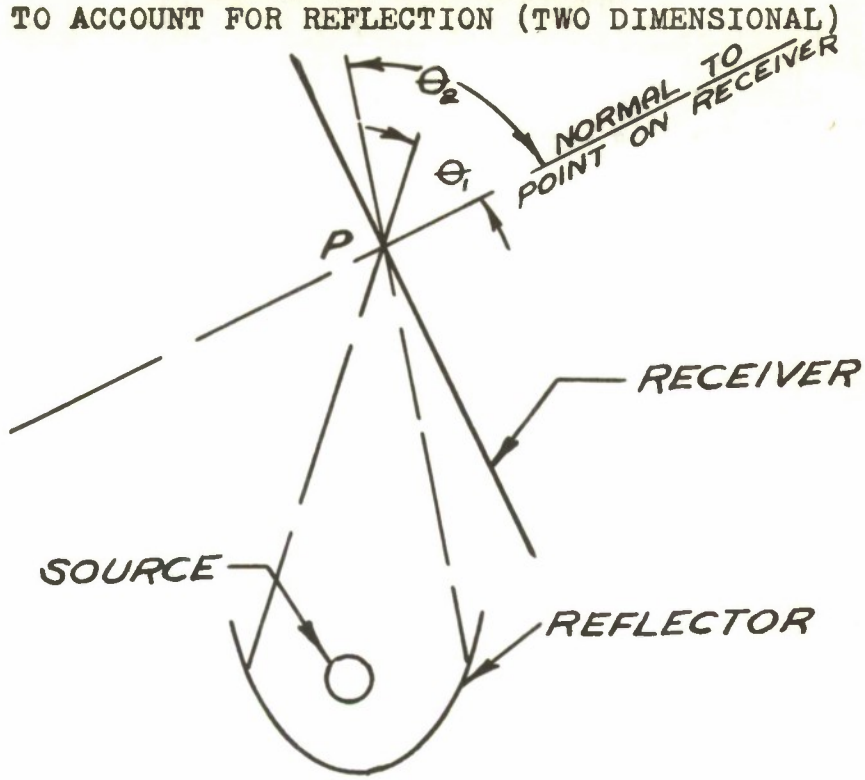
$$F_R' = .96\,\frac{\pi}{2}\left\{\left[\frac{\pi}{4}+\frac{8}{3}\left(\frac{2}{\pi}\right)\cos\alpha\cos\phi\left(\sin^2\phi+2\right)+7\left(\frac{2}{\pi}\right)^2\cos^2\alpha\left[-\sin^3\phi\cos\phi\right.\right.\right.$$
$$\left.+\frac{3}{2}\left(\phi-\frac{1}{2}\sin 2\phi\right)\right]+\frac{56}{5}\left(\frac{2}{\pi}\right)^3\cos^3\alpha\left[\sin^4\phi\cos\phi+\frac{4}{3}\cos\phi\left(\sin^2\phi+2\right)\right]$$
$$+\frac{35}{3}\left(\frac{2}{\pi}\right)^4\cos^4\alpha\left[-\sin^5\phi\cos\phi-\frac{5}{4}\sin^3\phi\cos\phi+\frac{15}{8}\left(\phi-\frac{1}{2}\sin 2\phi\right)\right]$$
$$+8\left(\frac{2}{\pi}\right)^5\cos^5\alpha\left[\sin^6\phi\cos\phi+\frac{6}{5}\left\{\sin^4\phi\cos\phi+\frac{4}{3}\cos\phi\left(\sin^2\phi+2\right)\right\}\right]$$
$$+\frac{1}{2}\left(\frac{2}{\pi}\right)^6\cos^6\alpha\left[-\sin^7\phi\cos\phi-\frac{7}{6}\sin^5\phi\cos\phi+\frac{35}{24}\left\{-\sin^3\phi\cos\phi+\frac{3}{2}\left[\phi-\frac{1}{2}\sin 2\phi\right]\right\}\right]$$
$$+\frac{8}{7}\left(\frac{2}{\pi}\right)^7\cos^7\alpha\left[\sin^8\phi\cos\phi+\frac{8}{7}\sin^6\phi\cos\phi+\frac{48}{35}\left\{\sin^4\phi\cos\phi+\frac{4}{3}\cos\phi\left(\sin^2\phi+2\right)\right\}\right]$$
$$+\frac{1}{10}\left(\frac{2}{\pi}\right)^8\cos^8\alpha\left[-\sin^9\phi\cos\phi-\frac{9}{8}\sin^7\phi\cos\phi+\frac{63}{48}\left\{-\sin^5\phi\cos\phi+\frac{5}{4}\left[-\sin^3\phi\cos\phi\right.\right.\right.$$
$$\left.\left.\left.\left.\left.+\frac{3}{2}\left(\phi-\frac{1}{2}\sin 2\phi\right)\right]\right\}\right]\right]_{\frac{\pi}{2}}^{\phi_R}\Bigg\} \qquad (10)$$

The factor F_R' has been plotted for all values of ϕ_R and various values of α in Fig. 88 in order to eliminate the arduous task of solving Eq. (10). The factor F_L' may be obtained from the same Fig. by determining the value of ϕ_L to the left of dA_1. As mentioned previously the total correction factor, F', is equal to $F_R' + F_L'$. For the special case where the source is entirely on one side and does not extend thru the origin, Fig. 88 may still be used. Find the value of F' for an imaginary source extending from the origin to the beginning of the actual source and for a second imaginary source extending from the origin to the end of the real source; then subtract the former from the latter.

By definition, the factor, F', multiplied by the intensity determined by the chart method, corrects for finite source length and receiver reflection.

APPENDIX VII

CORRECTION FOR CHART METHOD OF RADIATION DISTRIBUTION TO ACCOUNT FOR REFLECTION (TWO DIMENSIONAL)



Consider the two dimensional case shown in the above illustration. Energy impinges on point P on the receiver between the angles θ_1, and θ_2. A varying percentage of the rays between these two angles will be reflected from the surface in accordance with Fresnel's relationship. To account for this reflection loss, a correction factor was derived as shown in the following.

Modifying Lambert's Cosine Law to account for reflection, the energy intensity passing thru the surface at any point P on the receiver is:

$$\frac{Q'}{dA} = \int_{\theta_1}^{\theta_2} I \cos\theta \, d\theta \, (1-r) \qquad (1)$$

where

$\frac{Q'}{dA}$ = energy intensity passing thru the surface, BTU/hr, ft^2

I = intensity of normal incident radiation, BTU/hr, ft^2

r = fraction of energy reflected at any indident angle

θ = angle of incidence

The Fresnel reflection relationship is somewhat complex. It was found that Eq. (2), simpler in form, could be used with but little error to express the relationship between reflection and angle of incidence for glass or plexiglas (see Fig. 87 for comparison of the two equations).

$$r = .04 + .96\left(\frac{\theta}{\pi/2}\right)^8 \tag{2}$$

Substituting Eq (2) into Eq (1)

$$\frac{Q'}{dA} = \int_{\theta_1}^{\theta_2} I \cos\theta \, d\theta \left[.96 + .96\left(\frac{\theta}{\pi/2}\right)^8\right]$$

$$= .96 I \sin\theta\Big]_{\theta_1}^{\theta_2} - .96 i \int_{\theta_1}^{\theta_2} \left(\frac{\theta}{\pi/2}\right)^8 \cos\theta \, d\theta \tag{3}$$

The second term of Eq. (3) can be integrated as is, but for evaluation purposes it proved simpler to express cos θ in infinite series form and then integrate; only the first few terms are significant.

$$\frac{Q'}{dA} = .96 I \sin\theta\Big]_{\theta_1}^{\theta_2} - .96 I \int_{\theta_1}^{\theta_2} \left(\frac{\theta}{\pi/2}\right)^8 \left[1 - \frac{\theta^2}{2!} + \frac{\theta^4}{4!} - \frac{\theta^6}{6!} + \frac{\theta^8}{8!} - \cdots\right] d\theta$$

$$= .96 I \sin\theta - .96 I \left(\frac{2}{\pi}\right)^8 \left(\frac{\theta^9}{9} - \frac{\theta^{11}}{11 \times 2!} + \frac{\theta^{13}}{13 \times 4!} - \frac{\theta^{15}}{15 \times 6!} + \frac{\theta^{17}}{17 \times 8!} - \cdots\right)\Big]_{\theta_1}^{\theta_2} \tag{4}$$

The above expression was evaluated for $\theta_1 = 0$ and ranging from 0 to $\pi/2$ and the results are presented in Fig. 89. The graph may be used for all cases, not only when $\theta_1 = 0$. For these other cases, determine the values from the chart for θ_1 and θ_2 and subtract the former from the latter.

APPENDIX VIII

CORRECTION FOR BLOCKAGE

Blockage is herein defined as the percentage of the total radiation from a radiator within a reflector which is reflected back onto the radiator. If the reflector material has a 0.0 emissivity and the radiator an emissivity of 1.0 there is not any energy loss involved in blockage. The energy given off by the radiator, which is blocked, is merely returned to the radiator. However, the effective radiating area of the source is decreased by the blockage phenomena.

In Appendix V, it was shown that the radiation received on dA_1 from an infinitely long strip source, containing elements parallel to dA_1 is:

$$\frac{Q}{dA_1} = \int_{-\infty}^{\infty} \frac{I \cos\theta_1 \, dx_2 \, dl_2 \cos\theta_2}{r^2}$$

$$= \frac{I \frac{\pi}{2} dl_2 \cos\alpha \cos\gamma}{h}$$

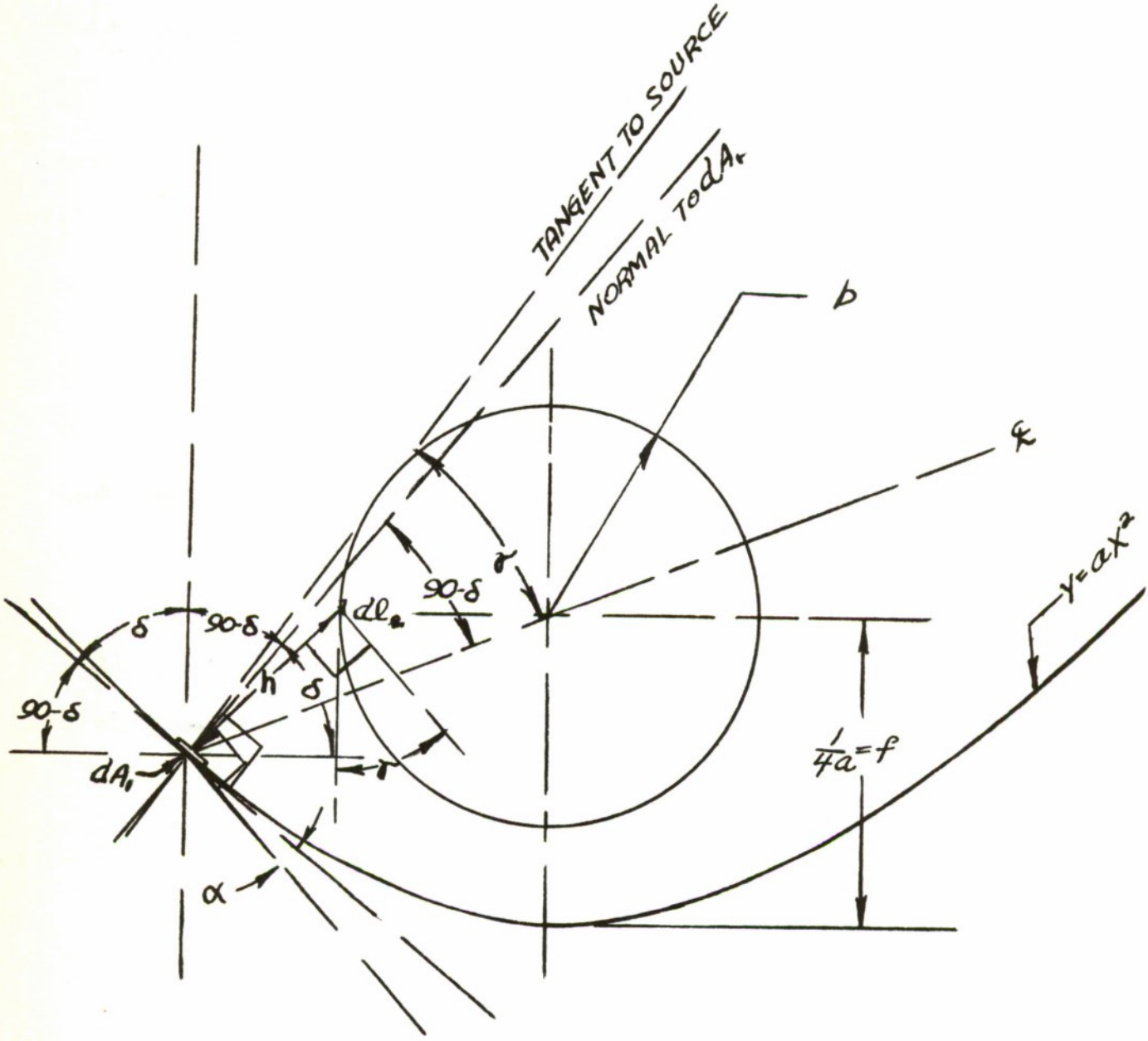
(Refer to Appendix V for sketch and nomenclature.)

Now consider the infinitely long, narrow strip, dl_2, located on the perimeter of a circular radiator which is located at the focus of the parabola. The receiver element dA_1 is located on the reflector surface.

In order to find the total radiation from the circular source which will be reflected from dA_1 back onto the source, sum up the contribution from each element dl_2.

$$\frac{dl_2 \cos\gamma}{h} = d\alpha$$

Because of the properties of this source-reflector combination, only the elements in the angle $2[\delta - (90-\delta) + \gamma - \delta]$ will contribute.



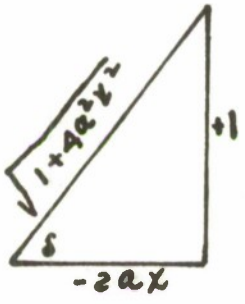
$$2\int_0^{\delta-(90-\delta)+\nu-\delta} \frac{\varphi}{dA_1} = 2I\frac{\pi}{2}\int_0^{\delta-(90-\delta)+\nu-\delta} \cos\alpha\, d\alpha = \frac{\varphi''}{dA_1}$$

δ = angle between the normal to dA_1 and a perpendicular to the reflector axis

ν = angle at dA_1 formed by a tangent to the source and line going through the center of the source.

$$\frac{\varphi''}{dA_1} = \pi I \sin\alpha\Big]_0^{\nu+\delta-90} = -\pi I \cos(\nu+\delta)$$

$$= -\pi I\left[\cos\nu\cos\delta - \sin\nu\sin\delta\right]$$

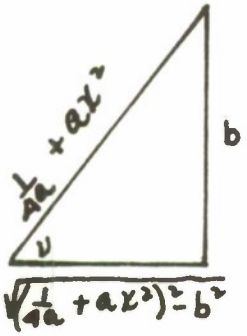


$$\delta = \tan^{-1}\frac{1}{-dy/dx}$$

The equation of the parabolic reflector is $y = ax^2$

$$dy/dx = 2ax$$

$$\therefore \delta = \tan^{-1}\frac{1}{-2ax}$$



$$\nu = \sin^{-1}\frac{b}{\frac{1}{4a}+ax^2}$$

$$\frac{\varphi''}{dA_1} = -\pi I\left[\frac{\sqrt{(\frac{1}{4a}+ax^2)^2-b^2}\,(-2ax)}{(\frac{1}{4a}+ax^2)\sqrt{1+4a^2x^2}} - \frac{b}{(\frac{1}{4a}+ax^2)\sqrt{1+4a^2x^2}}\right] \quad (2)$$

The equation of the parabolic reflector is $y = ax^2$.

Also

$$dA_1 = dl_1 \cdot dz$$

now
$$dl_1 = dx\sqrt{1+\left(\frac{dy}{dx}\right)^2}$$

$$= dx\sqrt{1+(2ax)^2}$$

$$= dx\sqrt{1+4a^2x^2}$$

And summing up the blocked out radiation reflected from all of the contributing strips on the reflector.

$$\frac{Q''}{dz} = \pi I \int_{-x_L}^{x_L} \frac{\left(-2ax\sqrt{\left(\frac{1}{4a}+ax^2\right)^2-b^2}+b\right)}{\frac{1}{4a}+ax^2}\,dx$$

It was found that after a graphical check the negative value of the radical yielded the correct answer. The total radiation given off by the unit cylindrical source is $2\pi b\pi I$.

$$\text{Blockage} = \frac{\frac{Q''}{dz}}{2\pi b\pi I} = \frac{1}{\pi b}\int_0^{x_L} \frac{\left(-2a\sqrt{\left(\frac{1}{4a}+ax^2\right)^2-b^2}+b\right)}{\frac{1}{4a}+ax^2}\,dx$$

Now the limit, x_L, is determined by setting $\theta = 0$, see Eq. 6)

$$2ax\sqrt{\left(\frac{1}{4a}+ax^2\right)^2-b^2} = b$$

$$\sqrt{\left(\frac{1}{4a}+ax^2\right)^2-b^2} = \frac{b}{2ax}$$

$$\left(\frac{1}{4a}+ax^2\right)^2-b^2=\frac{b^2}{4a^2x^2}$$

$$\frac{(1+4a^2x^2)^2}{16a^2}=\frac{b^2}{4a^2x^2}(1+4a^2x^2)$$

$$\frac{1+4a^2x^2}{16a^2}=\frac{b^2}{4a^2x^2}$$

$$16a^4x^4+4a^2x^2=16a^2b^2$$

$$4a^2x^2+\frac{1}{2}=\sqrt{16a^2b^2+\frac{1}{4}}$$

$$2ax=\pm\sqrt{\sqrt{16a^2b^2+\frac{1}{4}}-\frac{1}{2}}$$

$$\text{Blockage}=\frac{1}{\pi b}\int_0^{x_L}\frac{b\,dx}{\frac{1}{4a}+ax^2}-\frac{1}{\pi b}\int_0^{x_L}\frac{2ax\sqrt{\left(\frac{1}{4a}+ax^2\right)^2-b^2}}{\frac{1}{4a}+ax^2}\,dx$$

$$\frac{1}{\pi b}\int_0^{x_L}\frac{b\,dx}{\frac{1}{4a}+ax^2}=\frac{1}{\pi b}\int_0^{x_L}\frac{4ab\,dx}{1+4a^2x^2}=\frac{2}{\pi}\tan^{-1}2ax\Big]_0^{x_L}$$

Substituting x_L in above

$$=\frac{2}{\pi}\tan^{-1}\sqrt{\sqrt{16a^2b^2+\frac{1}{4}}-\frac{1}{2}}$$

let $\quad r=\frac{1}{4a}+ax^2$

$$dr=2ax\,dx$$

$$-\frac{1}{\pi b}\int_0^{x_L}\frac{2ax\sqrt{\left(\frac{1}{4a}+ax^2\right)^2-b^2}}{\frac{1}{4a}+ax^2}\,dx=-\frac{1}{\pi b}\int_0^{x_L}\frac{\sqrt{r^2-b^2}}{r}\,dr$$

$$=-\frac{1}{\pi b}\left[\sqrt{r^2-b^2}-b\cos^{-1}\frac{b}{r}\right]_0^{x_L}$$

Substituting for r

$$= +\frac{1}{\pi}\left[-\sqrt{\frac{\left(\frac{1}{4a}+ax^2\right)^2}{b^2}-1} + \cos^{-1}\frac{b}{\frac{1}{4a}+ax^2}\right]_0^{x_L}$$

$$= \frac{1}{\pi}\left[-\sqrt{\frac{(1+4a^2x^2)^2}{16a^2b^2}-1} + \cos^{-1}\frac{4ab}{1+4a^2x^2}\right]_0^{x_L}$$

Substituting for x_L

$$= \frac{1}{\pi}\left[-\sqrt{\frac{\left(\sqrt{16a^2b^2+\frac{1}{4}}+\frac{1}{2}\right)^2-1}{16a^2b^2}} + \cos^{-1}\frac{4ab}{\sqrt{16a^2b^2+\frac{1}{4}}+\frac{1}{2}}\right.$$

$$\left. + \sqrt{\frac{1}{16a^2b^2}-1} - \cos^{-1}4ab\right]$$

Collecting terms

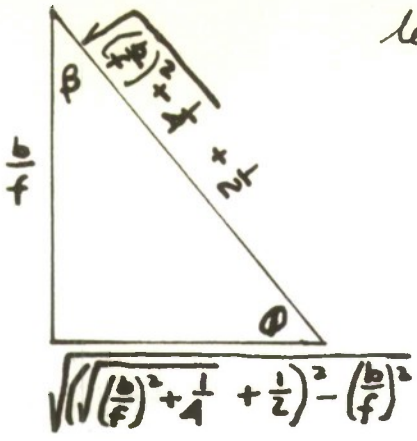
$$\text{Blockage} = \frac{1}{\pi}\left[2\tan^{-1}\sqrt{\sqrt{16a^2b^2+\frac{1}{4}}-\frac{1}{2}} - \sqrt{\frac{\left(\sqrt{16a^2b^2+\frac{1}{4}}+\frac{1}{2}\right)^2-1}{16a^2b^2}}\right.$$

$$\left. + \cos^{-1}\frac{4ab}{\sqrt{16a^2b^2+\frac{1}{4}}+\frac{1}{2}} + \sqrt{\frac{1}{16a^2b^2}-1} - \cos^{-1}4ab\right]$$

let $f = \frac{1}{4a}$

$$\text{Blockage} = \frac{1}{\pi}\left[2\tan^{-1}\sqrt{\sqrt{\left(\frac{b}{f}\right)^2+\frac{1}{4}}-\frac{1}{2}} - \frac{f}{b}\sqrt{\left(\sqrt{\left(\frac{b}{f}\right)^2+\frac{1}{4}}+\frac{1}{2}\right)^2-\left(\frac{b}{f}\right)^2}\right.$$

$$\left. + \cos^{-1}\frac{b/f}{\sqrt{\left(\frac{b}{f}\right)^2+\frac{1}{4}}+\frac{1}{2}} + \frac{f}{b}\sqrt{1-\left(\frac{b}{f}\right)^2} - \cos^{-1}\frac{b}{f}\right]$$



let $\beta = \cos^{-1} \dfrac{\frac{b}{f}}{\sqrt{(\frac{b}{f})^2+\frac{1}{4}}+\frac{1}{2}}$

Note: angles β and φ are not the same angles used in Appendices V & VI

$$\varphi = \tan^{-1} \frac{b/f}{\sqrt{(\sqrt{(\frac{b}{f})^2+\frac{1}{4}}+\frac{1}{2})^2-(\frac{b}{f})^2}}$$

$$= \tan^{-1} \frac{b/f}{\sqrt{(\frac{b}{f})^2+\frac{1}{4}+\sqrt{(\frac{b}{f})^2+\frac{1}{4}}+\frac{1}{4}-(\frac{b}{f})^2}}$$

$$= \tan^{-1} \frac{b/f}{\sqrt{\sqrt{(\frac{b}{f})^2+\frac{1}{4}}+\frac{1}{2}}} \cdot \frac{\sqrt{\sqrt{(\frac{b}{f})^2+\frac{1}{4}}-\frac{1}{2}}}{\sqrt{\sqrt{(\frac{b}{f})^2+\frac{1}{4}}-\frac{1}{2}}}$$

$$= \tan^{-1} \frac{\frac{b}{f}\sqrt{\sqrt{(\frac{b}{f})^2+\frac{1}{4}}-\frac{1}{2}}}{\sqrt{(\sqrt{(\frac{b}{f})^2+\frac{1}{4}})^2-\frac{1}{4}}}$$

$$\varphi = \tan^{-1} \frac{\frac{b}{f}\sqrt{\sqrt{(\frac{b}{f})^2+\frac{1}{4}}-\frac{1}{2}}}{\sqrt{(\frac{b}{f})^2+\frac{1}{4}-\frac{1}{4}}} = \tan^{-1} \sqrt{\sqrt{(\frac{b}{f})^2+\frac{1}{4}}-\frac{1}{2}}$$

also $\tan \beta = \frac{f}{b}\sqrt{(\sqrt{(\frac{b}{f})^2+\frac{1}{4}}+\frac{1}{2})^2-(\frac{b}{f})^2} = \frac{f}{b}\sqrt{\sqrt{(\frac{b}{f})^2+\frac{1}{4}}+\frac{1}{2}}$

then

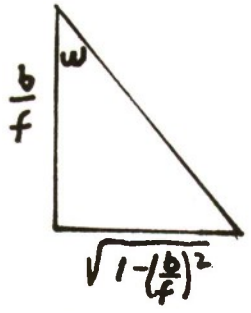
$$2\tan^{-1}\sqrt{\sqrt{\left(\frac{b}{f}\right)^2+\frac{1}{4}}-\frac{1}{2}}-\frac{f}{b}\sqrt{\left(\sqrt{\left(\frac{b}{f}\right)^2+\frac{1}{4}}+\frac{1}{2}\right)^2-\left(\frac{b}{f}\right)^2}+\cos^{-1}\frac{b/f}{\sqrt{\left(\frac{b}{f}\right)^2+\frac{1}{4}}+\frac{1}{2}}$$

may be replaced by

$$2\phi-\tan\beta+\beta=2\left(\frac{\pi}{2}-\beta\right)-\tan\beta+\beta$$

$$=\pi-\beta-\tan\beta$$

$$=\pi-\frac{f}{b}\sqrt{\sqrt{\left(\frac{b}{f}\right)^2+\frac{1}{4}}+\frac{1}{2}}-\tan^{-1}\frac{f}{b}\sqrt{\sqrt{\left(\frac{b}{f}\right)^2+\frac{1}{4}}+\frac{1}{2}}$$



$$\omega=\cos^{-1}\frac{b}{f}$$

then

$$\frac{f}{b}\sqrt{1-\left(\frac{b}{f}\right)^2}-\cos^{-1}\frac{b}{f}=\tan\omega-\omega$$

$$=\tan\left(\cos^{-1}\frac{b}{f}\right)-\cos^{-1}\frac{b}{f}$$

therefore

$$\text{Blockage}=\frac{1}{\pi}\left[\pi-\frac{f}{b}\sqrt{\sqrt{\left(\frac{b}{f}\right)^2+\frac{1}{4}}+\frac{1}{2}}-\tan^{-1}\frac{f}{b}\sqrt{\sqrt{\left(\frac{b}{f}\right)^2+\frac{1}{4}}+\frac{1}{2}}\right.$$

$$\left.-\cos^{-1}\frac{b}{f}+\tan\left(\cos^{-1}\frac{b}{f}\right)\right]$$

To save computation time, the above equation has been solved for all possible values of (b/f), (0 to $\pi/2$), and the results plotted in Fig. 91.

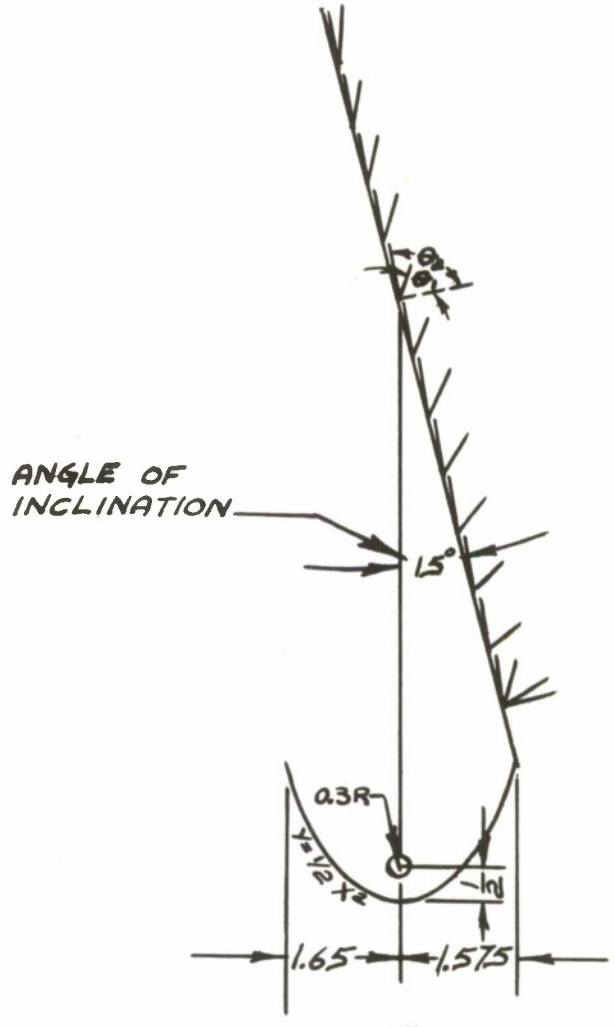
APPENDIX IX

SAMPLE CALCULATION FOR EXPERIMENTAL REFLECTOR TESTS

The detailed calculations for run no. 1, Figure 94, are presented herein.

Predicted Results

The incident radiant energy distribution on a 12 inch length receiver was determined for an infinitely long radiator by the semi-graphical method. A design chart, similar to Figure 82 was constructed for the parabola curve $y = \frac{1}{2}x^2$ with a 0.6 inch circular source at the focus. A sheet of paper, representing the receiver, was oriented with respect to the chart reflector as in the actual test set-up. The intercepted angle, the angle over which the source can be 'seen' directly or by reflection, was determined at 12 equally spaced stations on the receiver. The intensity at each station was then



determined by Eq. (2) of Appendix IV.

$$\frac{Q}{dA_1} = \frac{\pi I}{2} \sin \theta \Big]_{\theta_1}^{\theta_2}$$

The result of this computation is shown in column two of Table I.

The angle, ϕ_R, shown in the diagram of Appendix V was determined by trigonometric means for each station. The effective length of the source was 24.25 inches on each side of the receiver row of stations. The angle was measured to the center of the source extreme. Because the source is symmetrically located, the angle ϕ to the left and right are equal. The value of ϕ for each station is listed in column three of Table I.

The correction for finite length and reflection from the receiver surface was next determined from Figure 88 for a constant $a = 75^\circ$. This is the complement of the angle formed by the receiver plane and the centerline of the parabola, the angle of inclination. In the derivation of the equation for Figure 88, it was indicated that a was an average value of θ_1 and θ_2 at each point. Use of such values yielded intensity variations twice as great and average intensities 10% greater than that obtained by considering a a constant for any angle of inclination. Because the latter method agreed so much better with experimental results, it was used in the comparison. However, it is possible that the variation of absorbed energy is as indicated by the former method and the conduction of heat within the Plexiglas made the experimental temperature distribution more uniform.

The correction factors, F', as determined from Figure 88 and multiplied by 2 to account for both the left and right sides are shown in column four.

The product of $\frac{Q}{dA}$ and F', column 5, represents the intensity of radiant energy, from the source-reflector combination, passing through the surface of the receiver. For a plexiglas receiver and low source temperature, it also represents the absorbed energy. The average intensity is $.104 \times \frac{W}{2}$ and the maximum variation is 10/1. The source covering was chrome-steel. Assuming an effective reflectivity of reflector of 0.95, a source emissivity of 0.65, the value of W at 640°F is determined as follows:

$$W = \epsilon \sigma T^4 = .95 \times .65 \times .173 \left(\frac{1100}{100}\right)^4 = 1560 \text{ BTU / hr, ft}^2$$

TABLE I

1	2	3	4	5
Station	Q/dA BTU/hr,ft²	φ degrees	F'	$\frac{Q'}{dA_1} = \frac{Q}{dA_1} \times F'$
1	.422 × $\frac{\pi_2}{2}$	4.4	.664	.280 × $\frac{W}{2}$
2	.367	6.0	.664	.244
3	.219	7.8	.664	.146
4	.190	9.8	.664	.126
5	.133	12.0	.662	.088
6	.133	14.0	.662	.088
7	.100	16.2	.66	.066
8	.093	18.3	.66	.062
9	.085	20.1	.658	.056
10	.059	22.4	.654	.038
11	.048	24.3	.652	.032
12	.043	26.2	.65	.028
			Sum	1.254 × $\frac{W}{2}$
			Average	.104 × $\frac{W}{2}$

Max. Variation $= \frac{.280}{.028} = 10/1$

Hence the average heat absorption is:

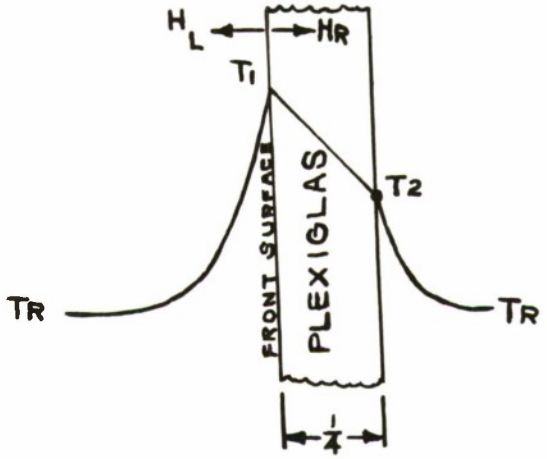
$$\frac{Q'}{dA_1} = .104\,\frac{W}{2} = \frac{.104 \times 1560}{2} = 81 \quad BTU/hr, ft^2$$

Experimental Results

The pertinent test results were as follows:

Room temperature = 81°F
Average receiver surface temperature rise = 23.5°F
Maximum receiver surface temperature rise variation = 10.6/1
Source surface temperature = 640°F

From the above data, the heat loss from the receiver, and hence the heat gain by radiation, was determined in the following manner. The radiation was assumed to be absorbed in a very thin layer at the plexiglas front surface (See Figure 33).



The natural convection coefficient at the midpoint was calculated from (Ref. 27):

$$h_c = 0.28\left(\frac{\Delta T}{.5}\right)^{0.25} \quad BTU/hr, ft^2, °F$$

The radiation coefficient for the radiation loss from the surface to the surroundings, is:

$$h_r = \frac{\left[\left(\frac{T}{100}\right)^4 - \left(\frac{T_R}{100}\right)^4\right] \times .173}{T - T_R} \quad BTU/hr, ft^2, °F$$

The conductivity of plexiglas, k, is 1.5 BTU/hr, ft^2 $^\circ$F/in

For $T_R = (81 + 460)^\circ F$ and average $\Delta T = 23.5^\circ F$ the calculated value of $(h_c + h_r)$ is 1.91 BTU/hr, ft^2, $^\circ$F. Hence the heat loss to the left is:

$$H = 1.92 \times 23.5 = 45 \text{ BTU/hr, ft}^2$$

The heat loss to right was solved by a trial and error method. On the last try, it was assumed that the combined coefficient for the back surface, $(h_c + h_r)$ was equal to 1.84. The back surface temperature, T_z, was therefore:

$$T_z = 81 + 23.5 \frac{k/x}{\frac{k}{x} + (h_c + h_r)}$$

$$T_z = 81 + 23.5 \frac{1.5/.25}{\frac{1.5}{.25} + 1.84} = 99^\circ F$$

Substituting this temperature into the equations for h_c and h_r yields 1.84, which checks with the original assumption. Hence the heat loss to the right is:

$$H_R = (h_c + h_r)\Delta T = 1.84\,(99-81) = 33.1 \text{ BTU/hr, ft}^2$$

The total loss is therefore:

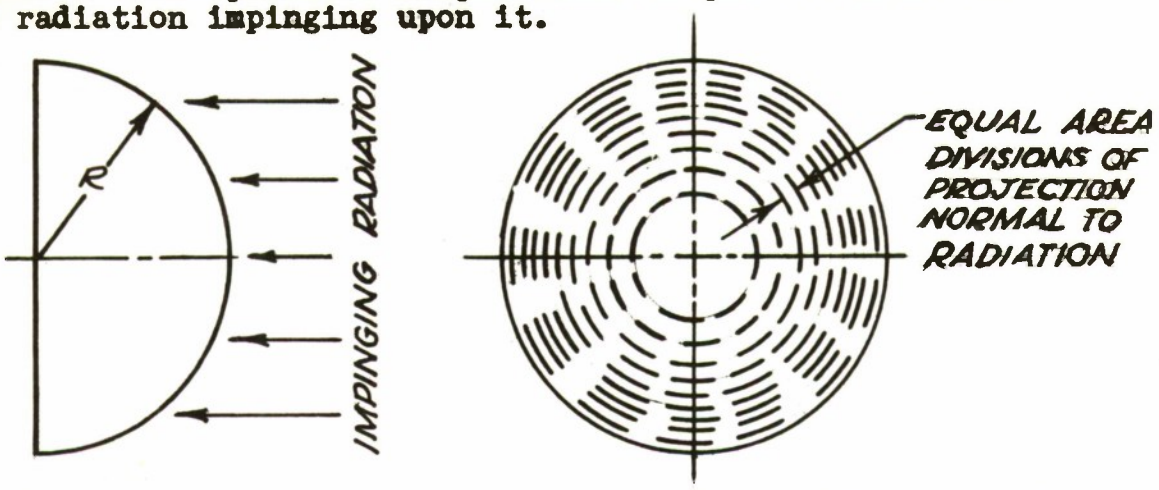
$$\frac{Q'}{dA_1} = H_R + H_c = 45 + 33.1 = 78.1 \text{ BTU/hr}$$

This compares well with the predicted value. Since these calculations are fairly rough, the close agreement in this particular case is fortuitous.

APPENDIX X

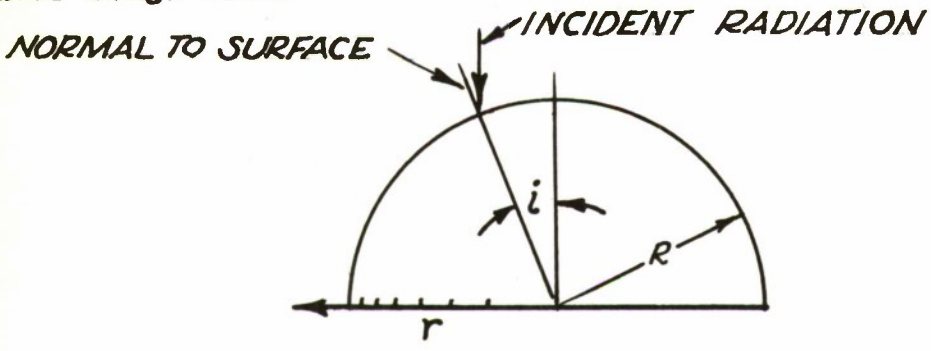
REFLECTION FROM A WATER DROPLET

Assume a hemi-spherical shaped water droplet with normal parallel radiation impinging upon it.



Equal area annular rings, of the projection of the droplet on a plane perpendicular to the incident radation, will contain equal amounts of incident energy. For the purposes of this calculation, the projection was divided into ten such equal annular areas. The ratio of the radius of the center of each of these rings to the droplet radius is listed in Column 2 of Table I.

The angle of incidence between the radiation path and the normal to the surface was computed at the center of each of these annular rings from:



$$i = \tan^{-1} \frac{r/R}{\sqrt{1-(r/R)^2}}$$

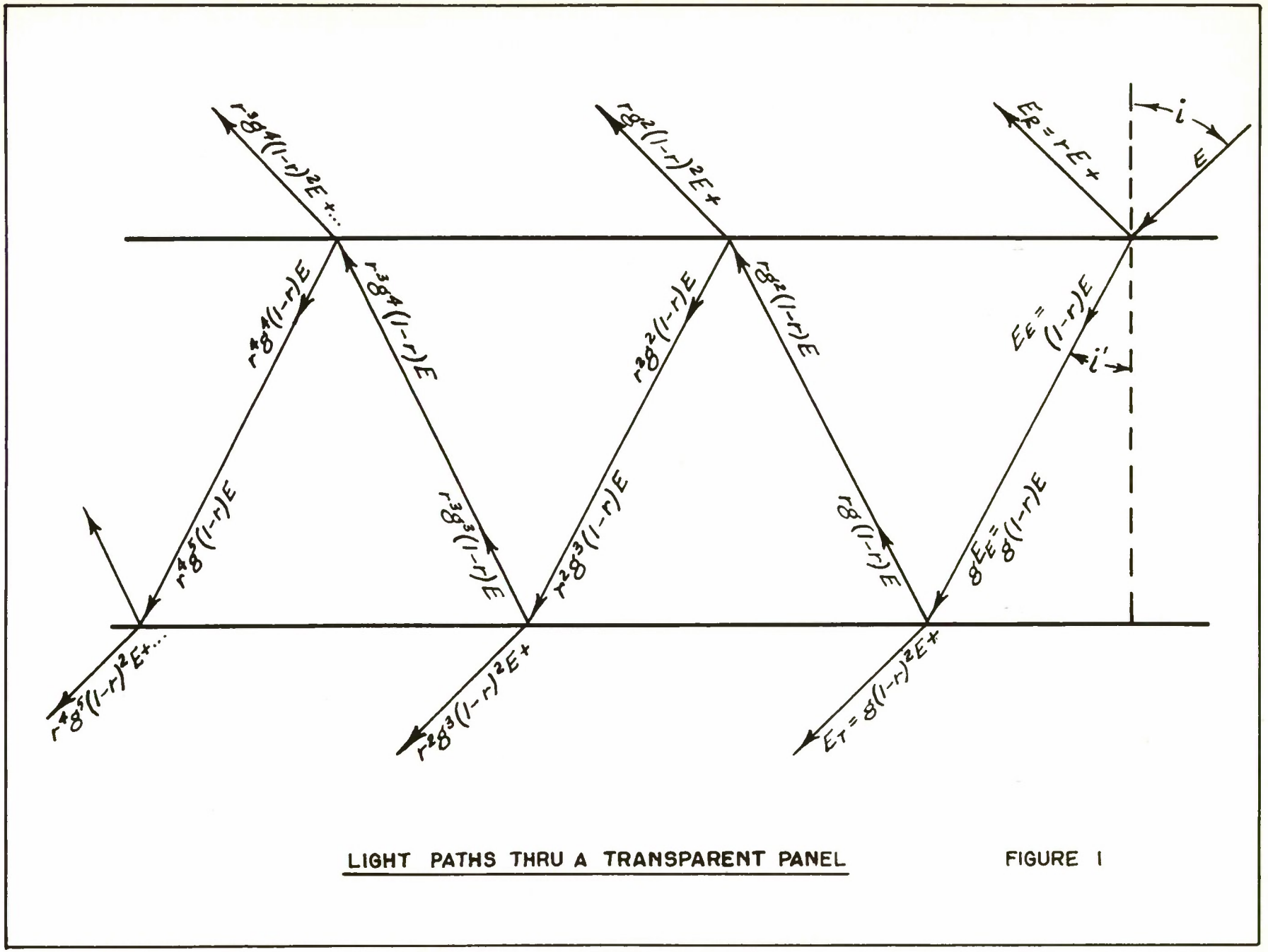
The computed angles are listed in Column 3 of the Table. Using a refractive index of 1.33 for water, the reflection was calculated from Fresnel's equation (Eq. 4, Section I) for each of these angles and are tabulated in Column 4. Since annular rings were chosen which had equal amounts of impinging energy, the average value of Column 4, 6 %, is the average reflection coefficient.

TABLE I

Annular Ring No.	Ratio of Ring to Droplet Radius, $r/_R$	Angle of Incidence, i Degrees	Reflection Coefficient %
1	.158	9.	2.1
2	.382	22.5	2.1
3	.498	30	2.1
4	.590	36	2.3
5	.670	42	2.5
6	.741	48	3.0
7	.806	55	4.3
8	.866	60	5.9
9	.922	67	10.2
10	.974	70	25.7
		10	60.2
		Average	6.0 %

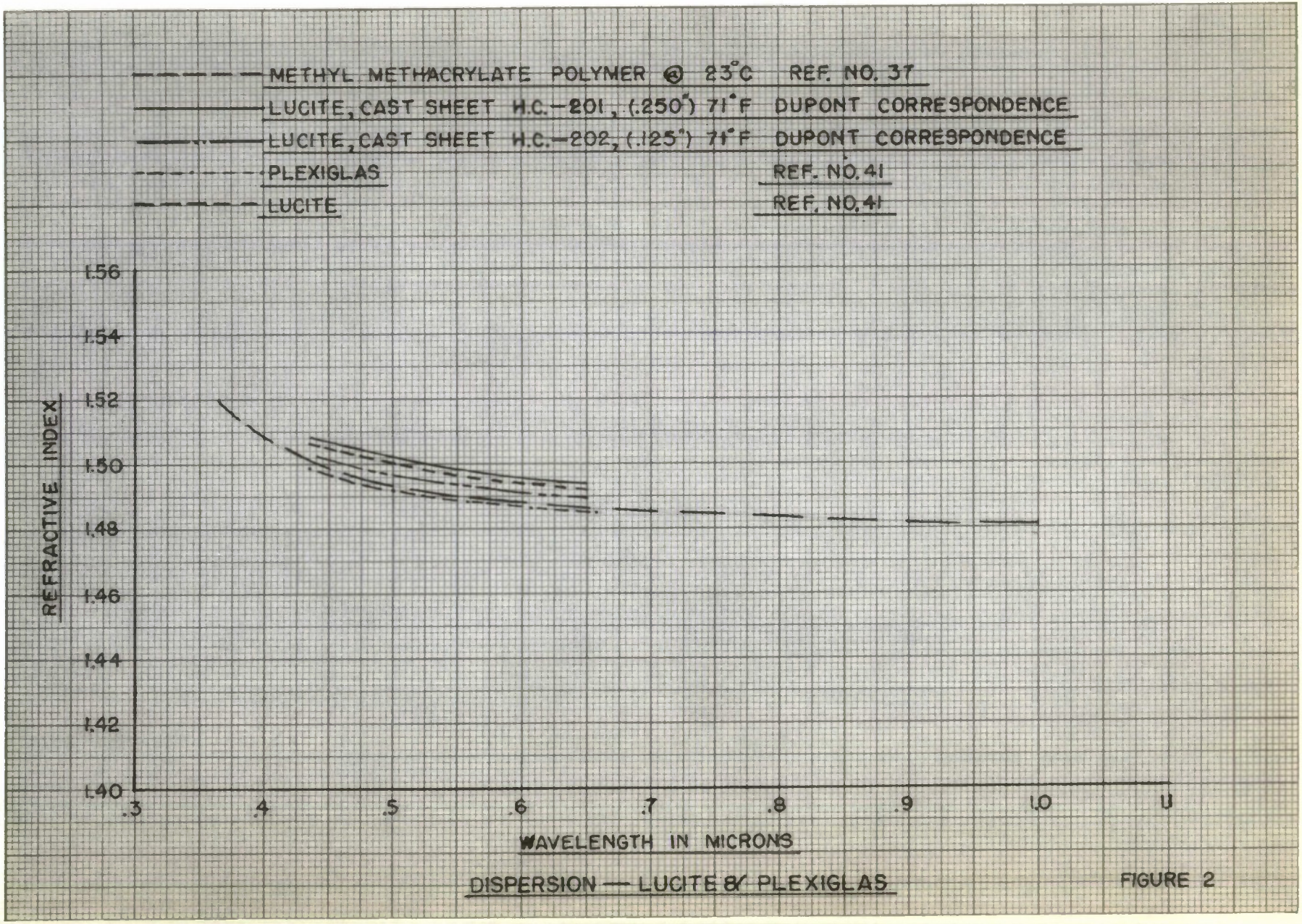
AFTR 5874

90



LIGHT PATHS THRU A TRANSPARENT PANEL

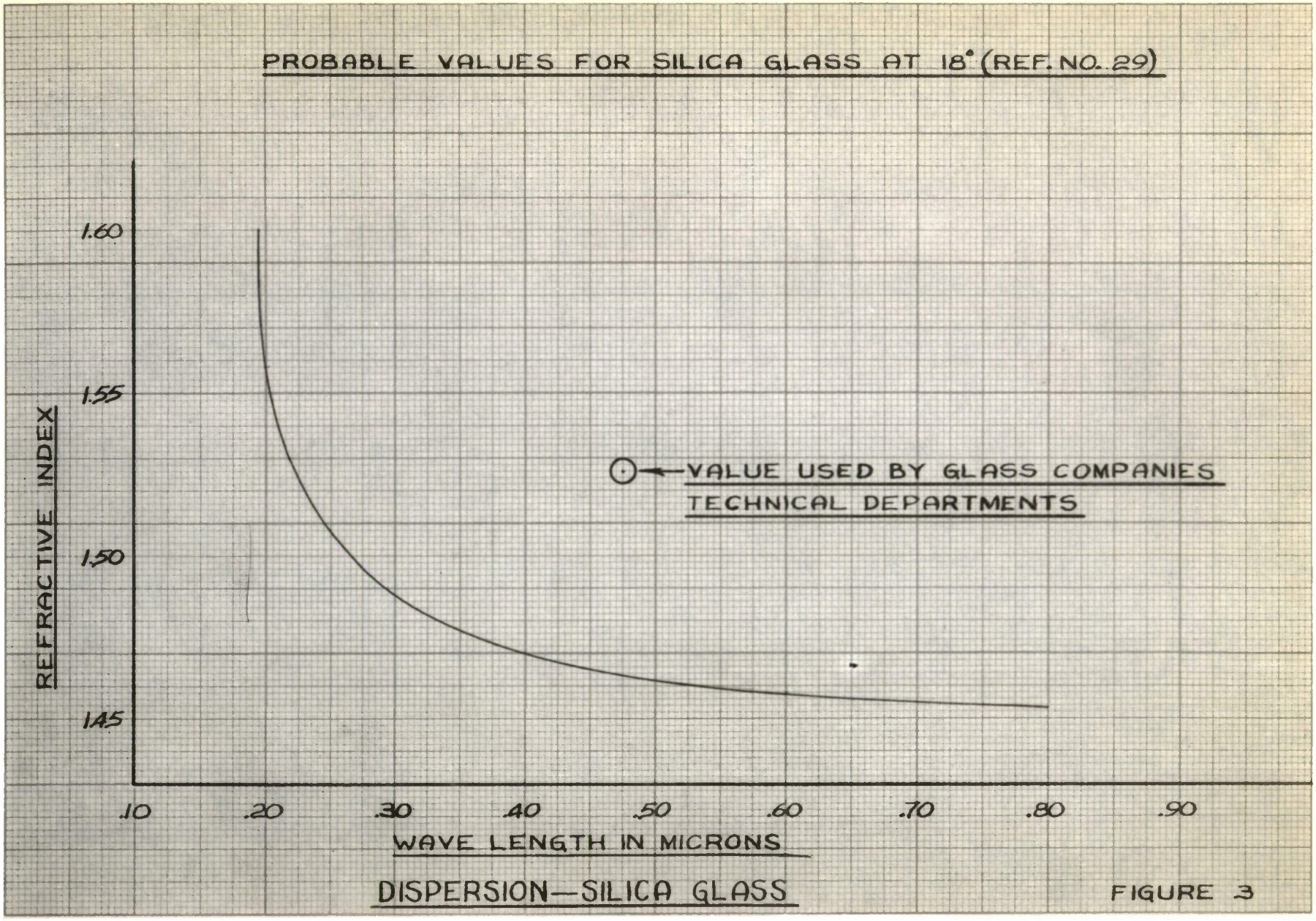
FIGURE 1



DISPERSION — LUCITE & PLEXIGLAS

FIGURE 2

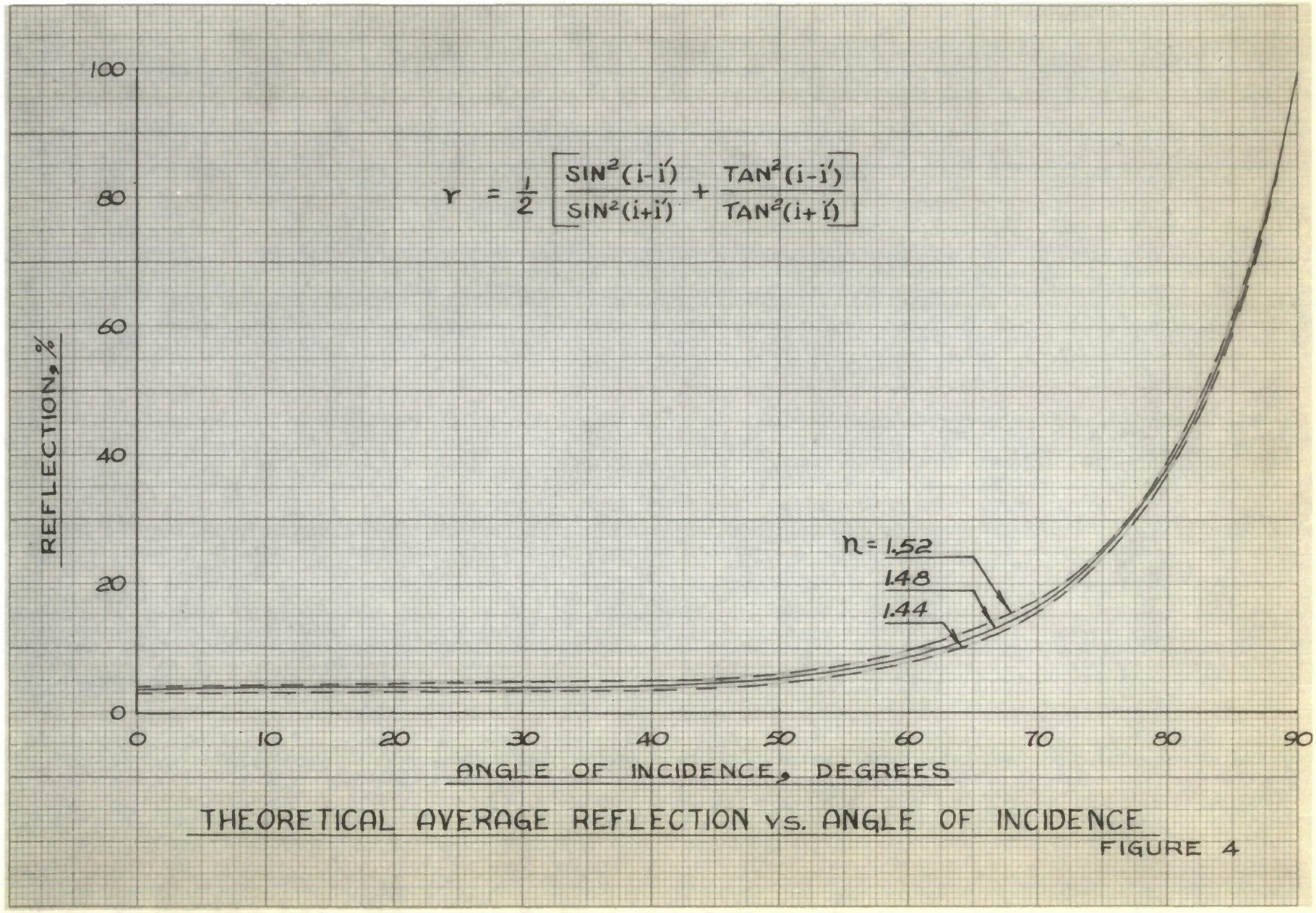
AFTR 5074



DISPERSION—SILICA GLASS

FIGURE 3

APER 58724

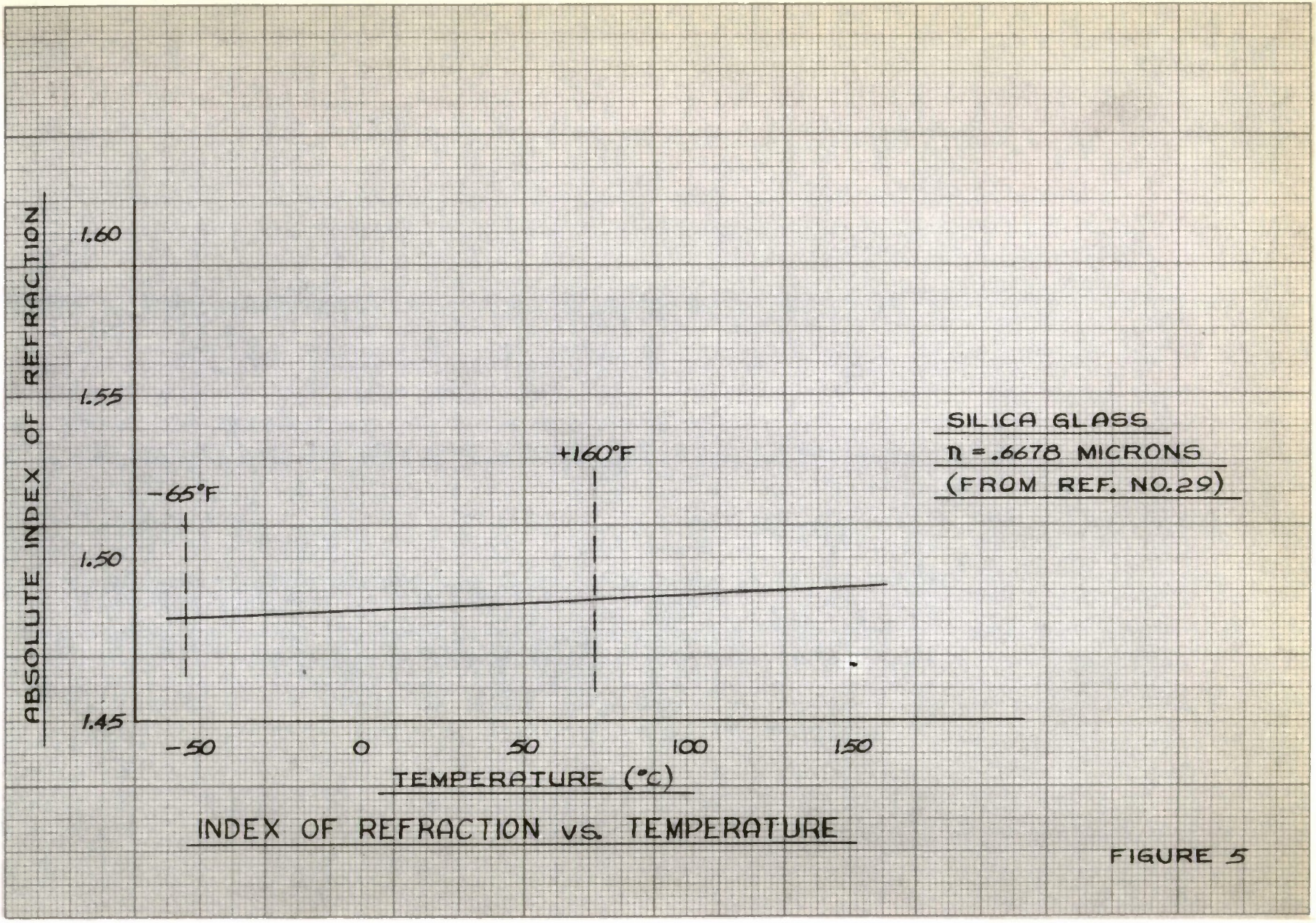


THEORETICAL AVERAGE REFLECTION vs. ANGLE OF INCIDENCE

FIGURE 4

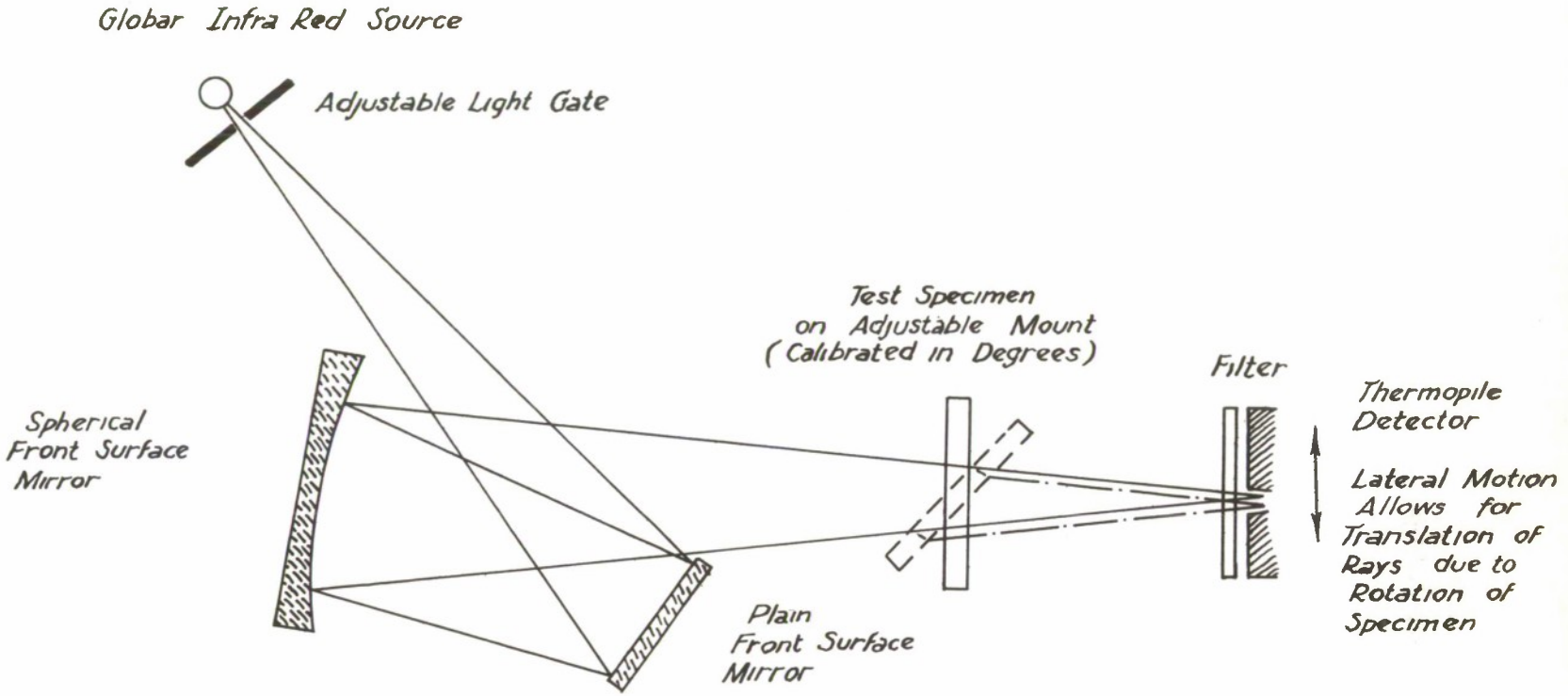
AFTR 5874

94



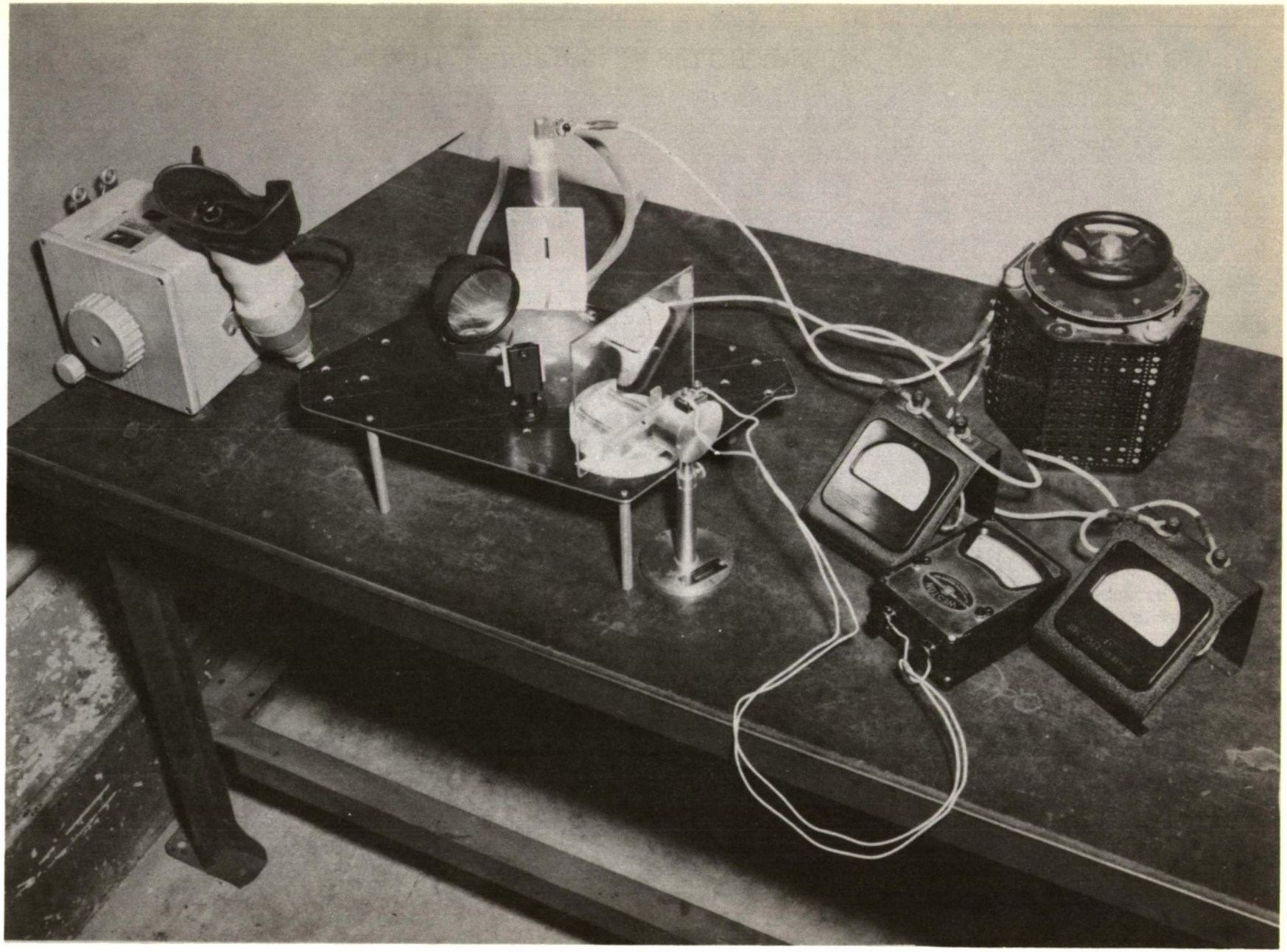
INDEX OF REFRACTION vs. TEMPERATURE

FIGURE 5



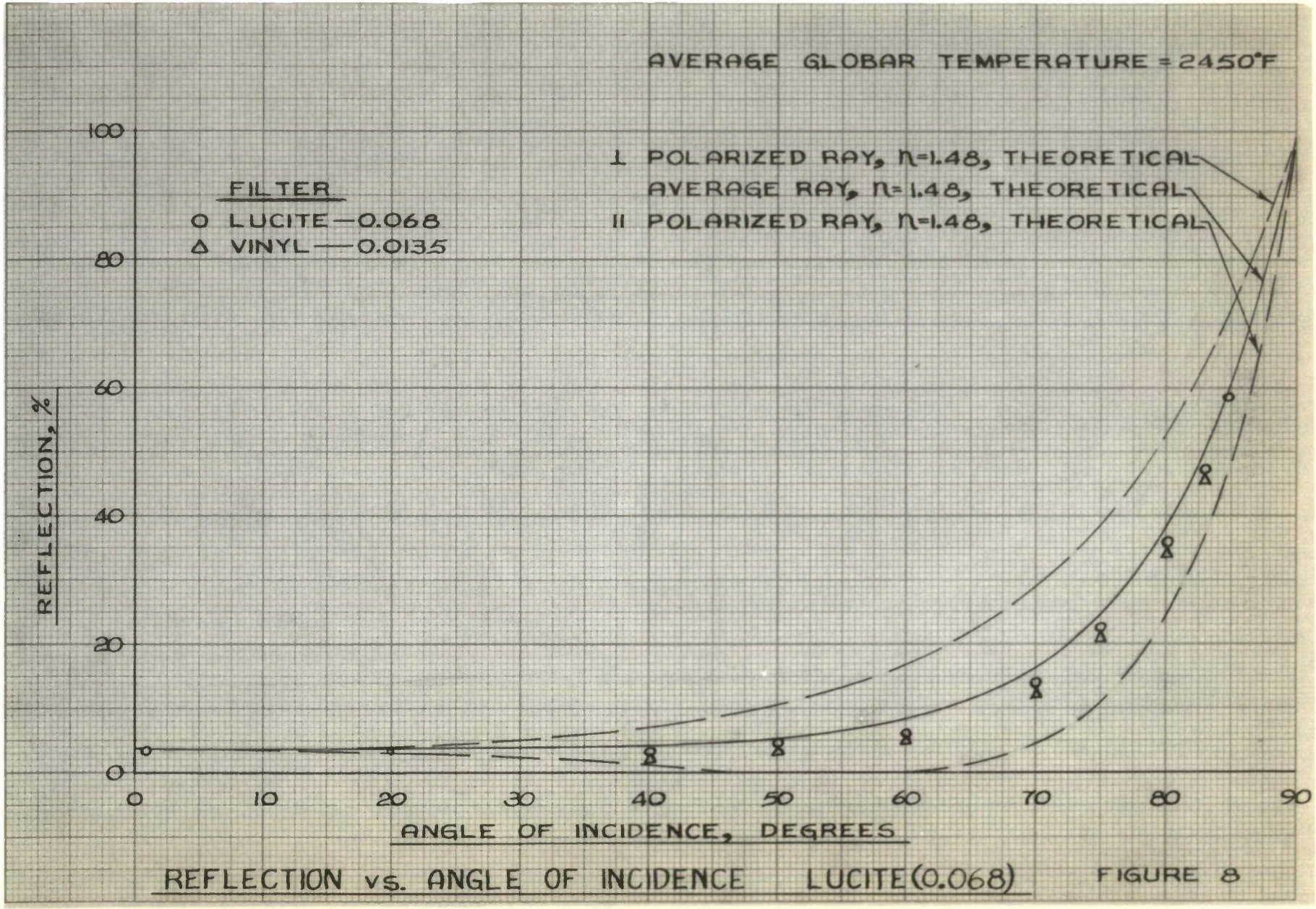
SCHEMATIC — PORTABLE SPECTROMETER

FIGURE 6



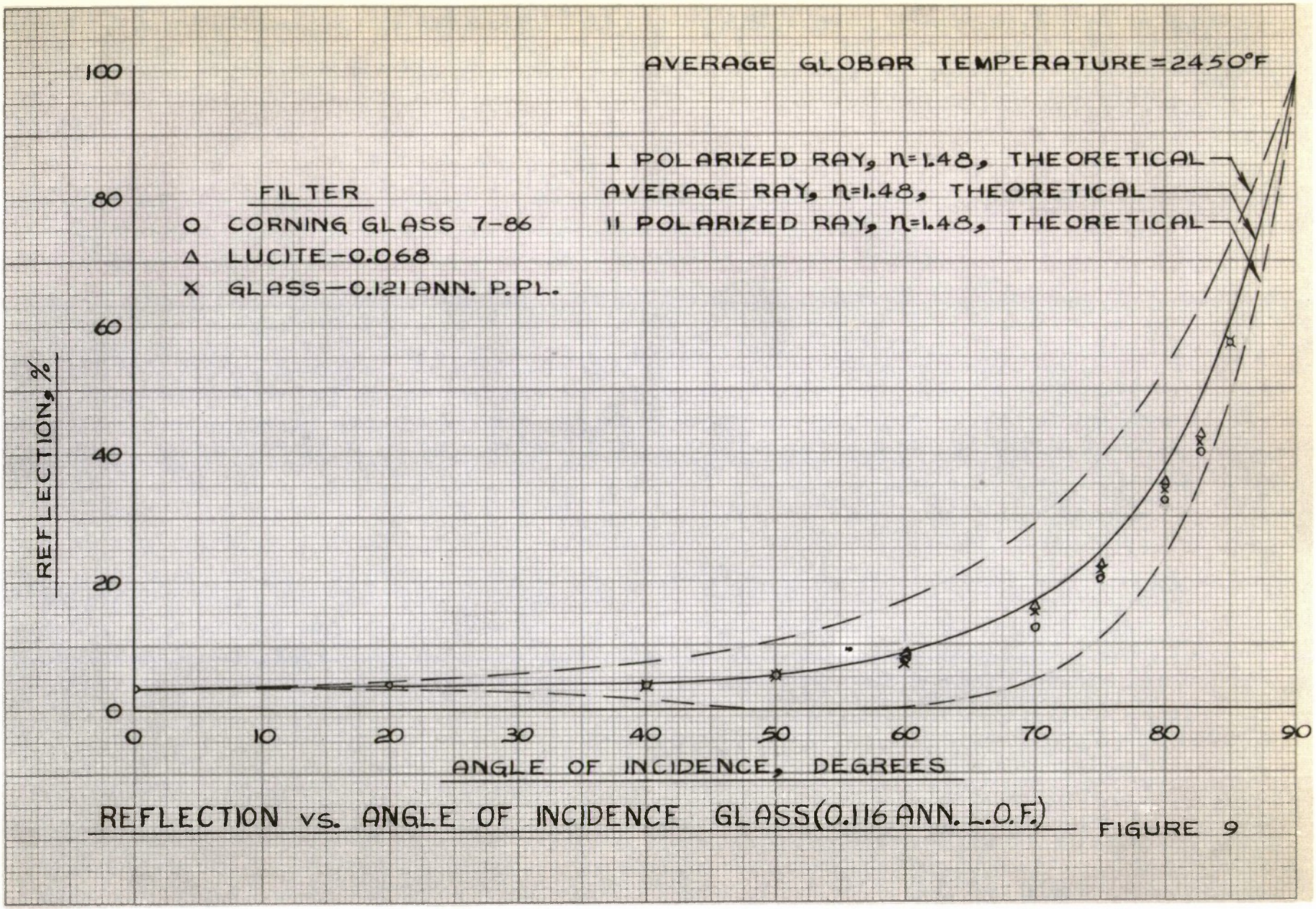
PORTABLE SPECTROMETER SET-UP

FIGURE 7



REFLECTION vs. ANGLE OF INCIDENCE LUCITE (0.068) FIGURE 8

AFTR 5874



REFLECTION vs. ANGLE OF INCIDENCE GLASS(0.116 ANN. L.O.F.)

FIGURE 9

AFTR 5874

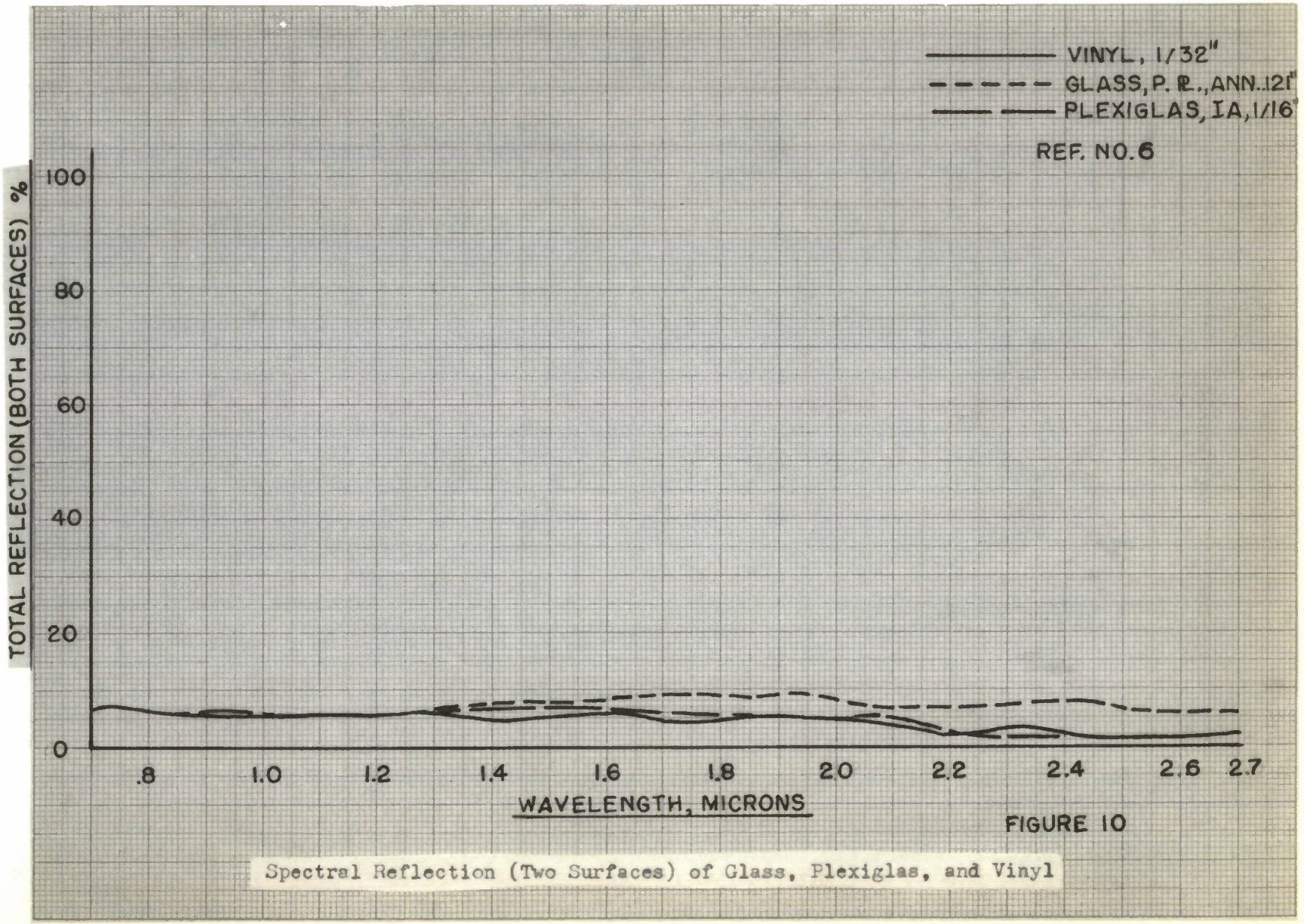
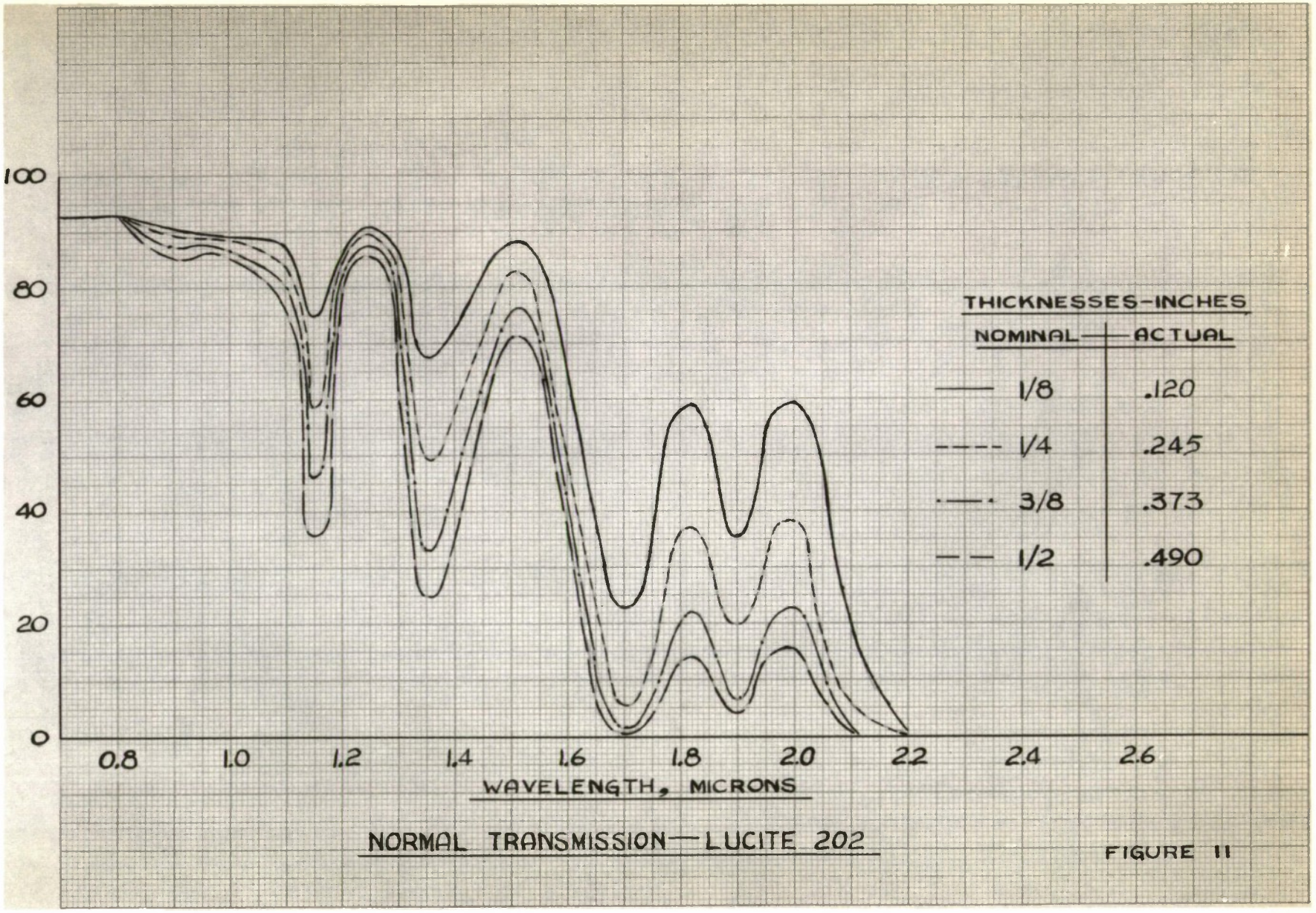


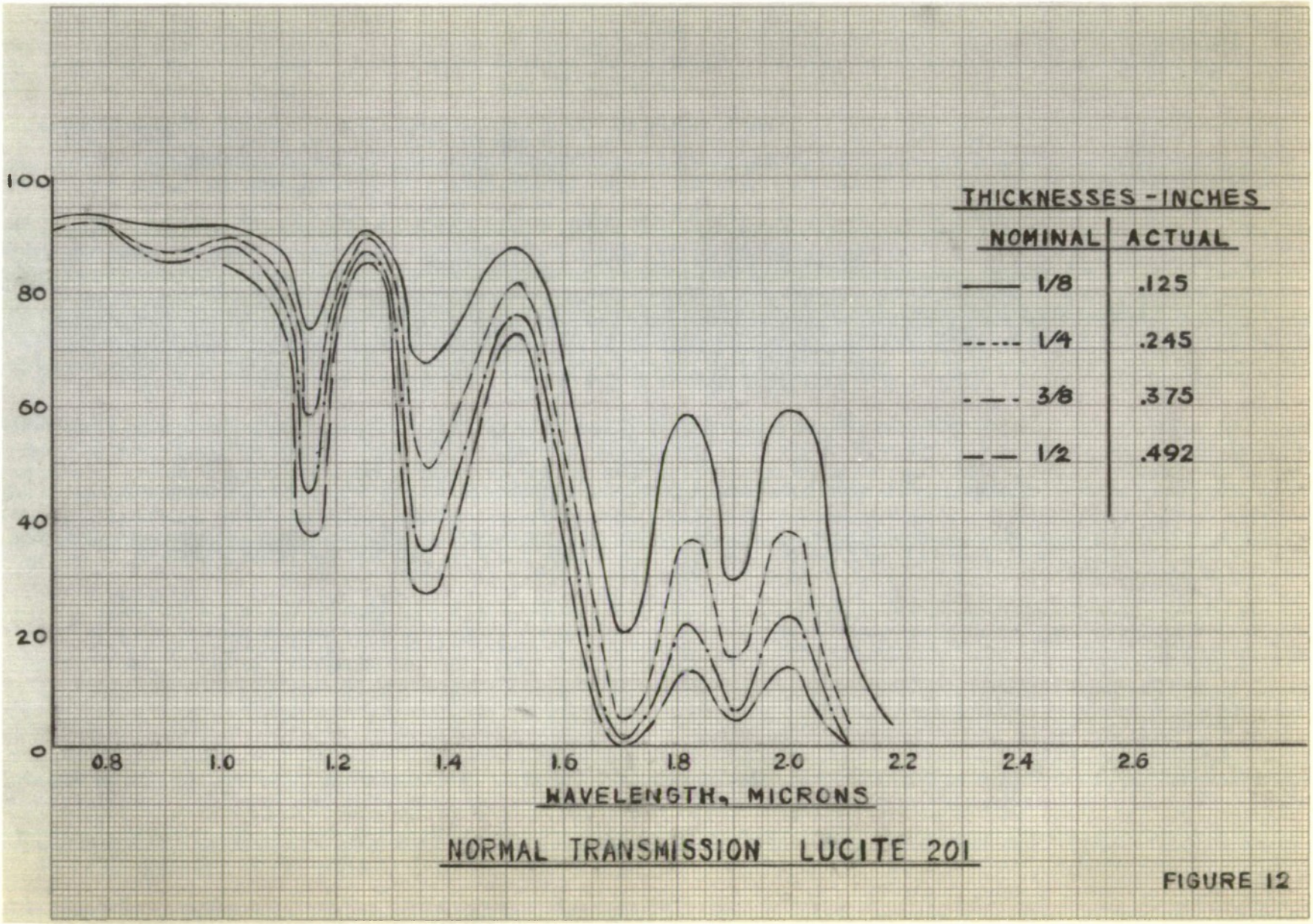
FIGURE 10

Spectral Reflection (Two Surfaces) of Glass, Plexiglas, and Vinyl



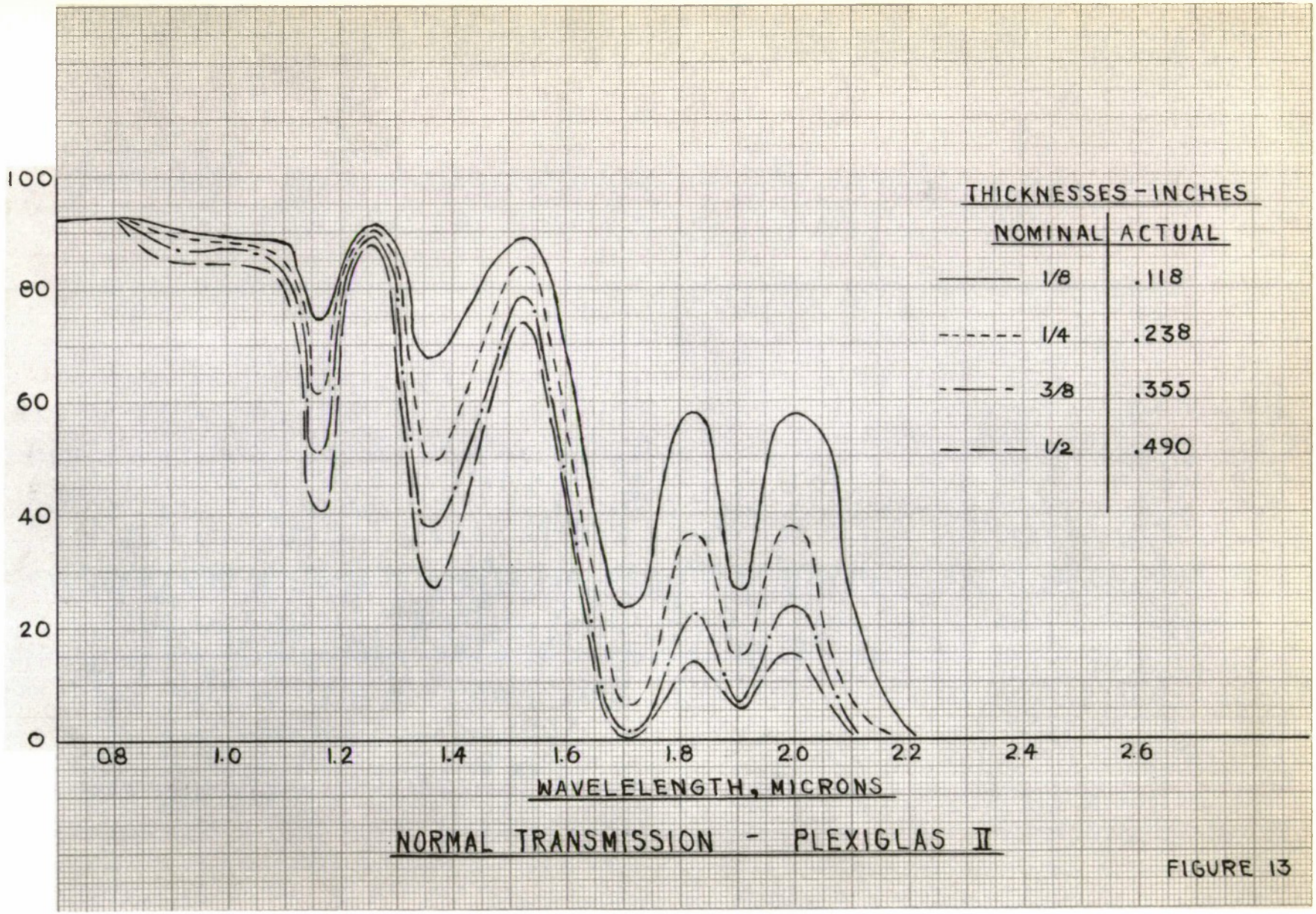
NORMAL TRANSMISSION — LUCITE 202

FIGURE 11



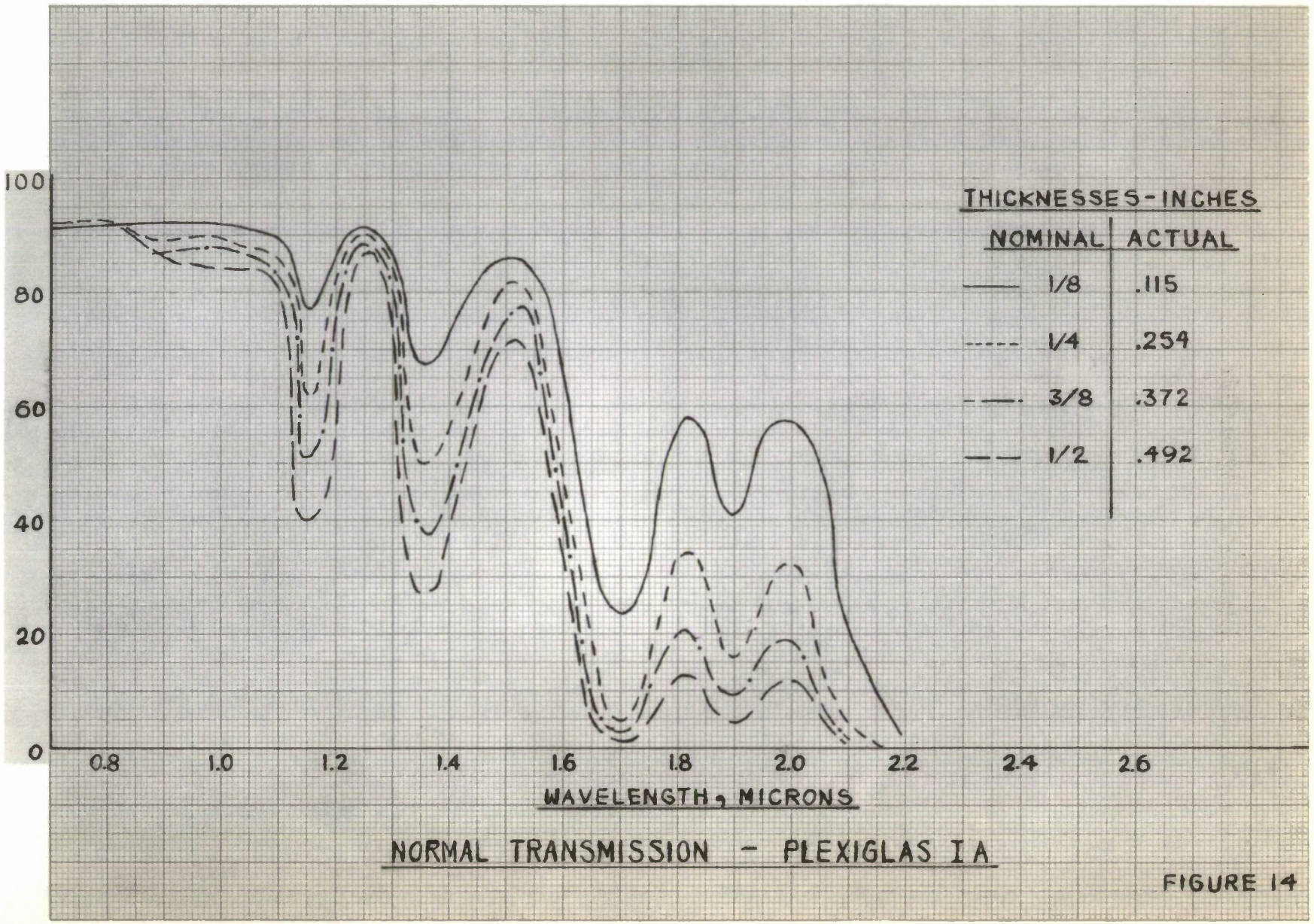
NORMAL TRANSMISSION LUCITE 201

FIGURE 12



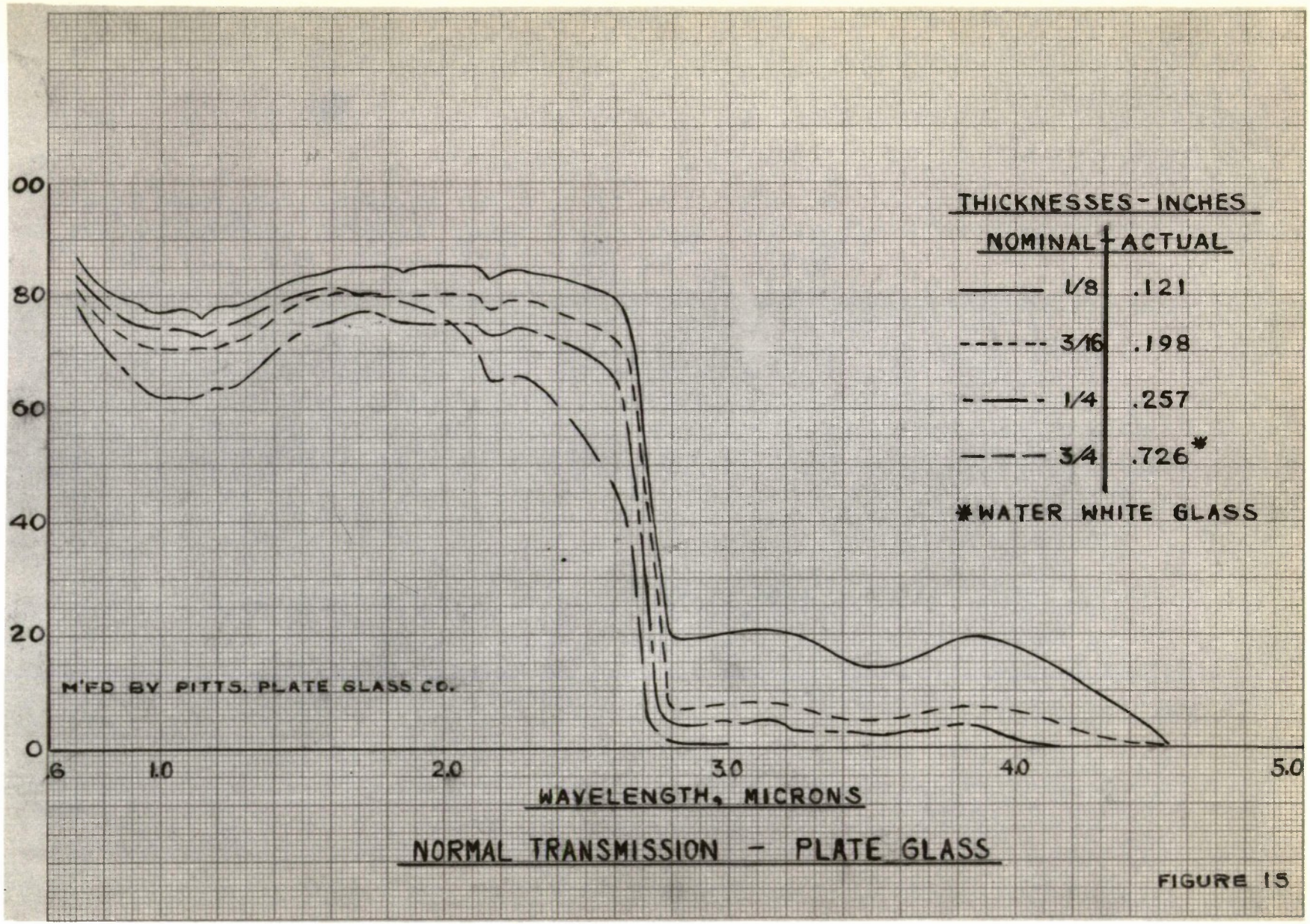
NORMAL TRANSMISSION - PLEXIGLAS II

FIGURE 13



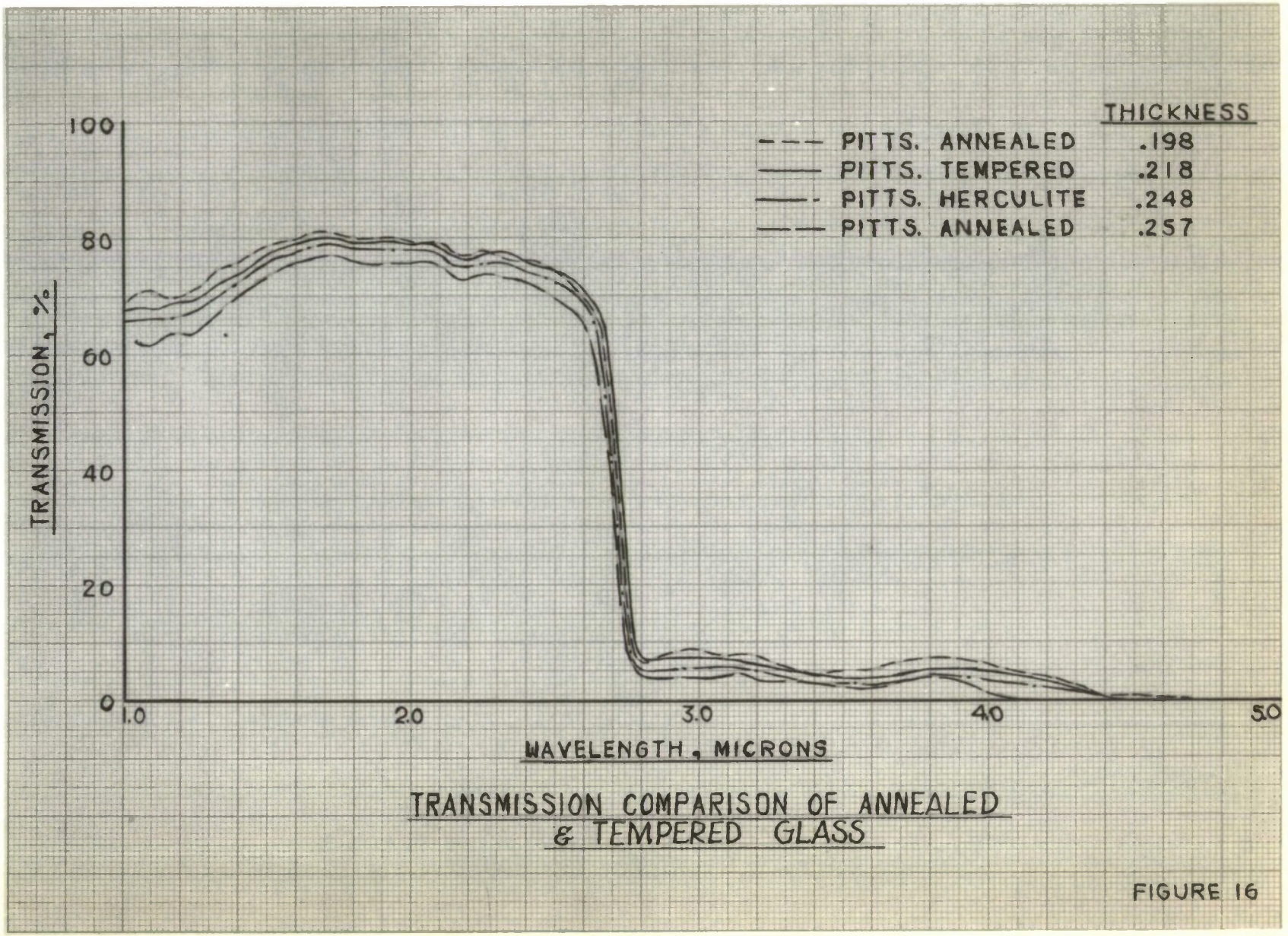
NORMAL TRANSMISSION - PLEXIGLAS I A

FIGURE 14



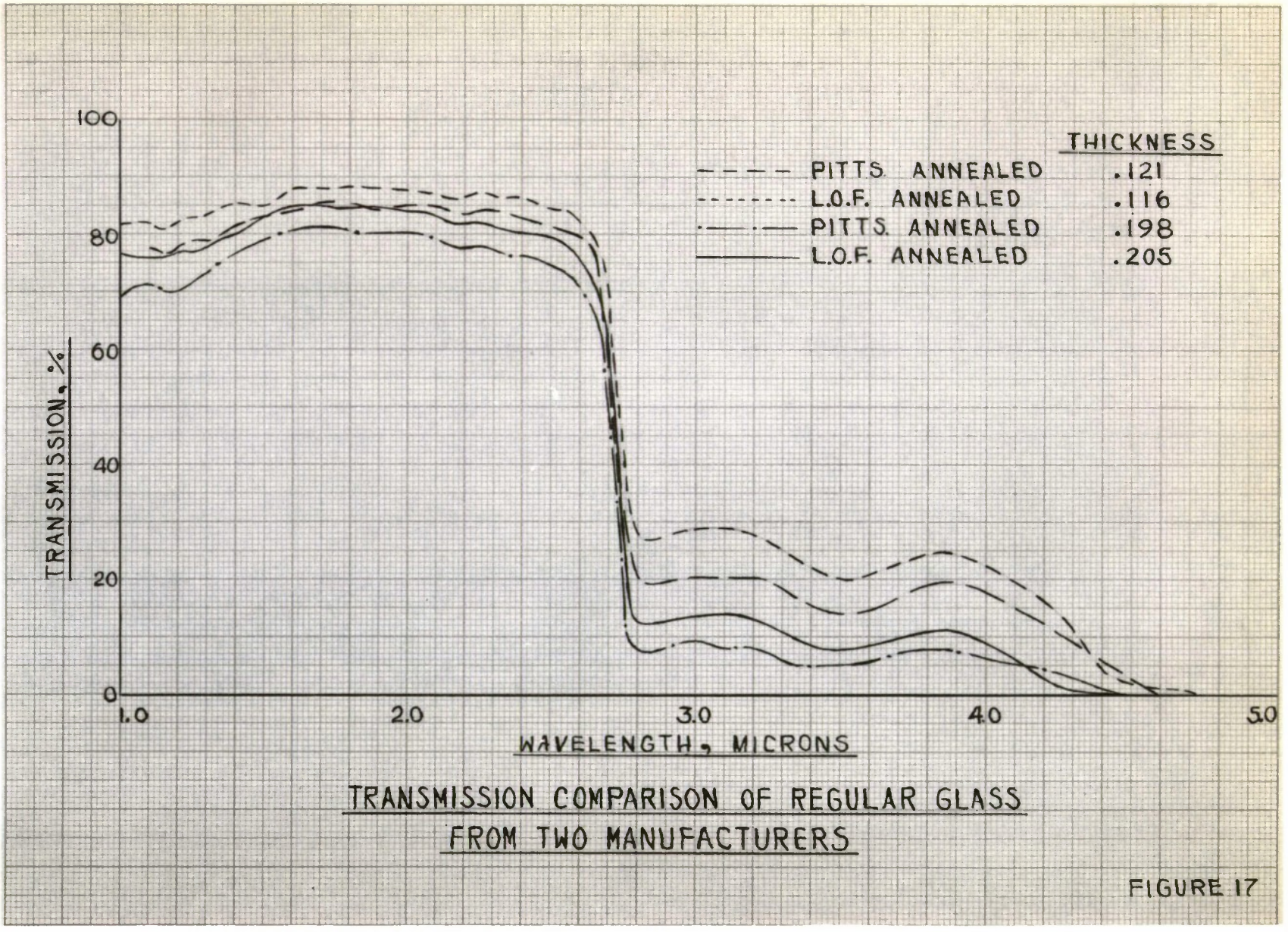
NORMAL TRANSMISSION - PLATE GLASS

FIGURE 15



TRANSMISSION COMPARISON OF ANNEALED & TEMPERED GLASS

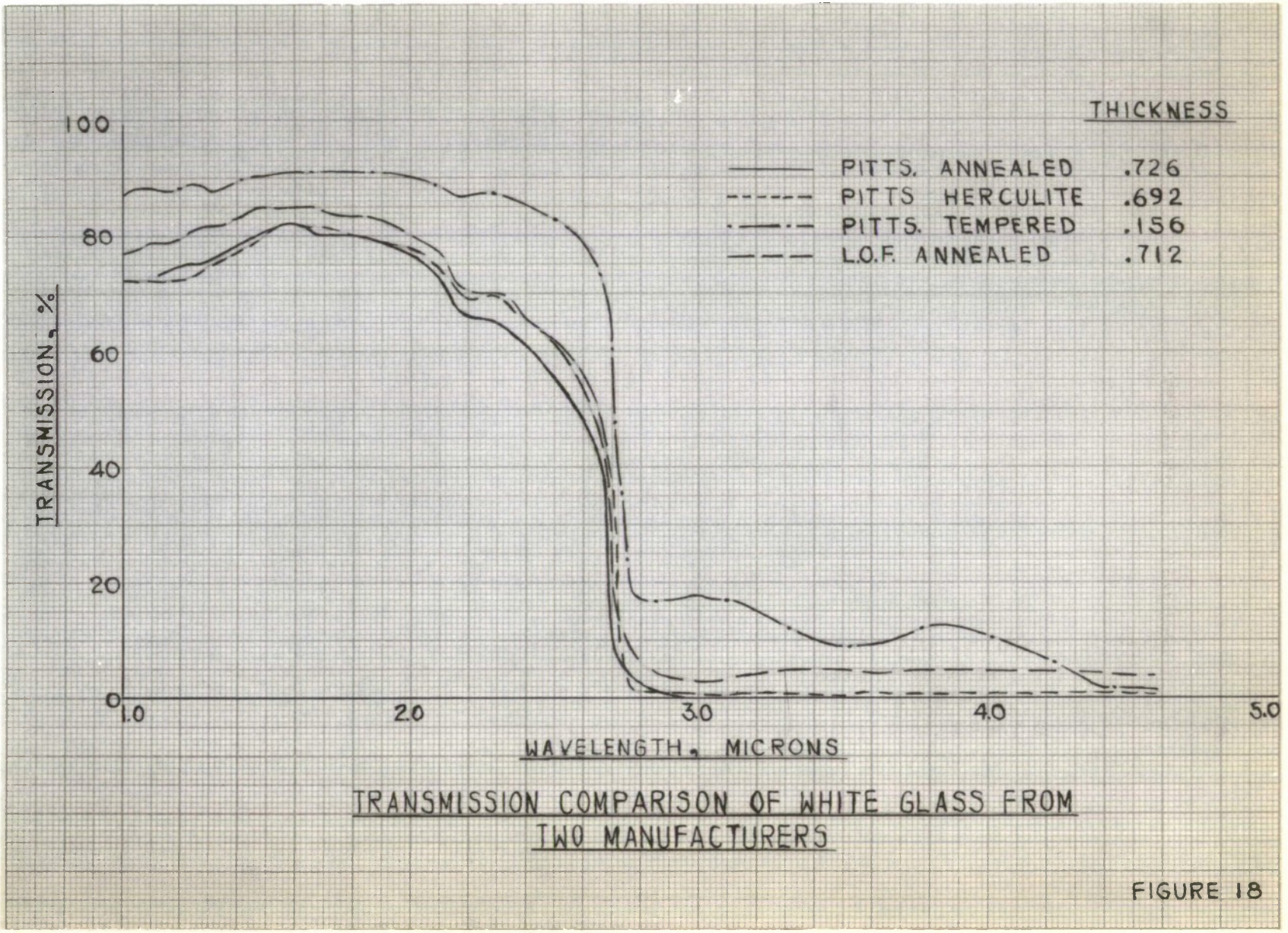
FIGURE 16



TRANSMISSION COMPARISON OF REGULAR GLASS FROM TWO MANUFACTURERS

FIGURE 17

AFTR 5854

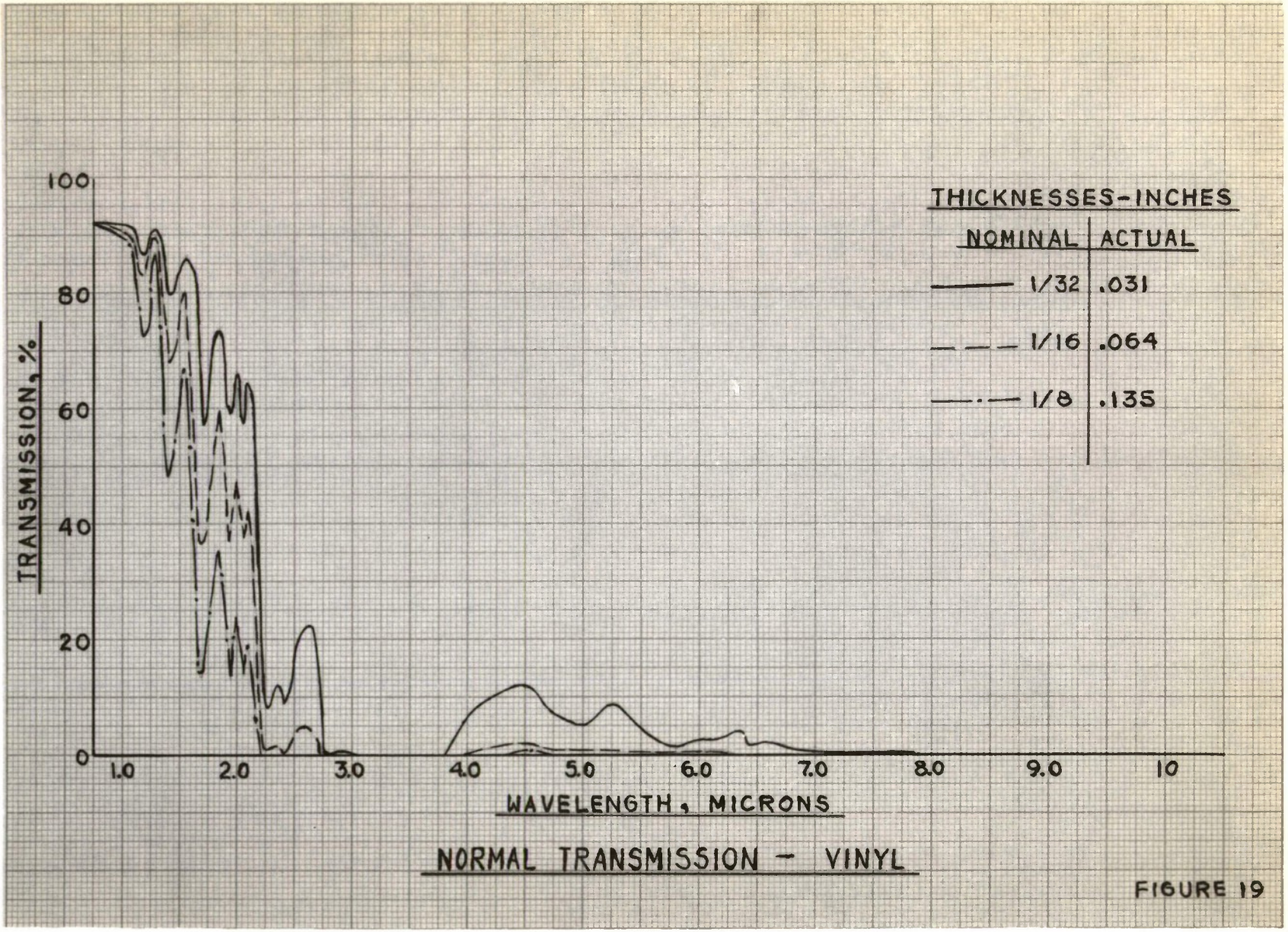


TRANSMISSION COMPARISON OF WHITE GLASS FROM TWO MANUFACTURERS

FIGURE 18

AFTR 5874

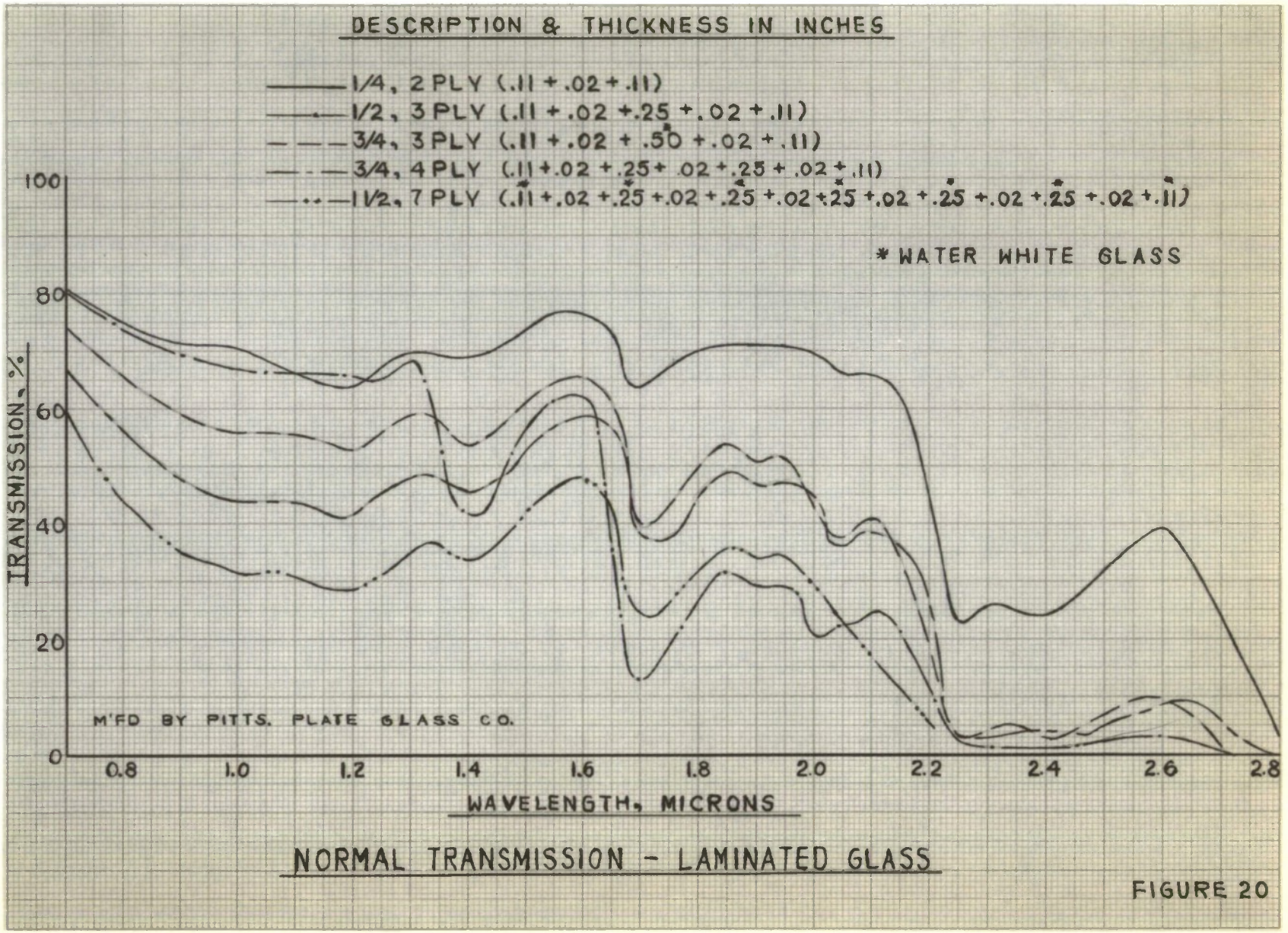
108



NORMAL TRANSMISSION - VINYL

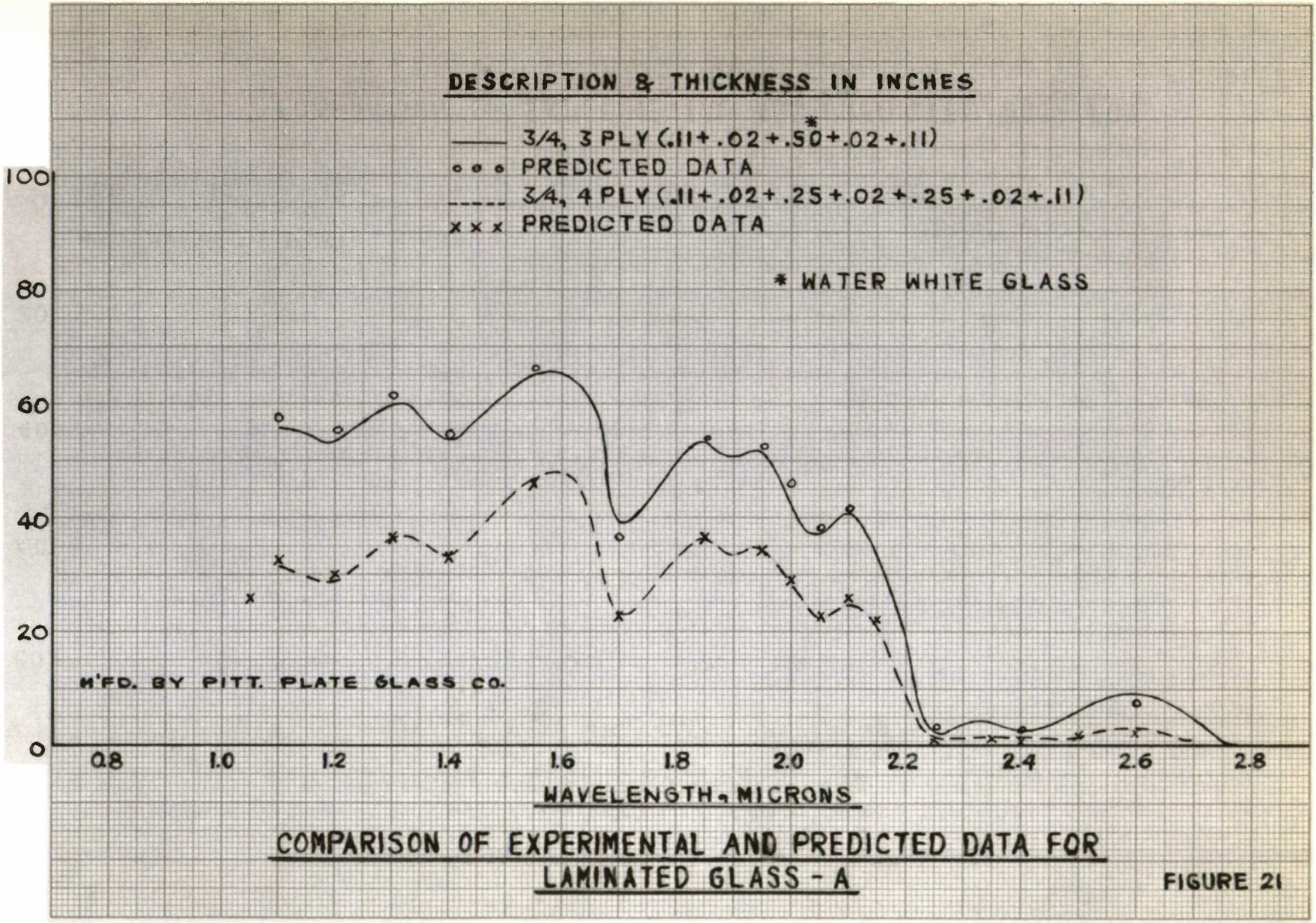
FIGURE 19

AFTR 5874



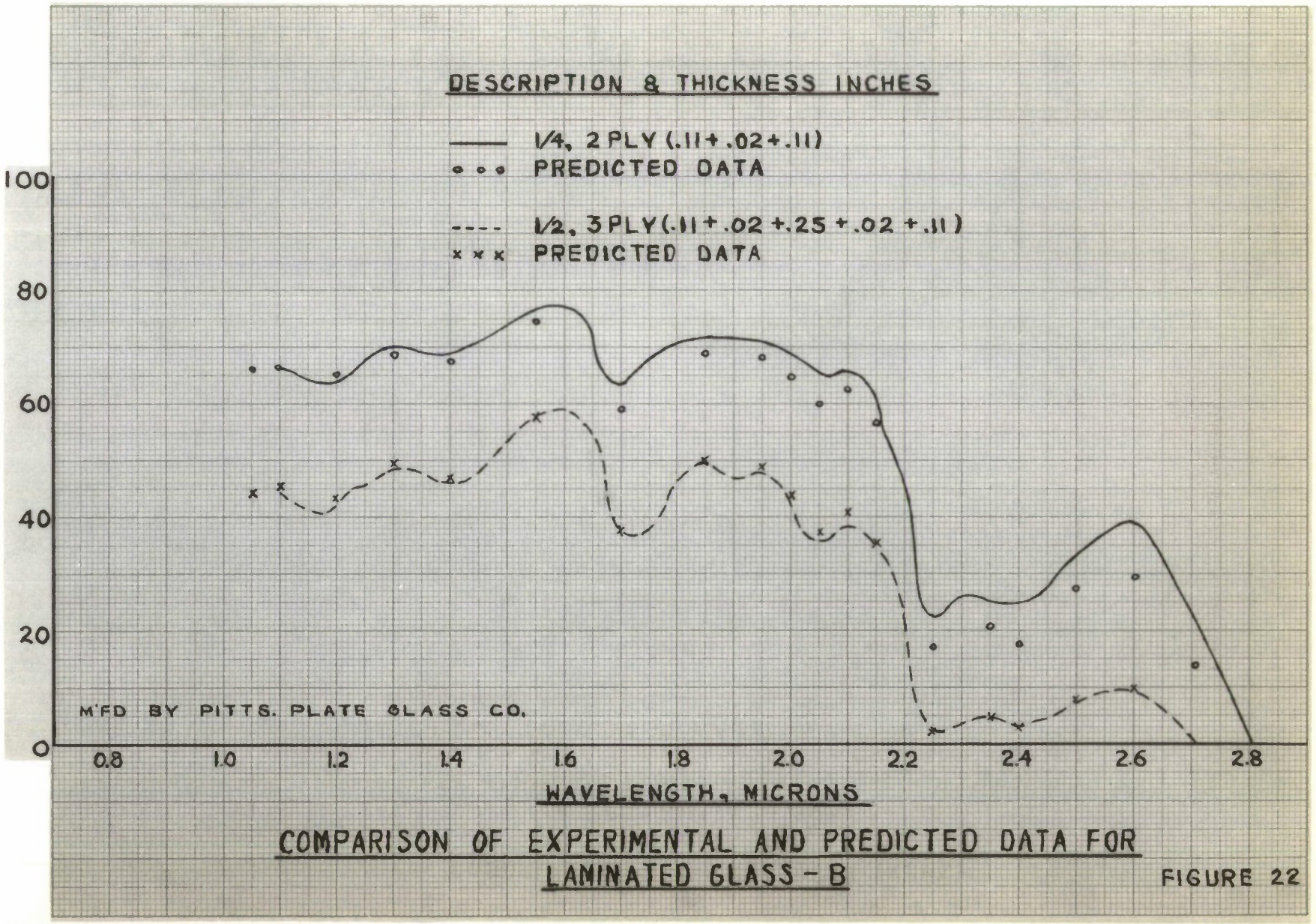
NORMAL TRANSMISSION - LAMINATED GLASS

FIGURE 20



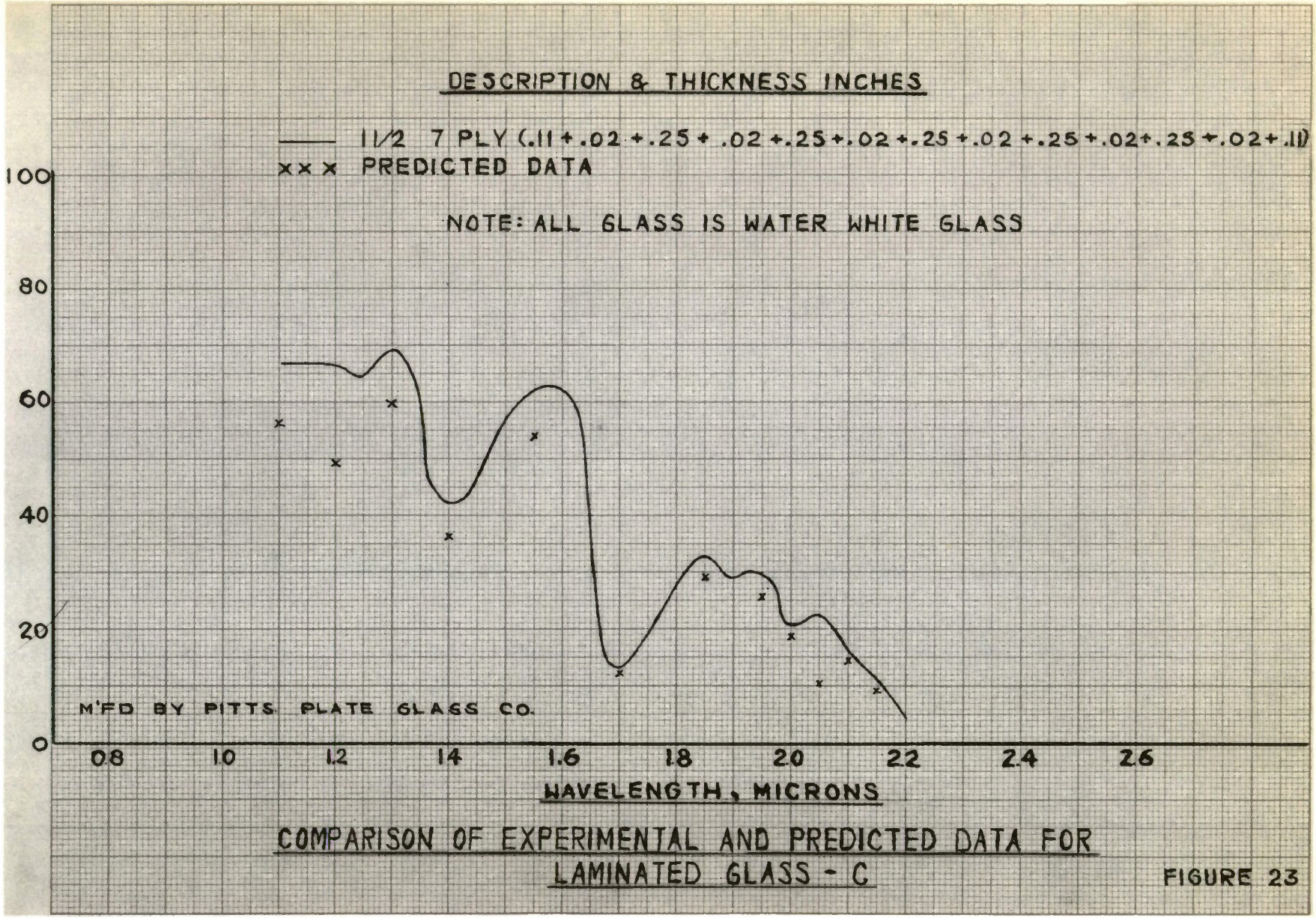
COMPARISON OF EXPERIMENTAL AND PREDICTED DATA FOR LAMINATED GLASS - A

FIGURE 21



COMPARISON OF EXPERIMENTAL AND PREDICTED DATA FOR LAMINATED GLASS - B

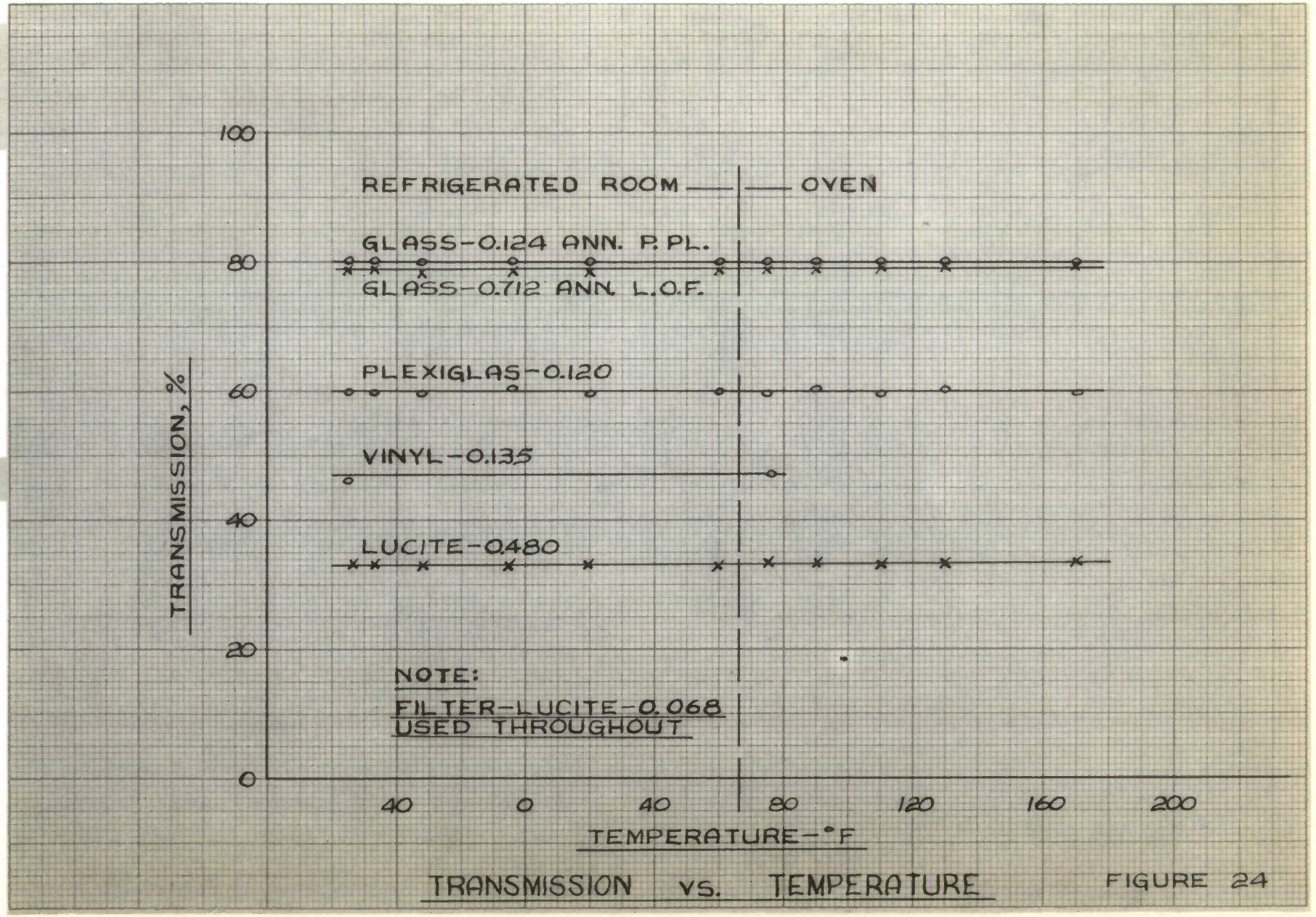
FIGURE 22



COMPARISON OF EXPERIMENTAL AND PREDICTED DATA FOR LAMINATED GLASS - C

FIGURE 23

AFTR 5874

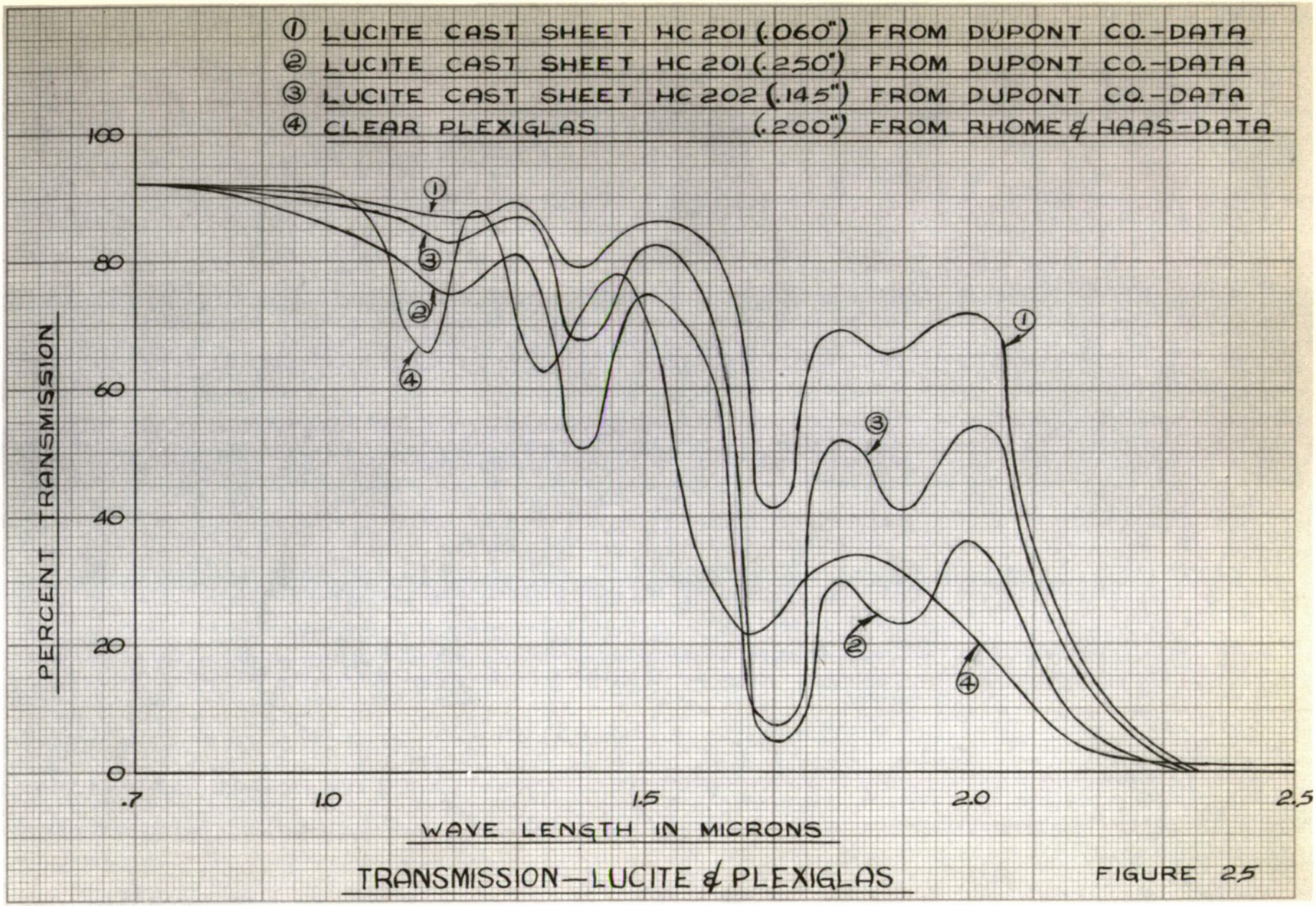


TRANSMISSION VS. TEMPERATURE

FIGURE 24

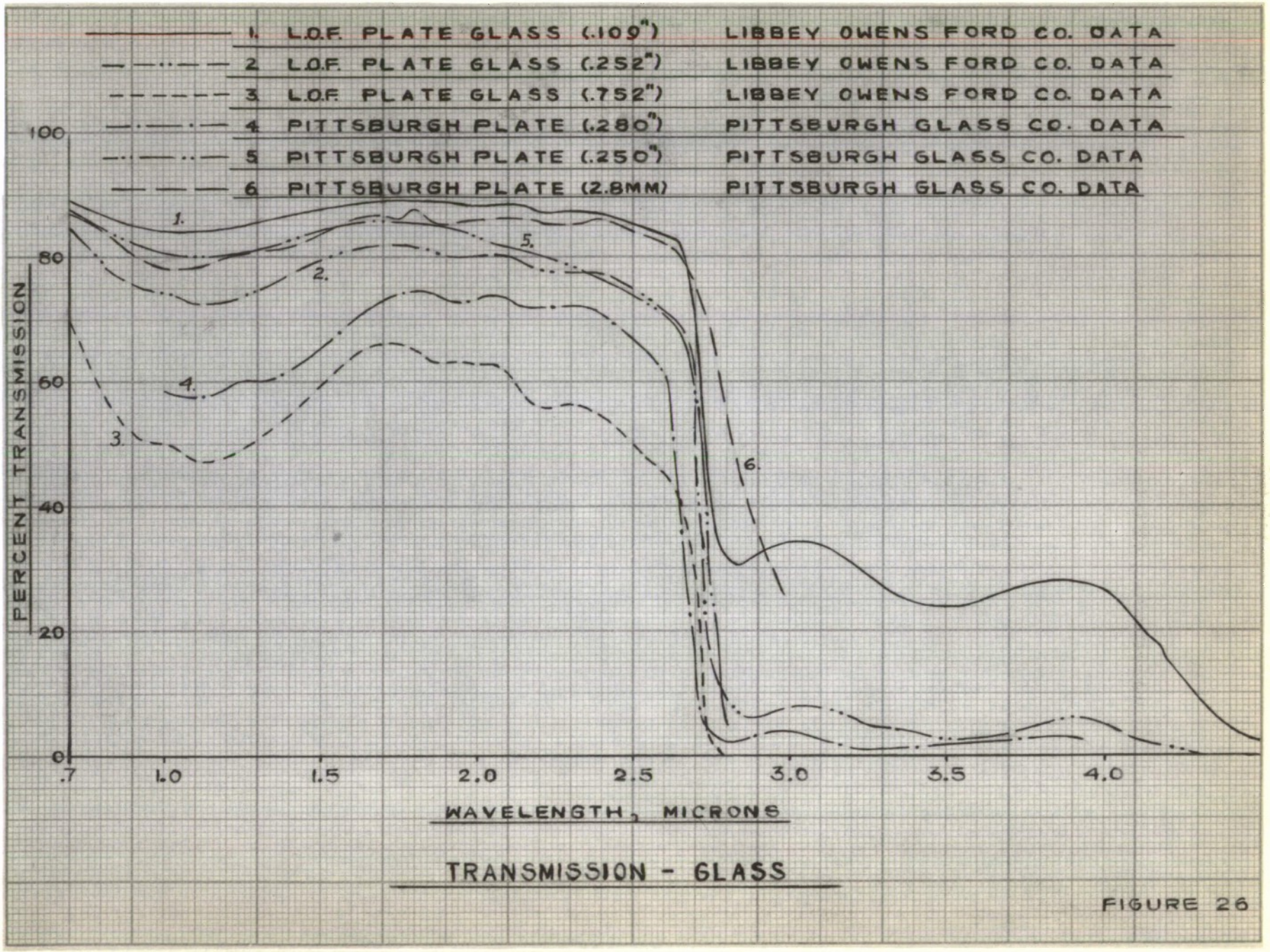
AFTR 5674

114



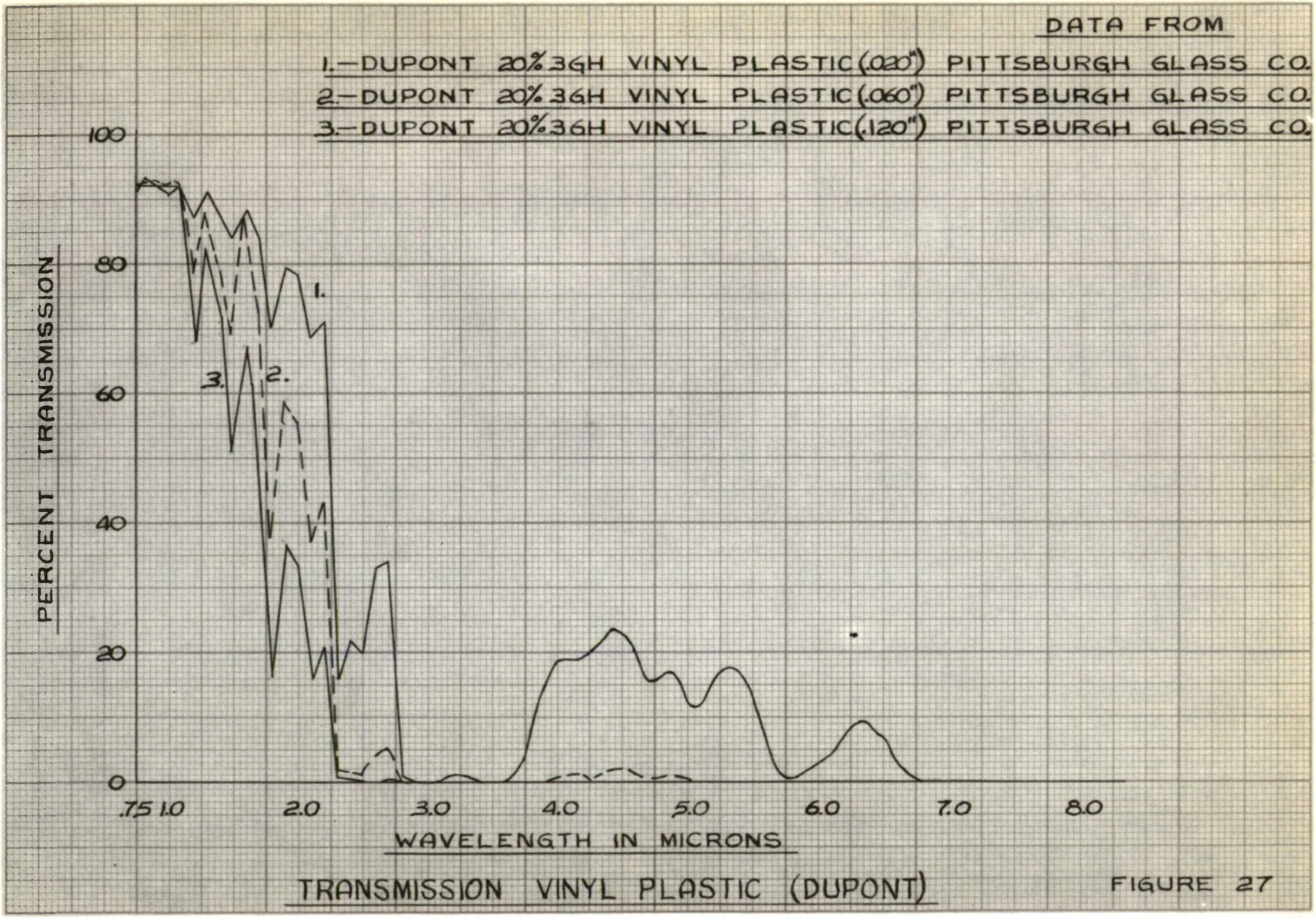
TRANSMISSION—LUCITE & PLEXIGLAS

FIGURE 25



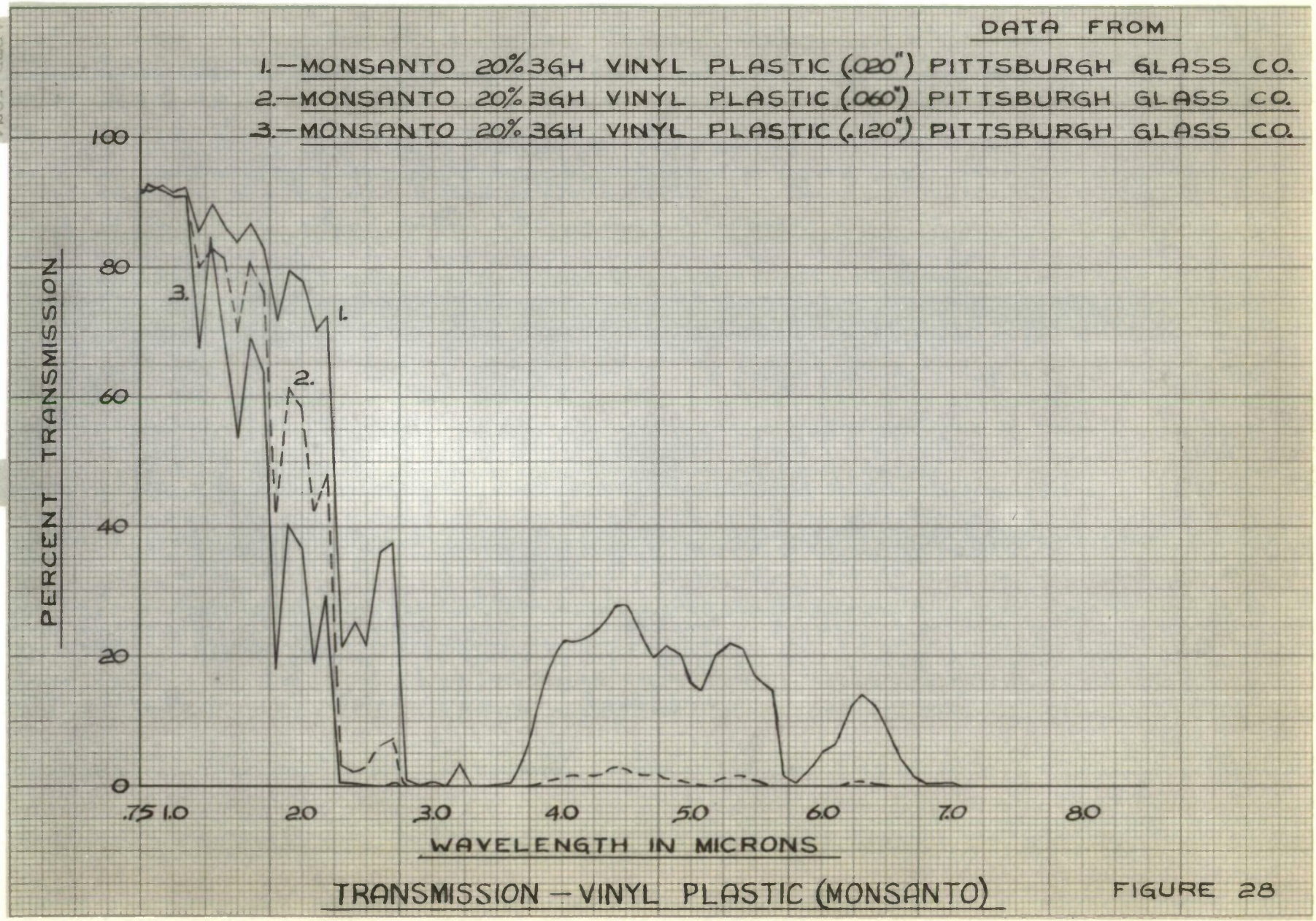
TRANSMISSION - GLASS

FIGURE 26



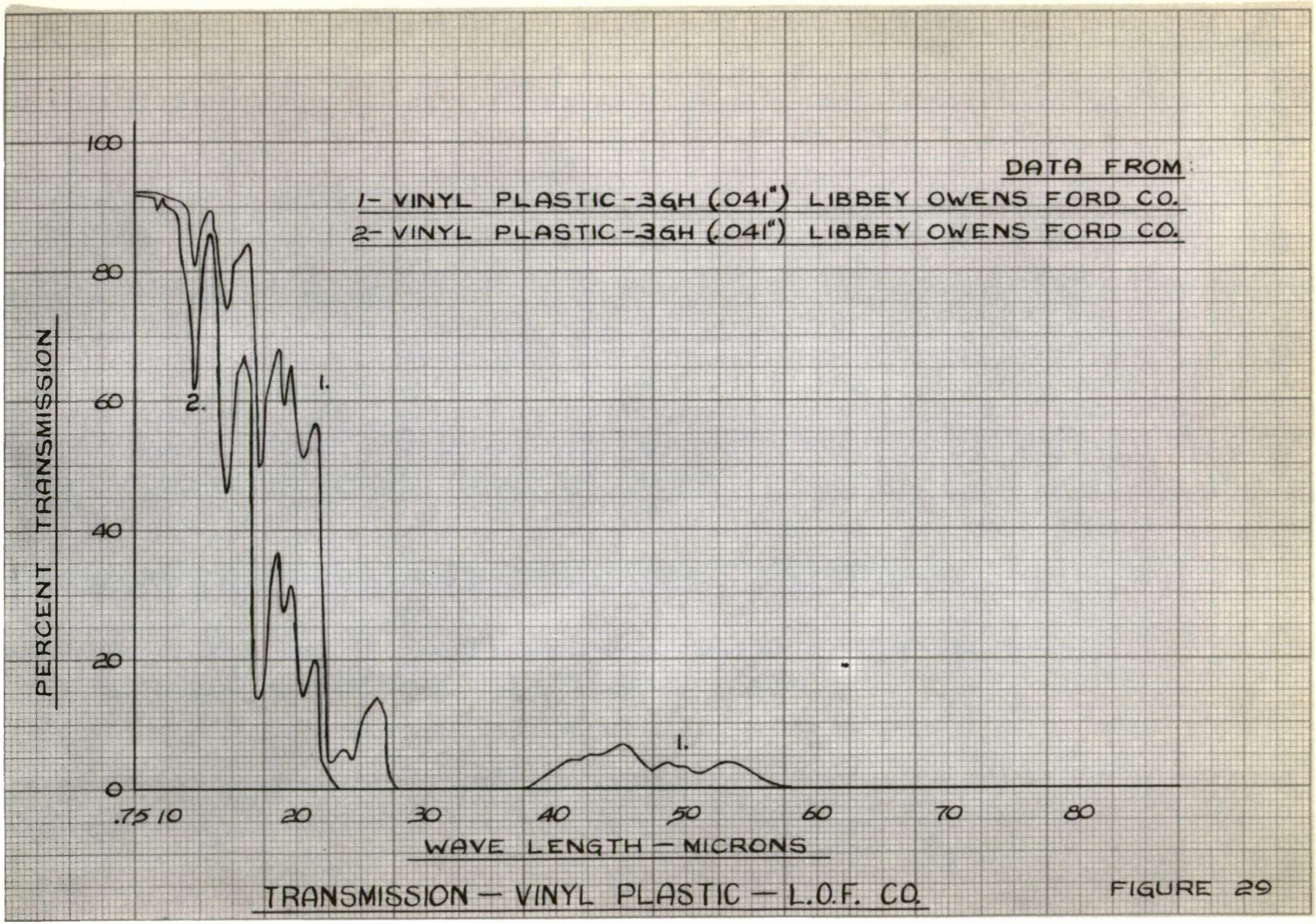
TRANSMISSION VINYL PLASTIC (DUPONT)

FIGURE 27



TRANSMISSION — VINYL PLASTIC (MONSANTO)

FIGURE 28

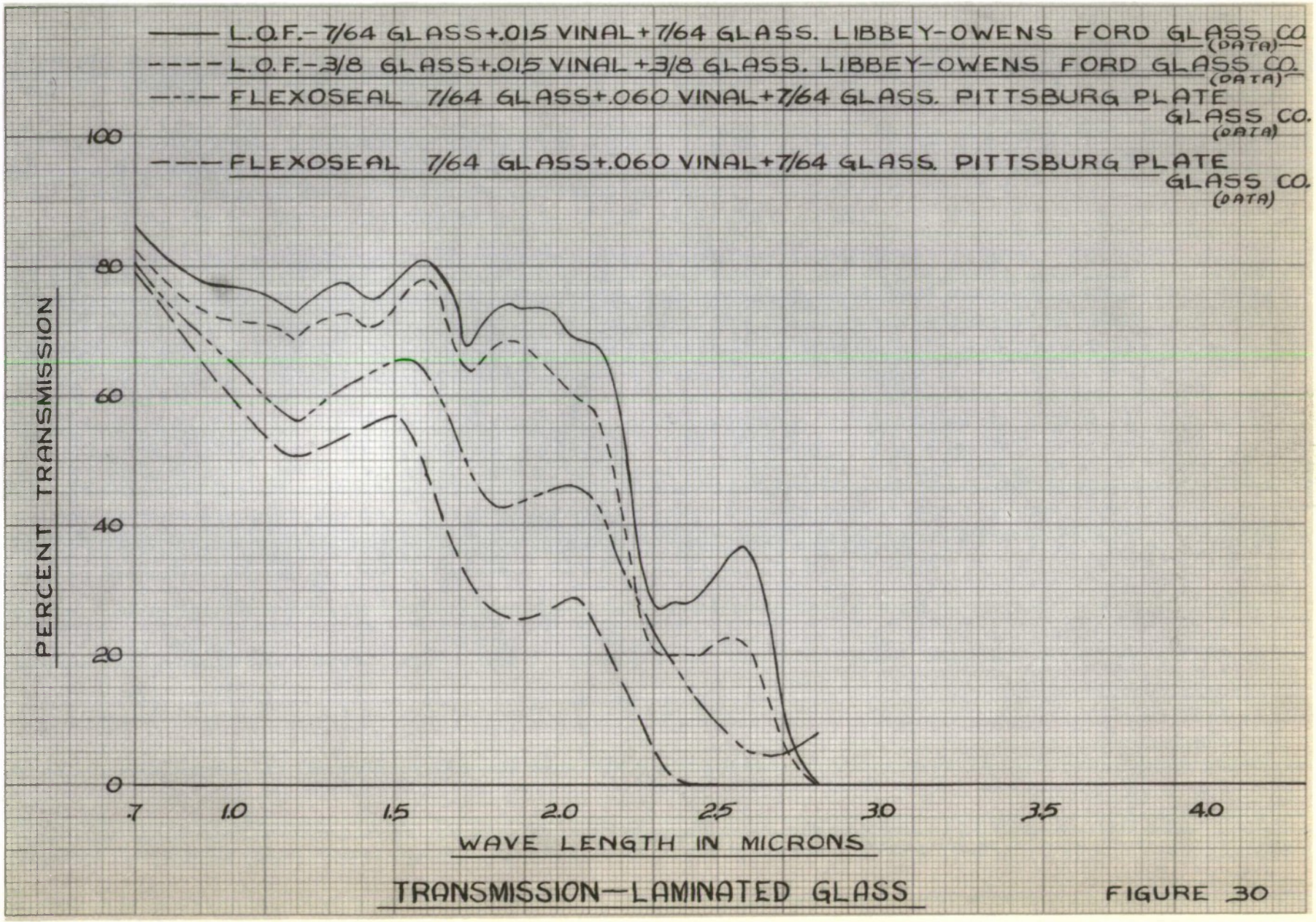


TRANSMISSION — VINYL PLASTIC — L.O.F. CO.

FIGURE 29

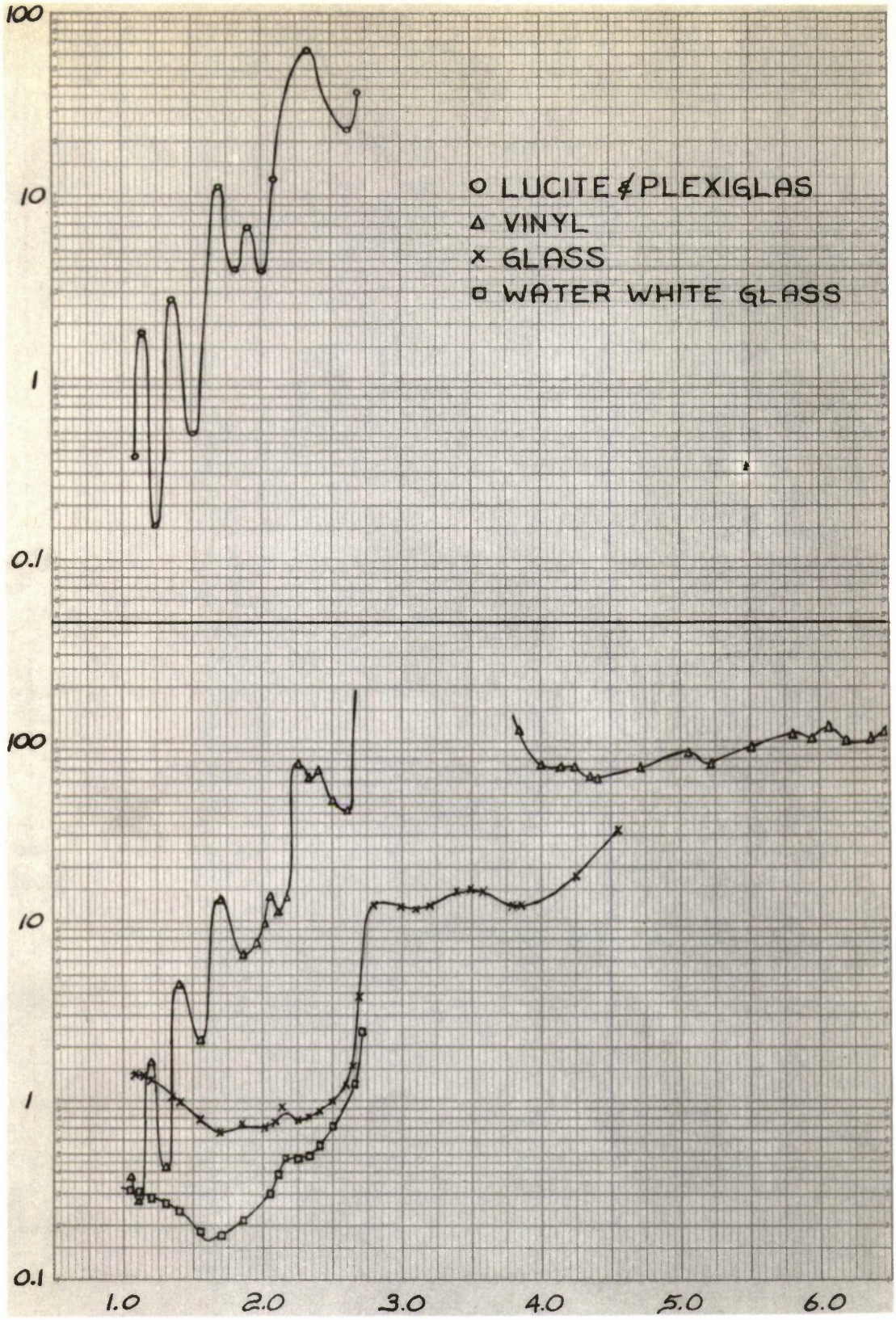
AFTR 5874

119

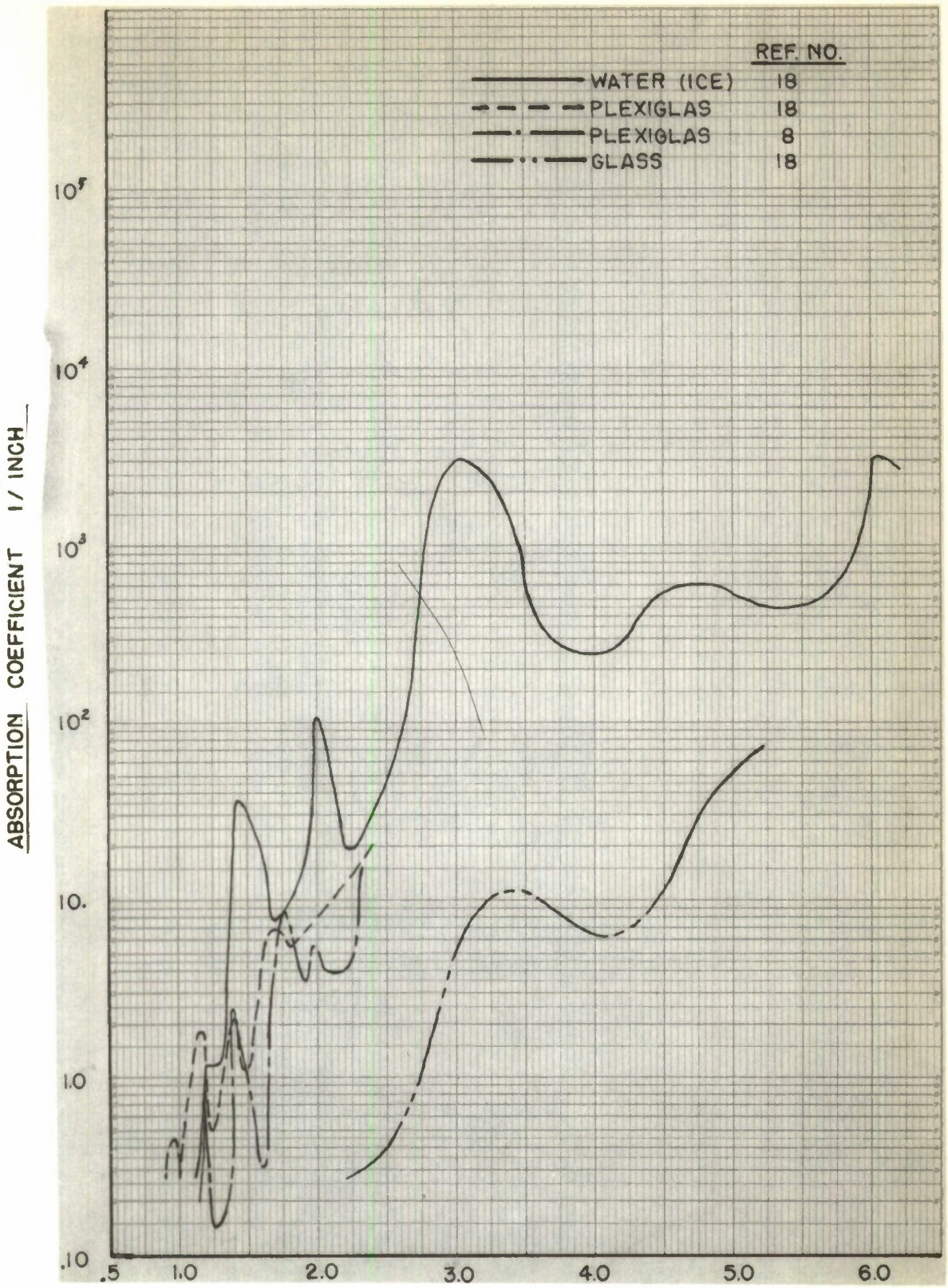


TRANSMISSION—LAMINATED GLASS

FIGURE 30

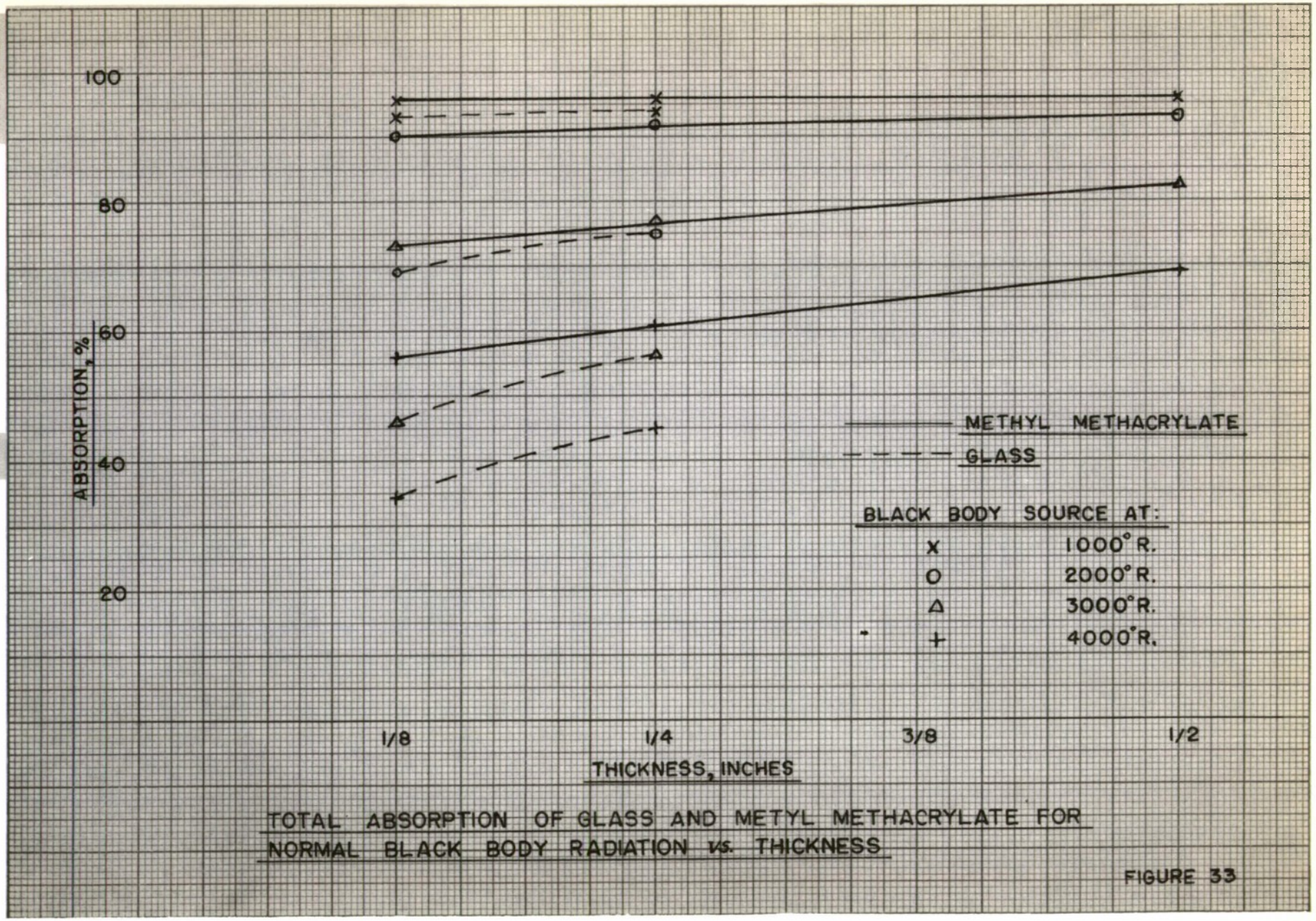


ABSORPTION COEFFICIENTS OF TRANSPARENT MATERIALS



ABSORPTION COEFFICIENTS OF TRANSPARENT MATERIALS FROM TWO REFERENCES

FIGURE 32



TOTAL ABSORPTION OF GLASS AND METYL METHACRYLATE FOR NORMAL BLACK BODY RADIATION *vs.* THICKNESS

FIGURE 33

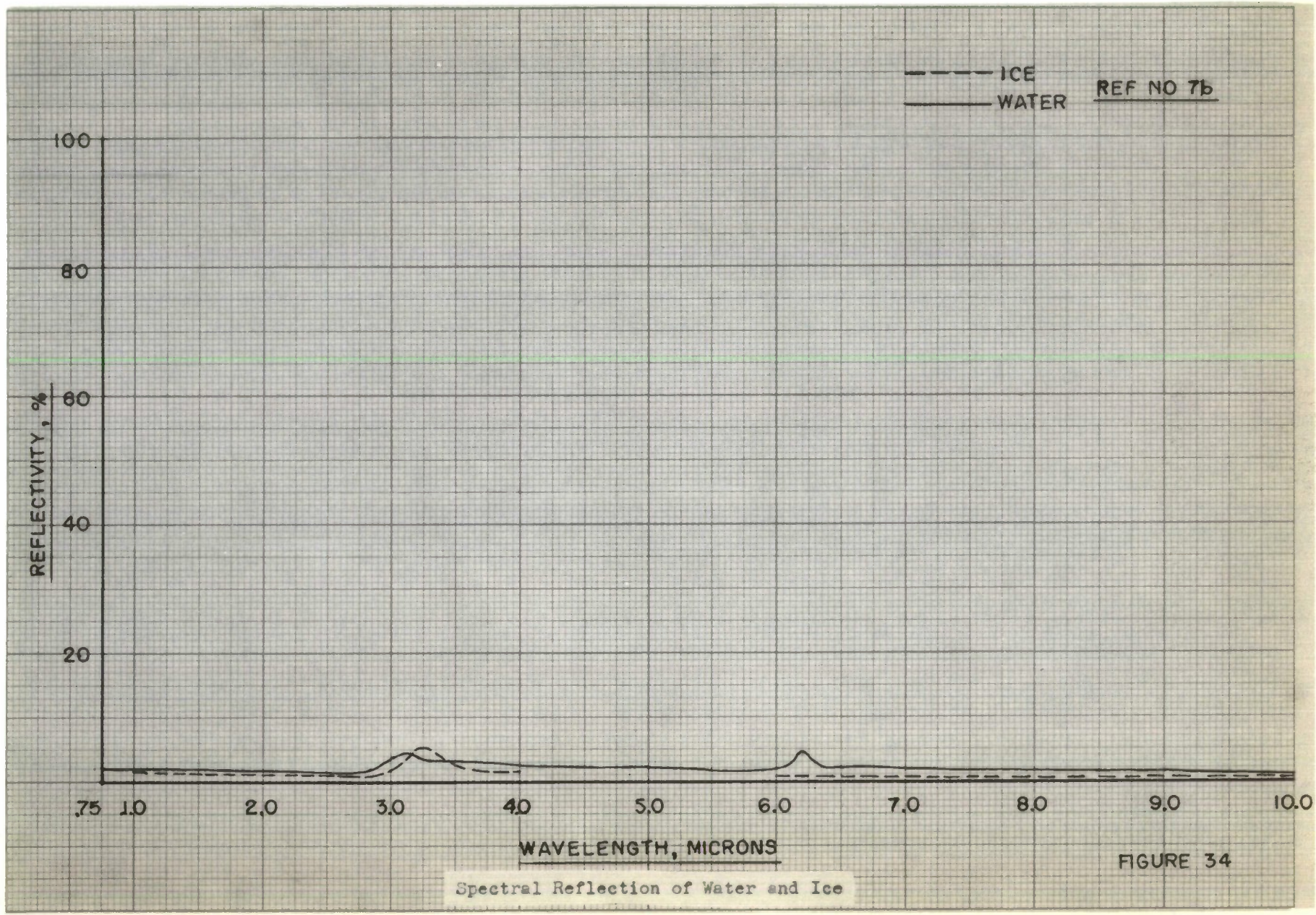
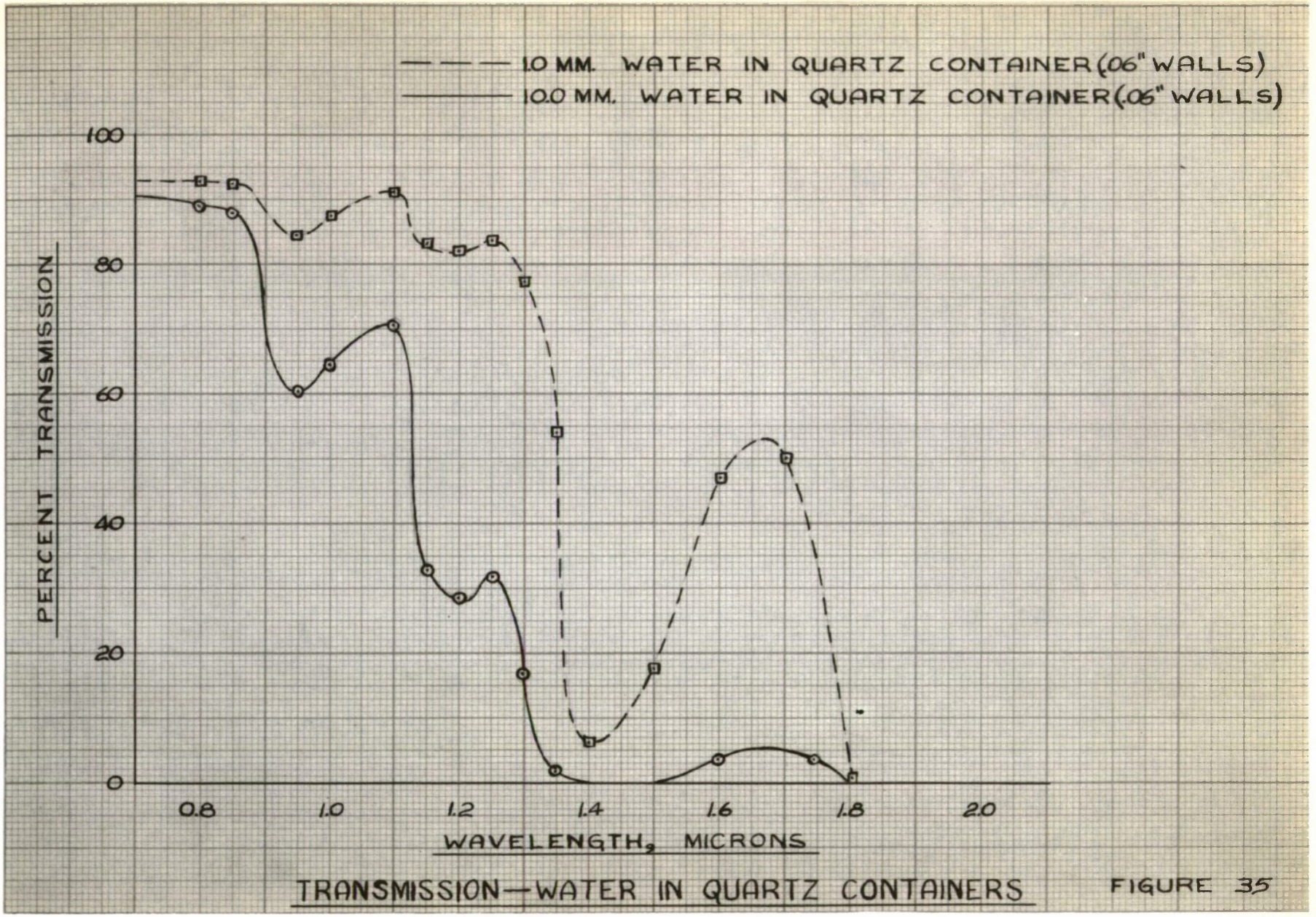


FIGURE 34

Spectral Reflection of Water and Ice

AFTR 5874

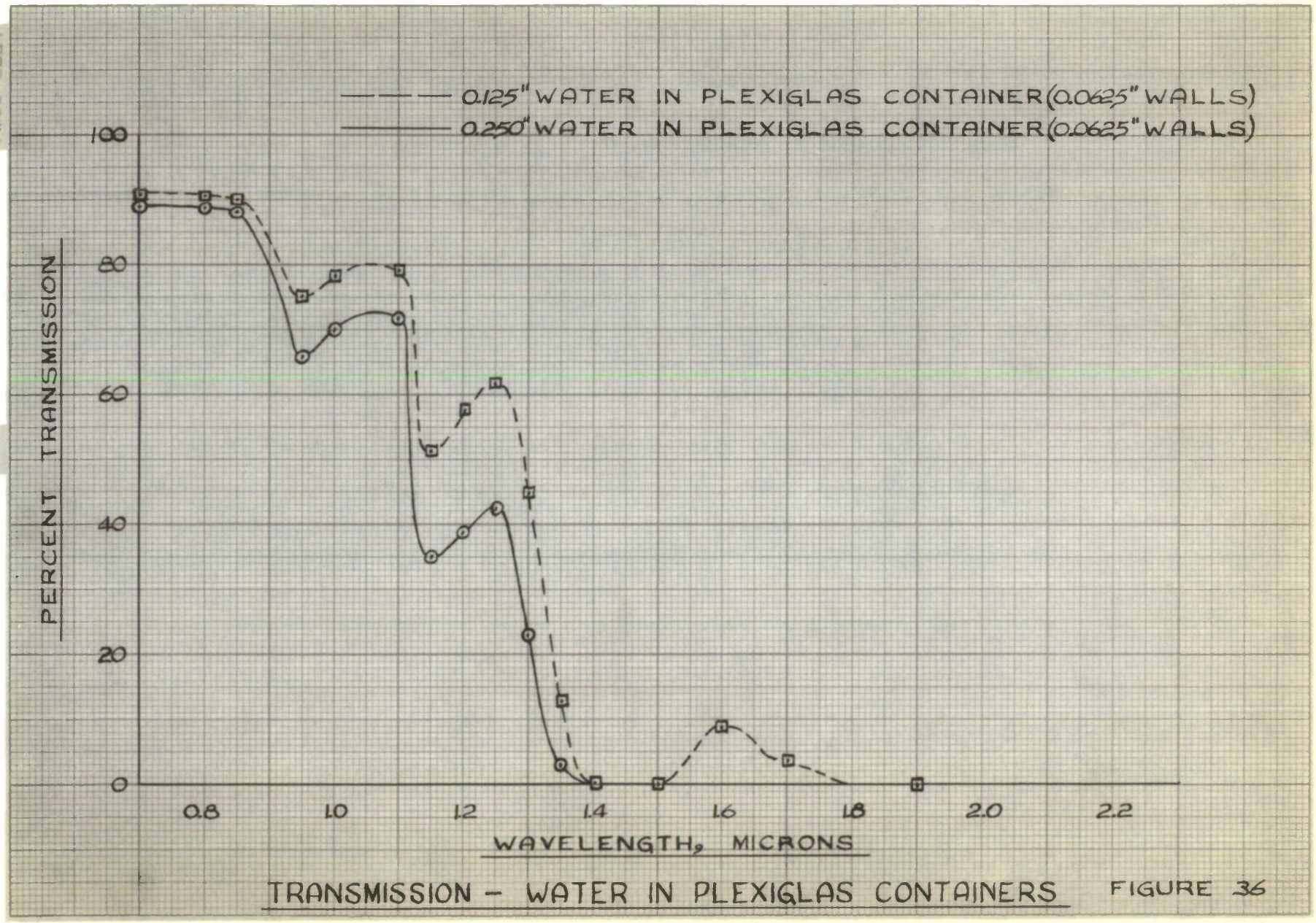
124



TRANSMISSION—WATER IN QUARTZ CONTAINERS

FIGURE 35

AFTR 5874



TRANSMISSION – WATER IN PLEXIGLAS CONTAINERS FIGURE 36

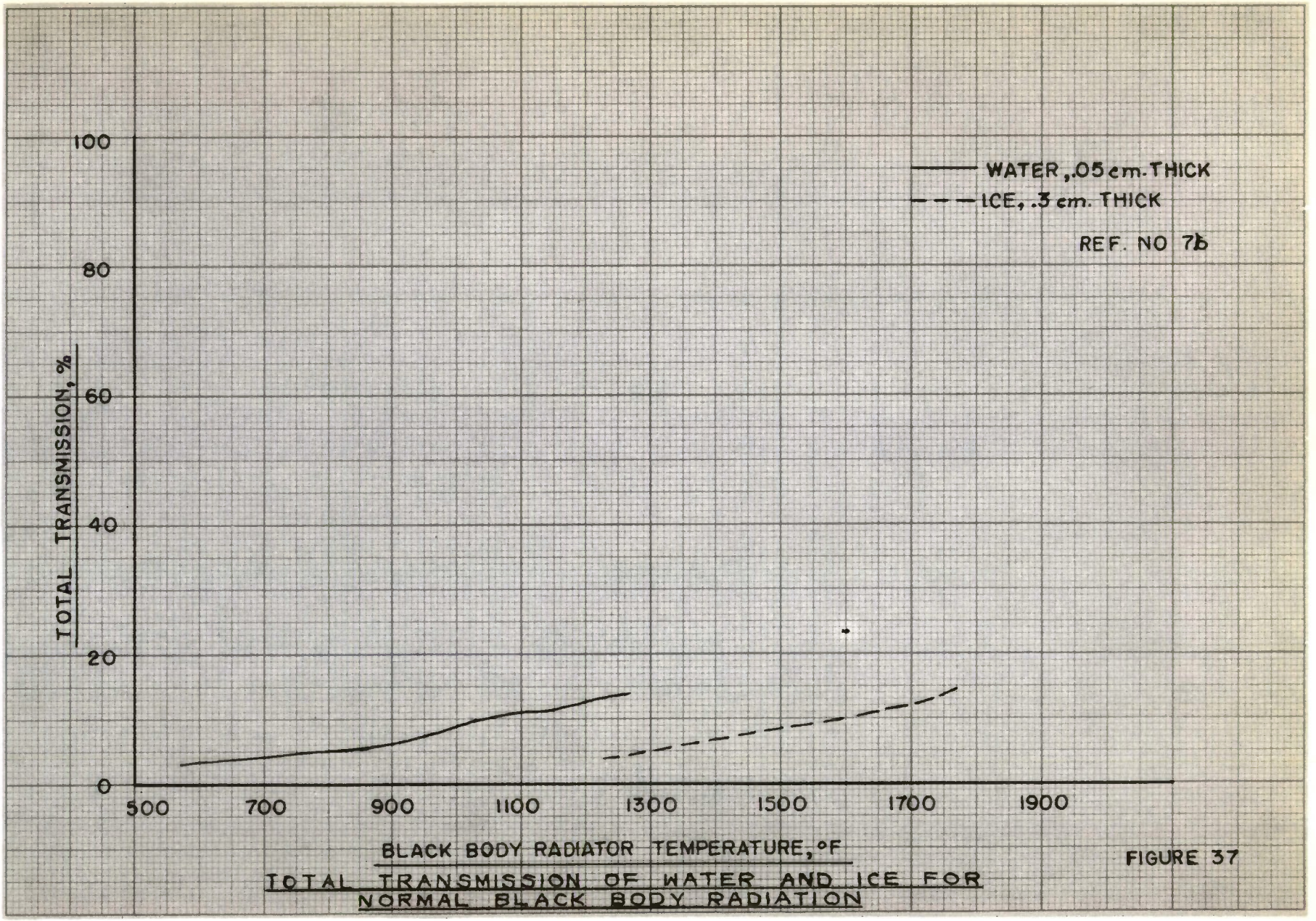
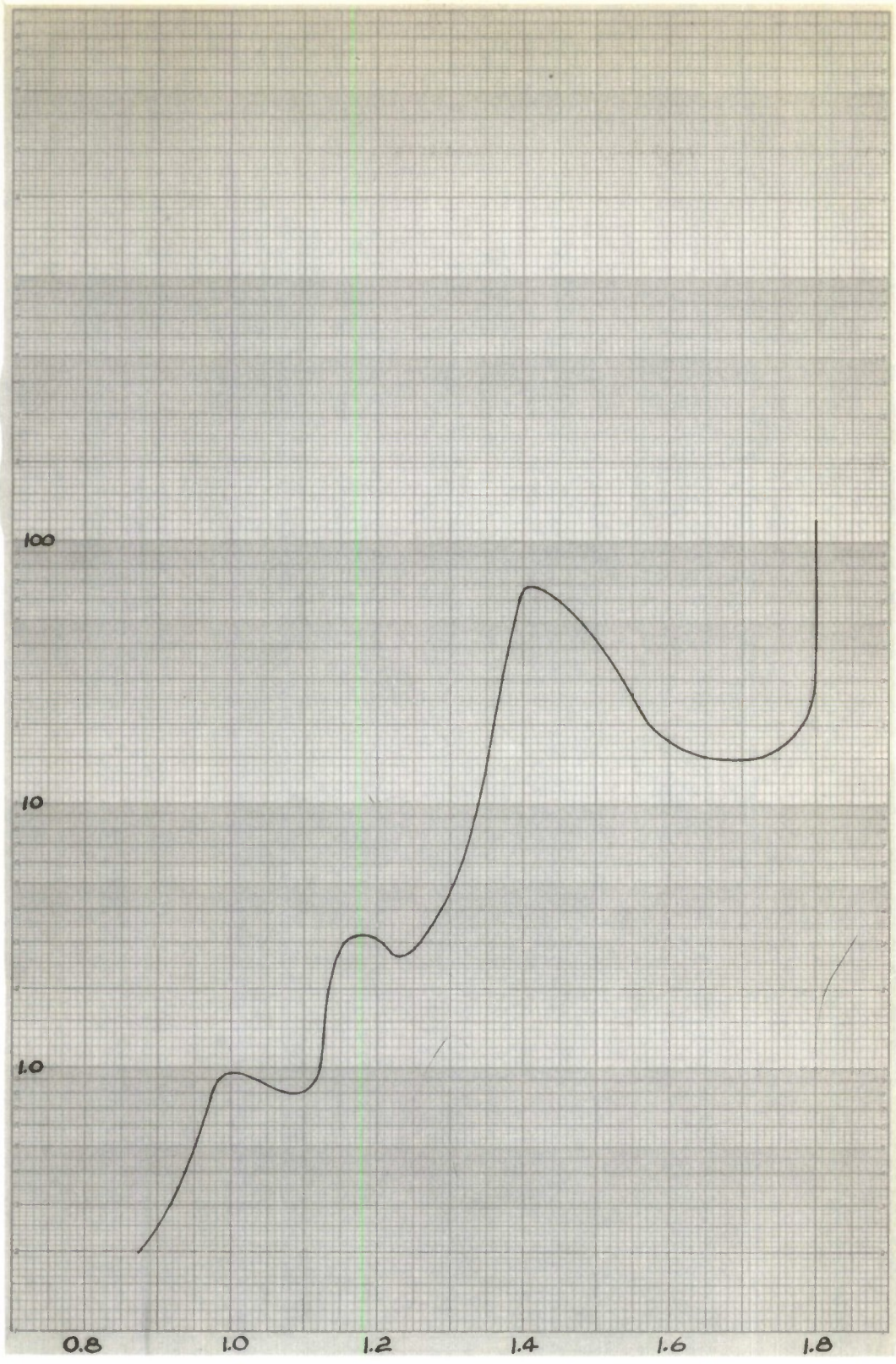


FIGURE 37

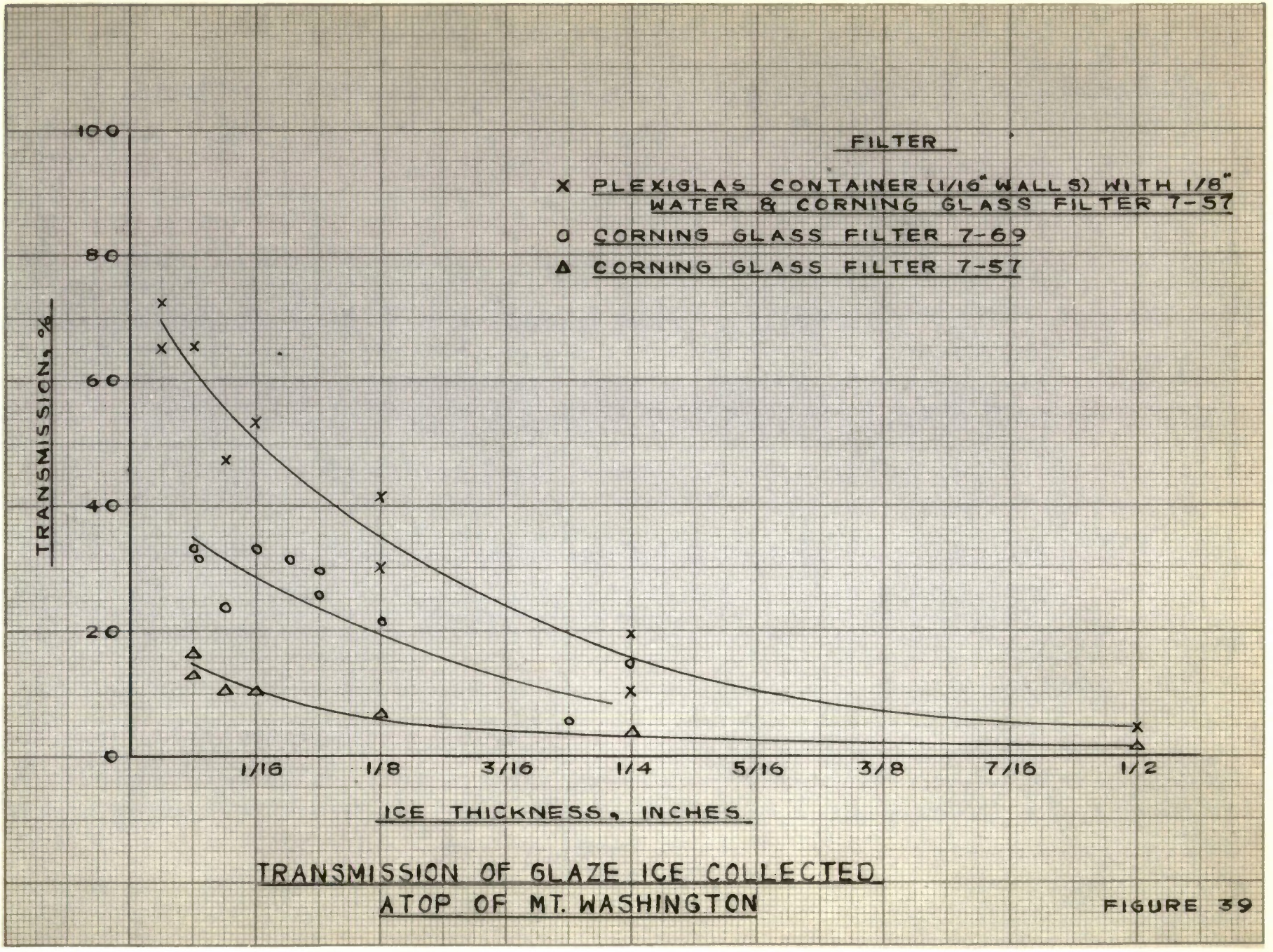
TOTAL TRANSMISSION OF WATER AND ICE FOR NORMAL BLACK BODY RADIATION



ABSORPTION COEFFICIENT-WATER

FIGURE 38

AFIT 58-74

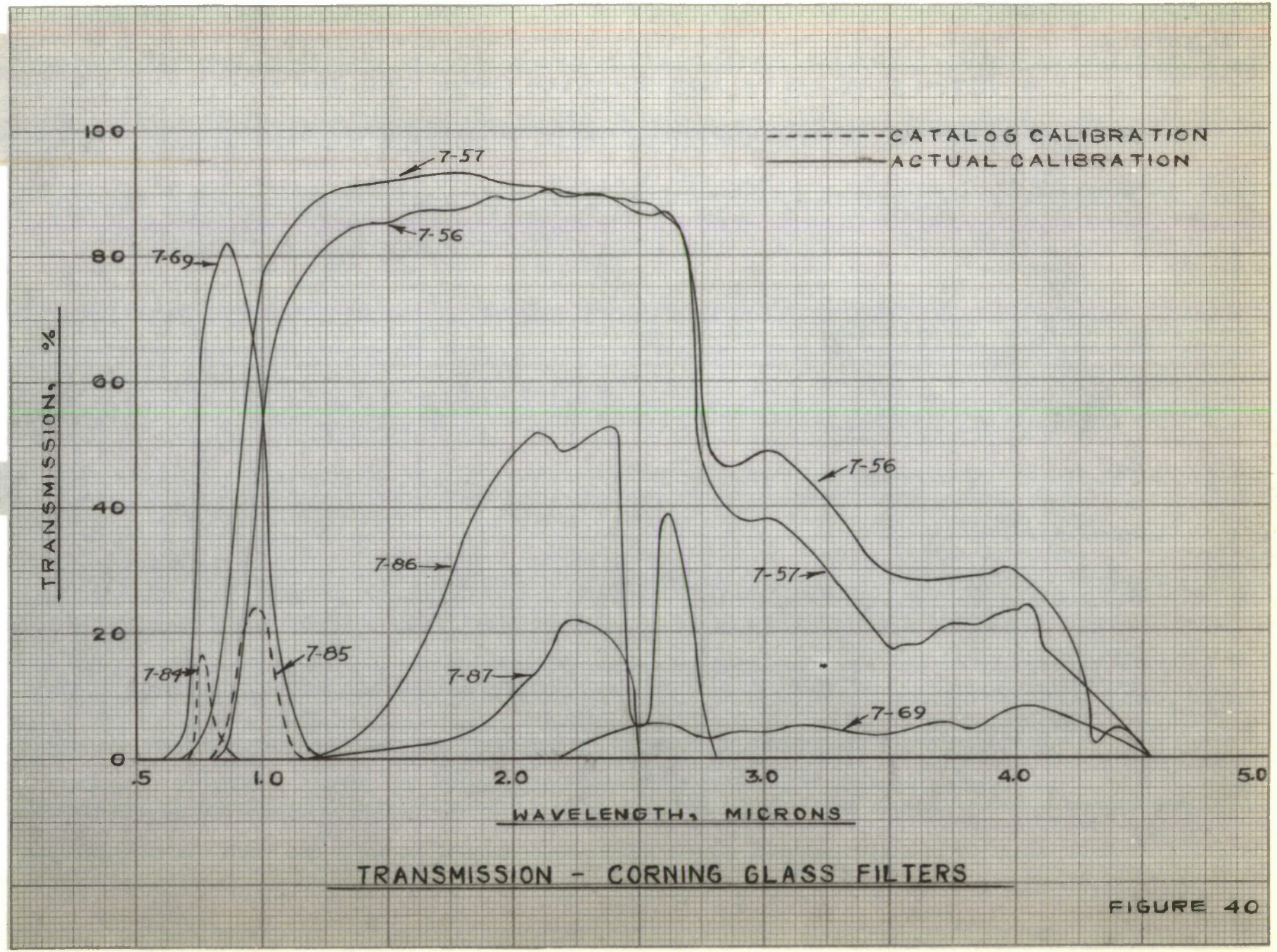


TRANSMISSION OF GLAZE ICE COLLECTED ATOP OF MT. WASHINGTON

FIGURE 39

128

AFTR 5874



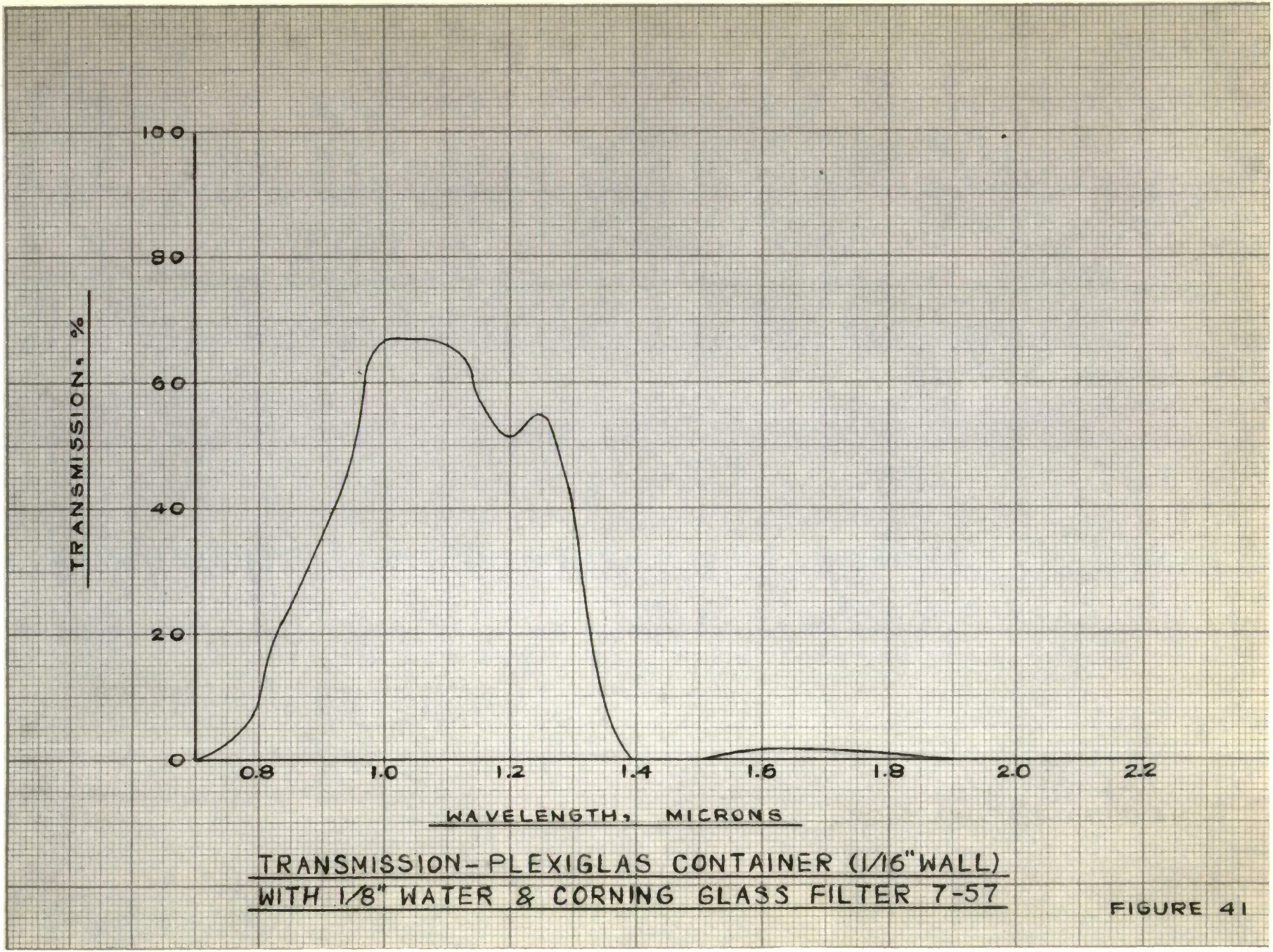
TRANSMISSION - CORNING GLASS FILTERS

FIGURE 40

129

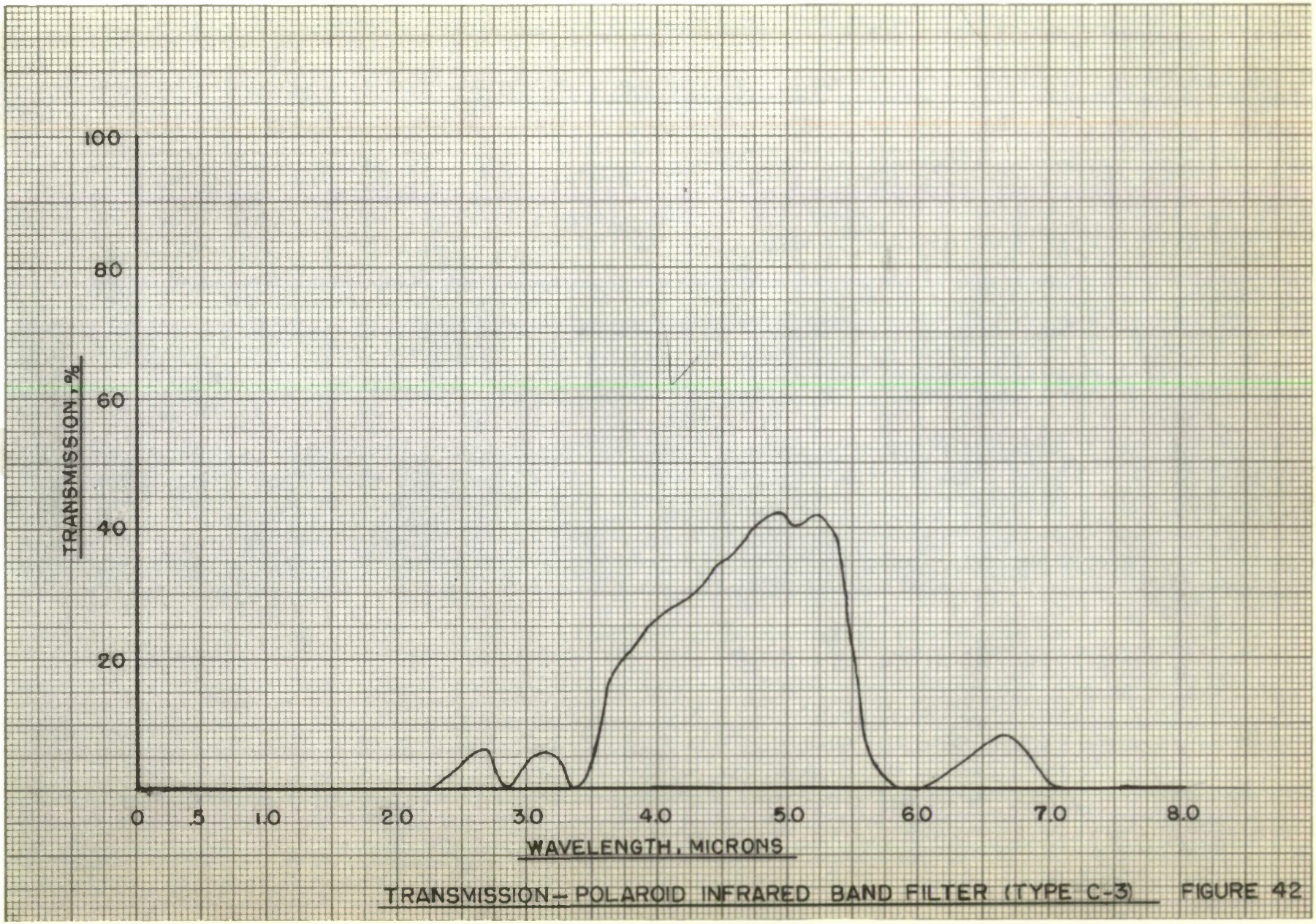
AFIR 5874

120



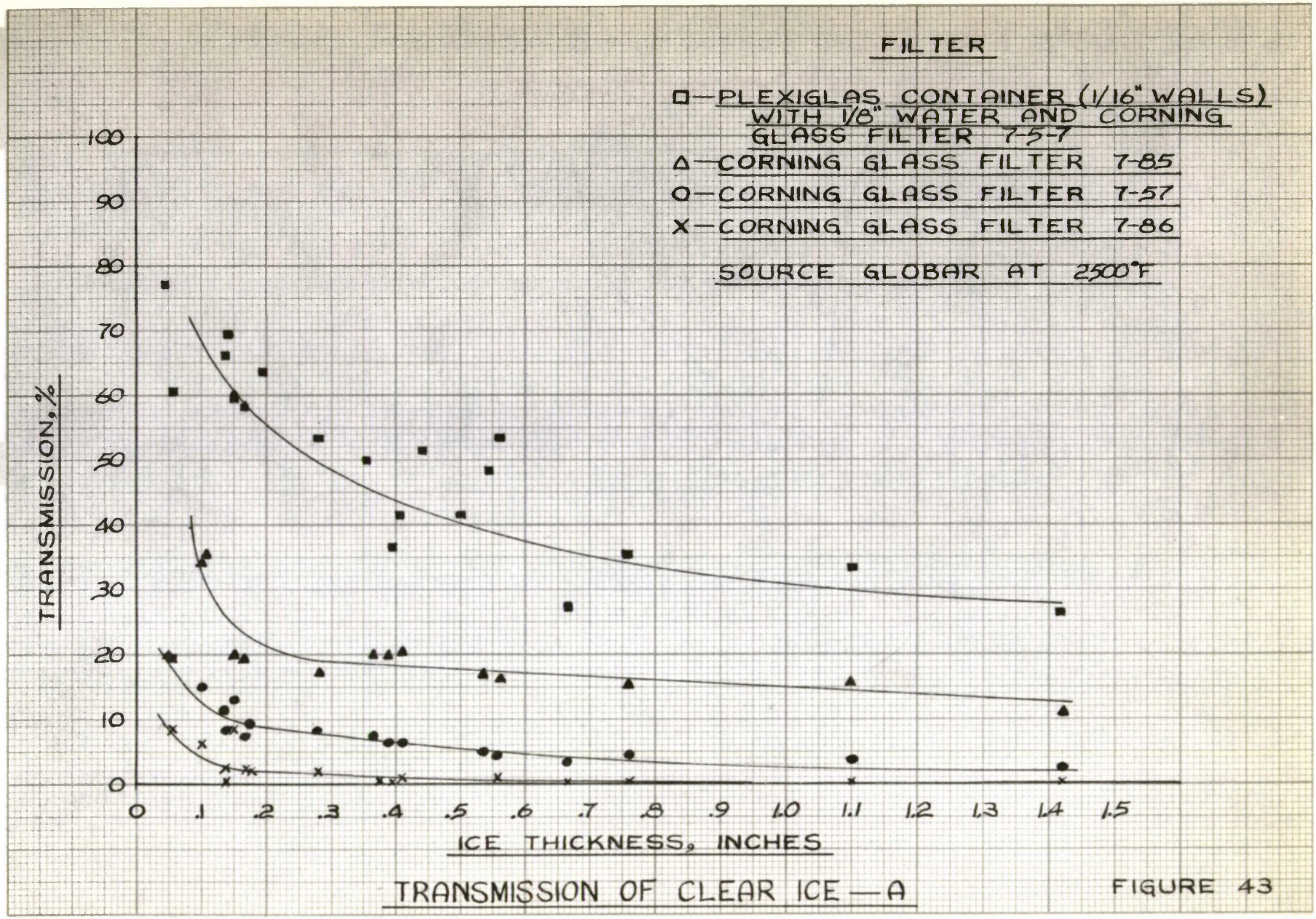
TRANSMISSION - PLEXIGLAS CONTAINER (1/16" WALL)
WITH 1/8" WATER & CORNING GLASS FILTER 7-57

FIGURE 41



TRANSMISSION – POLAROID INFRARED BAND FILTER (TYPE C-3) FIGURE 42

AFTR 5374

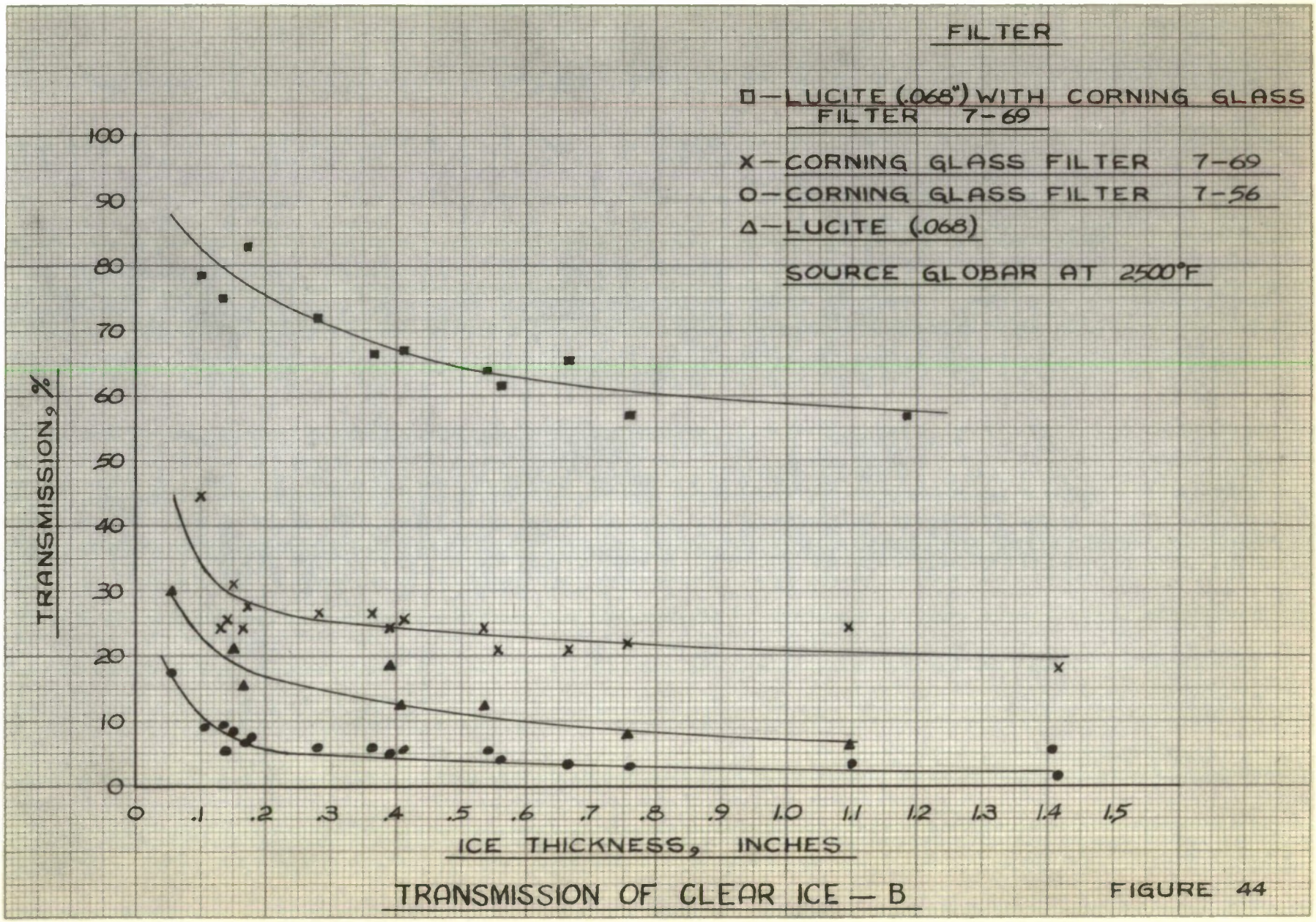


TRANSMISSION OF CLEAR ICE — A

FIGURE 43

133

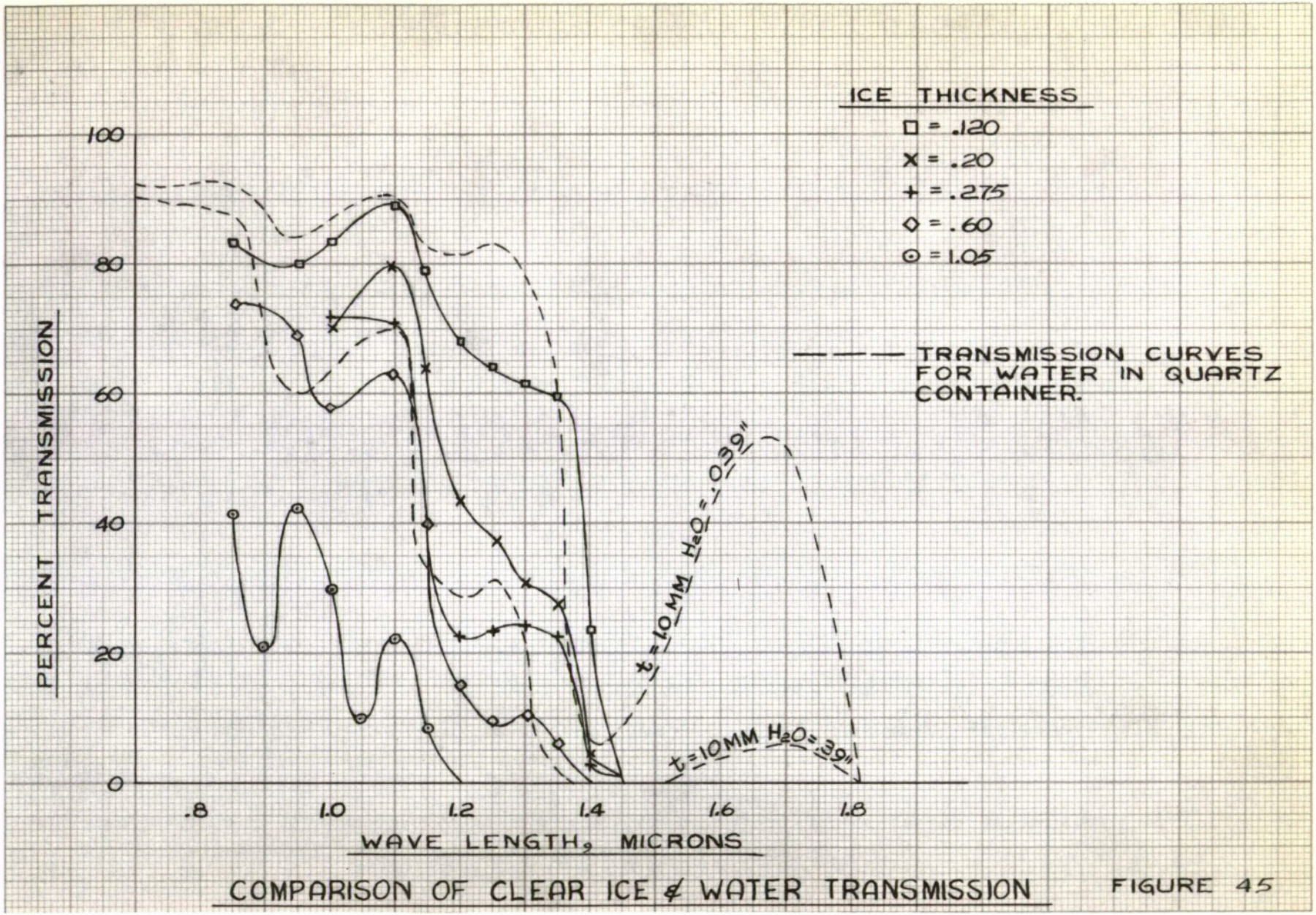
AFTR 5674



TRANSMISSION OF CLEAR ICE — B

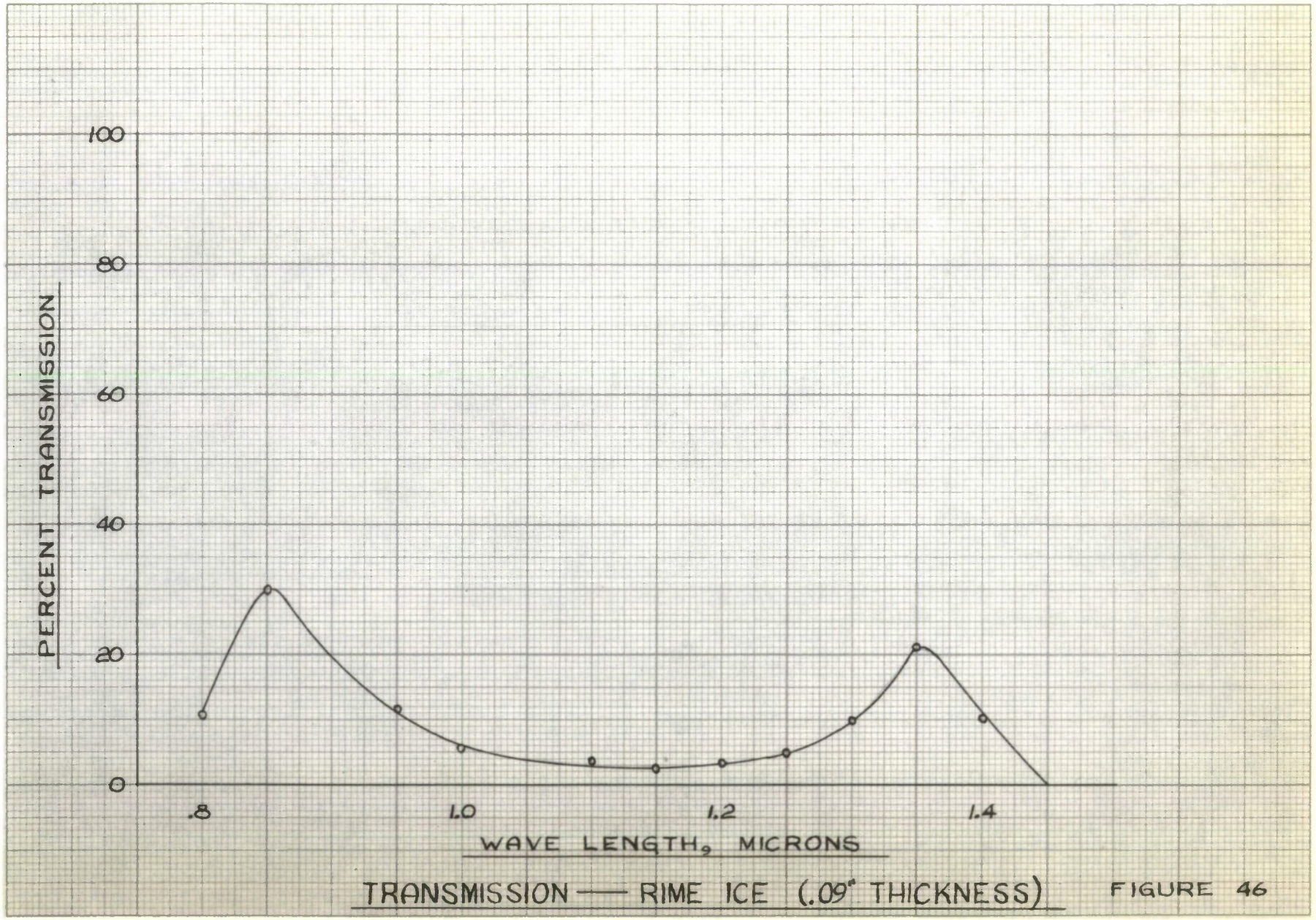
FIGURE 44

AFTR 5874



COMPARISON OF CLEAR ICE & WATER TRANSMISSION FIGURE 45

134



TRANSMISSION — RIME ICE (.09" THICKNESS) FIGURE 46

AFTR 5874

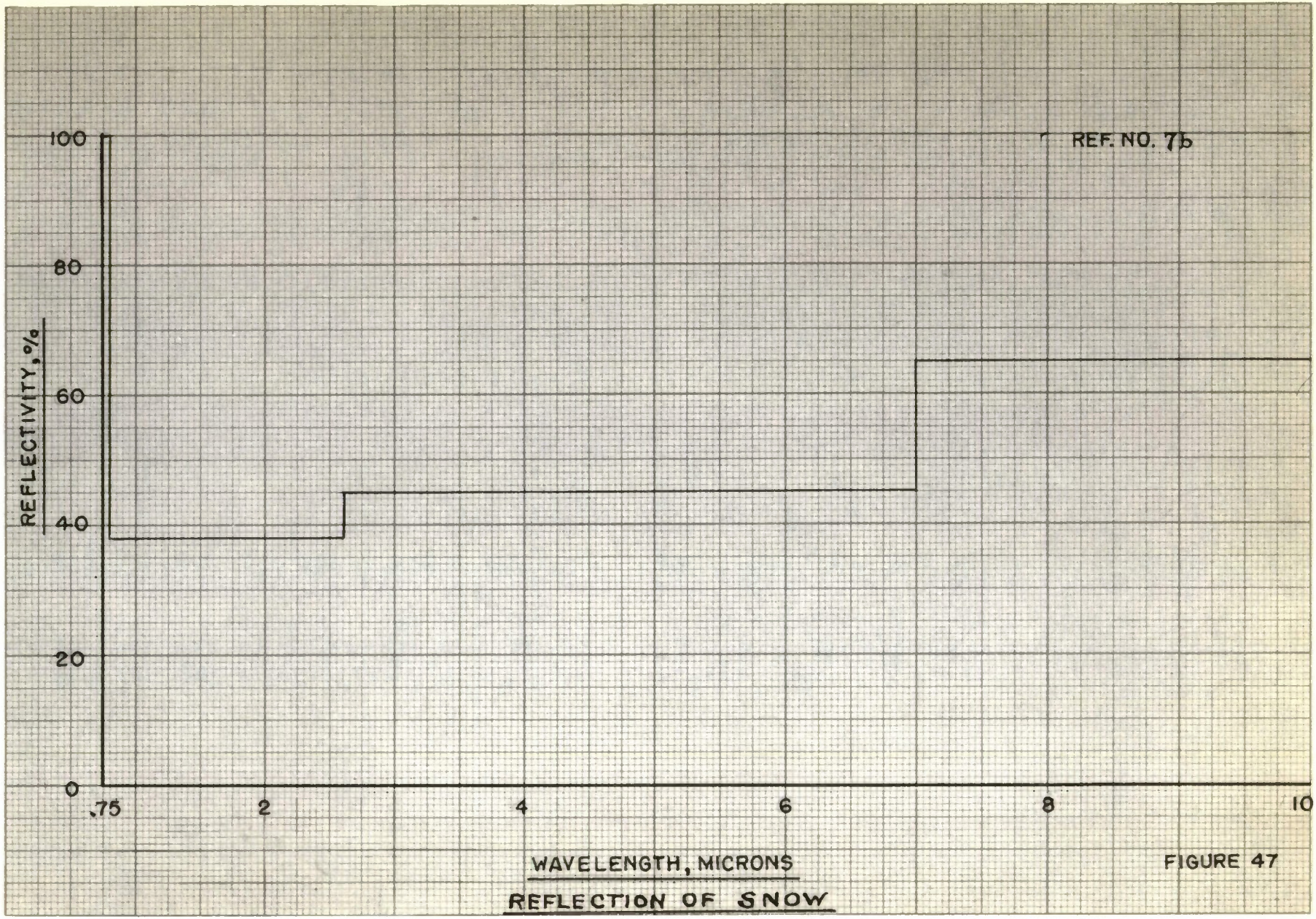
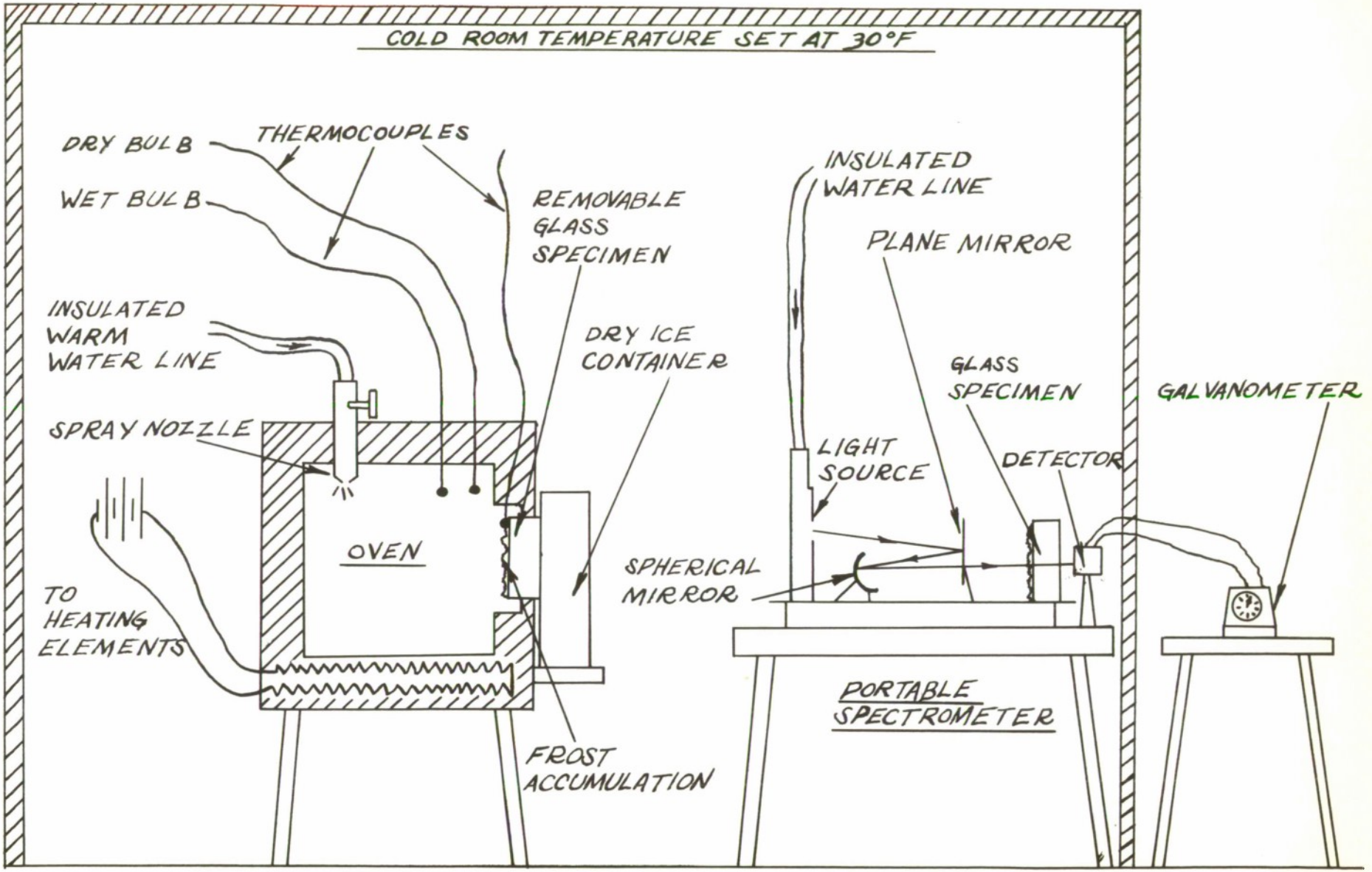


FIGURE 47

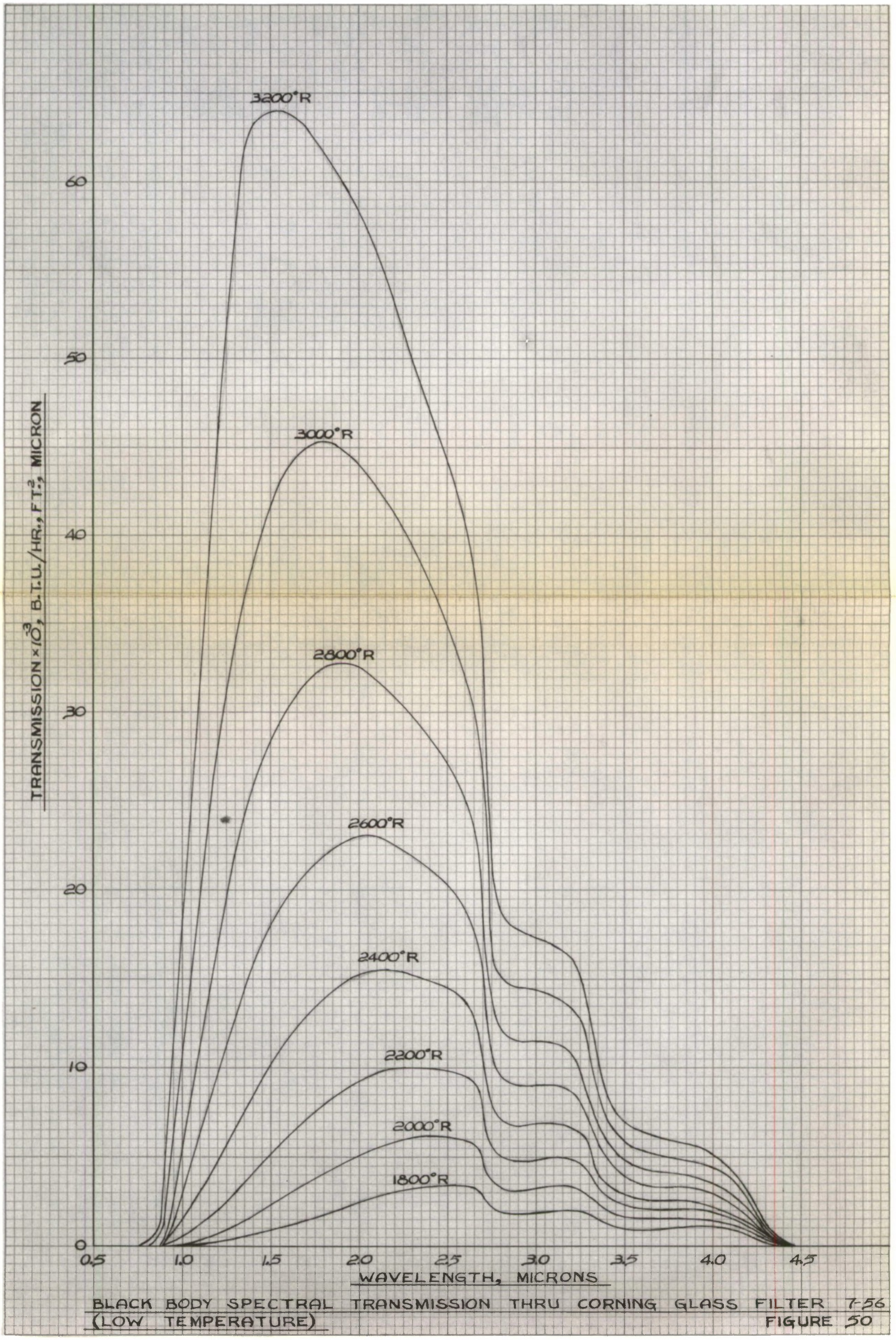
REFLECTION OF SNOW



LABORATORY FROST ACCRETION SETUP

FIGURE 48

AFTR 5874

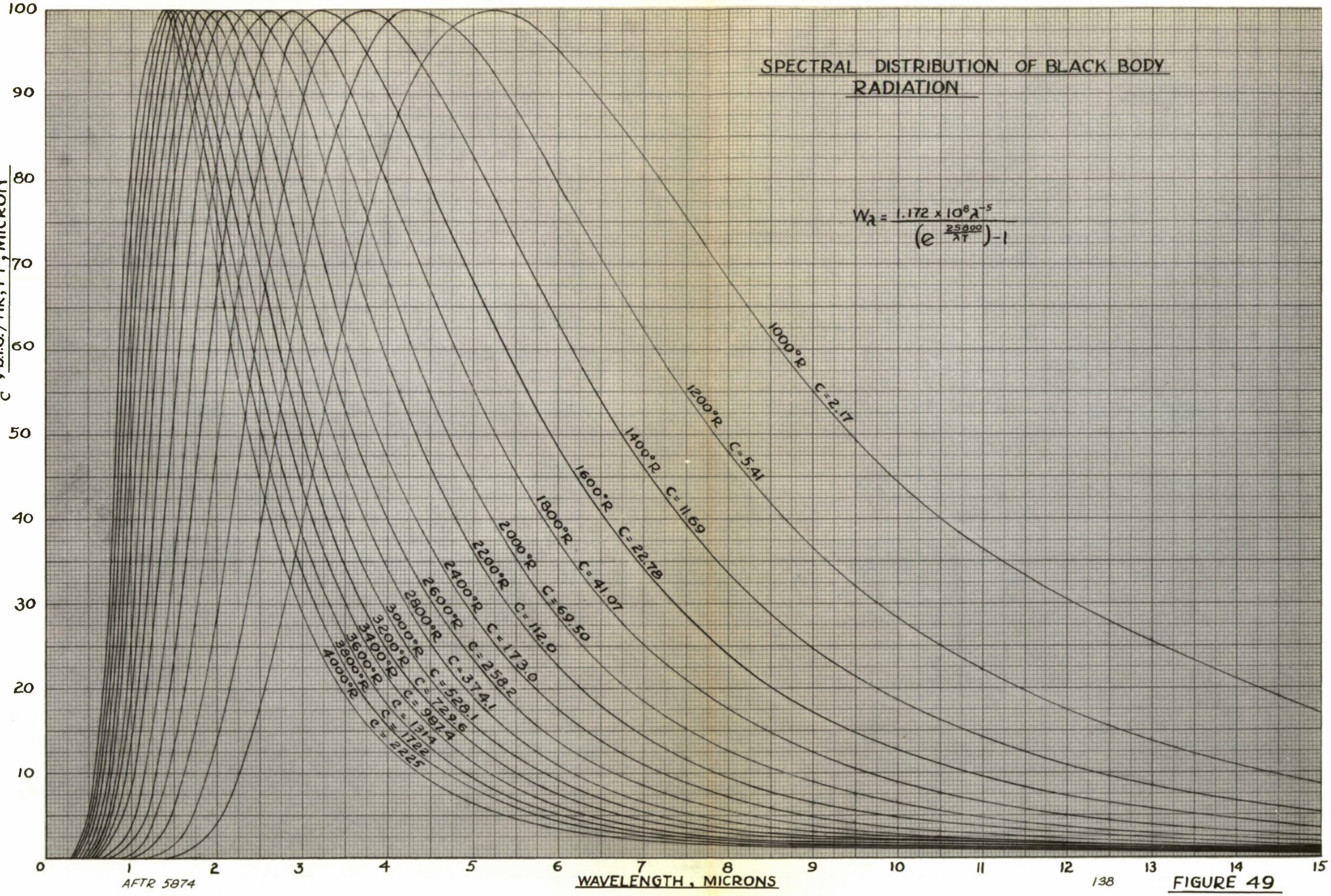


BLACK BODY SPECTRAL TRANSMISSION THRU CORNING GLASS FILTER 7-56
(LOW TEMPERATURE)

FIGURE 50

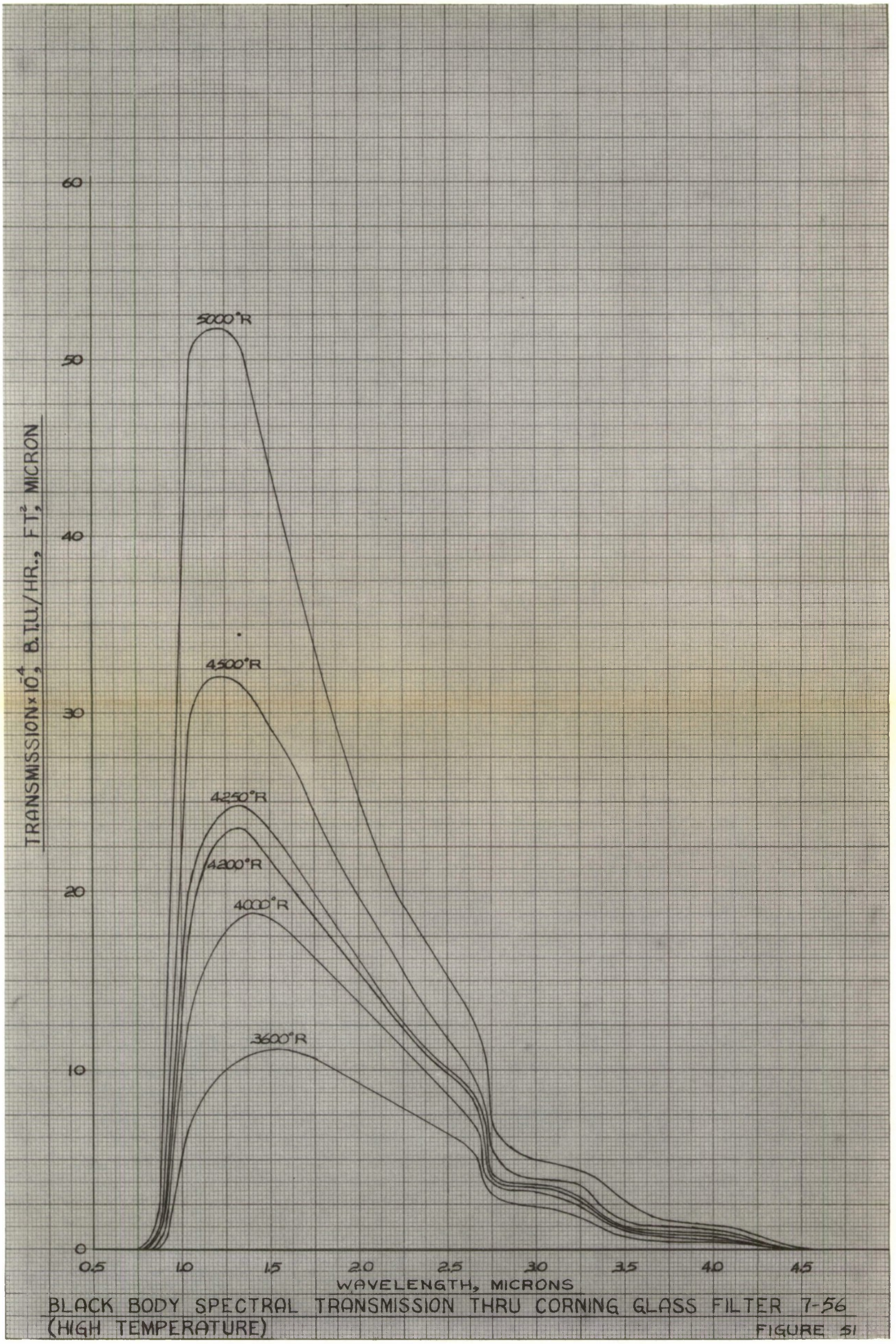
SPECTRAL DISTRIBUTION OF BLACK BODY RADIATION

$$W_\lambda = \frac{1.172 \times 10^8 \lambda^{-5}}{\left(e^{\frac{25800}{\lambda T}}\right) - 1}$$



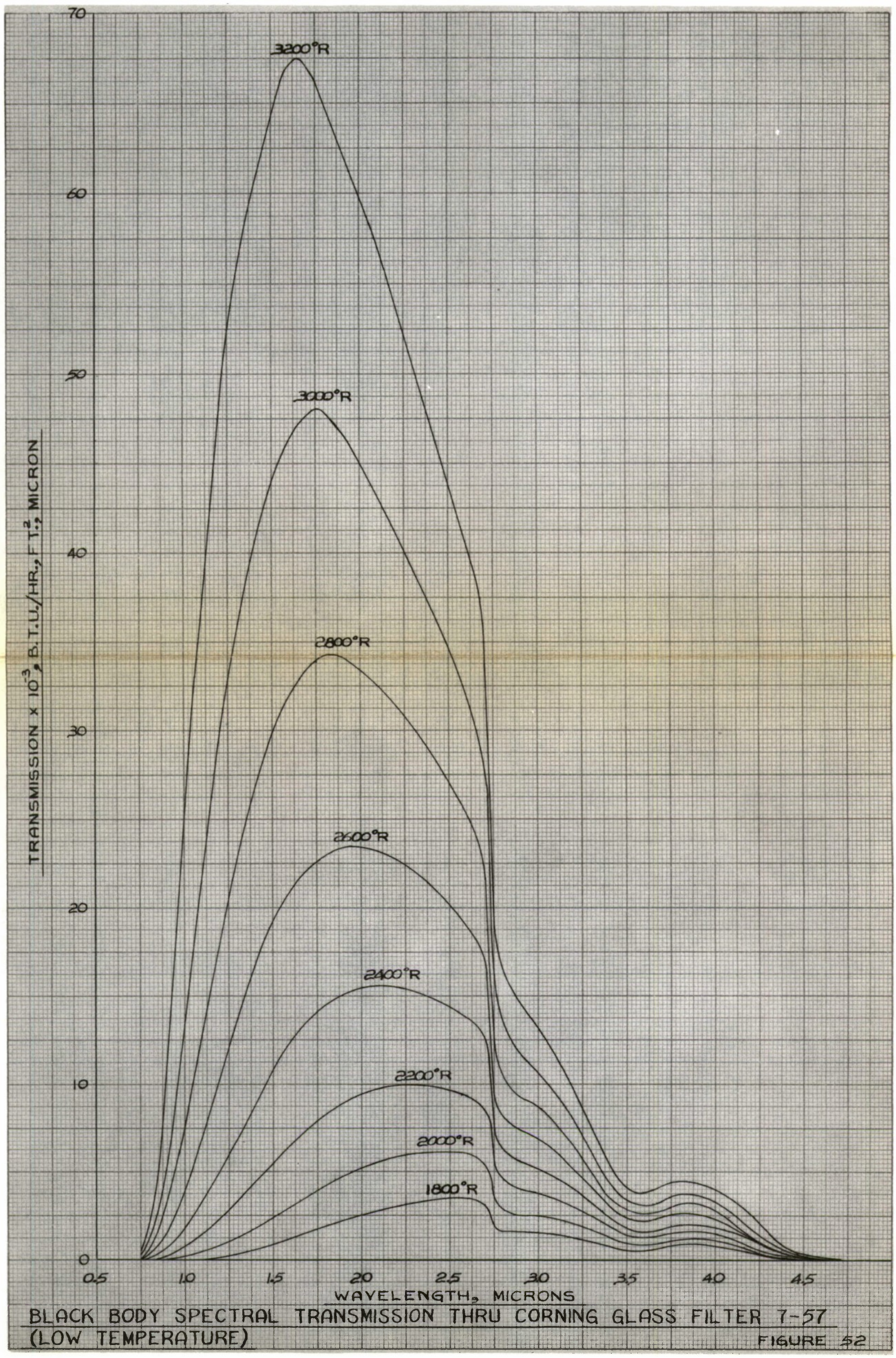
AFTR 5874

FIGURE 49



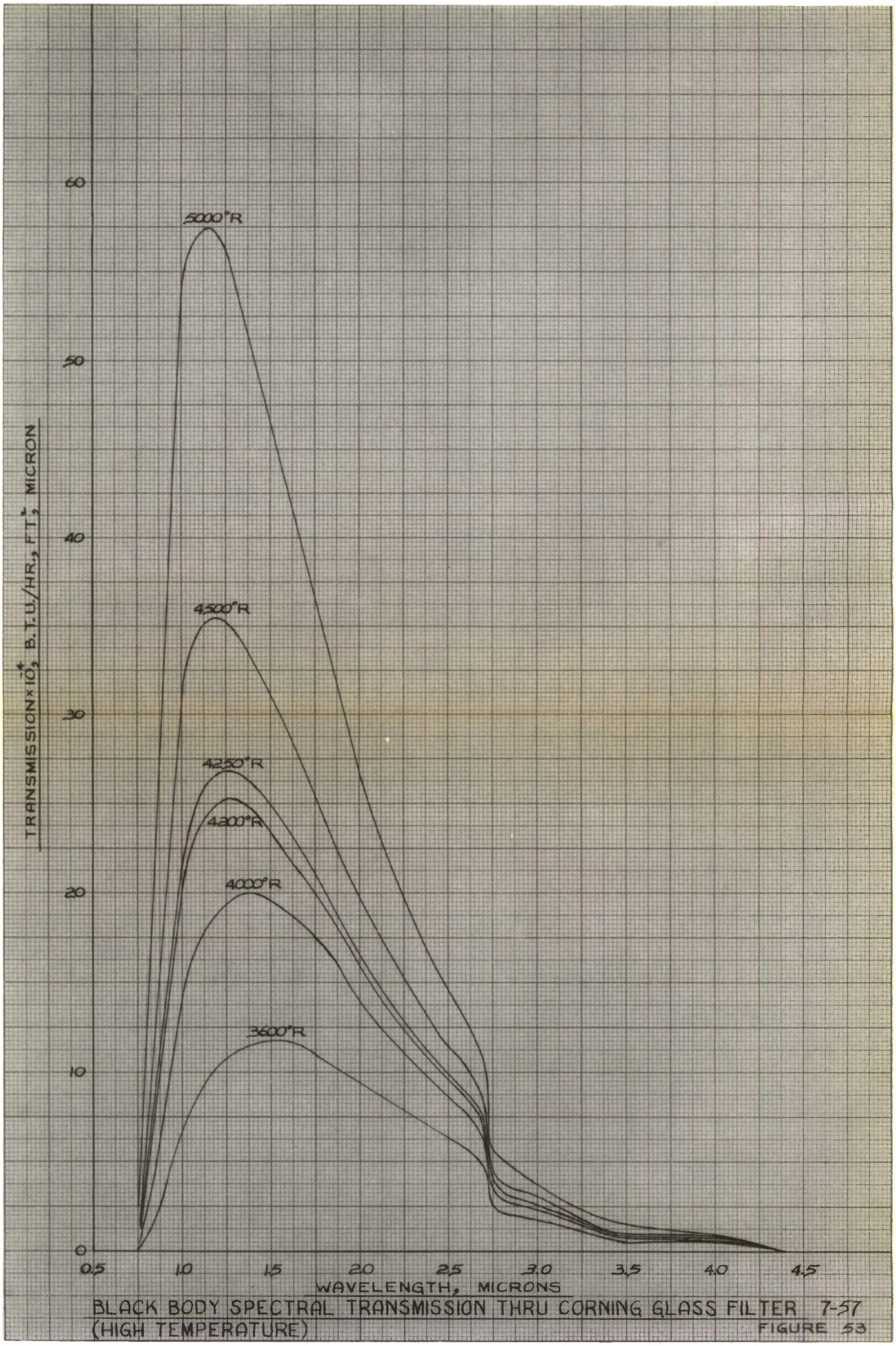
BLACK BODY SPECTRAL TRANSMISSION THRU CORNING GLASS FILTER 7-56 (HIGH TEMPERATURE)

FIGURE 51



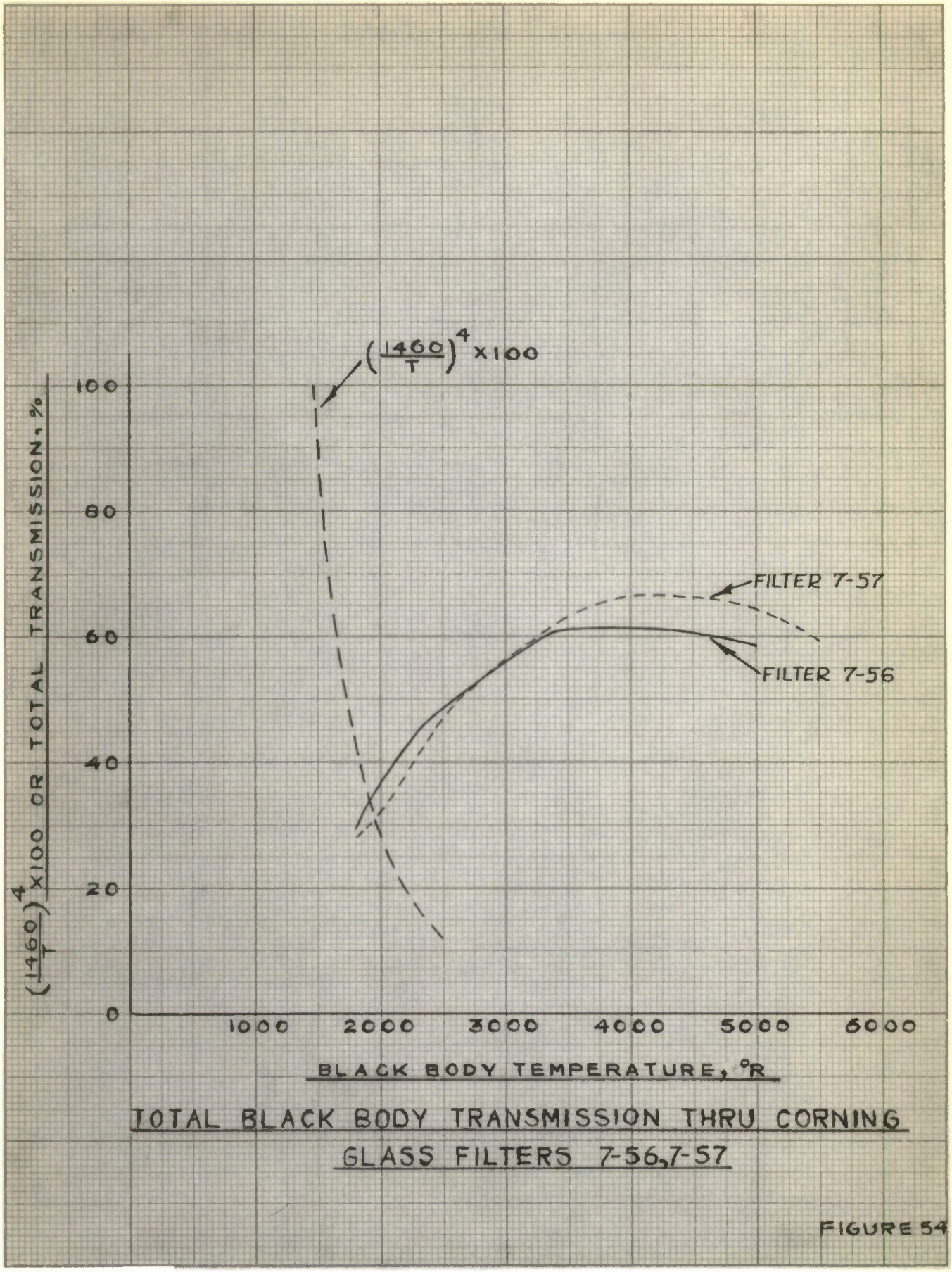
BLACK BODY SPECTRAL TRANSMISSION THRU CORNING GLASS FILTER 7-57 (LOW TEMPERATURE)

FIGURE 52



BLACK BODY SPECTRAL TRANSMISSION THRU CORNING GLASS FILTER 7-57
(HIGH TEMPERATURE)

FIGURE 53

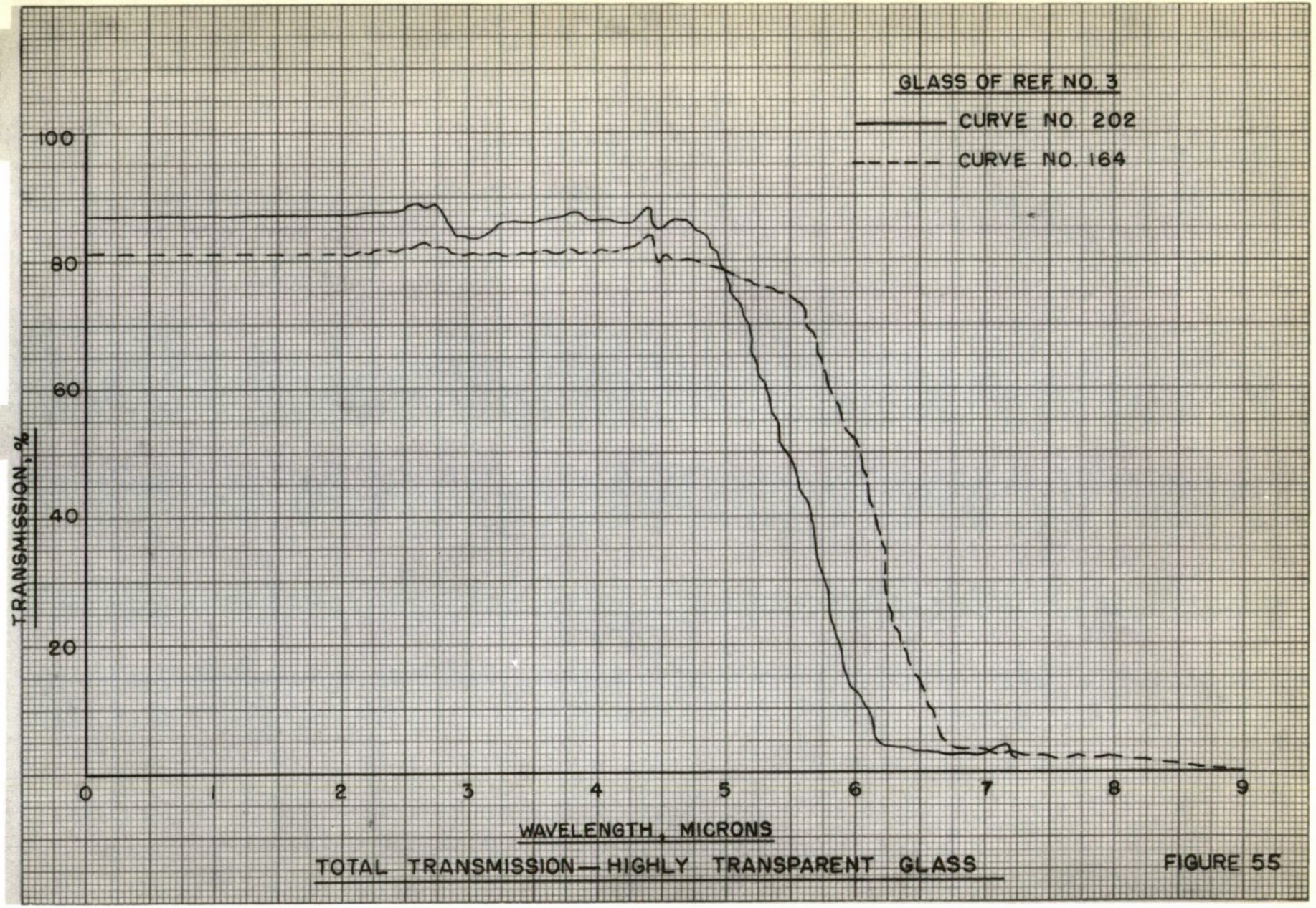


TOTAL BLACK BODY TRANSMISSION THRU CORNING GLASS FILTERS 7-56, 7-57

FIGURE 54

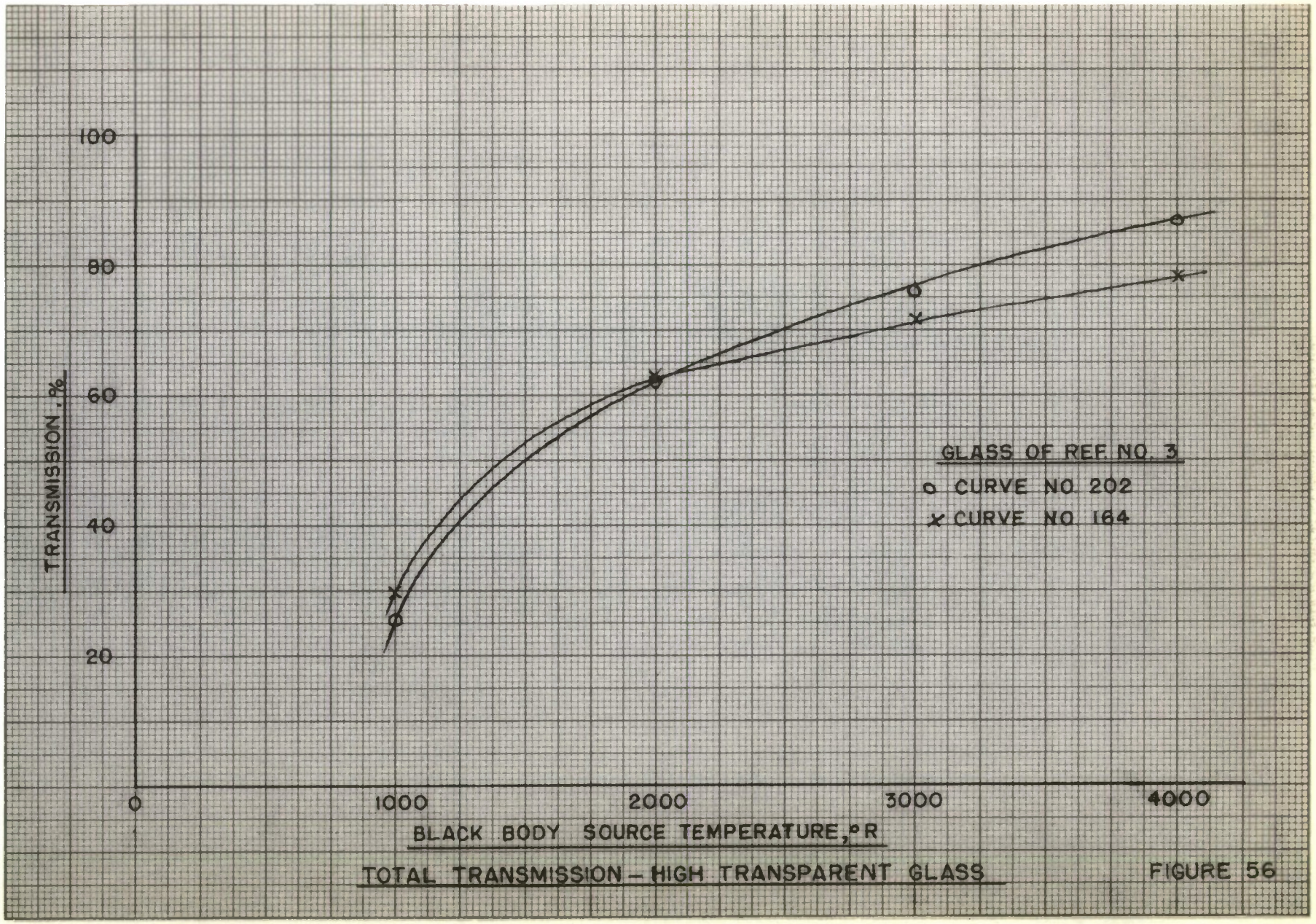
AFTR 5874

144



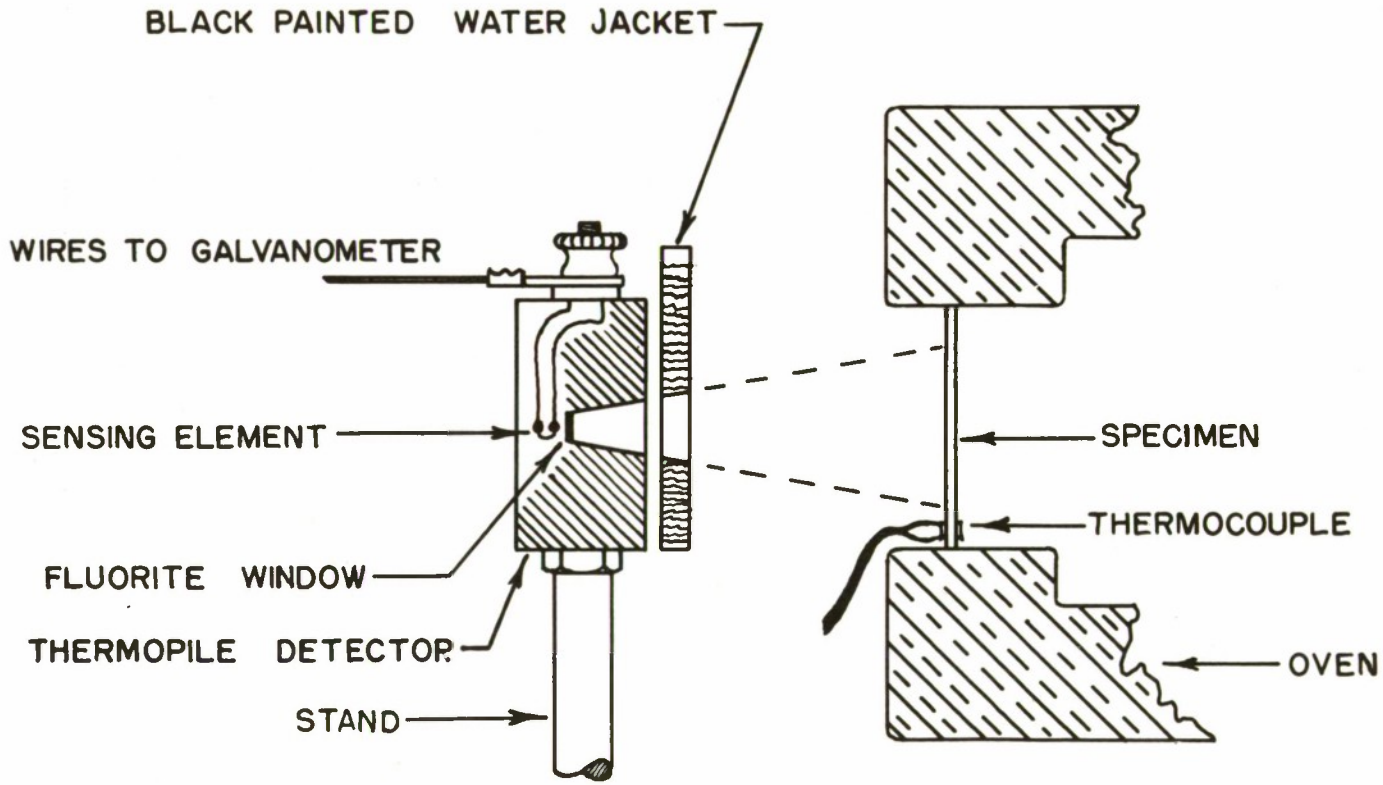
TOTAL TRANSMISSION — HIGHLY TRANSPARENT GLASS

FIGURE 55



TOTAL TRANSMISSION – HIGH TRANSPARENT GLASS

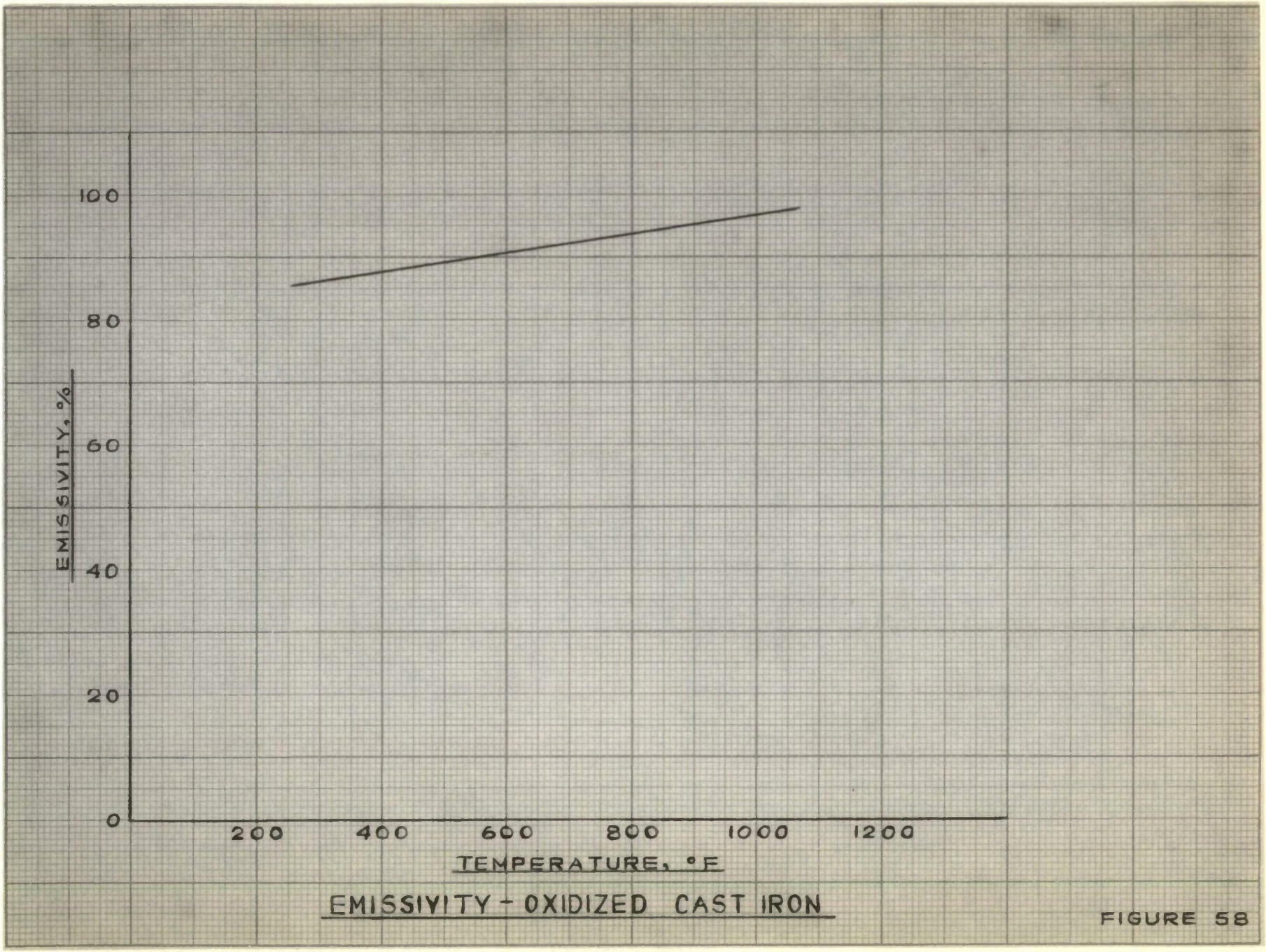
FIGURE 56



SCHEMATIC OF EMISSIVITY SET-UP

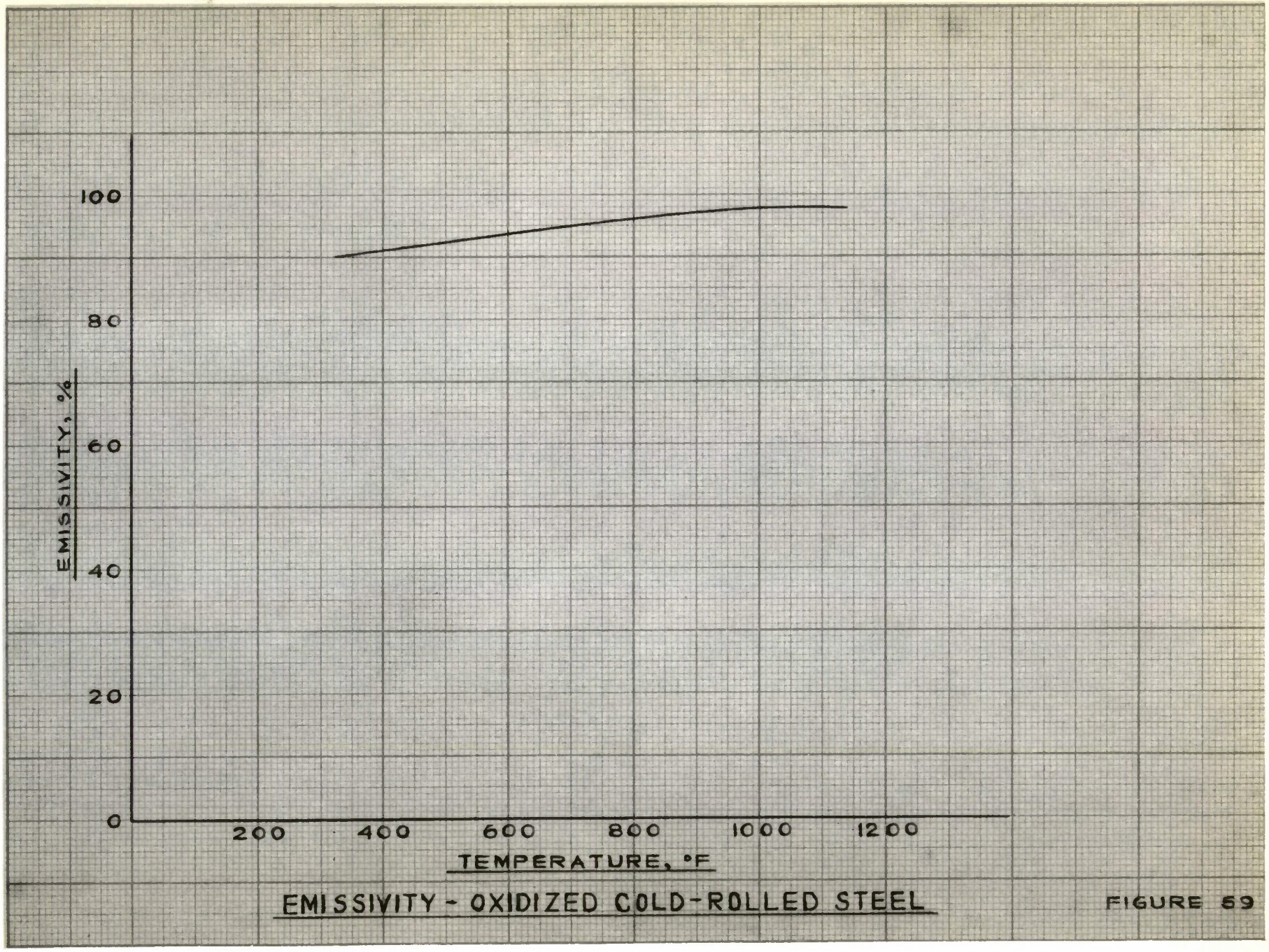
FIGURE 57

AFTR 5874



EMISSIVITY - OXIDIZED CAST IRON

FIGURE 58

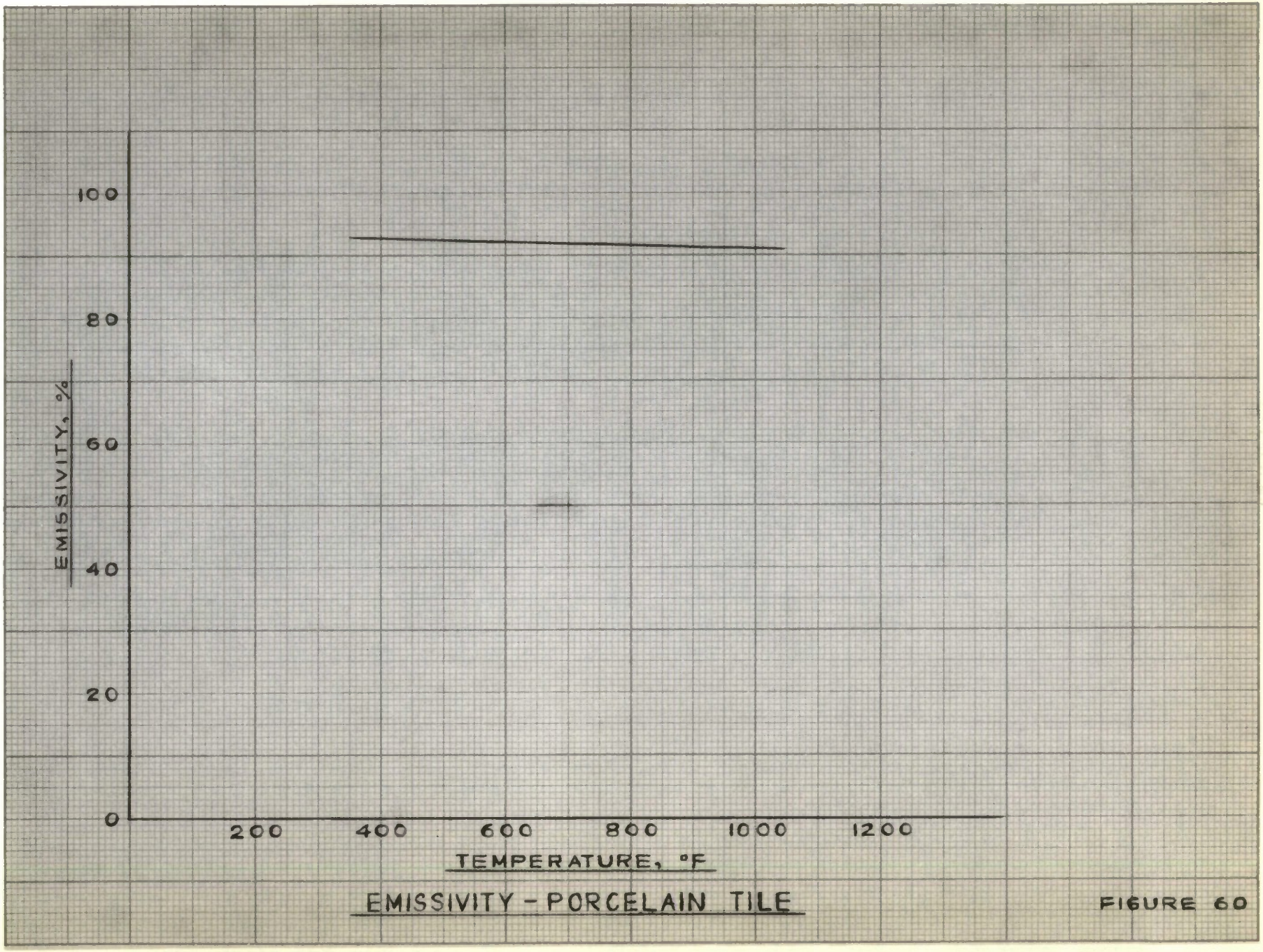


EMISSIVITY - OXIDIZED COLD-ROLLED STEEL

FIGURE 69

AFTR 5874

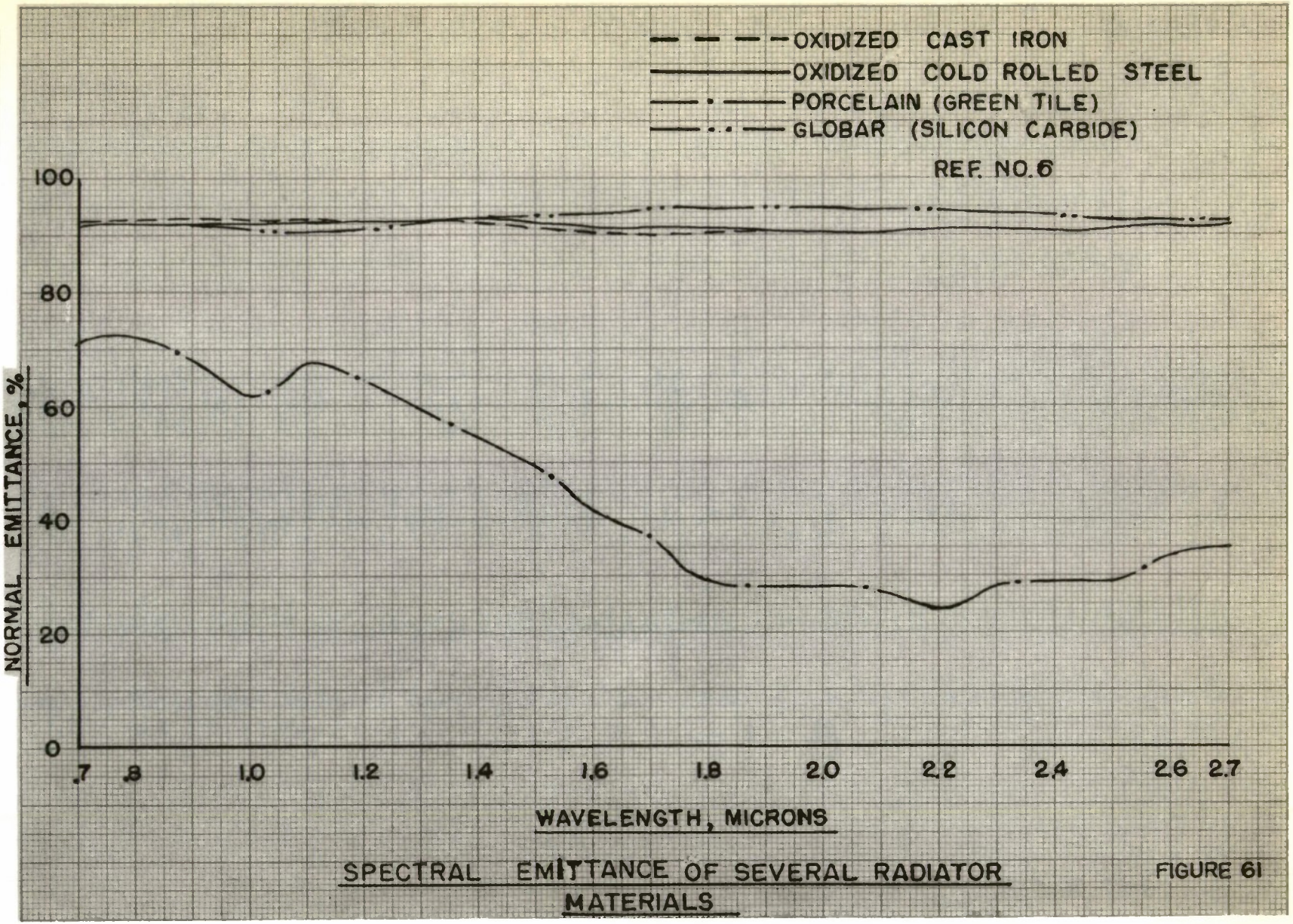
149



EMISSIVITY - PORCELAIN TILE

FIGURE 60

AFTR 5874



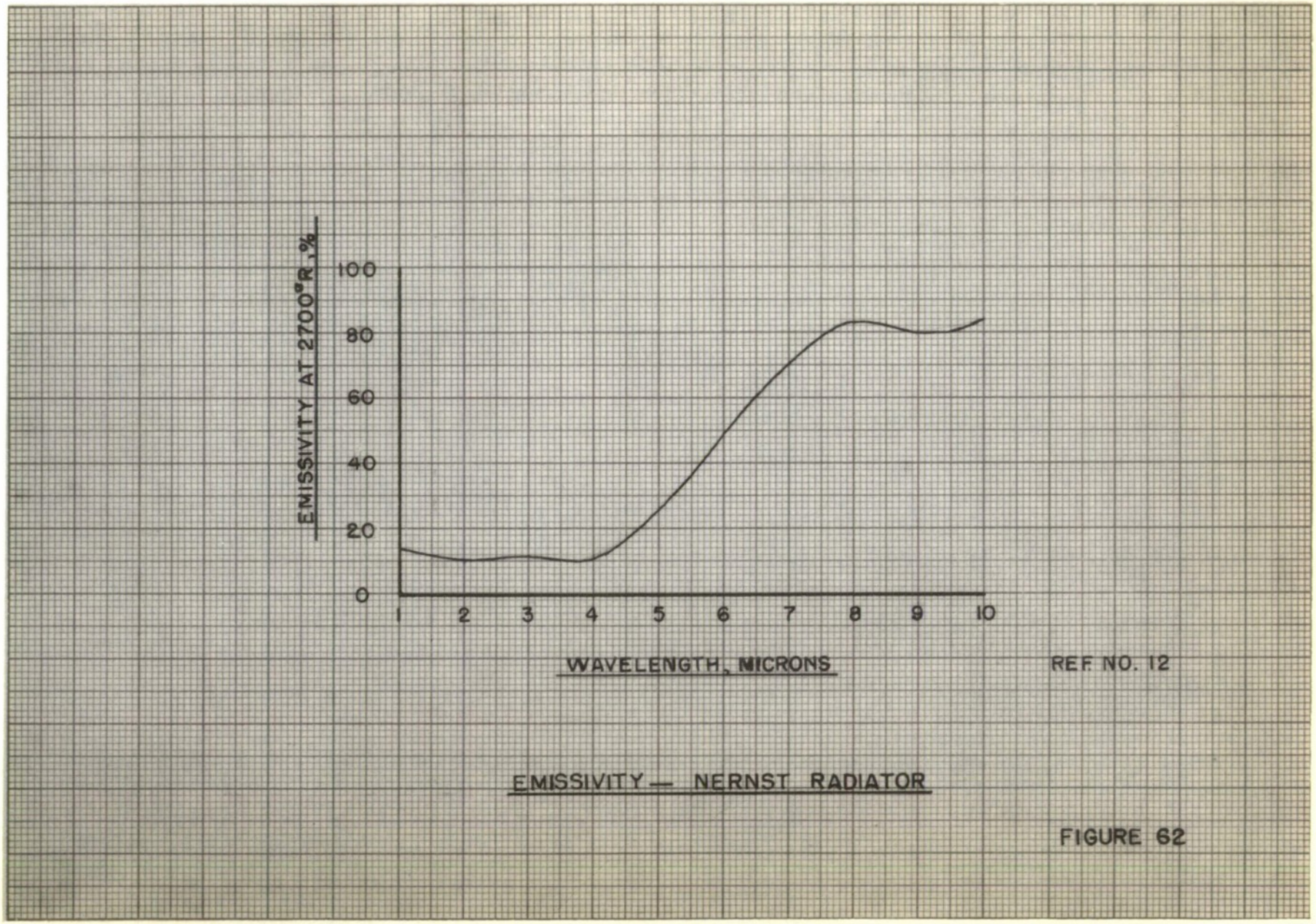
SPECTRAL EMITTANCE OF SEVERAL RADIATOR MATERIALS

FIGURE 61

150

AFTR 5874

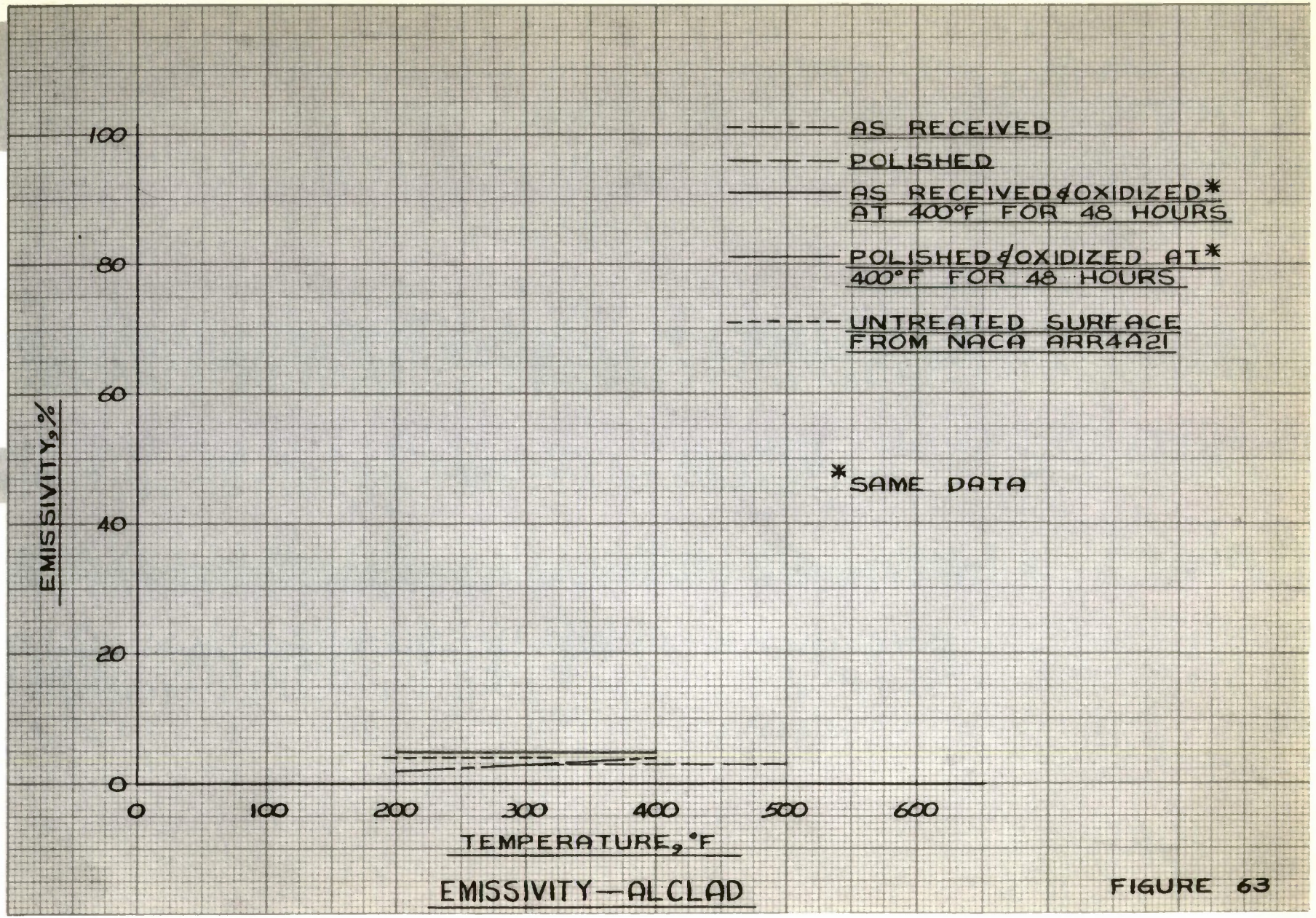
151



EMISSIVITY — NERNST RADIATOR

FIGURE 62

AFTR 5974

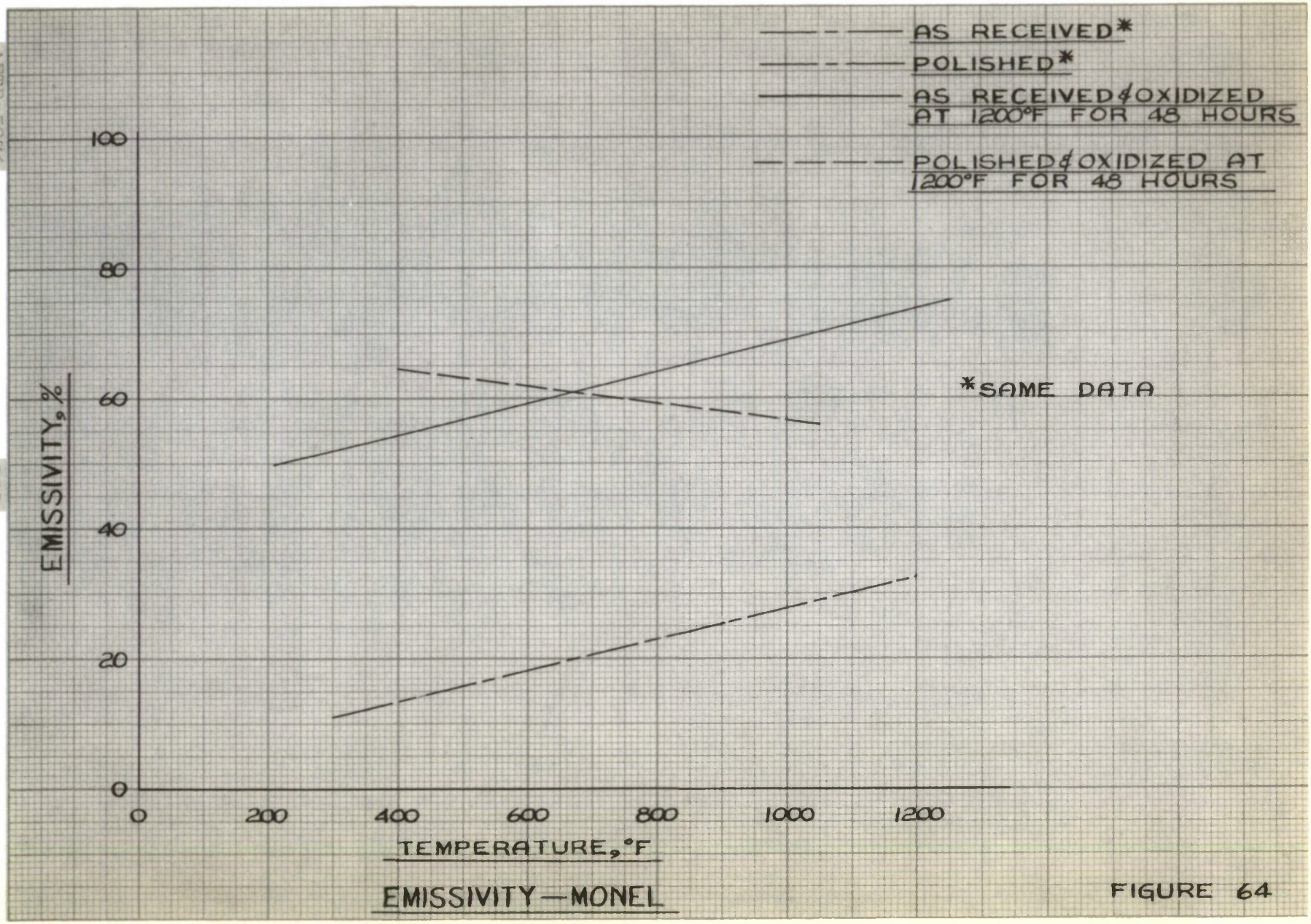


EMISSIVITY—ALCLAD

FIGURE 63

AFTR 5874

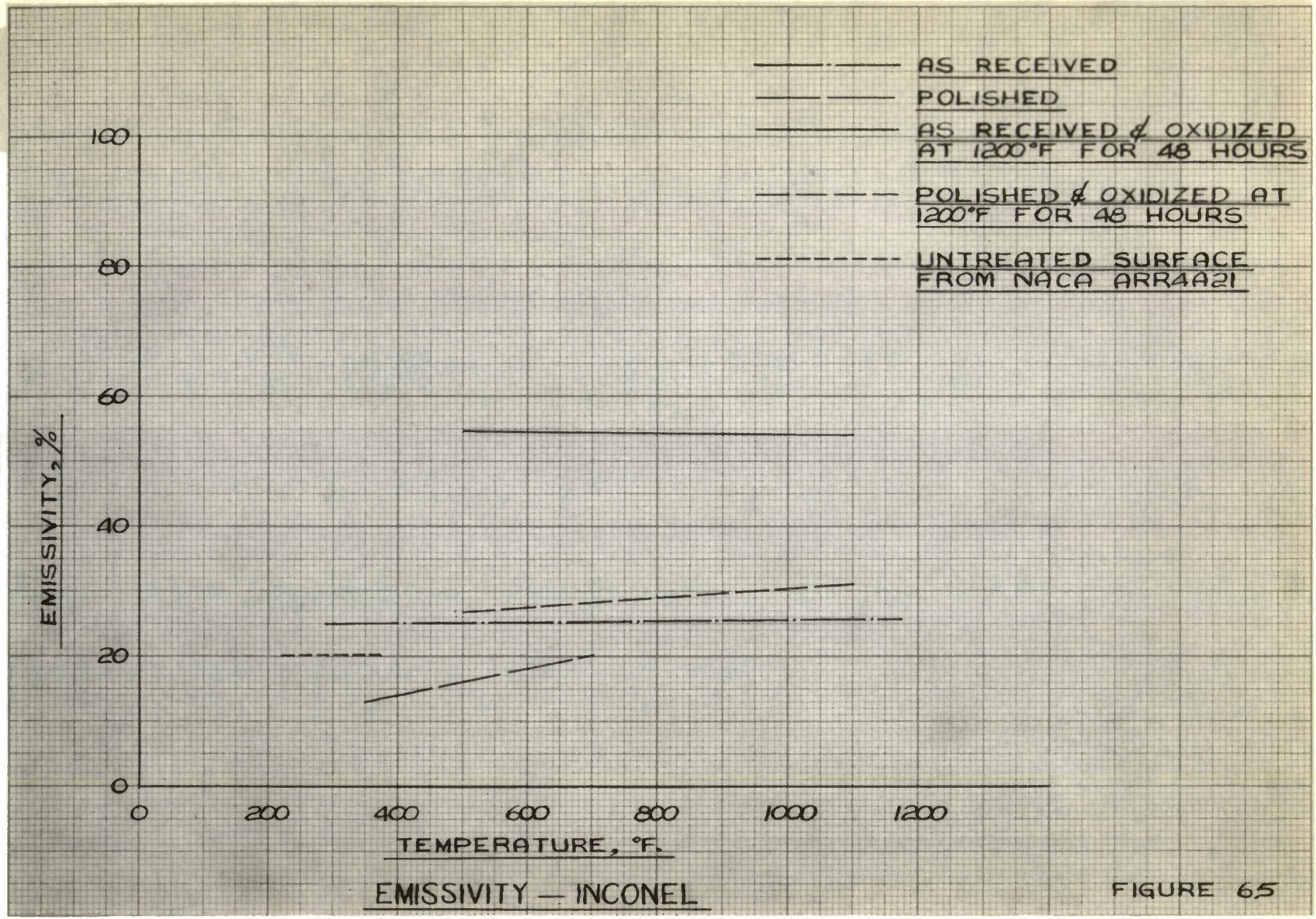
153



EMISSIVITY—MONEL

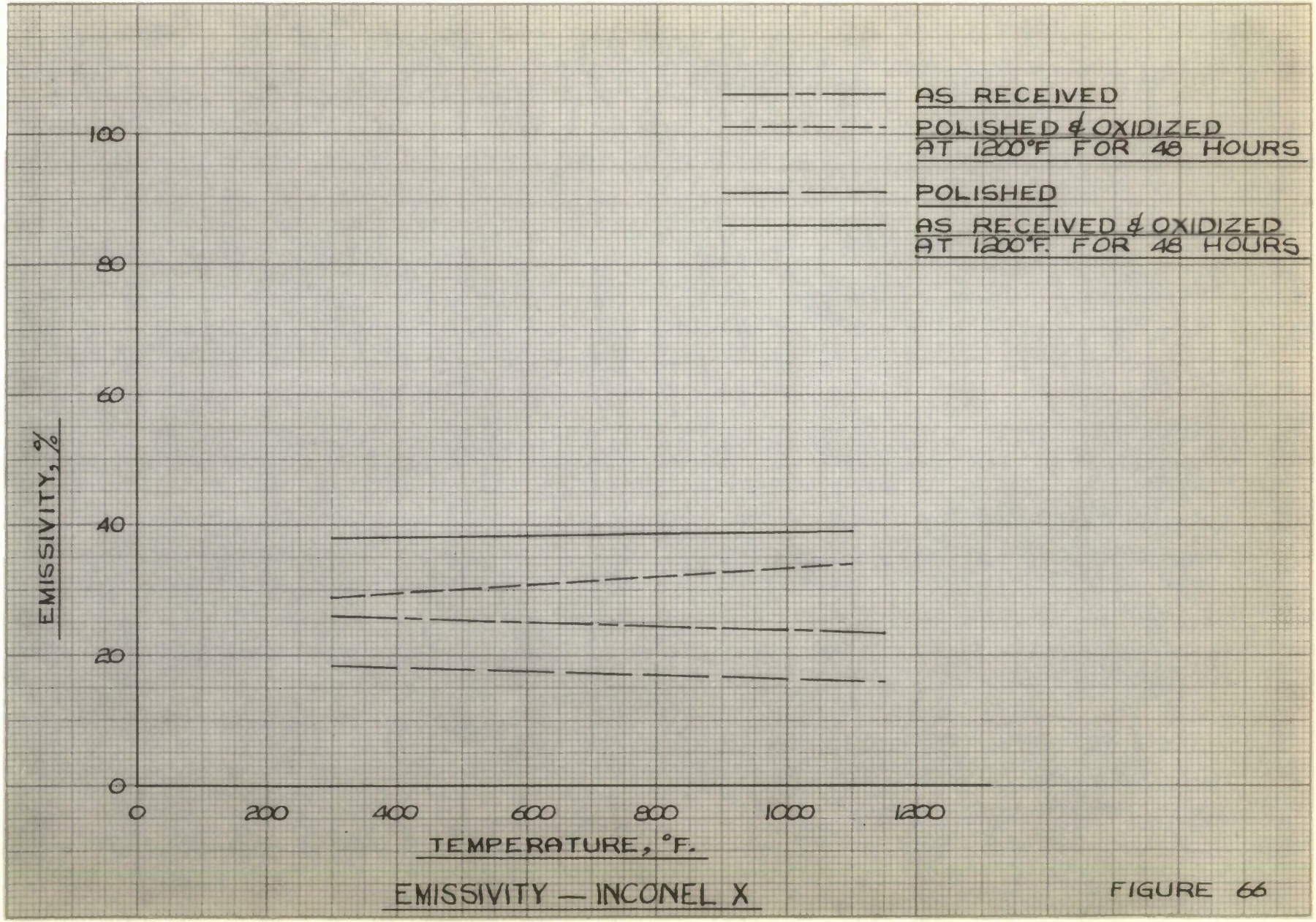
FIGURE 64

AFTR 5874



EMISSIVITY — INCONEL

FIGURE 65



EMISSIVITY — INCONEL X

FIGURE 66

AFTR 5674

156

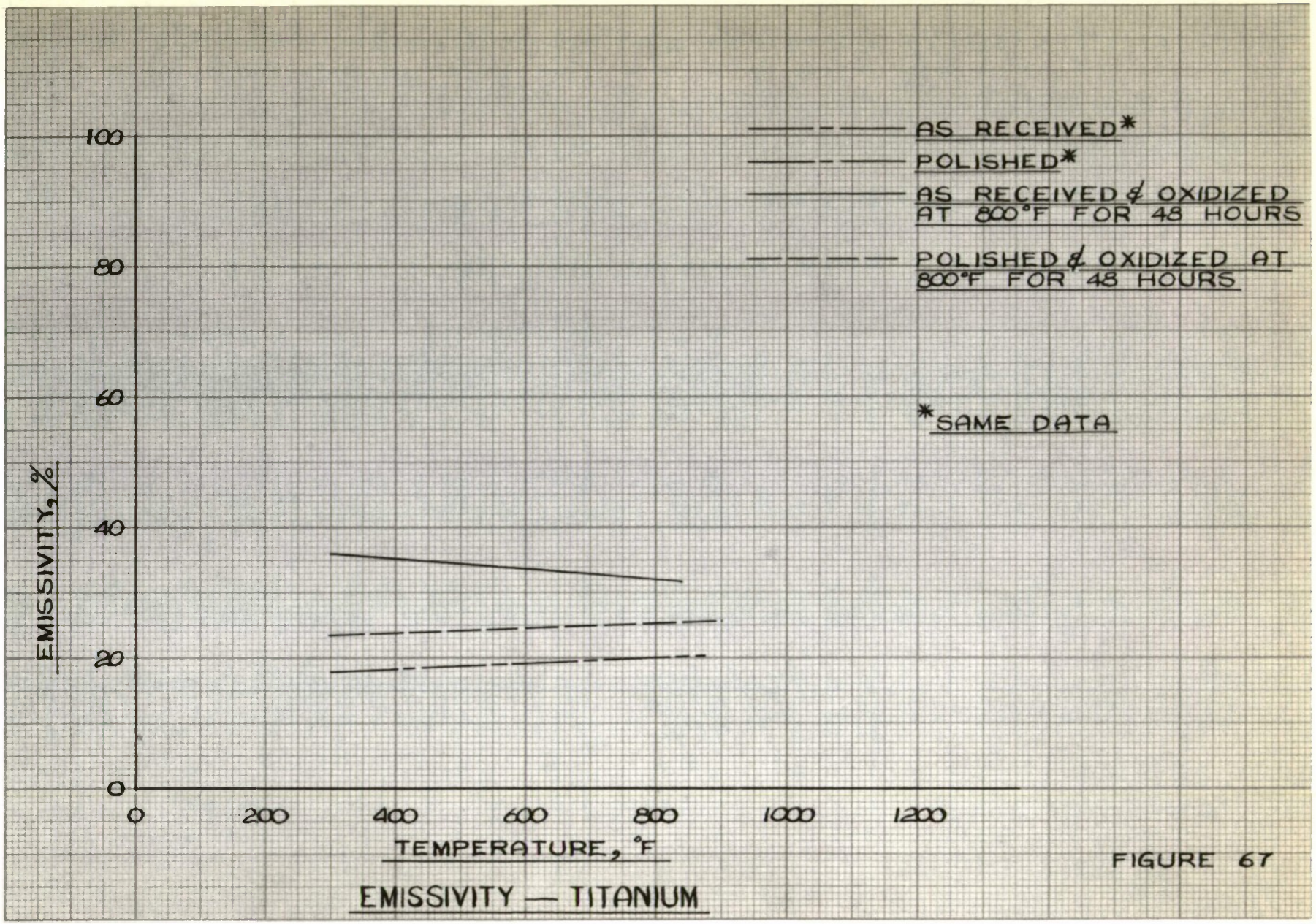
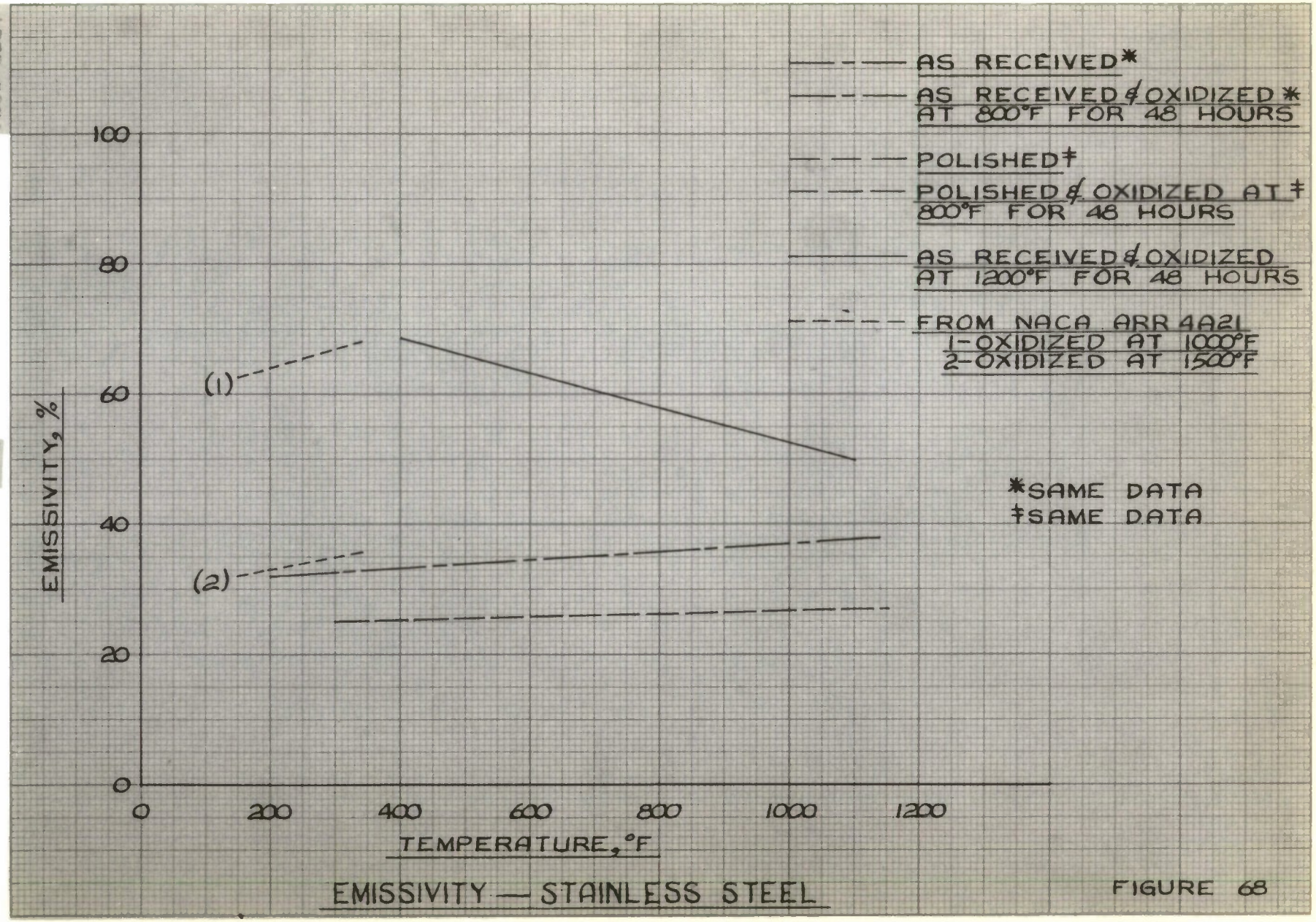


FIGURE 67

EMISSIVITY — TITANIUM

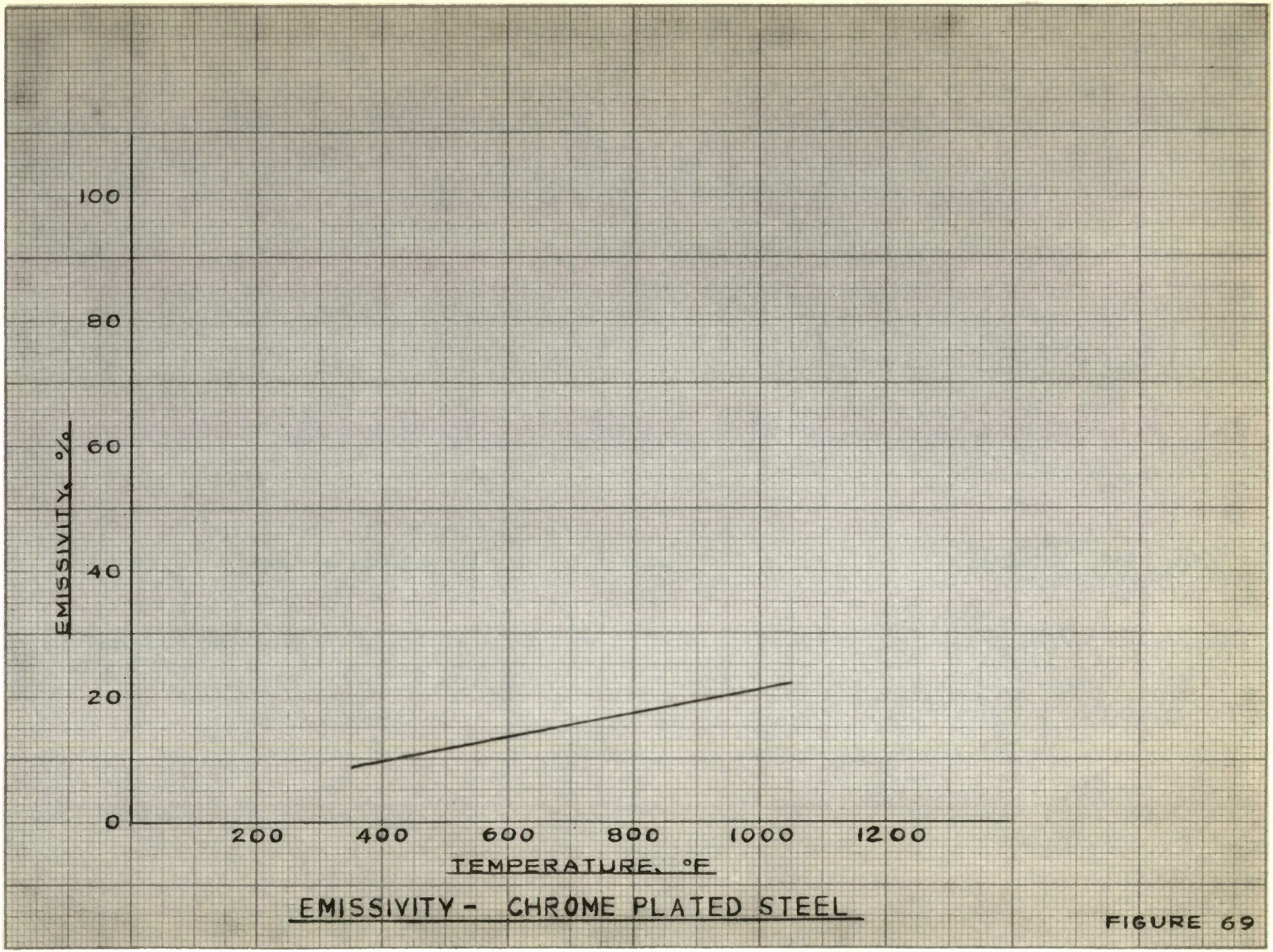
AFTR 5874



EMISSIVITY — STAINLESS STEEL

FIGURE 68

157

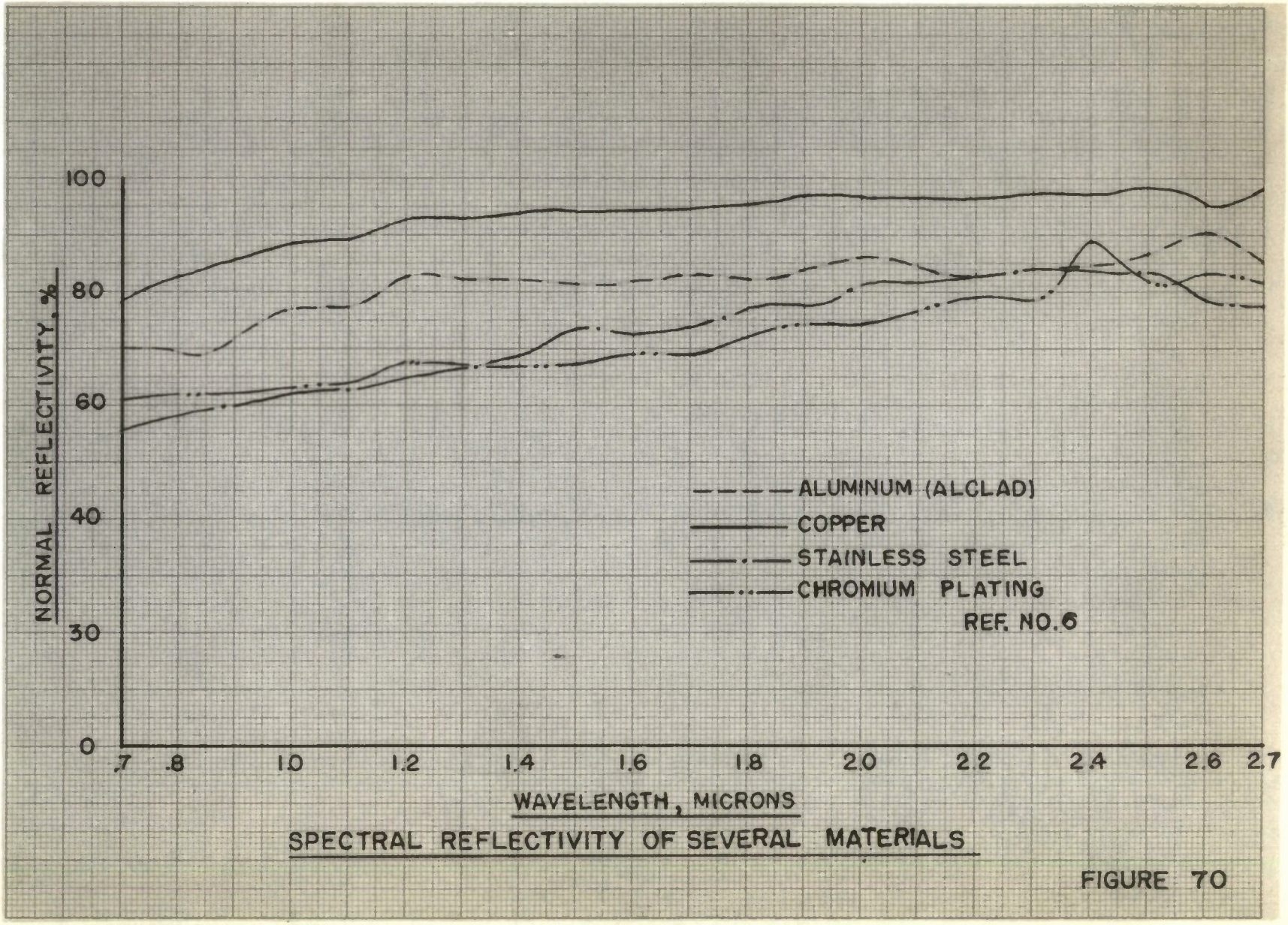


EMISSIVITY - CHROME PLATED STEEL

FIGURE 69

AFFR 5874

159

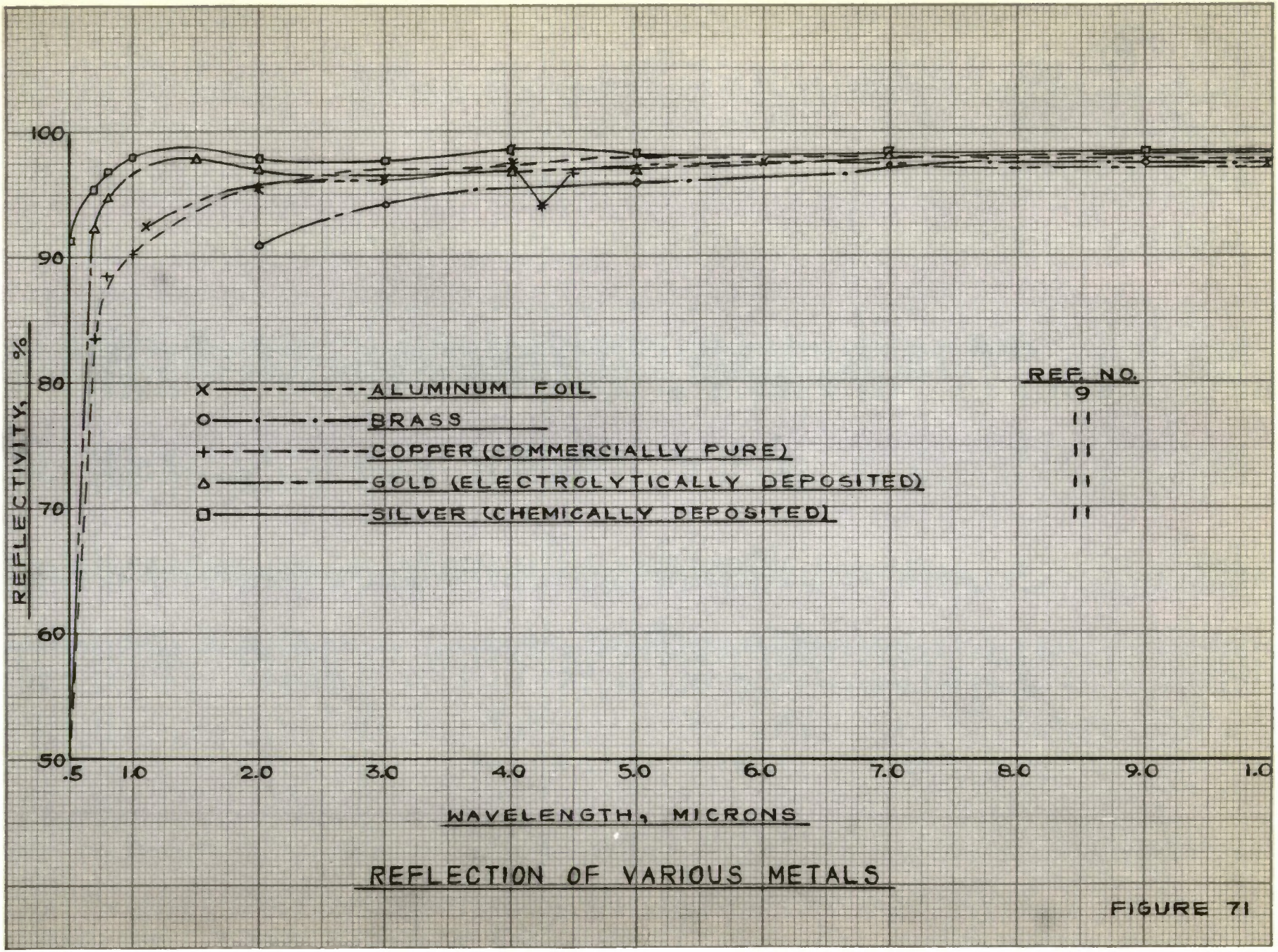


SPECTRAL REFLECTIVITY OF SEVERAL MATERIALS

FIGURE 70

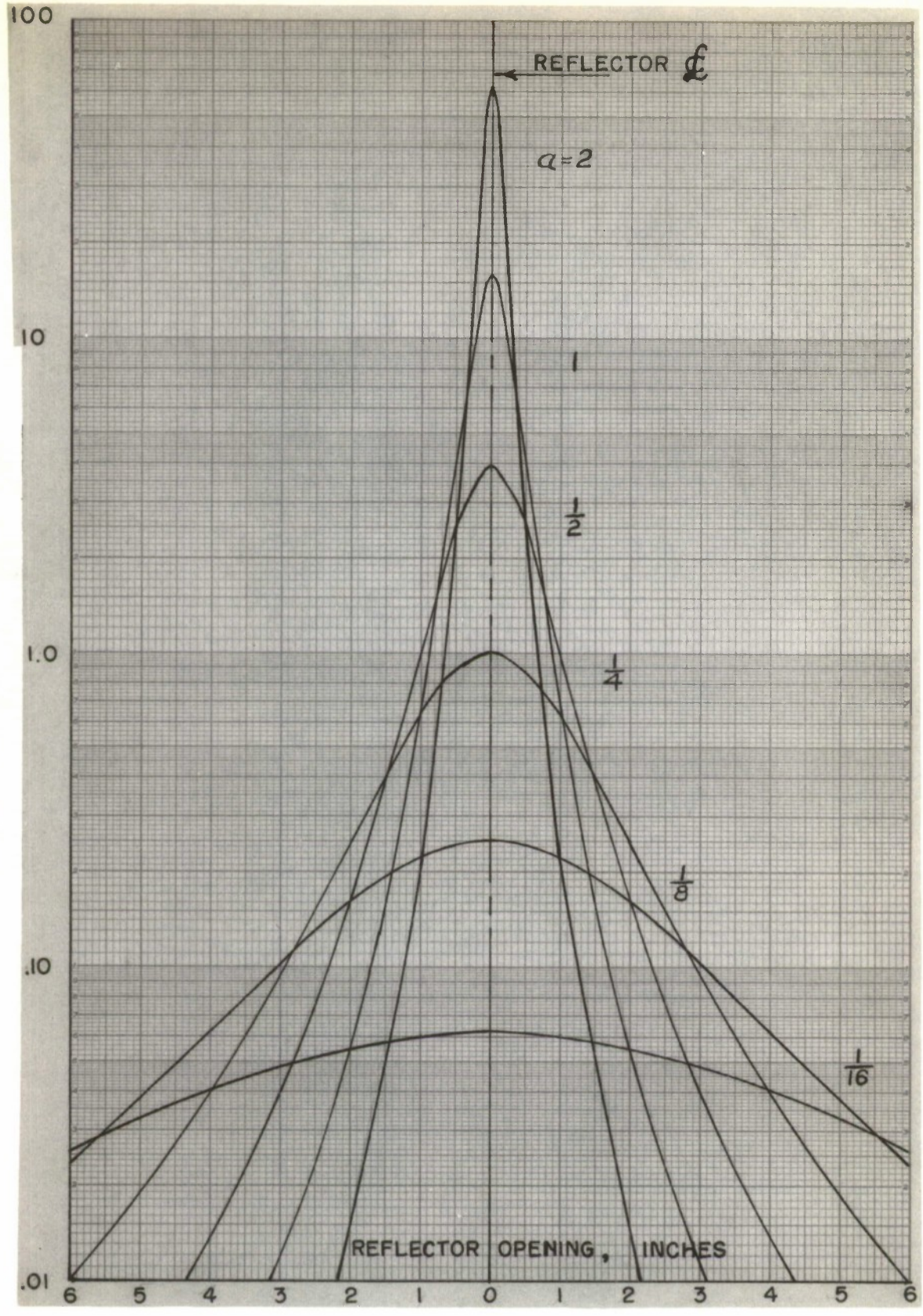
AFTR 5874

160



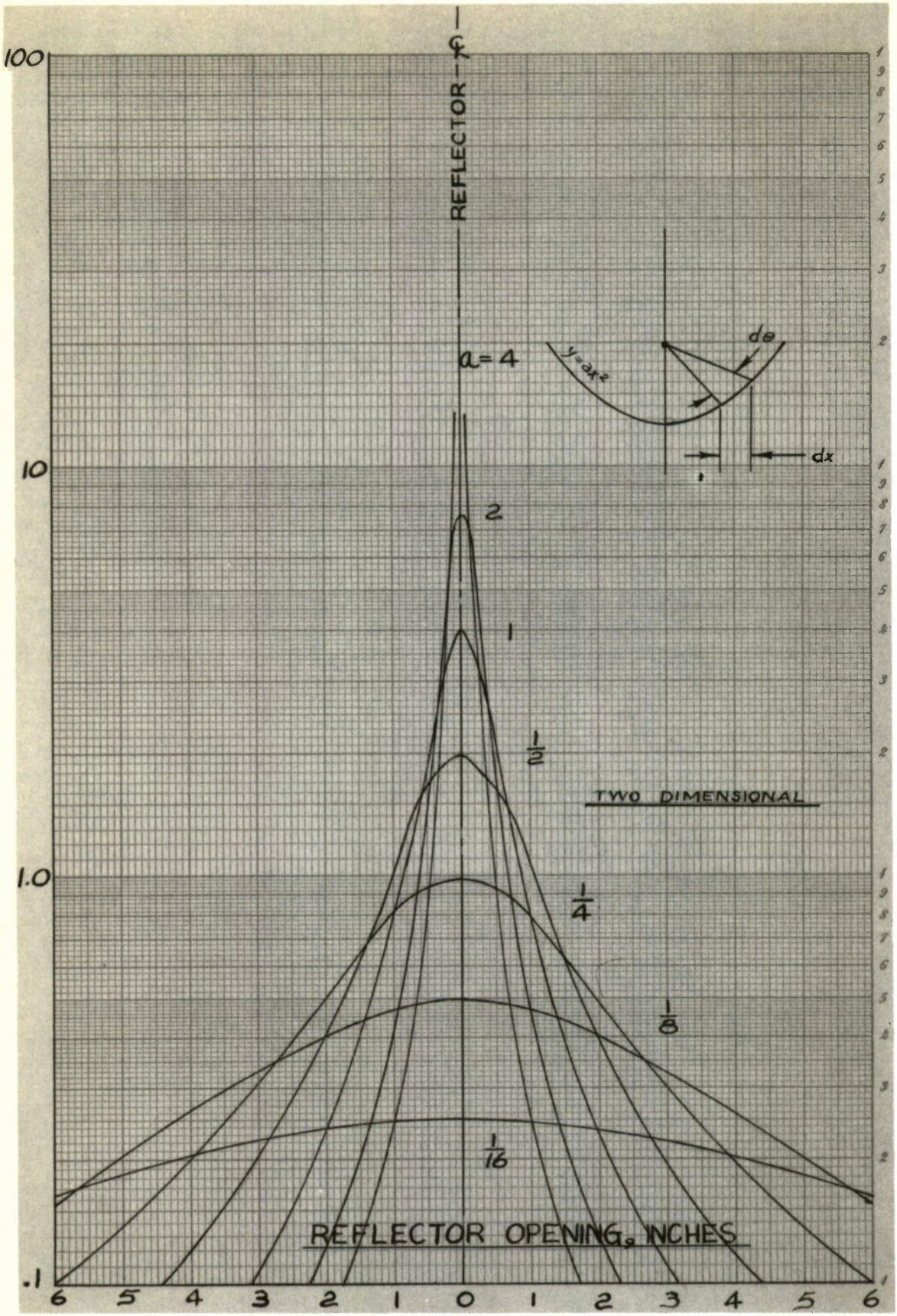
REFLECTION OF VARIOUS METALS

FIGURE 71



DISTRIBUTION OF REFLECTED ENERGY FROM A PARABOLOID CONTAINING A POINT SOURCE AT FOCUS

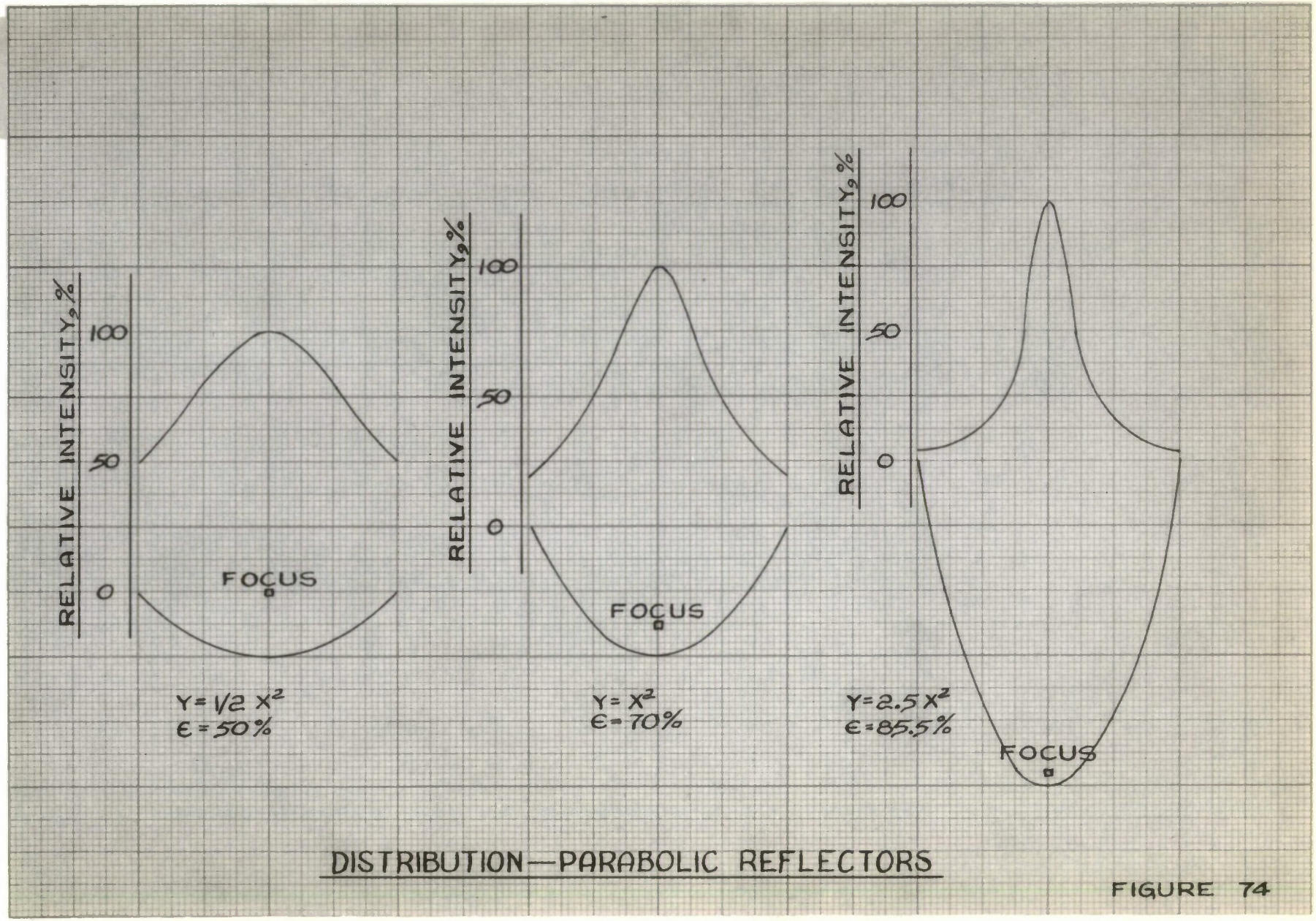
FIGURE 72



DISTRIBUTION OF REFLECTED ENERGY FROM A POINT SOURCE ENCLOSED WITHIN A PARABOLIC REFLECTOR

FIGURE 73

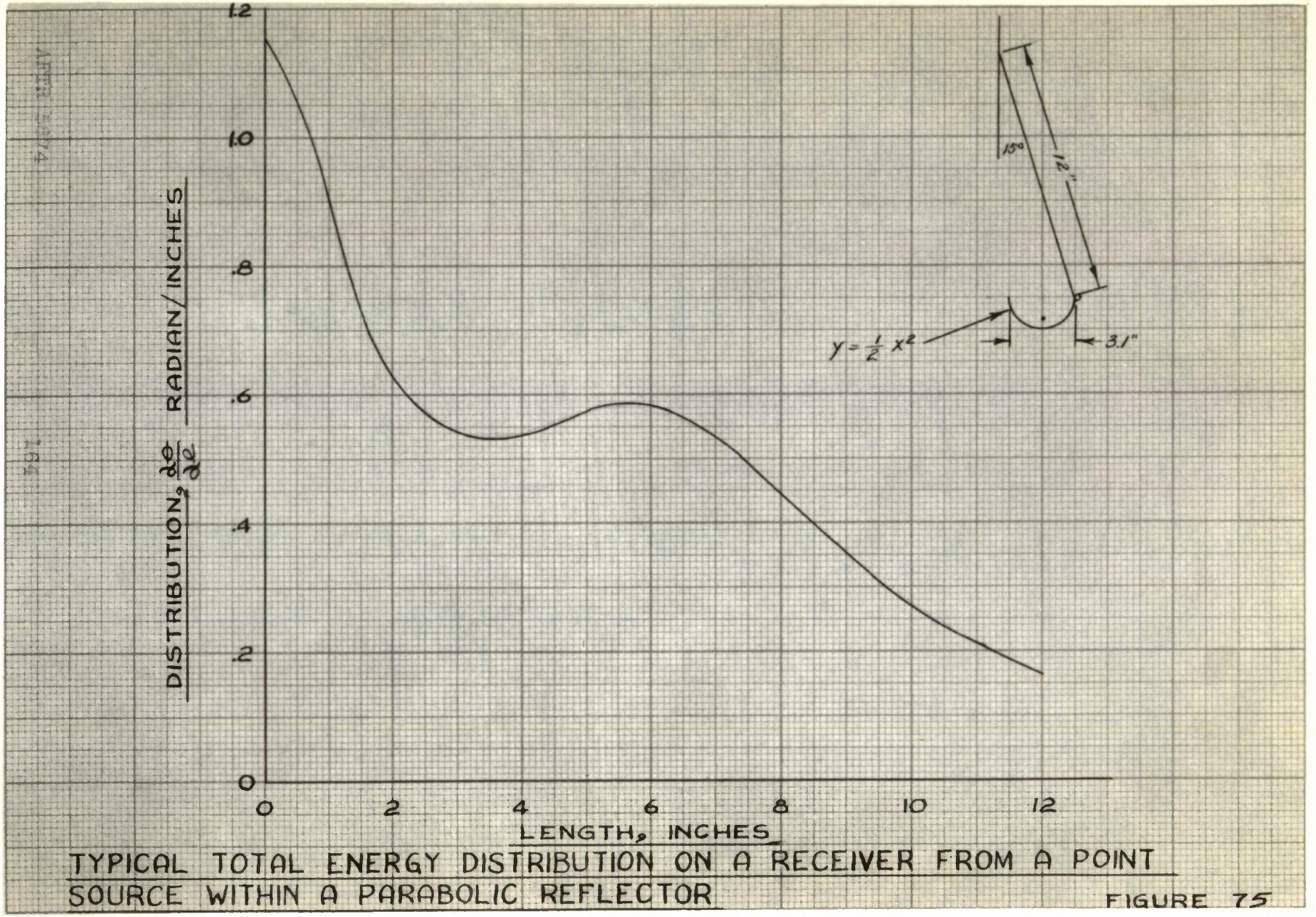
AFTR 5874



DISTRIBUTION—PARABOLIC REFLECTORS

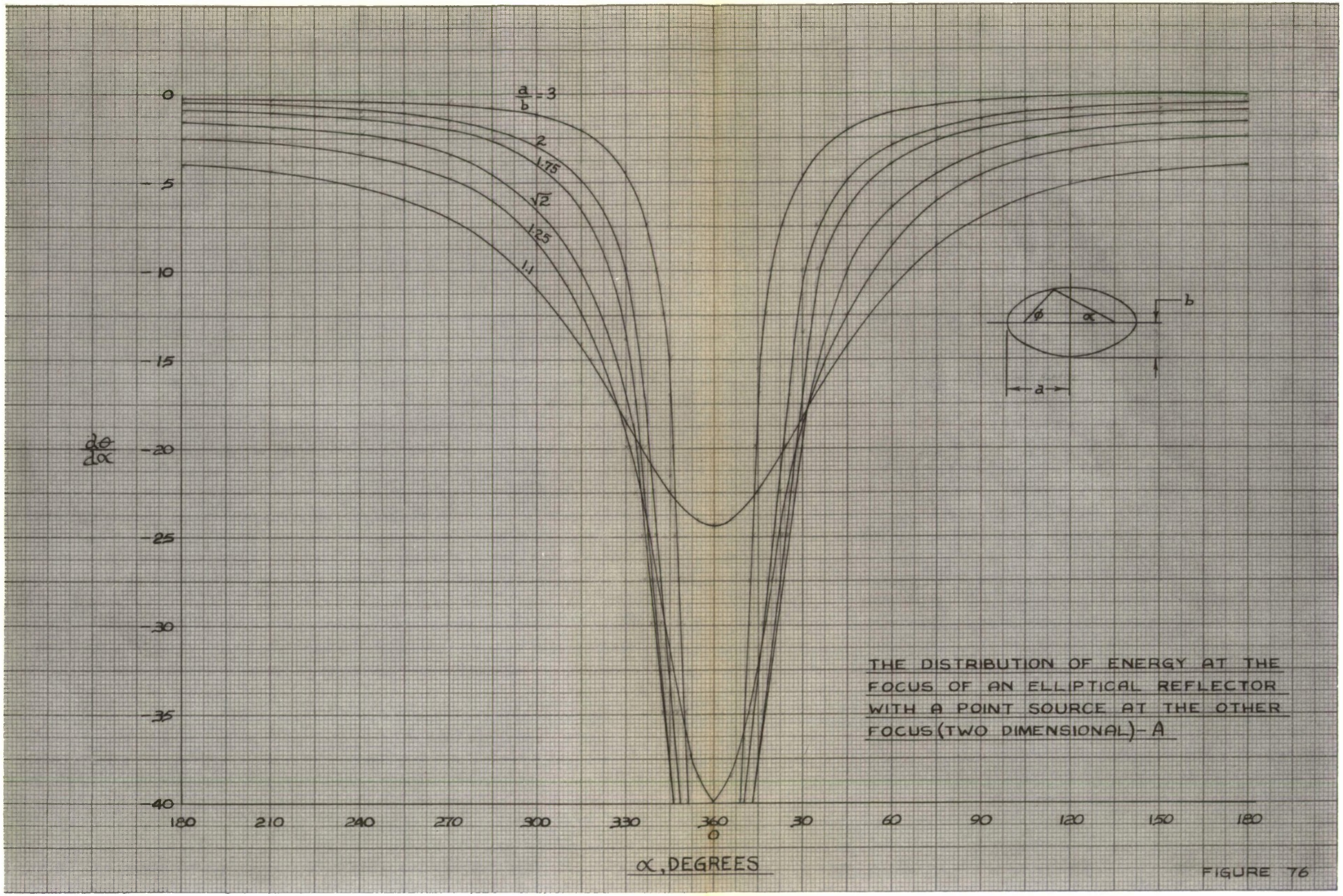
FIGURE 74

162



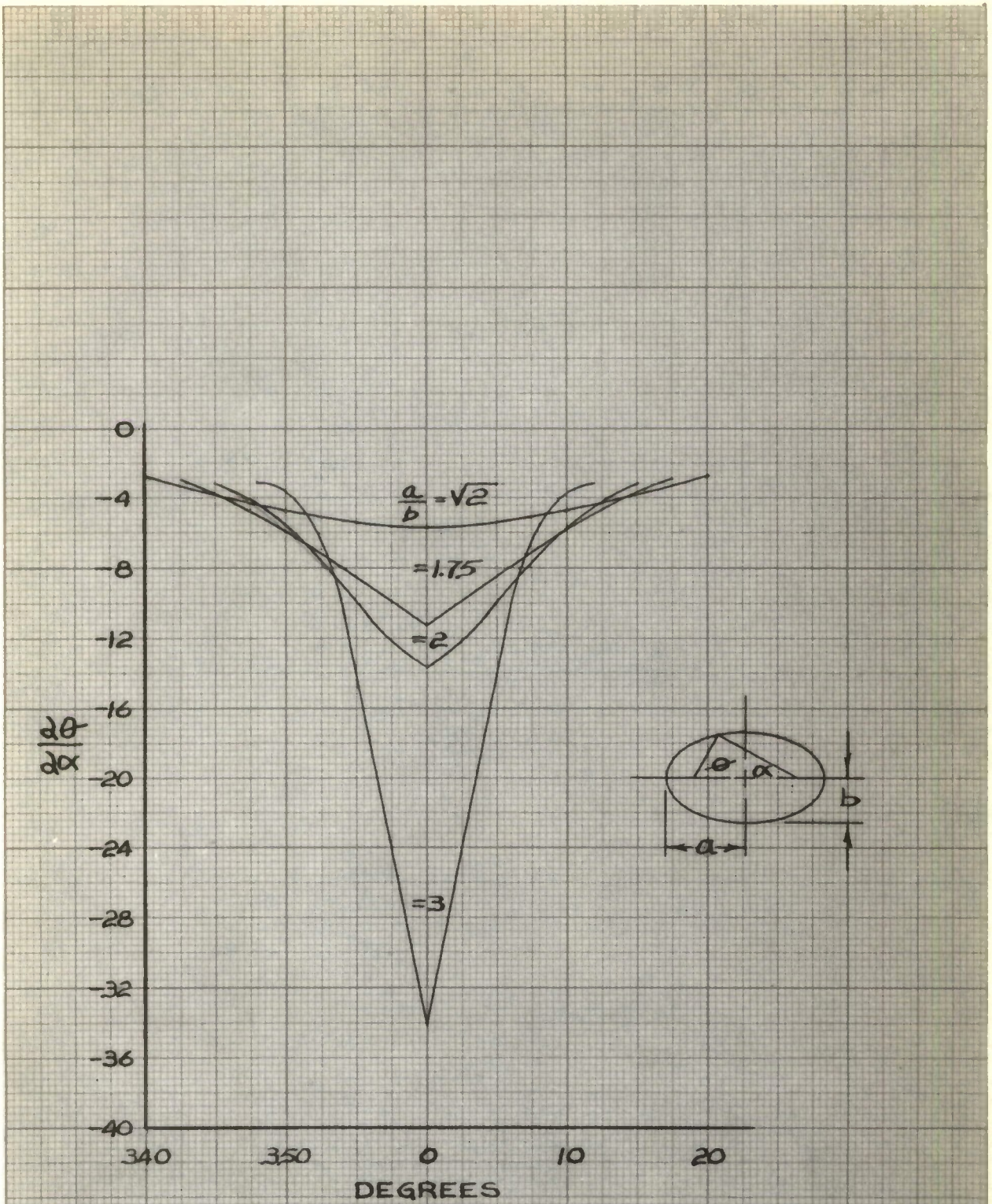
TYPICAL TOTAL ENERGY DISTRIBUTION ON A RECEIVER FROM A POINT SOURCE WITHIN A PARABOLIC REFLECTOR

FIGURE 75



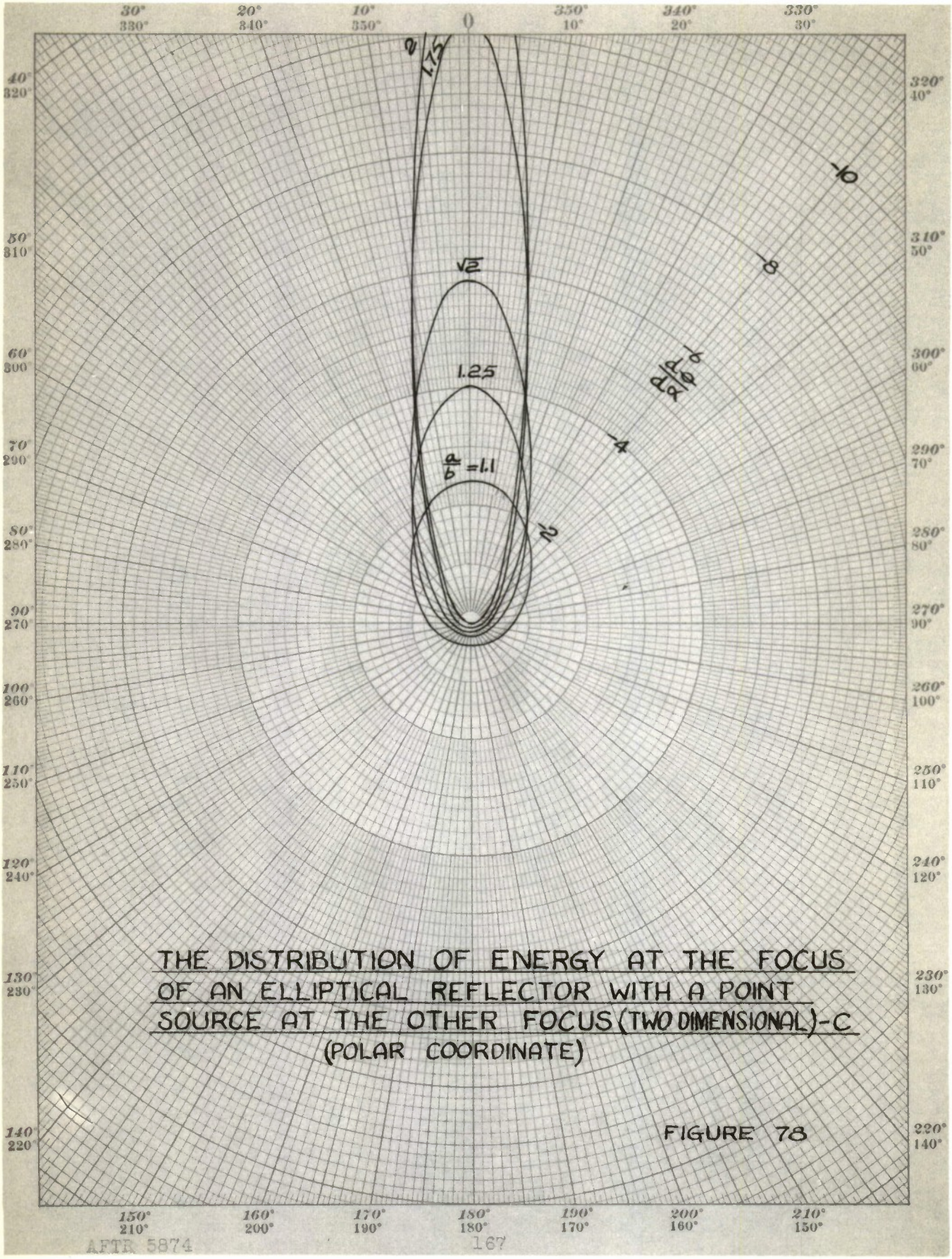
THE DISTRIBUTION OF ENERGY AT THE FOCUS OF AN ELLIPTICAL REFLECTOR WITH A POINT SOURCE AT THE OTHER FOCUS (TWO DIMENSIONAL) - A

FIGURE 76



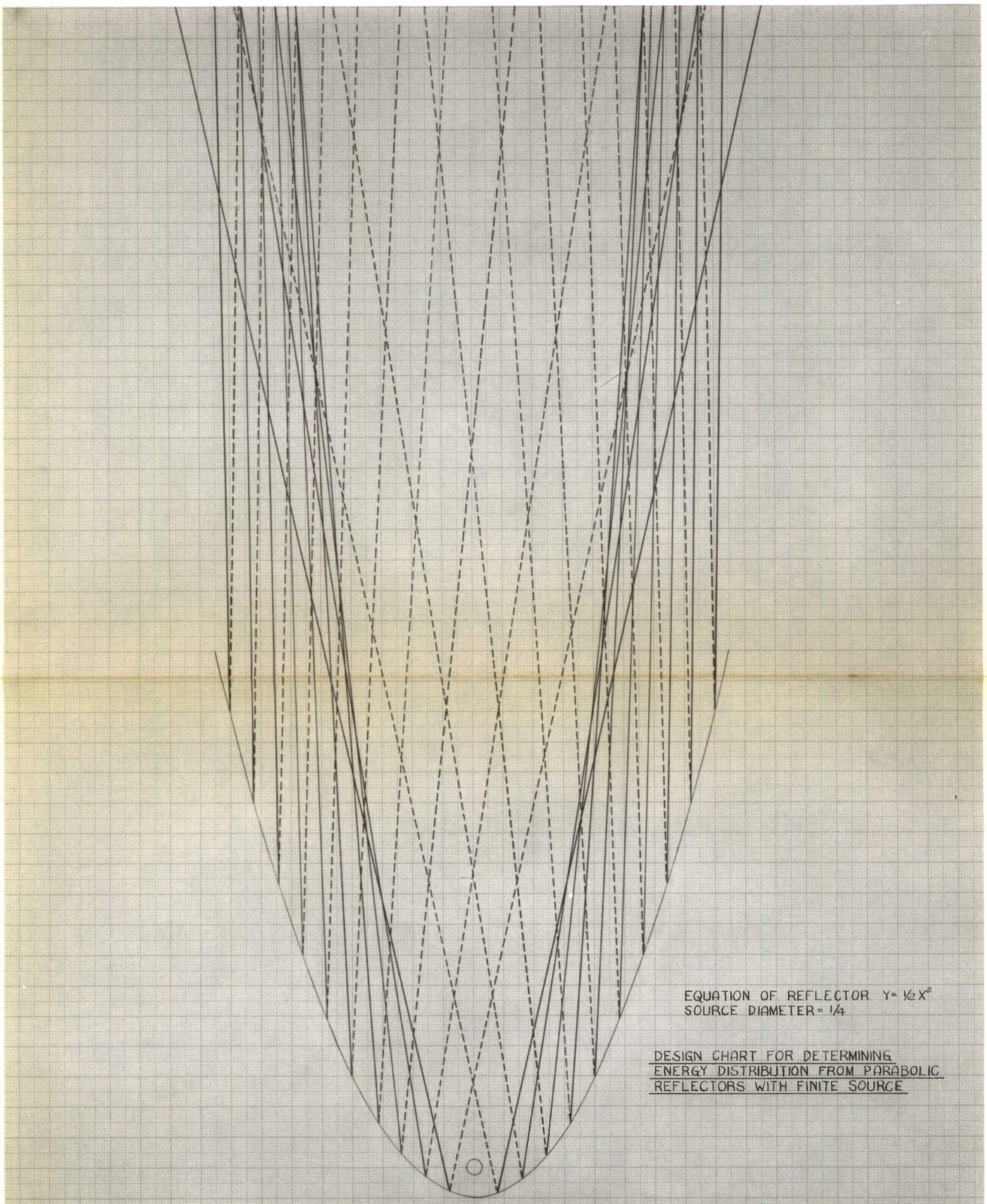
THE DISTRIBUTION OF ENERGY AT THE FOCUS OF AN ELLIPTICAL REFLECTOR WITH A POINT SOURCE AT THE OTHER FOCUS (TWO DIMENSIONAL)-B

FIGURE 77



THE DISTRIBUTION OF ENERGY AT THE FOCUS OF AN ELLIPTICAL REFLECTOR WITH A POINT SOURCE AT THE OTHER FOCUS (TWO DIMENSIONAL)-C
(POLAR COORDINATE)

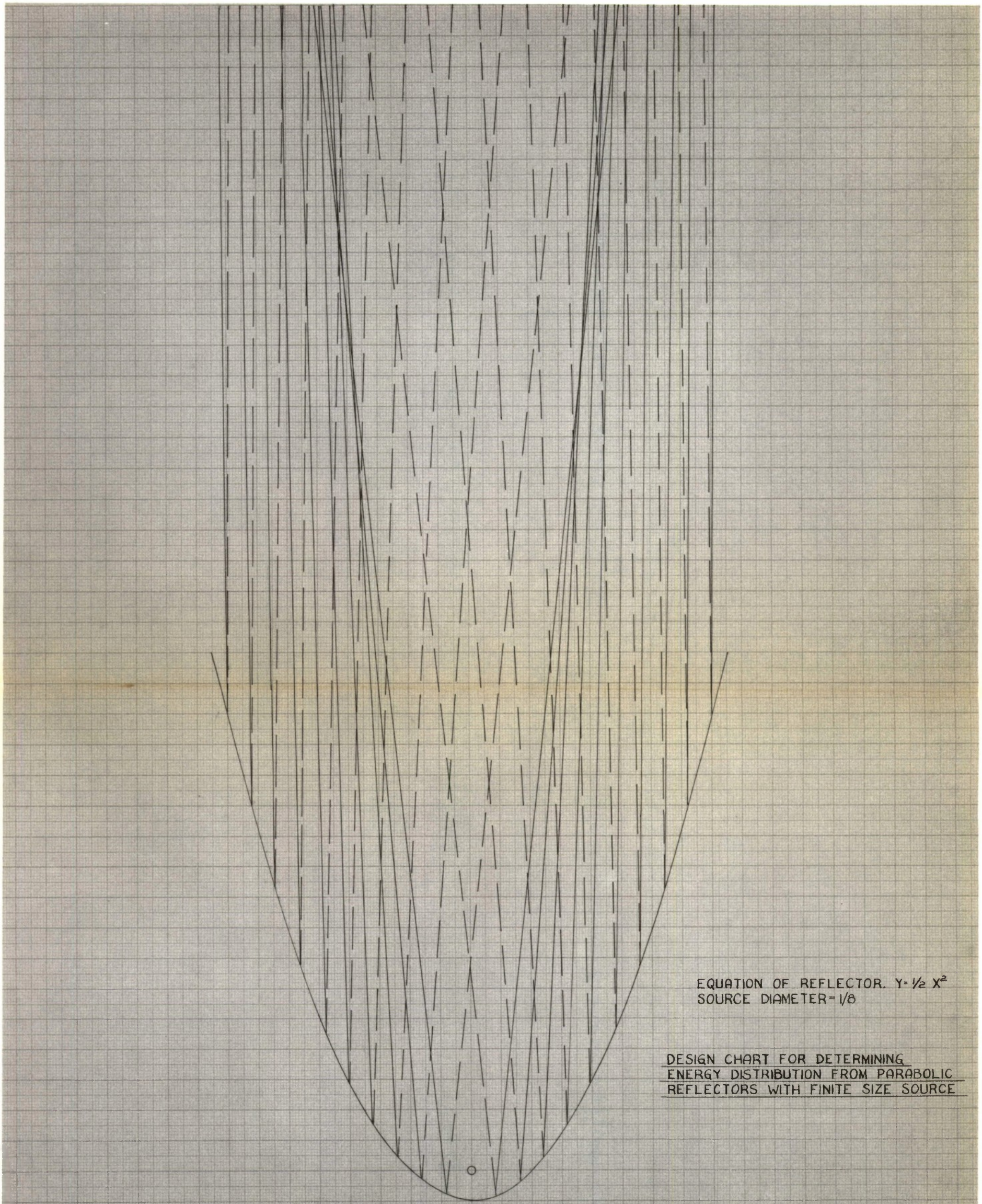
FIGURE 78



EQUATION OF REFLECTOR $Y = \frac{1}{2}X^2$
SOURCE DIAMETER = 1/4

DESIGN CHART FOR DETERMINING ENERGY DISTRIBUTION FROM PARABOLIC REFLECTORS WITH FINITE SOURCE

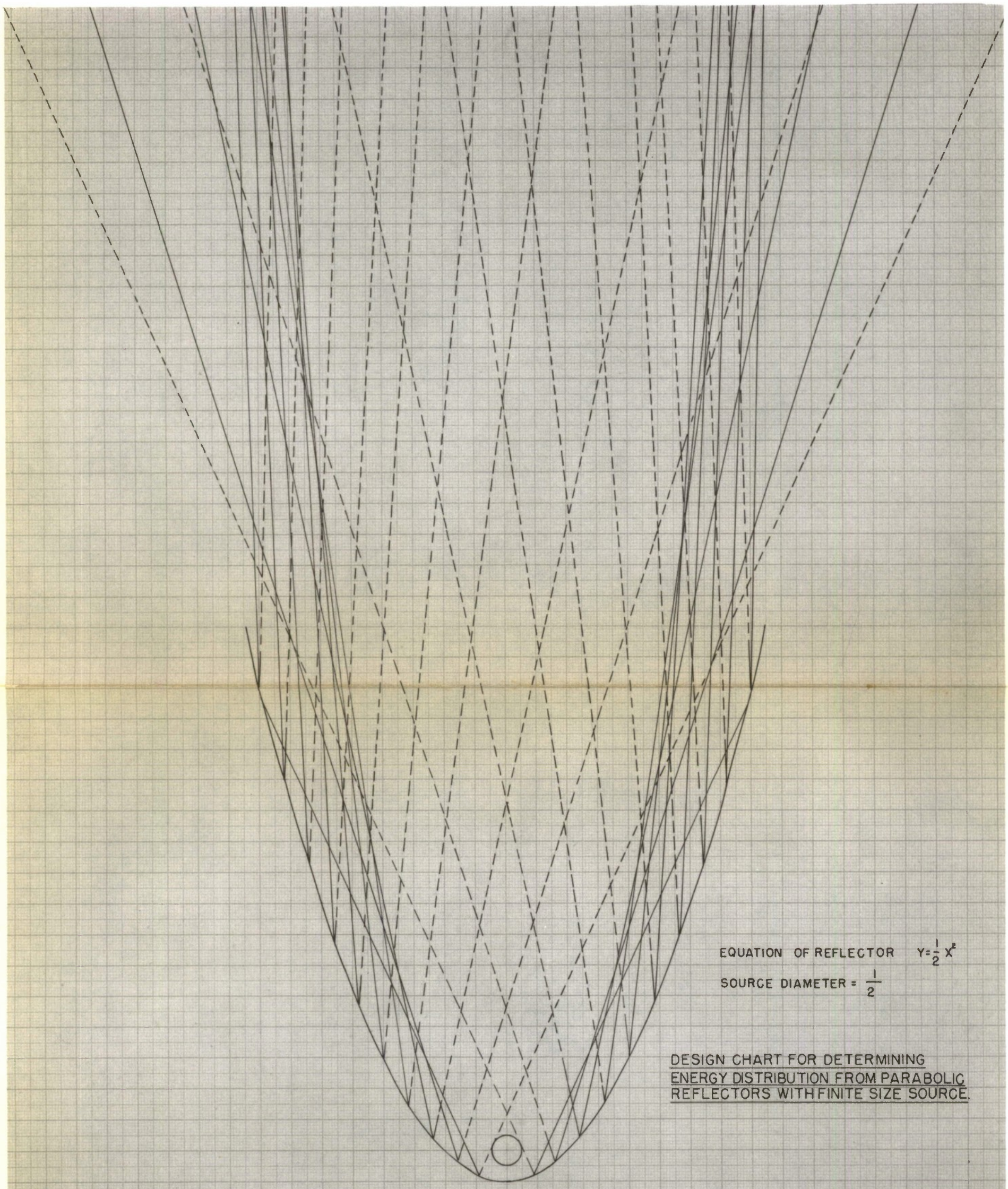
FIGURE 80



EQUATION OF REFLECTOR. $Y = \frac{1}{2} X^2$
SOURCE DIAMETER = 1/8

DESIGN CHART FOR DETERMINING ENERGY DISTRIBUTION FROM PARABOLIC REFLECTORS WITH FINITE SIZE SOURCE

FIGURE 79

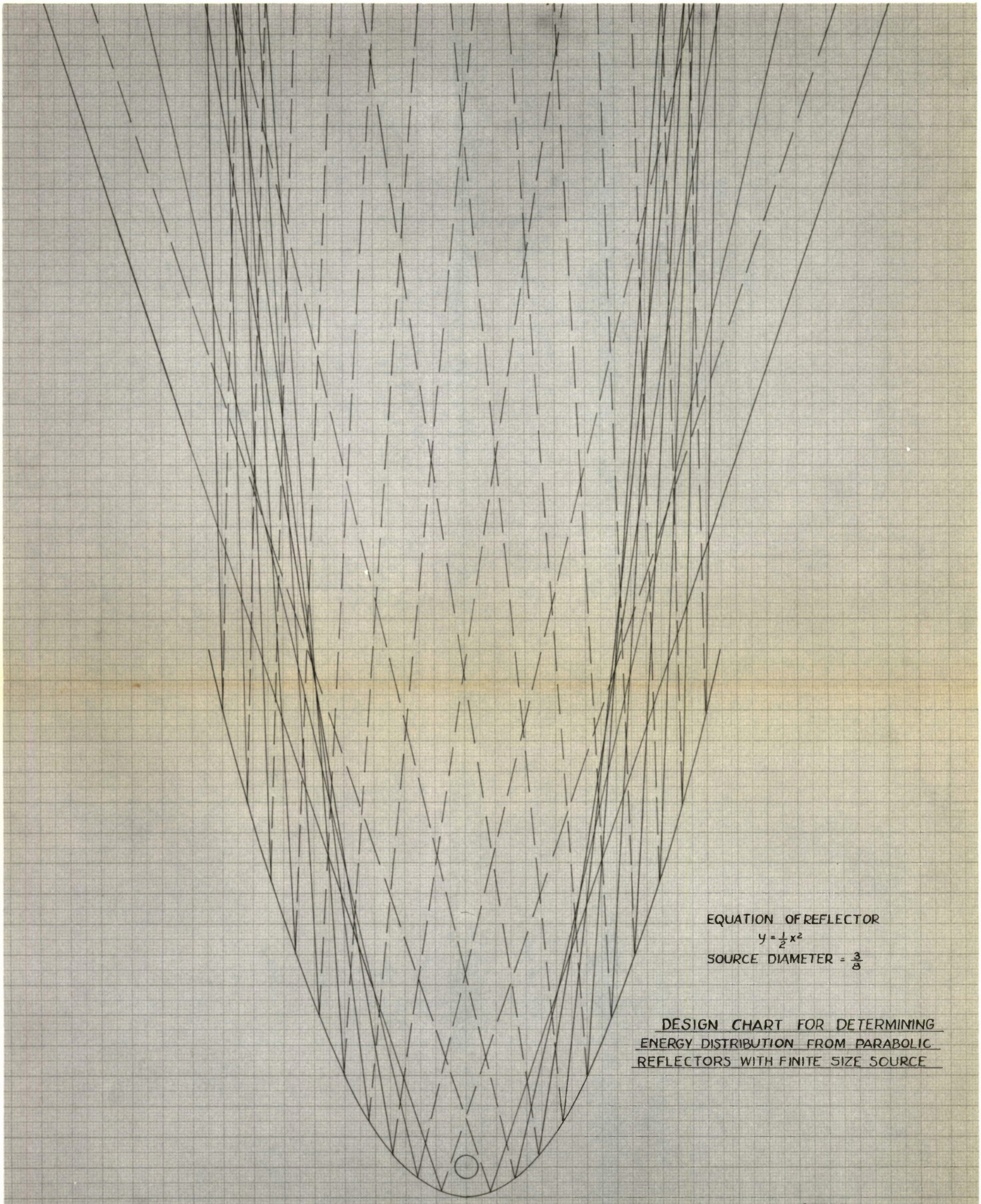


EQUATION OF REFLECTOR $Y = \frac{1}{2} X^2$

SOURCE DIAMETER = $\frac{1}{2}$

DESIGN CHART FOR DETERMINING ENERGY DISTRIBUTION FROM PARABOLIC REFLECTORS WITH FINITE SIZE SOURCE.

FIGURE 82



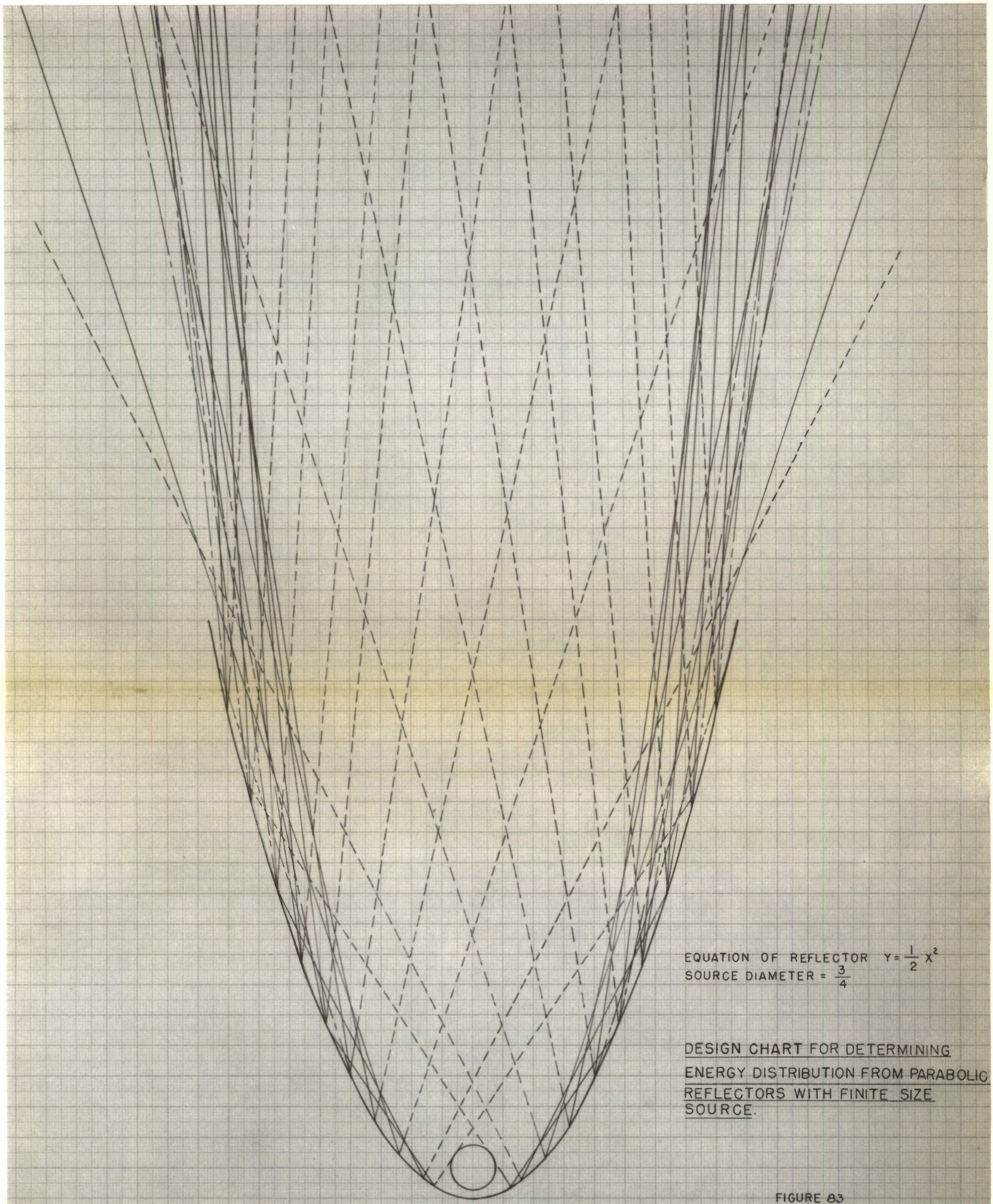
EQUATION OF REFLECTOR

$y = \frac{1}{2}x^2$

SOURCE DIAMETER = $\frac{3}{8}$

DESIGN CHART FOR DETERMINING ENERGY DISTRIBUTION FROM PARABOLIC REFLECTORS WITH FINITE SIZE SOURCE

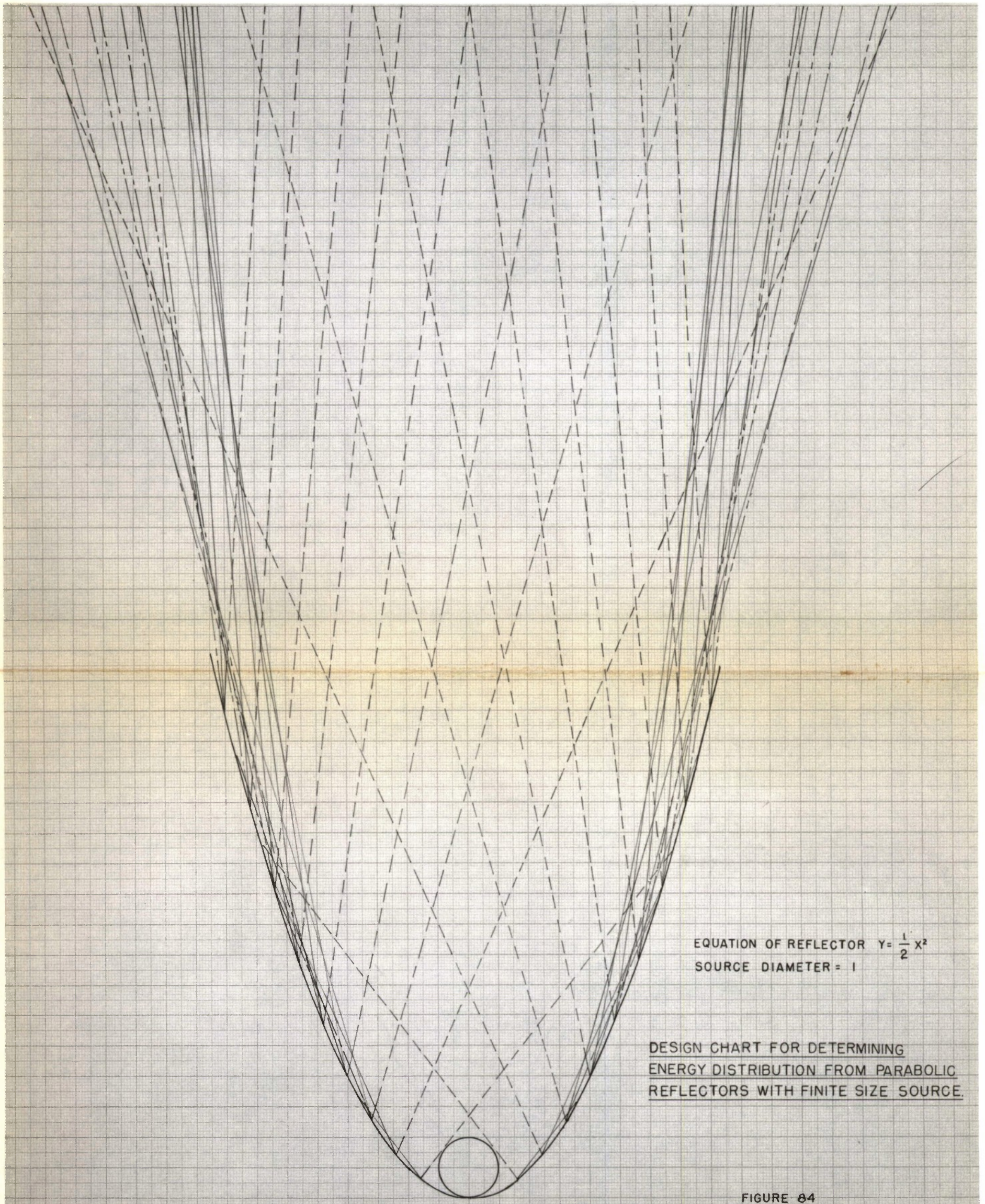
FIGURE 81



EQUATION OF REFLECTOR $Y = \frac{1}{2} X^2$
SOURCE DIAMETER = $\frac{3}{4}$

DESIGN CHART FOR DETERMINING ENERGY DISTRIBUTION FROM PARABOLIC REFLECTORS WITH FINITE SIZE SOURCE.

FIGURE 83

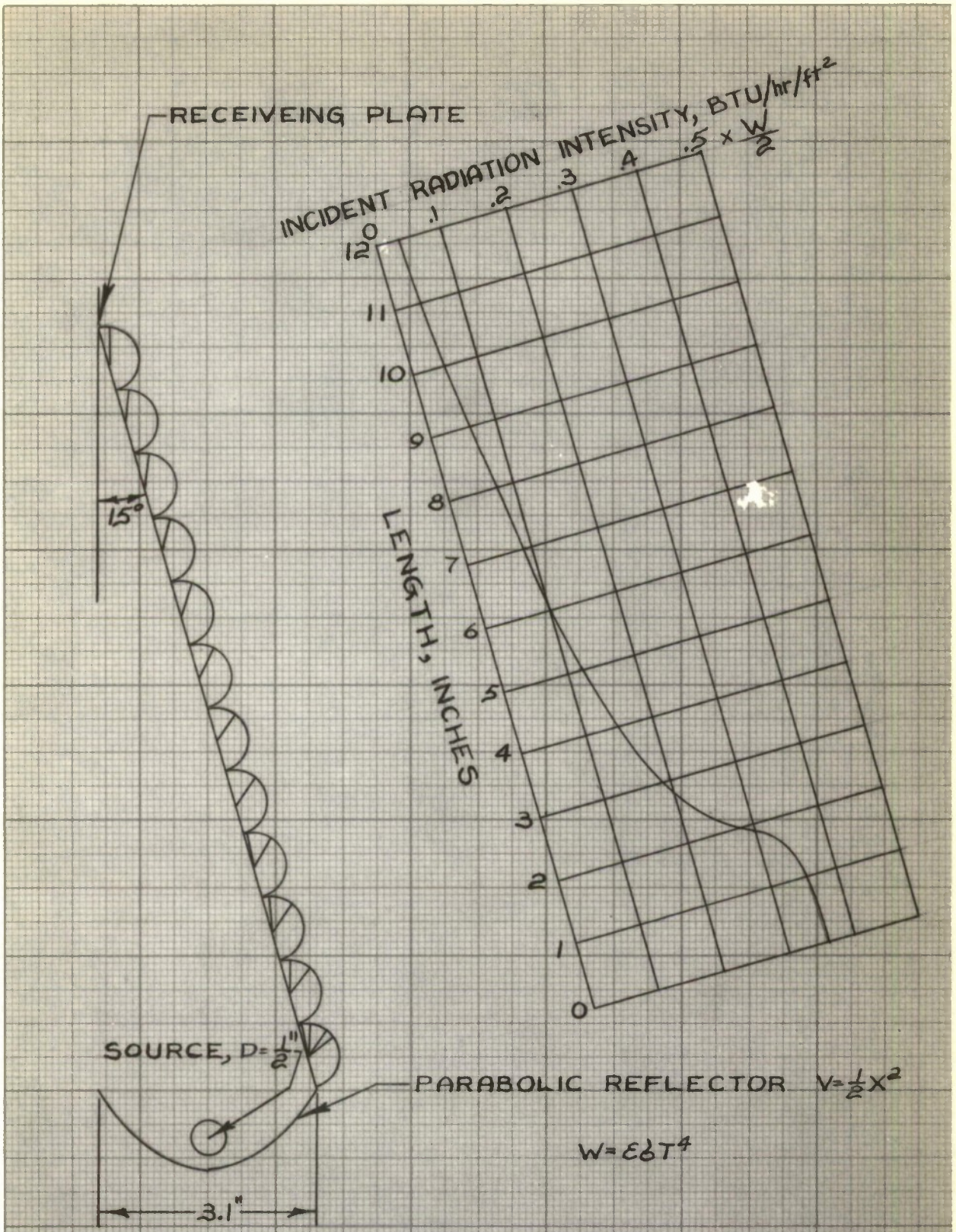


EQUATION OF REFLECTOR $Y = \frac{1}{2} X^2$

SOURCE DIAMETER = 1

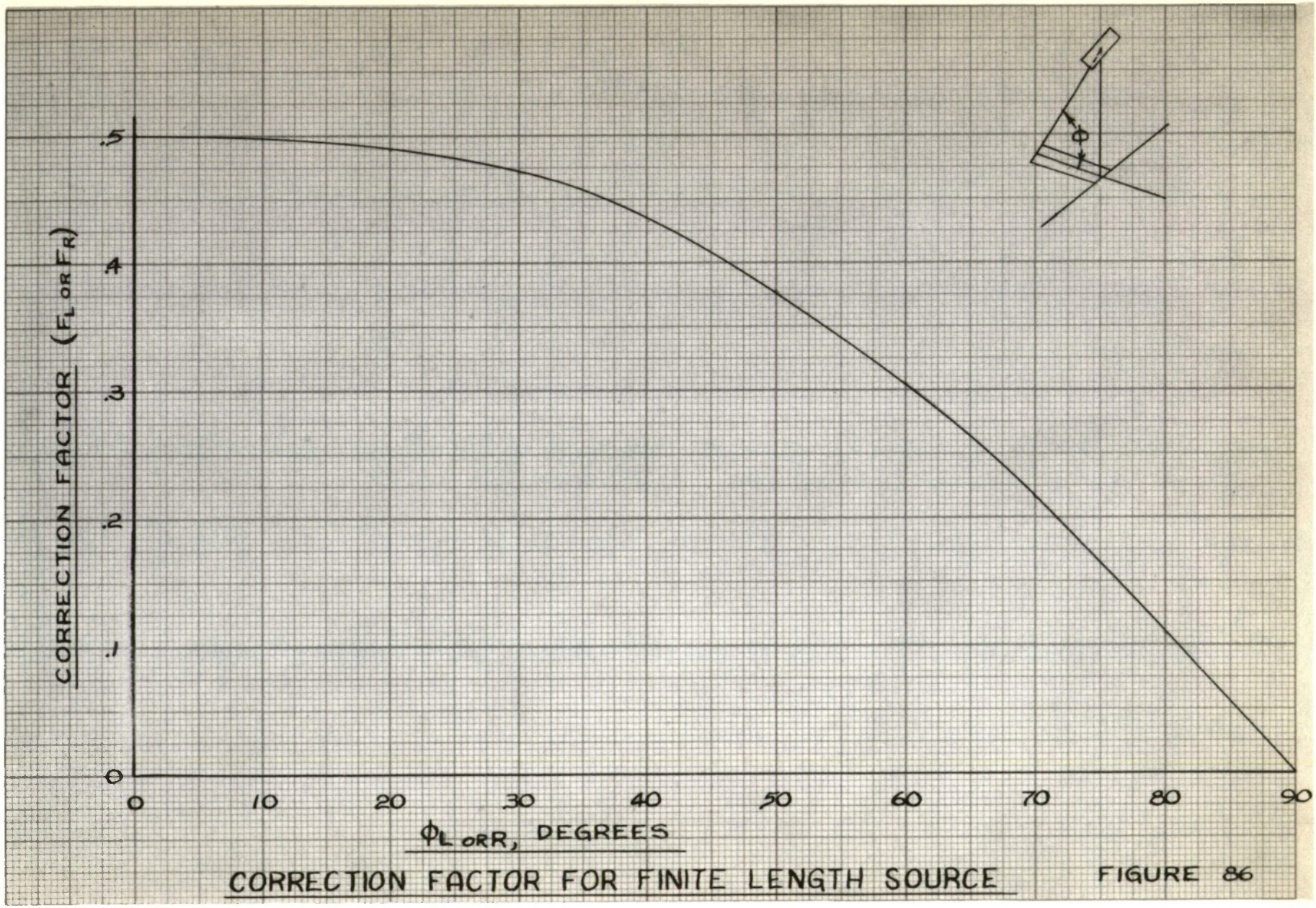
DESIGN CHART FOR DETERMINING ENERGY DISTRIBUTION FROM PARABOLIC REFLECTORS WITH FINITE SIZE SOURCE.

FIGURE 84

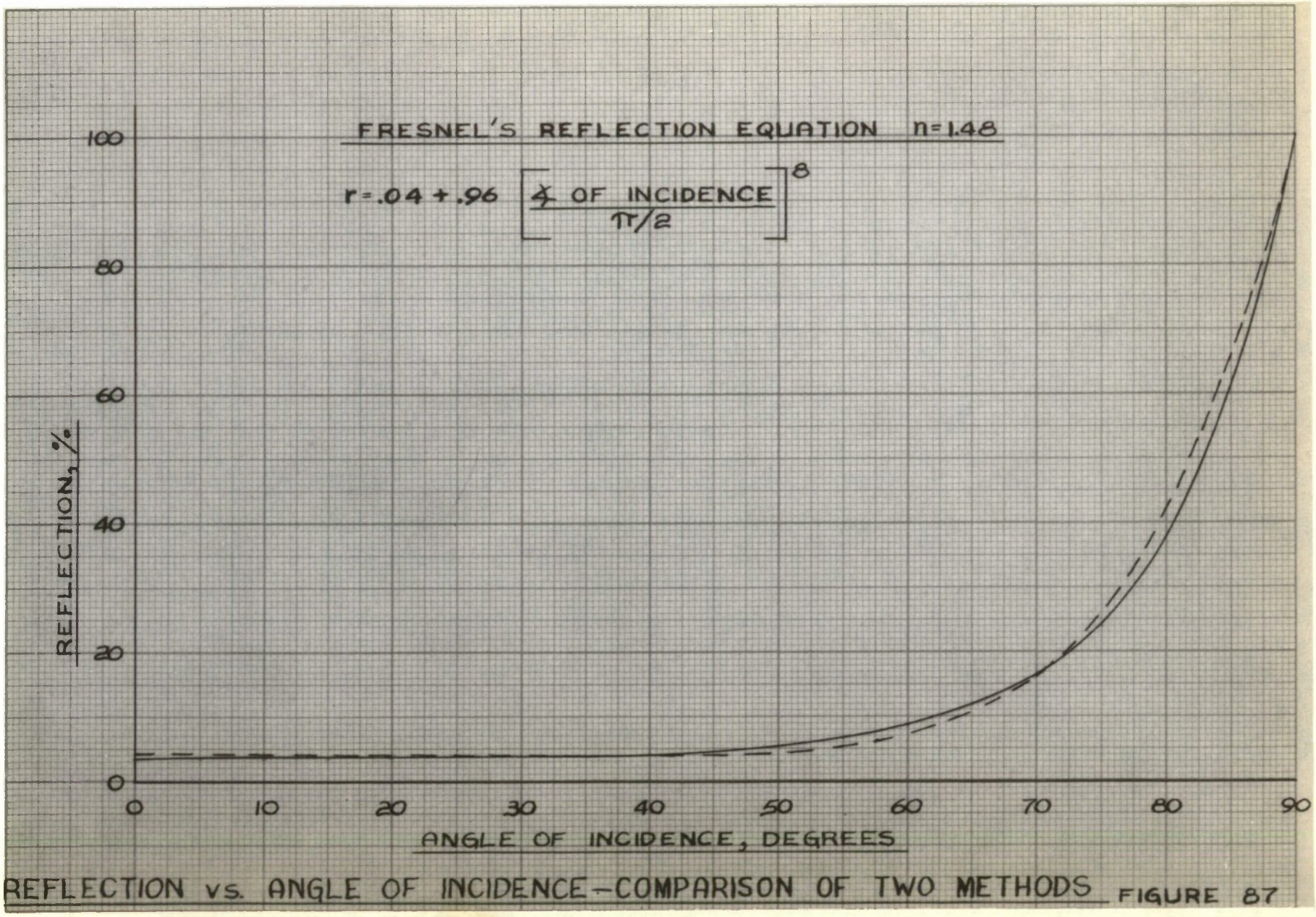


TYPICAL ENERGY DISTRIBUTION ON PLATE ABOVE A PARABOLIC REFLECTOR CONTAINING A FINITE DIAMETER OF A FINITE LENGTH

FIGURE 85

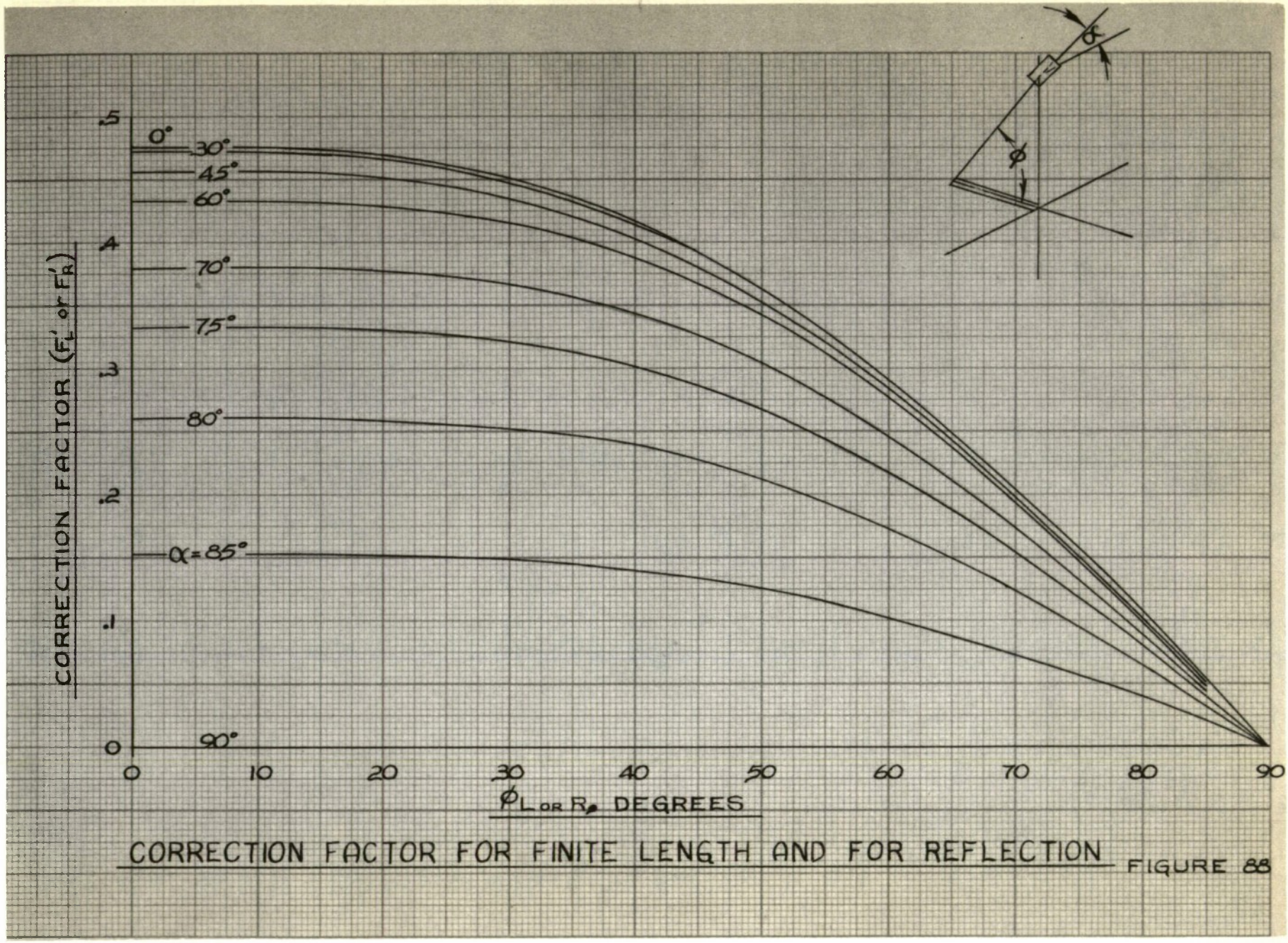


CORRECTION FACTOR FOR FINITE LENGTH SOURCE FIGURE 86

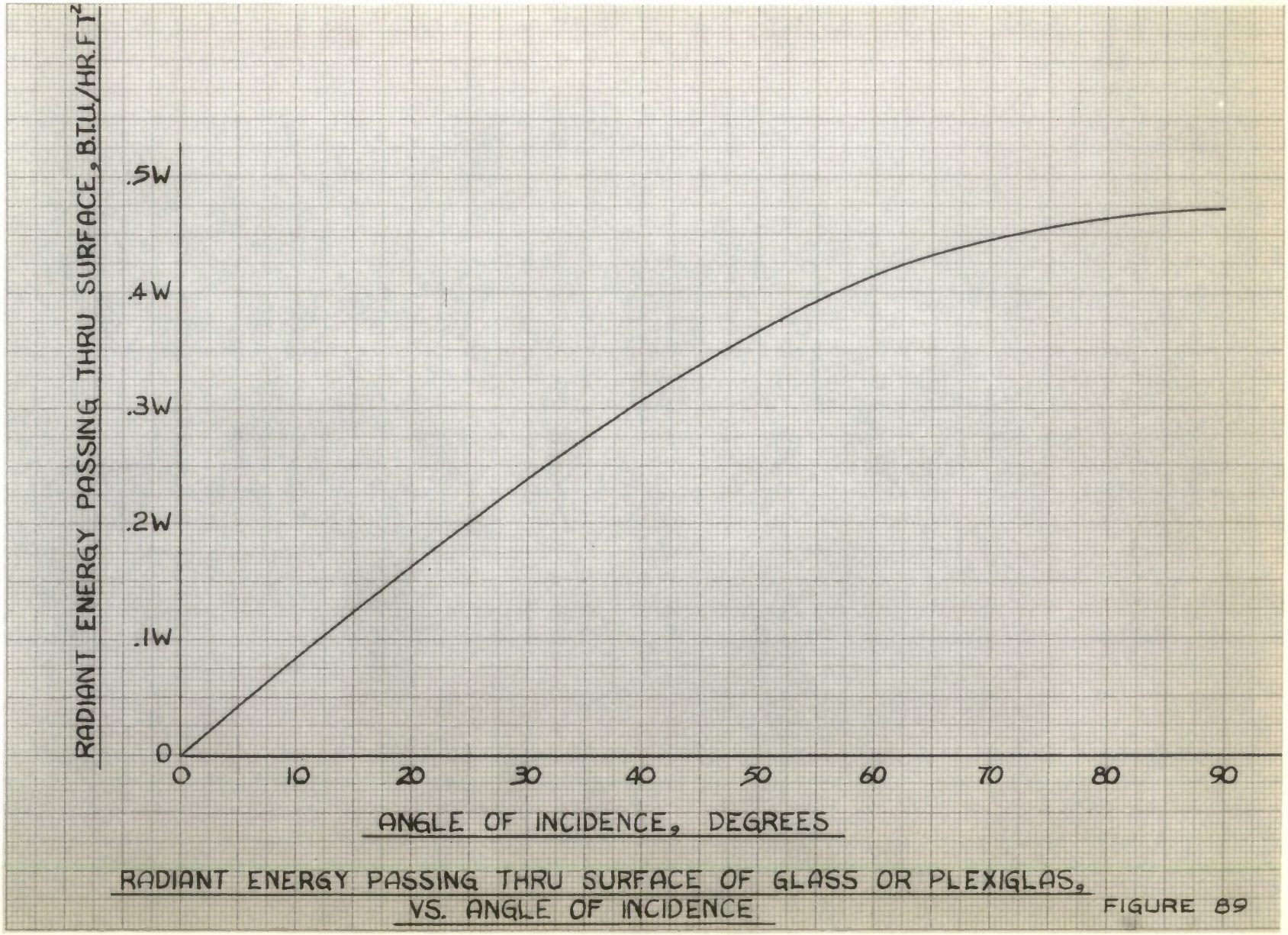


REFLECTION vs. ANGLE OF INCIDENCE—COMPARISON OF TWO METHODS FIGURE 87

AFTR 5874

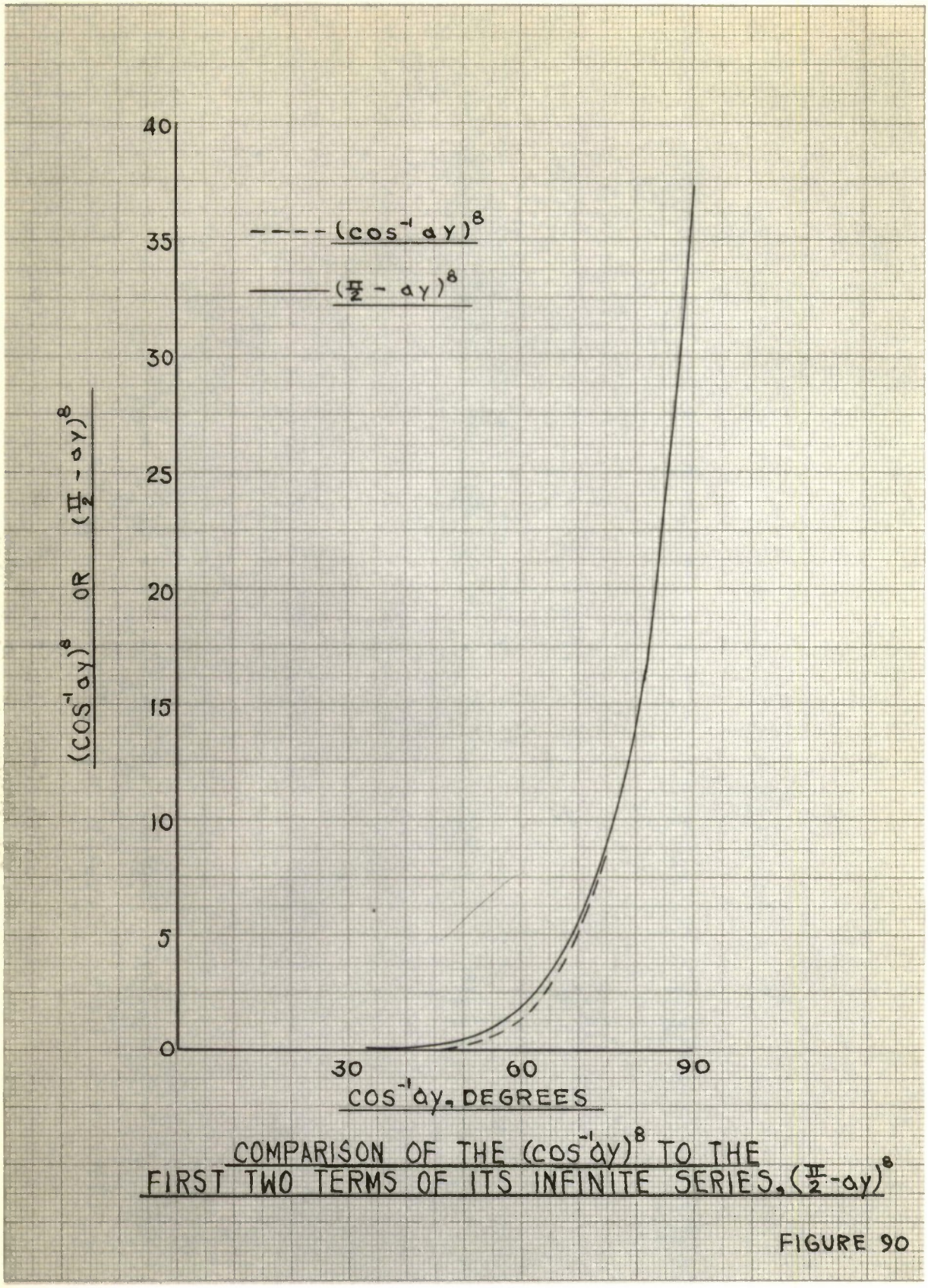


CORRECTION FACTOR FOR FINITE LENGTH AND FOR REFLECTION FIGURE 88



RADIANT ENERGY PASSING THRU SURFACE OF GLASS OR PLEXIGLAS, VS. ANGLE OF INCIDENCE

FIGURE 89



COMPARISON OF THE $(\cos^{-1} ay)^8$ TO THE FIRST TWO TERMS OF ITS INFINITE SERIES, $(\frac{\pi}{2} - ay)^8$

FIGURE 90

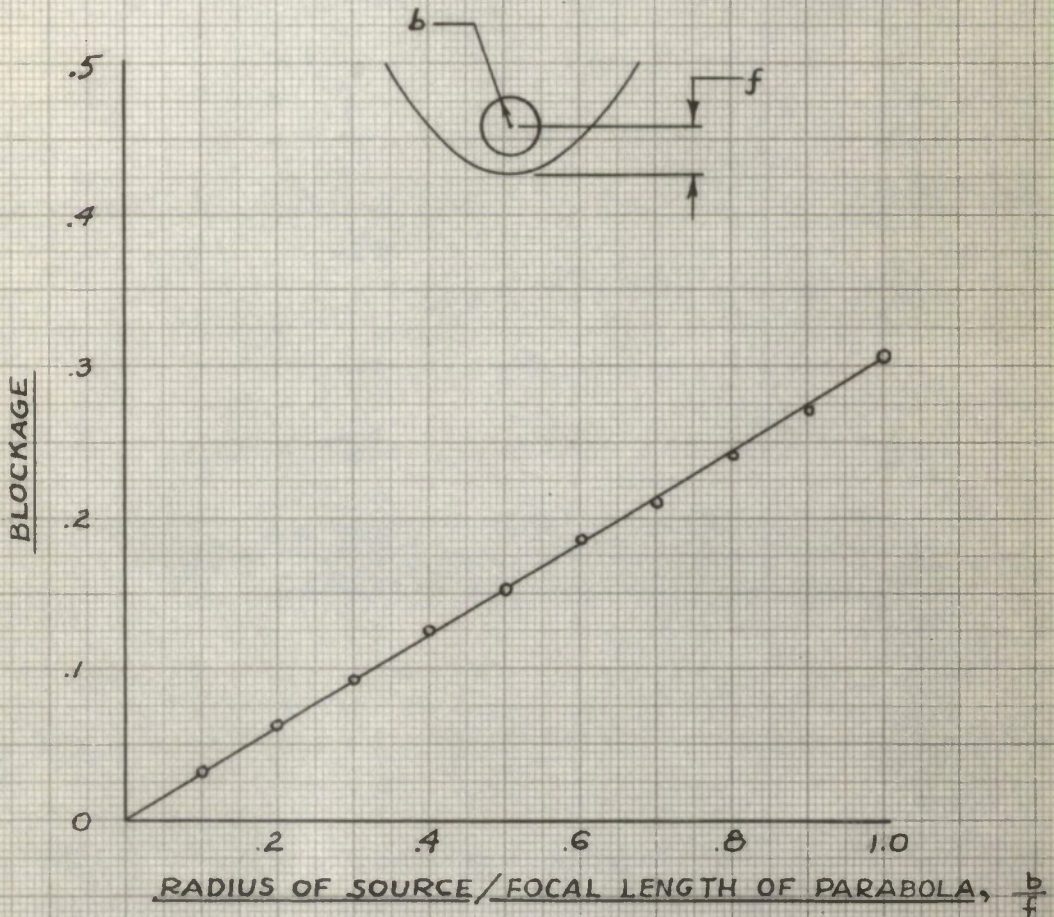
THEORETICAL EQUATION

$$\text{BLOCKAGE} = \frac{1}{\pi}\left[\pi - \frac{f}{b}\sqrt{\sqrt{\left(\frac{b}{f}\right)^2+\frac{1}{4}}\ \frac{1}{2}} - \text{Tan}^{-1}\ \frac{f}{b}\sqrt{\sqrt{\left(\frac{b}{f}\right)^2+\frac{1}{4}}+\frac{1}{2}}\right.$$

$$\left. - \text{Cos}^{-1}\ \frac{b}{f} + \text{Tan}\left(\text{Cos}^{-1}\frac{b}{f}\right)\right]$$

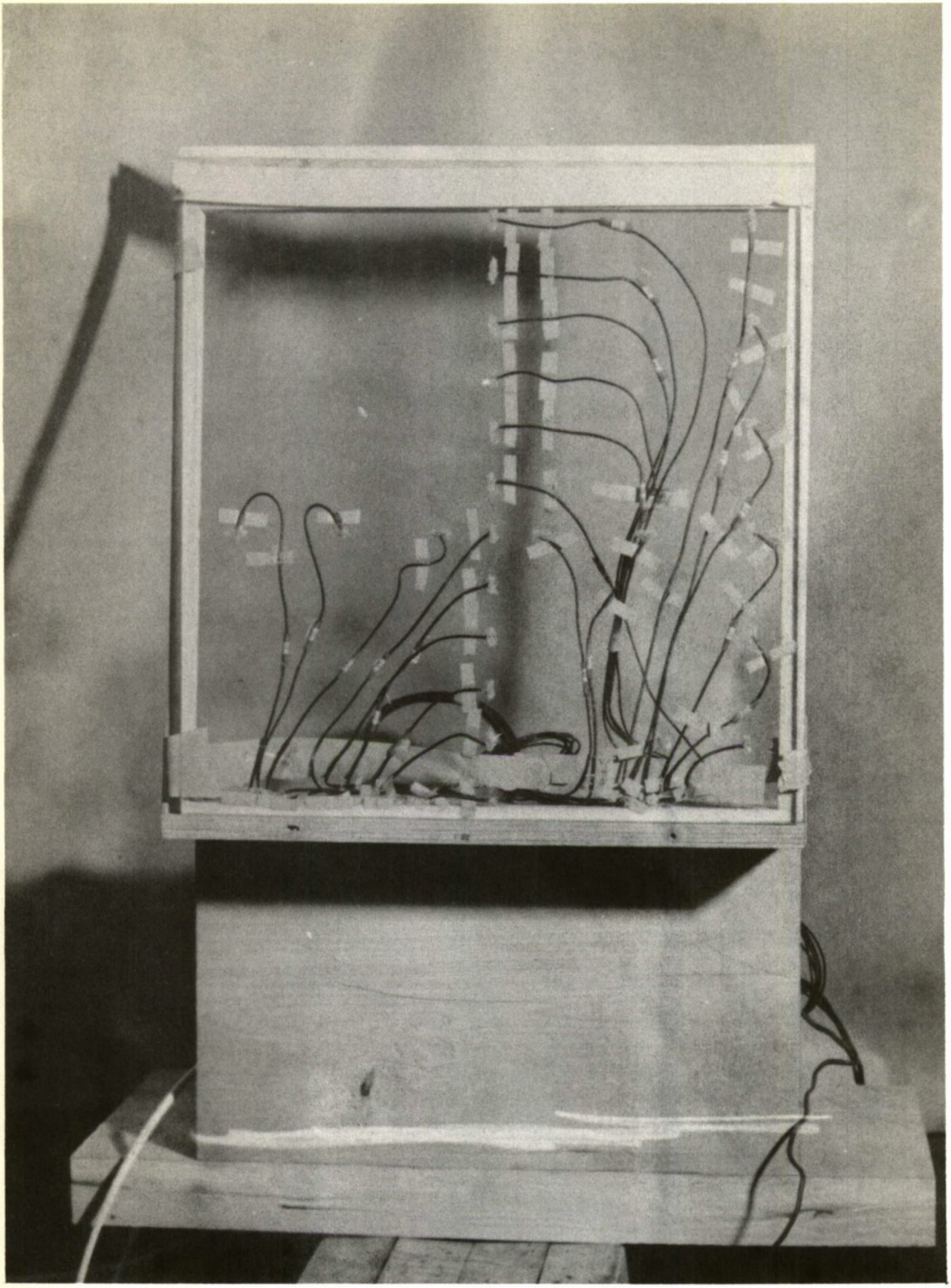
APPROX. EQUATION

$$\text{BLOCKAGE} = .307\,\frac{b}{f}$$

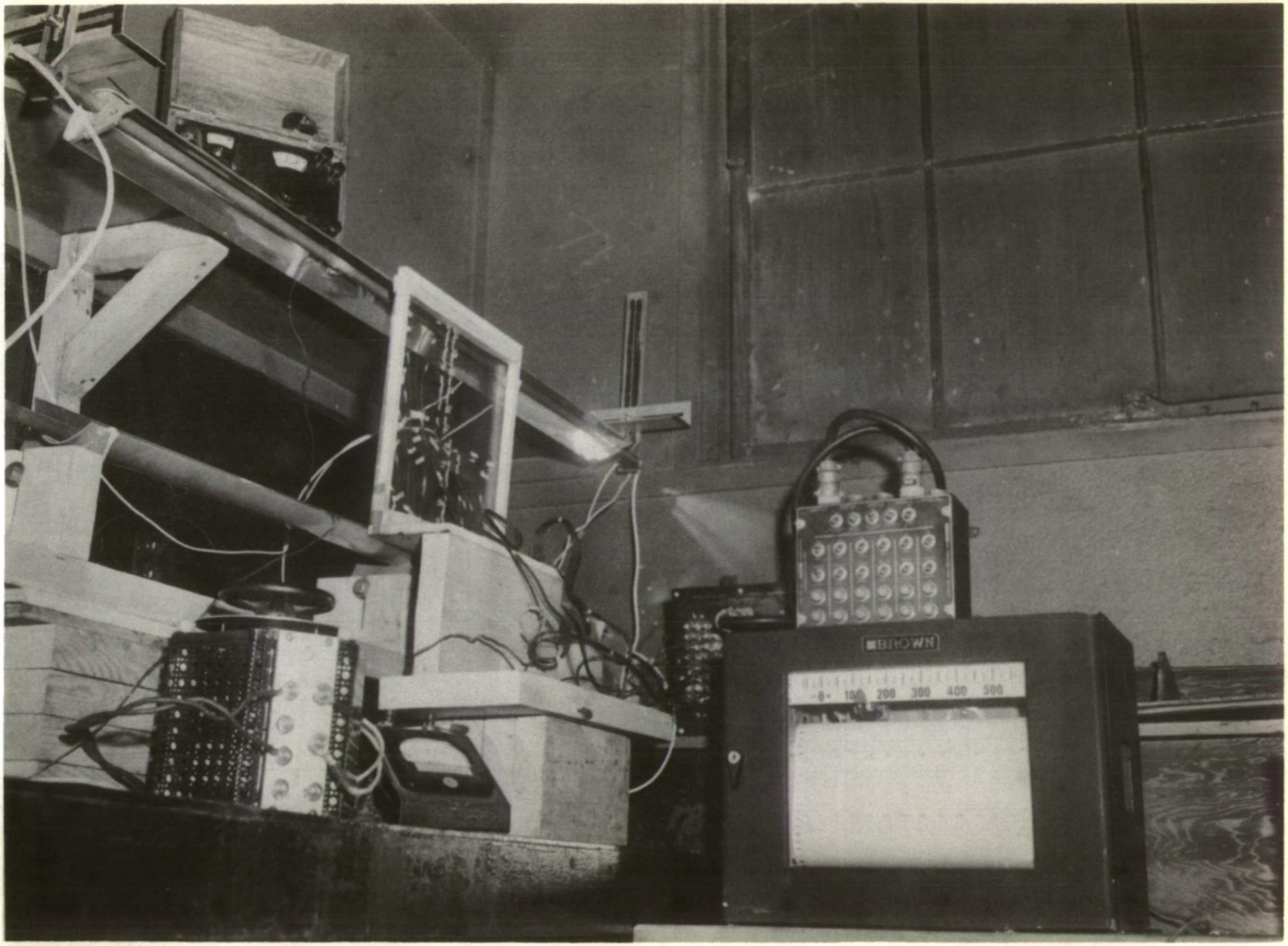


BLOCKAGE OF AN INFINITELY LONG CYLINDRICAL SOURCE WITHIN A PARABOLIC REFLECTOR

FIGURE 91



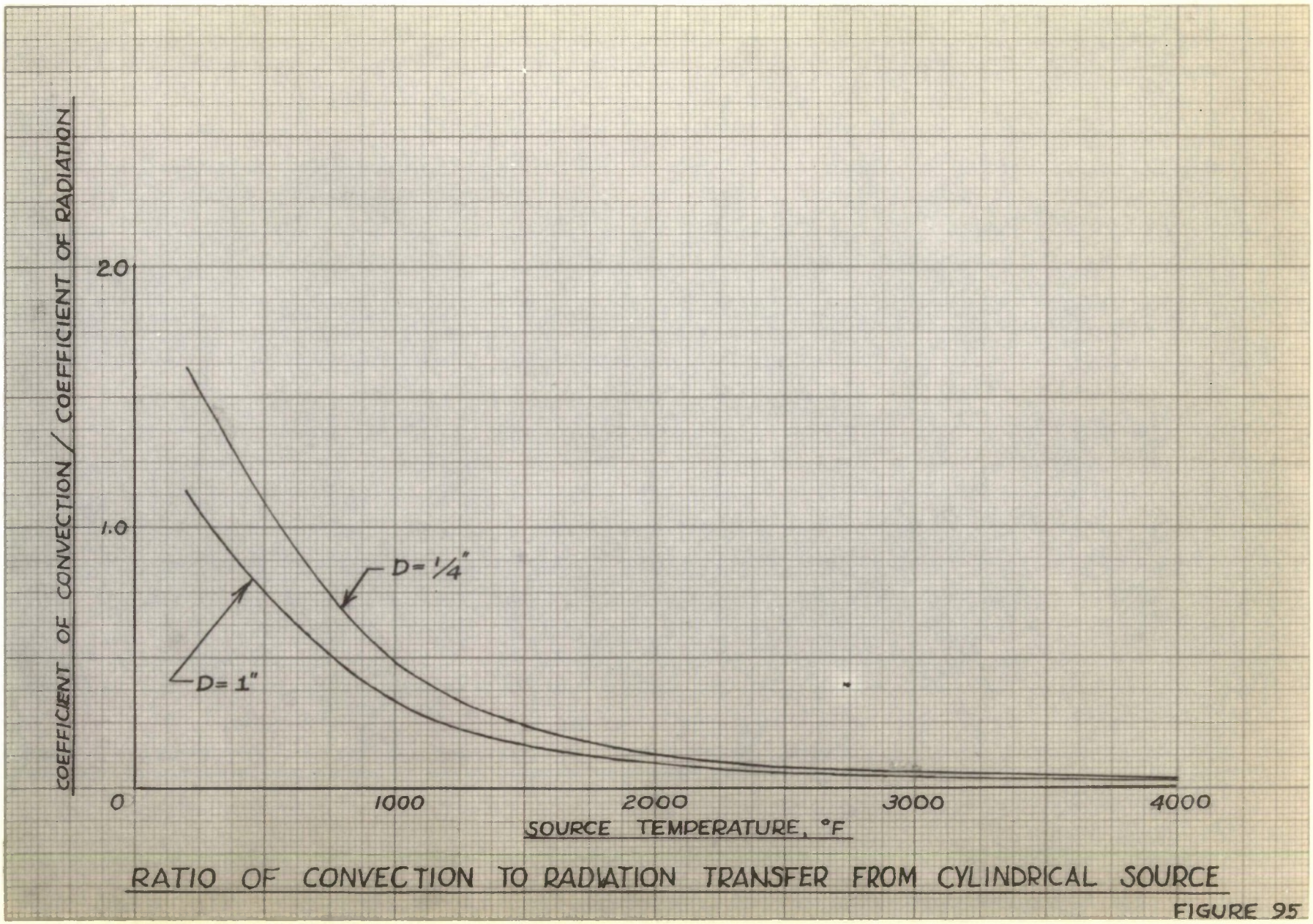
PLEXIGLAS RECEIVER INSTRUMENTED WITH SURFACE THERMOCOUPLES



EXPERIMENTAL REFLECTOR TEST SET-UP FIGURE 93

RUN NO.	NUMBER OF SOURCE-REFLECTOR COMBINATIONS	EFFECTIVE SOURCE LENGTH, INCHES	SOURCE TEMP, °F	RECEIVER ∠ OF INCLINATION, DEGREES	TEMP VARIATION (MAX)		AVERAGE RADIATION ABSORPTION RATE, BTU/hr, ft²	
					EXPERIMENTAL	THEORETICAL	CALCULATED FROM EXPERIMENTAL DATA	THEORETICAL
1	1 ABOVE RECEIVER	48.5	640	15	10.6/1	10/1	78.1	81
2	1 ABOVE RECEIVER	48.5	640	20	11.5/1	10.7/1	88.3	99.5
3	1 ABOVE RECEIVER	48.5	635	10	8.1/1	7.6/1	68.4	52.8
4	1 ABOVE RECEIVER	12	635	15	12.5/1	16.3/1	70.6	72.7
5	1 ABOVE RECEIVER	12	735	15	11.5/1	16.3/1	119.2	102
6	1 BELOW RECEIVER	48.5	605	15	4.2/1 including convection	10/1 radiation only	147.9 including convection	71.5 radiation only
7	2 ABOVE & BELOW RECEIVER	48.5	UPPER 630 LOWER 605	15	2.6/1 including convection	2.1/1 radiation only	233.9 including convection	149.6 radiation only 226.0 including convection

COMPARISON OF EXPERIMENTAL & PREDICTED REFLECTOR RESULTS FIGURE 94



RATIO OF CONVECTION TO RADIATION TRANSFER FROM CYLINDRICAL SOURCE

FIGURE 95